CARRIER PHASE-BASED LONG-RANGE GPS KINEMATIC POSITIONING

SHAOWEI HAN

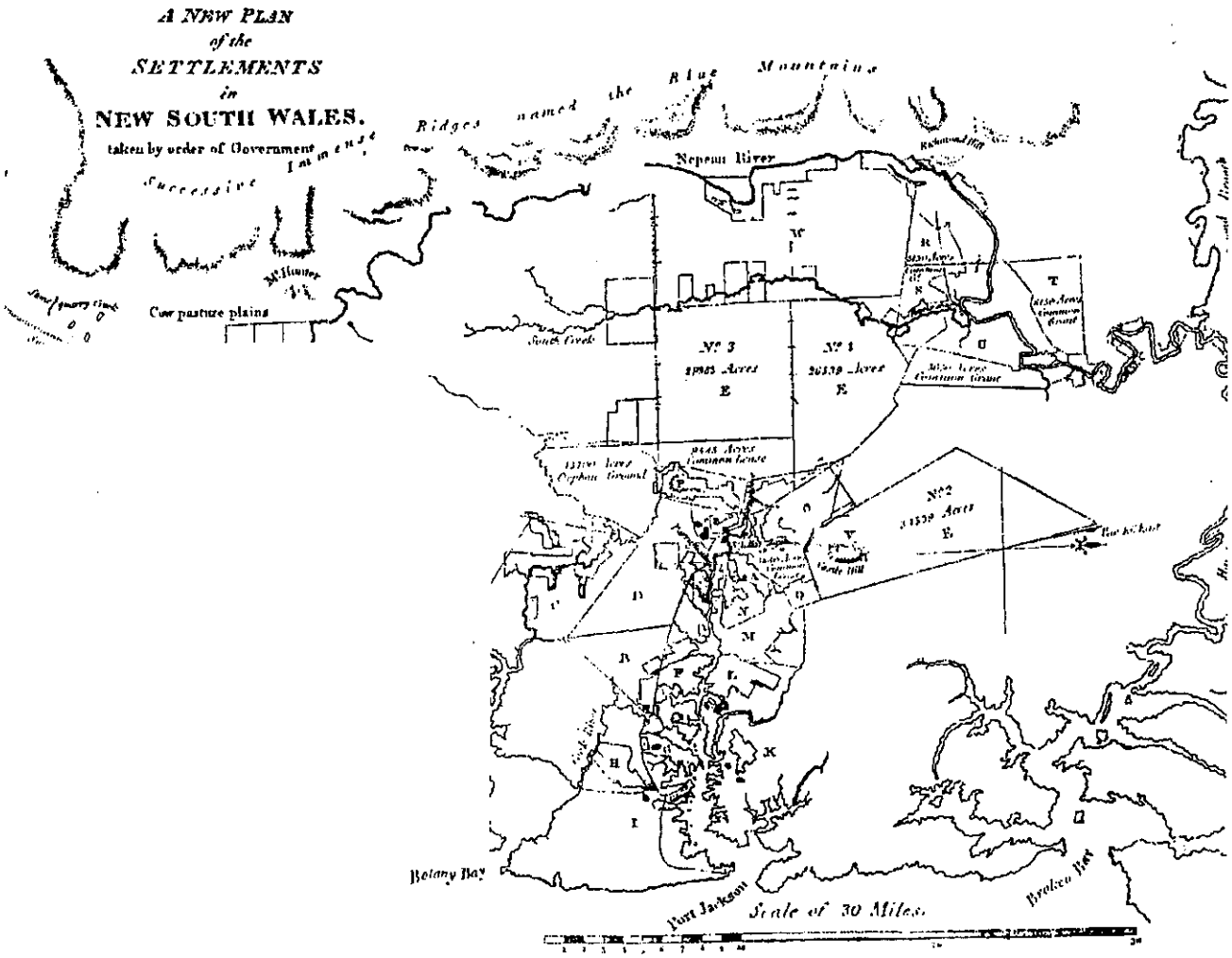

UNISURV S-49, 1997

Reports from

SCHOOL OF GEOMATIC ENGINEERING

THE UNIVERSITY OF NEW SOUTH WALES SYDNEY NSW 2052 AUSTRALIA

UNISURV REPORT S-49, 1997

CARRIER PHASE-BASED LONG-RANGE GPS KINEMATIC POSITIONING

SHAOWEI HAN

Received: March, 1997
Accepted: August, 1997

SCHOOL OF GEOMATIC ENGINEERING
UNIVERSITY OF NEW SOUTH WALES
SYDNEY NSW 2052
AUSTRALIA

National Library of Australia

Card No. and ISBN 0 85839 074 4

ABSTRACT

Carrier phase-based long-range GPS kinematic positioning can potentially provide sub-decimetre accuracy trajectories even when the separation between the roving receiver and reference receiver is many hundreds of kilometres. To realise this potential, three techniques have been proposed in this thesis.

An ambiguity resolution on-the-fly algorithm, using data from multiple reference stations for medium-range kinematic positioning (<100 km), is proposed. This technique is based on a linear combination functional model, formed from the single-differenced functional equation for baselines from the roving receiver to three or more reference receivers. In this way, the orbit bias and ionospheric delay can be eliminated, and, in addition, the tropospheric delay, multipath and observation noise can be significantly reduced. Hence, the ambiguity resolution technique similar to that used for the short-range case can be employed. This technique requires that the reference stations be located such that they surround the survey area and the roving receiver is less than 100 km from the nearest reference station, in order to effectively account for the ionospheric delay. Experiments have shown that ambiguities can be resolved using a single epoch of data.

Ambiguity recovery techniques for long-range kinematic positioning (up to many hundreds of kilometres) have been proposed. One of the techniques requires precise pseudo-range observations, which when combined with carrier phase observations can estimate the cycle slips on the widelane and an observable combination with maximum wavelength (14.65 m). All integer ambiguity candidates derived from the cycle slip estimates can be tested by validation criteria to determine the correct integer ambiguity set. This technique can repair data gaps up to 1-5 minutes in length depending on the receiver type and the ionospheric conditions. If the dual-frequency, full wavelength carrier phase observations are available, but no precise pseudo-range data, the Ambiguity Function Method with Kalman filtering is a powerful combination for detecting and repairing cycle slips. This technique can repair data gaps up to a few seconds in length. These two ambiguity recovery techniques require the precise ephemeris in order to determine sub-decimetre accuracy positions.

The third technique assumes that only the trajectory of the roving receiver relative to itself is required to be of high accuracy. The biased position derived using incorrectly fixed ambiguities can be corrected to sub-decimetre accuracy using the known position of the start point and end point of the survey, based on the approximately linear characteristic of the effect of biases on results over a short period (half hour or so).

In the process of deriving the above three techniques in this thesis, important contributions have been made, and new algorithms developed, in the areas of orbit bias elimination procedures, ionospheric delay interpolation technique using an epoch-by-epoch and satellite-by-satellite model, three-step quality control improvements, a new method for constructing multi-satellite ambiguity combinations, a study of the effect of temporal correlation on ambiguity resolution, and multipath extraction and mitigation methods.

TABLE OF CONTENTS

LIST OF TABLES

LIST OF FIGURES

Figure

ACKNOWLEDGEMENTS

This research thesis was carried out from June, 1994 to March 1997 under the supervision of Professor Chris Rizos. I am grateful to my supervisor Prof. Rizos for his encouragement, valuable advice, and patient guidance during this work. I also wish to thank members of the Satellite Navigation And Positioning (SNAP) group in the School of Geomatic Engineering, Dr. Wan-Xuan Fu, the late Mr. Bernd Hirsch, Mr. David Lin, Mr. Craig Roberts, Dr. Mustafa Subari, Mr. Ken Wong, Ms. Evelyn Koeller, and some new members, for valuable discussions, and assistance in collecting GPS data.

I would also like to thank the Overseas Postgraduate Research Scholarship (OPRS) scheme and support from Australian Research Council.

I am indebted to Professor Pinhao Shi, Wuhan Technical University of Surveying and Mapping (WTUSM), who encouraged me to develop GPS software in 1986 and who continued to give me a lot of advice on GPS research. The support of other members of the WTUSM GPS research group, especially Professor Jingnan Liu and Dr. Yanming Feng, is also appreciated.

Last, but not least, my final and deepest appreciation to my family, especially my parents, my wife (PhD student in the School of Geography, UNSW) and my son, Jeff, for their love, encouragement and understanding during my studies.

Chapter 1

INTRODUCTION

1.1 GPS Background

The Global Positioning System (GPS) is a satellite-based radio-positioning navigation and time transfer system designed, financed, deployed, and operated by the U. S. Department of Defense (DoD). The GPS system consists of three segments, the *Space Segment* comprising the 21+3 satellites which transmit the signals, the *Control Segment* consisting of the ground facilities carrying out the task of satellite tracking, orbit computations, telemetry and supervision necessary for the daily control of the space segment, and; the *User Segment* which includes the entire spectrum of applications equipment and computational techniques that must provide the users with the positioning results. GPS was developed as a military force enhancement system and will continue to play this role. However, GPS has also demonstrated a significant benefit to the civilian community.

The GPS ranging signal is broadcast at two L-band frequencies: a primary signal at 1575.42MHz (L1) and a secondary signal at 1227.6MHz (L2). Modulated onto the L1 carrier wave are two pseudo-random noise (PRN) ranging code: the 1-millisecond-long C/A-code with a chipping rate of about 1.023MHz, and a week-long segment of the P-code with a chipping rate of 10.23MHz. Also modulated on the carrier is the navigation message which, among other items, includes the ephemeris data describing the predicted position of the satellite and the predicted satellite clock correction terms. The L2 carrier is modulated by the P-code and the navigation message, but no C/A-code. The pseudo-random binary sequences of C/A-code (C(t)), P-code (P(t)) and GPS message D(t) are modulated on the L1 and L2 carrier phase, and hence the two carrier signals leaving the satellite antenna can be represented by (Wells et al., 1987):

$$S_{L1}(t) = A_c C(t) D(t) \sin(2\pi f_1 t + \phi_c) + A_p P(t) D(t) \cos(2\pi f_1 t + \phi_{p1}) \qquad (1\text{-}1)$$

$$S_{L2}(t) = A_p P(t) D(t) \cos(2\pi f_2 t + \phi_{p2}) \quad (1\text{-}2)$$

The C/A code is used by the Standard Positioning Service (SPS). The P-code is used by the Precise Positioning Service (PPS). Because of its higher modulation bandwidth, the P-code ranging signal has higher measurement resolution and is therefore more precise. The GPS navigation message is a data sequence with a bit rate of 50 bps. One frame of D(t) has a length of 1500 bits, and hence a period of 30 seconds. The code and data phase modulation sequences can be modelled as sequences of ± 1 amplitude states.

The U. S. DoD has encrypted the P-code under a policy known as "Anti-Spoofing" (AS). The resulting Y-code is the modulo-two sum of the P-code and a substantially lower rate encrypting code W(t). It is difficult for civilian receivers to decode the Y-code, and hence the Y-code pseudo-ranges and L2 carrier phase measurements are difficult to obtain. In addition, the military operators of the system have the capability to intentionally degrade the accuracy of the C/A code by desynchronizing the satellite clock (δ – process), or by incorporating small errors (ε – process) in the broadcast ephemeris. This degradation is known as "Selective Availability" (S/A). The magnitude of the resulting range errors is typically 20 m, and results in rms horizontal position error of about 50 m, at the one sigma level. The DoD claim that horizontal errors will be less than 100 m, 95% of the time.

1.2 GPS Receivers and Observables

1.2.1 GPS Receivers

A GPS receiver consists of the antenna, radio frequency (RF) section, signal trackers, microprocessor, input control device, storage device and power supply. The antenna of a GPS receiver converts the energy in the electromagnetic waves arriving from the satellites into an electric current that can be handled by the electronics within the receiver. The RF section will combine the incoming signal with a pure sinusoidal signal generated by a local oscillator to transform the frequency of signals arriving at the antenna to a lower one, an intermediate frequency (IF), upon which measurements are made. The actual pseudo-range measurements are performed in tracking loop circuits. The code ranges are typically determined in the delay lock loop (DLL) using a code correlation technique. After removing the pseudo-random code from the incoming signal, and some filtering, the unmodulated (Doppler shifted) carrier wave is obtained.

The carrier wave is then passed to the phase lock loop (PLL) where the phase measurement is made. The observable is the (fractional) phase offset between the received signal and the reference signal generated in the receiver, and integer changes to the phase. Therefore, the initial phase measurement is ambiguous by an integer number of cycles (Langley, 1993).

If Anti-Spoofing were turned off, the C/A, P1 and P2 pseudo-ranges and L1 and L2 carrier phase observations are easily obtained. Unfortunately, under AS, the P-code has been changed to a Y-code, and this code sequence is not available to civilian users. What can GPS receiver measure when AS is turned on ? Recent developments in GPS receiver technology have focussed on extracting the precise pseudo-range and carrier phase information on L2. Typical techniques include the narrow-correlation technique, squaring, code correlation squaring, cross-correlation and P-W tracking (Hofmann-Wellenhof et al., 1994).

Narrow-Correlation technique: Code correlation technologies have been enhanced during the past few years. The most notable one is the development of the so-called narrow correlator, which improves the resolution of C/A code pseudo-ranges to the 10 centimetre level, compared with standard C/A code noise levels of 1-2 metres (Fenton et al., 1991). An example of such a receiver is the NovAtel family of instruments.

Squaring: Squaring, or auto-correlating L2, produces a half-wavelength carrier signal at twice the carrier frequency, resulting in a very low signal-to-noise ratio, approximately 30 dB lower than that obtained by correlation with the code (Counselman, 1987). A typical receiver was the Trimble 4000SST.

Code Correlation squaring: This technique involves correlating the L2 Y-code signal with a locally-generated replica of the underlying P-code, narrowing the bandwidth and subsequently squaring the signal (Hatch et al., 1992). This results in a half-wavelength carrier phase observable and a signal-to-noise 17dB lower than that obtained by correlating with the P-code. A typical receiver of this variety was the Leica SR299.

Cross-Correlation: This technique uses the fact that the unknown Y-code is identical on both L1 and L2 carriers, which enables cross correlation of the L1 and L2 signal. Because the velocity of Y-code on L2 is slightly slower than the Y-code on L1, the time delay necessary to match the L1 signal with the L2 signal in the receiver is a measure of the travel time difference of the two signals. The observables resulting from the

correlation process are the range difference between the two signals obtained from the time delay of the Y-Code on the two carriers and a beat frequency carrier (L2-L1). Consequently, two full wavelength carrier phase observables, Y-code pseudo-range difference between L2 and L1, and the C/A pseudo-range are available (Hofmann-Wellenhof et al., 1994; Leick, 1995). Cross correlating results in a signal-to-noise 27dB lower than that obtained by correlating with the P-code. Typical receivers are the Trimble 4000SSE, Rogue SNR 8000.

P-W tracking: This technique takes advantage of the fact that the Y-code is the modulo-2 sum of the P-code and the W-code, which is a substantially lower rate encryption code of 512 kHz. The L1 and L2 signals are correlated with locally generating P-codes, and the bandwidth is reduced to that of the encryption code. The encryption code is estimated and removed from the received signal to allow locally generated code replicas to be locked with the P-code signals of L1 and L2 (Ashjaee & Lorenz, 1992). Consequently, two full wavelength carrier phase observables, L1 and L2 Y-code pseudo-ranges and the C/A-code pseudo-range can be obtained. This technique results in a signal-to-noise 14dB lower than that obtained by correlating with the P-code directly. The typical receiver is the Ashtech Z12.

1.2.2 GPS Observables

Based on the available observations that can be made from civilian receivers, GPS receivers can be classified into five classes, as listed in Table 1-1 (Han & Rizos, 1996g). New generation GPS receivers such as the Ashtech Z12, Leica GPS SR399 and Trimble 4000SSi, provide precise pseudo-range and full wavelength L1 and L2 carrier phase observations, even under AS. GPS receivers such as the Rogue SNR 8000 and Trimble 4000SSE provide C/A pseudo-range, L1 and L2 carrier phase and the so-called "sixth observable": the difference between the P2 and P1 pseudo-ranges. Older generation GPS receivers output C/A pseudo-range, L1 carrier phase and half-wavelength L2 carrier phase (due to the use of the "squaring" technique). The single frequency GPS receiver outputs C/A pseudo-range and L1 carrier phase. GPS navigation receivers output C/A pseudo-range, though some of them provide L1 Doppler observations as well, or just coordinates in the WGS-84 datum.

The performance of the ambiguity resolution algorithm employed depends on the type of GPS receiver used. For short-range static or kinematic positioning, phase ambiguities can be resolved using a single epoch of data if receiver type 1 is used, a few minutes of

observations if receiver type 2 is used, about 10 minutes of observations if receiver type 3 is used, and more than 10 minutes of observations if receiver type 4 is used, assuming state-of-art algorithms are implemented (Han, 1996; 1994c). For long-range static or kinematic positioning, receiver types 1 and 2 are preferred (Han, 1995b; Han & Rizos, 1995d).

Table 1-1. GPS receiver classification scheme

No.	Types	Type of Observations available	Typical receivers
1	New generation receiver (precise pseudo-range available)	P1 (Y1), and/or P2 (Y2), and/or precise C/A pseudo-ranges, L1 and L2 carrier phase (and sometimes L1 and L2 Doppler)	Ashtech Z12, Leica SR 399, Trimble 4000SSi, and NovAtel Millennium
2	Dual-frequency receiver (cross-correlation type)	C/A pseudo-range, L1 and L2 carrier phase and the difference between the P2 and P1 pseudo-ranges	Rogue SNR 8000, Trimble 4000SSE
3	Dual frequency receivers (signal squaring type)	C/A pseudo-range, L1 carrier phase and half-wavelength L2 carrier phase	Leica SR 299 (WM102), Trimble 4000SST, etc.
4	Single frequency receivers	C/A pseudo-range and L1 carrier phase	Trimble 4000SE, WM101, Ashtech 3DF, GSS1, NovAtel, etc.
5	Navigation receiver	C/A pseudo-range, though some also provide L1 Doppler	Magnavox MX200, Magellan 1000, etc.

1.3 Modelling GPS Observations

1.3.1 Pseudo-Range Observation Equation

The basic pseudo-range observable is the difference between the time of transmission from a satellite (in the satellite time scale t) and the time of arrival at a receiver (in the receiver time scale T) of a particular signal. The mathematical expression is (e.g., Wells et al., 1987):

$$R = \rho + d\rho + c\cdot(dt - dT) + d_{ion} + d_{trop} + d_{mp}^{R} + \varepsilon_R \qquad (1\text{-}3)$$

where R: the pseudo-range observation
ρ: $= \left\|X^s - X\right\|$, X^s is the satellite position vector, X is the station position vector
$d\rho$: the effect of ephemeris errors, including S/A effects
dt: the satellite clock error with respect to GPS time, including S/A effects
dT: the receiver clock error with respect to GPS time
d_{ion}: the ionospheric delay on the pseudo-range
d_{trop}: the tropospheric delay
d_{mp}^{R}: the multipath on the pseudo-range
ε_R: the pseudo-range measurement noise

1.3.2 Carrier Phase Observation Equation

The basic carrier phase observable is a measure of the difference between the carrier signal generated by a receiver's internal oscillator and the carrier signal from the satellite. Although the observable is essentially the number of full carrier cycles, and the fractional cycle, between the antennas of the satellite and the receiver, the problem is that a GPS receiver has no way of distinguishing one carrier cycle from another. The best it can do is to measure the fractional phase and keep track of *changes* to the phase; hence the initial phase is undetermined, or ambiguous, by an integer number of cycles. To use the carrier phase as an observable for positioning this unknown number of cycles, or the phase ambiguity, must be estimated or accounted for in some way (Wells et al., 1987).

$$\phi = \rho + d\rho + c\cdot(dt - dT) + \lambda\cdot N - d_{ion} + d_{trop} + d_{mp}^{\phi} + \varepsilon_\phi \qquad (1\text{-}4)$$

where ϕ: the carrier phase observation in unit of metres
d_{mp}^{ϕ}: the multipath on the carrier phase
ε_ϕ: the carrier phase observation noise
λ: the wavelength of the carrier phase
N: the integer ambiguity

The other terms, ρ, $d\rho$, dt, dT, d_{ion} and d_{trop} are the same as in equation (1-3). Note that the ionospheric delay for carrier phase observations is the same magnitude as the ionospheric delay for pseudo-range, but has the opposite sign.

The data processing necessary to determine the value of the integer ambiguity is referred to as "Ambiguity Resolution". Ambiguity resolution without requiring a GPS receiver to remain stationary for any length of time is also referred to as Ambiguity Resolution On-The-Fly (OTF), and ambiguity resolution using a single epoch data is referred to here as Instantaneous Ambiguity Resolution.

1.4 GPS Positioning and Applications

1.4.1 Point Positioning

GPS point positioning, sometimes also called *absolute positioning*, employs one receiver to output position information in the World Geodetic System 1984 (WGS-84) datum (the system in which the satellite ephemeris is derived). Using one-way ranging data from four or more GPS satellites (that are also broadcasting their positions), four unknowns must be determined; typically, they are: latitude, longitude, altitude, and a correction to the receiver's clock. If altitude or time are already known, a lower number of satellites can be used. Carrier phase observations can be used to contribute to the velocity determination for kinematic applications, or improve the pointing accuracy for static point positioning. GPS point positioning is easy to implement for real-time applications such as navigation in the air, at sea, or on land.

Note that the ephemeris bias and satellite clock bias are ignored in the point positioning processing model. Therefore, if S/A is turned on the positioning accuracy is significantly reduced. DoD state that horizontal errors will be limited to less 100 m, 95% of time. Therefore, the applications using one GPS receiver in point positioning mode will be restricted to those with low accuracy requirements.

1.4.2 Relative Positioning

GPS *relative positioning* requires the determination of the coordinates of an unknown point with respect to a known (reference) point which, for most applications, is stationary. Relative positioning is most effective if simultaneous observations are made at both the reference and the unknown point because the differenced observable can be formed between two points and the biases due to imprecise ephemeris information (including the S/A ε – effect), satellite clock (including the S/A δ – effect), ionospheric and tropospheric delays, can be reduced, to an extent that is largely dependent on the

distance between the points. Hence, relative positioning, also refered to as *differential positioning*, yields positioning accuracy that is much higher than point positioning .

Pseudo-range-based DGPS

Differential GPS (DGPS) is a technique that significantly improves both the accuracy and the integrity of GPS. DGPS requires high quality GPS reference receivers at known surveyed locations. The reference station estimates the slowly varying error components of each satellite range measurement and generates a correction for each GPS satellite. This correction is broadcast to all DGPS users over some convenient communication link. With differential corrections, the SPS navigation accuracy can be improved to better than 1m, one sigma, provided the correction data age is less than 10 seconds, and the user is within 50 km of the reference station. As the correction data age, or the distance from the reference station increases, the accuracy of DGPS degrades. DGPS can still provide improvements greater than that of the PPS accuracy. DGPS using one reference station is suitable for operations over a small area, typically about 150 km across, and is often referred to as Local Area DGPS (LADGPS)

If a network of reference stations can be used to form a vector correction for each satellite, consisting of individual correction components for the satellite clock, three components of the satellite ephemeris, and parameters of an ionospheric delay model, the correction is valid over a much greater geographical area. This concept is generally referred to as Wide Area DGPS (WADGPS). The accuracy of WADGPS is almost independent on the geographical separation of the user from the nearest reference station, though the validity of the correction still decreases with an increase in latency, or age, of the correction data (Kee, 1996).

The Wide Area Augmentation System (WAAS) consists of geostationary satellites to augment GPS satellites and ground reference stations. Geostationary satellites provide a ranging signal that is GPS-like and which can be received by slightly modified GPS receivers, and therefore provides additional range measurements for the GPS user. The reference stations are widely dispersed data collection sites that receive and process signals received from the GPS and geostationary satellites, and forward their measurements to data processing sites, referred to as wide area master stations. The master stations process the raw data to determine integrity, differential corrections, residual errors, and ionospheric delay information for each monitored satellite. They also compute ephemeris and clock information for the geostationary satellites. All these data

are packed into the WAAS message, which is sent to Navigation Earth Stations (NES). The NES uplink this message to the geostationary satellites, which then broadcast the "GPS-like" signal. The WAAS therefore augments GPS with the following three services: a ranging function (which improves availability and reliability); differential GPS corrections (which improve accuracy); and integrity monitoring (which improves safety) (Enge & Ven Dierendonck, 1996).

The LADGPS, WADGPS and WAAS applications include land vehicle navigation and tracking, marine applications, air traffic control, aircraft automatic landing approach, etc.

Carrier phase-based DGPS

Carrier phase-based DGPS uses carrier phase observations for high precision positioning, and therefore involves an ambiguity resolution procedure. Carrier phase-based DGPS can be categorised according to applications or positioning mode:

Short-Range Vs. Long-Range: The short-range positioning mode generally refers to scenarios where the baseline length (between reference and user receiver) is short enough so that the residual ionospheric delay and orbit biases in single-differenced observations between receivers can be ignored. Typically this is of the order of about 15km, but very dependent on the variability of the ionosphere and the amplitude of orbit biases. Hence the *constraint* introduced by the ionospheric delay and orbit biases in the cases of medium-range (up to 100 km) and long-range (up to many hundreds of kilometres) applications cannot be neglected, as is done for the short-range case.

Static Positioning Vs. Kinematic Positioning: For static positioning a GPS receiver can collect at least two epochs of data at a survey mark and only three coordinate parameters will be contained in the observation equation(s). However, in the case of kinematic positioning, the antenna is not stationary, and hence the number of coordinate parameters will be three times the number of observation epochs.

Real-Time Processing Vs. Post-Processing: Real-time processing requires the use of a causal filter, such as a Kalman filter, or sequential least squares. In the case of post-processing there is no such requirement. Theoretically, a non-causal filter will result in better accuracy than a causal filter. In general, the transmission latency for real-time applications is a very restrictive specification.

Attitude Determination: Attitude determination is an important GPS application, requiring the use of multiple GPS antennas and/or receivers, with the receiver(s) typically in motion. It is possible to use external information such as known (inter-antenna) baseline lengths, fixed antenna configurations and perhaps independent attitude-related information from external non-GPS sensors (Lu, 1995). There are two ways to specify the reference receiver for relative positioning of the GPS array: the reference receiver maybe static or in motion as well.

Applications of carrier phase-based DGPS include precision landing of aircraft using integrity beacons, spacecraft attitude control using GPS carrier phase data, GPS surveying, attitude determination, orbit determination, definition and maintenance of earth-centred, earth-fixed Cartesian coordinate systems such as the International Terrestrial Reference Frame (ITRF).

1.5 Motivation

Differential GPS navigation generally refers to the pseudo-range based systems, such as Wide Area Differential GPS (WADGPS) or Wide Area Augmentation Systems (WAAS), which are designed to deliver accuracies at the few metre level. WADGPS or WAAS requires a network of master/monitor stations spread over a wide area. Because the biases will be modelled and corrected, the positioning accuracy will be almost independent of baseline length. Carrier phase observations in these systems will generally be used to smooth the pseudo-range data (Feng & Han, 1996; Feng et al., 1996). However, for some applications requiring decimetre or sub-decimetre accuracy, carrier phase-based techniques for medium-range and long-range GPS kinematic positioning, in post processed or real-time mode, will be necessary.

The adoption of GPS kinematic positioning techniques has been growing rapidly for precise marine and airborne applications. However, there is a significant challenge when the GPS reference receiver(s) cannot be set up near the survey area, such as out on the continental shelf areas, and in remote and inaccessible land areas such as Antarctica, Australia's outback, Central Asia, Siberia, Greenland, etc. The distance from the fixed reference receiver(s) to the mobile user receiver(s) may range from tens to many hundreds of kilometres, yet the accuracy requirement may be at the decimetre level or higher. Once Wide Area DGPS systems or Wide Area Augmentation Systems are established and the appropriate data is transmitted, GPS carrier phase-based medium-

range or long-range kinematic positioning techniques may allow a user (with a single GPS receiver) to precisely position a moving receiver, even in real-time. Therefore, carrier phase-based long-range GPS kinematic positioning increasingly becomes a useful topic.

1.6 Previous Research on Carrier Phase-Based Long-Range GPS Kinematic Positioning

1.6.1 Error Mitigation for the Long-Range Case

The main problem in carrier phase long-range kinematic positioning is *error mitigation*. There are many on-the-fly ambiguity resolution techniques which are applicable for short-range GPS kinematic positioning, but all are based on the assumption that the orbit bias and ionospheric delay for double-differenced observations can be neglected. For long-range GPS kinematic positioning however, orbit bias and ionospheric delay cannot be ignored, and on-the-fly ambiguity resolution becomes a much more difficult problem to overcome.

The orbit bias is a baseline length dependent bias which must be reduced before implementing any ambiguity resolution procedure for long-range positioning. The precise ephemeris from the International GPS Service for Geodynamics (IGS) can be used, but there is a 10 day delay if 10cm accuracy is required, or a one day delay if 25cm accuracy is acceptable (Neilan, 1996). Colombo et al. (1995) proposed a two-step Kalman filter procedure to reduce the effect of orbit bias. The first step is to estimate the orbit bias using compressed observation data, and the second step is to hold fixed the corrected ephemeris while estimating the mobile receiver's trajectory on an epoch-by-epoch basis. This method is very difficult to implement in real-time. An alternative approach is to use reference station GPS data, the parameters of an appropriate error model which describes the distance dependent errors, including orbit bias, can be estimated and then disseminated to users in real-time (Wübbena et al., 1996). Wu (1994) has suggested that the linear combination of single-differenced observations between different reference stations and the mobile receiver can reduce the orbit bias. Han & Rizos (1996e) have proposed this method to reduce the effect of orbit bias for long-range ambiguity resolution. This method requires: (a) two reference receivers if the mobile receiver is on a line joining the two reference receivers; (b) three reference receivers if the mobile receiver is on the plane defined by the three reference receivers,

or; (c) four reference receivers if the mobile receiver is arbitrarily located. If more than four reference receivers are available, linear coefficient parameters can be determined which make the standard deviation of the linear combination of single-differenced observations a minimum.

Reference stations are sites with known coordinates, which typically are equipped with dual-frequency GPS receivers. The data from reference receivers should be processed in real-time in order to estimate the integer ambiguity set, and subsequently for ionospheric delay model determination. The initial ambiguity set for dual-frequency data should be determined when the system is first set up, and then real-time ambiguity recovery techniques (Blewitt, 1990; Han, 1995b) should be employed to maintain ambiguity continuity. The ionospheric delay value on the L1 carrier phase can be determined relative to the reference station, and the reference satellite, at each epoch. This is the so-called local epoch-by-epoch and satellite-by-satellite ionospheric delay model (Webster & Kleusberg, 1992; Wanninger, 1995).

1.6.2 Current Research on Ambiguity Resolution

The carrier phase observable has much higher measurement precision than the pseudo-range, and has been widely used in high accuracy static and kinematic positioning. Ambiguity resolution (AR) is therefore crucial and becoming increasingly important as GPS applications grow. The simplest AR method is to round off the estimated real-valued ambiguities to the nearest integer, but only if the real-valued ambiguity estimates are good enough. Typically this requires an observation span of at least 0.5 to 1 hour for short baselines (less than 15km), hence making high precision GPS positioning relatively inefficient. However a variety of AR techniques have been developed in the last decade. Generally speaking, there are five different kinds of AR techniques: (1) ambiguity resolution through a special operational mode, such as antenna swap, re-occupation, or "stop & go"; (2) ambiguity resolution using the pseudo-range data directly, in which use is made of linear combinations of L1 and L2 carrier phase with longer wavelength, and linear combinations of L1 and L2 P-code pseudo-ranges with lower noise; (3) AR through a search in the "coordinate domain", requiring the use of accurate initial coordinates, such as the Ambiguity Function Method; (4) AR through a search in the "estimated ambiguity domain", through first estimating ambiguities as real-valued parameters, and then determining the integer ambiguity through an integer least squares estimation process, and; (5) the integrated technique which uses other physical sensors to aid GPS ambiguity resolution.

Antenna swap and re-occupation modes are only suitable for short-range or static positioning. The "stop & go" mode can be used for long-range kinematic positioning, but it requires initialisation at the beginning of a survey session, and re-initialisation if cycle slips occur during the period the antenna is in motion.

The search technique in the measurement domain determines the L1 and L2 whole-cycle ambiguities with the aid of P-code pseudo-range data on L1 and L2, and was first suggested by Hatch (1986). However, it requires a comparatively long time to resolve the ambiguities due to the short wavelengths of the L1 and L2 carrier waves. Subsequently, Wübbena (1989), Dong & Bock (1989), Blewitt (1989), Abidin & Wells (1990) and Goad (1992) proposed the use of P-code pseudo-range data on L1 and L2 to determine the integer ambiguities of the widelane observations. The main advantage is that the ambiguities of widelane phase observables are easily determined, and largely independent of the baseline length. But for precise positioning the L1, L2 or ionosphere-free observations are used, not widelane observations. Hence the integer ambiguities of other independent combined observations should be resolved in order to determine the ambiguities for the L1 and L2 observations. The extra-widelaning technique (Wübbena, 1989) uses the widelane, narrowlane and the ionospheric signal phase combinations to determine the integer ambiguity of the widelane and narrowlane observations, aided by P-code pseudo-ranges on L1 and L2, for static positioning. Abidin & Wells (1990) also use this technique for kinematic positioning. Because the ionospheric effect dramatically increases with increasing baseline length, it is difficult to determine the integer ambiguities of the narrowlane carrier phase observation for long baselines. However, Dong & Bock (1989), Blewitt (1989) and Goad (1992) have used this technique to determine the integer ambiguity of the widelane carrier phase observable using dual-frequency precise pseudo-range data for long-range static baselines first, and then the ionosphere-free combination with L1 ambiguities and the known widelane ambiguity are used to compute the coordinates of the static site and the L1 ambiguities. In this way, the ionosphere-free combination can be processed with free ambiguity parameters, and the real-valued ambiguities can be obtained. Because a bias of 10.7cm in the real-valued ambiguities will cause a 1 cycle bias in the L1 ambiguities, the second step requires a relatively long static observation period to obtain high precision real-valued ambiguity estimates (less than a quarter of 10.7cm). Hence, the L1 ambiguity is not easy to determine for the long-range kinematic positioning mode (see Appendix B).

The search techniques in the coordinate domain, which are particularly suitable when good initial estimates of the coordinates are available, mainly use the Ambiguity Function Method (AFM) suggested by Counselman & Gourevitch (1981) and Remondi (1984). Mader (1992) proposed the ionospheric correction technique within the AFM using a trial suite of integers. Han (1993) suggested an integrated technique where the search region for the AFM is defined by the predicted position, and uncertainty, output by the Kalman filter used for kinematic position processing. A highly efficient computation procedure for the AFM using dual-frequency carrier phase observations was described by Han & Rizos (1996b). However, the ionospheric effect is the main obstacle for long-range kinematic applications, even if the precise ephemeris can be obtained, or the orbit biases estimated.

The search technique in the estimated ambiguity domain, using integer least squares estimation, is the most important technique for short-range applications, including for kinematic and rapid static positioning (Han, 1995c). Many practical searching procedures based on integer least squares estimation have been suggested, such as: Fast Ambiguity Resolution Approach (FARA) (Frei & Beutler, 1990); Cholesky Decomposition method (Landau & Euler, 1992); Spectral Decomposition method (Abidin, 1993); Least Squares Ambiguity Search Technique (Hatch, 1990); Fast Ambiguity Search Filter (FASF) (Chen, 1993), and; Least-squares AMBiguity Decorrelation Adjustment (LAMBDA) (Teunissen, 1994). The main reason these procedures are restricted to short-range applications are the orbit bias and ionospheric delay. For long-range applications, the ionosphere-free combination observable and the integer ambiguity should be searched, if the widelane ambiguity is fixed. However, the short wavelength will result in a large search region, and hence the searching will be difficult for long-range applications.

The integrated technique, such as using a combination GPS/INS, uses GPS observations with the addition of other physical sensors to aid ambiguity resolution. The physical sensors can provide *relative* information, and have no *absolute* information (Schwarz et al., 1994). Therefore this technique is suitable for cycle slip repair, even in the kinematic case, but makes no contribution to *initial* ambiguity resolution. If the initial ambiguities can be resolved by an initialization procedure, this technique is quite useful for long-range kinematic positioning. The main disadvantage is that the accurate physical sensor is usually very expensive.

The concept of using multiple reference stations, similar to the WADGPS system, has been proposed by several investigators, but few details have been presented (Han & Rizos, 1996e; Wübbena et al., 1996). Although the bias modelling using multiple reference stations has been developed for WADGPS (Kee, 1996), for the pseudo-range-based system, the accuracy is not good enough for ambiguity resolution. Though this concept can be used for carrier phase-based systems, the accuracy of the corrected observations will be degraded. A more efficient algorithm is needed for carrier phase-based long-range kinematic positioning.

1.7 Methodology

Current GPS research has concentrated on ambiguity resolution on-the-fly for short-range kinematic positioning on the one hand, and long-range static positioning on the other. *Ambiguity resolution on-the-fly for long-range kinematic positioning* is therefore a significant challenge. Carrier phase-based long-range GPS kinematic positioning requires that the integer ambiguity set be fixed and all biases, especially the baseline length-dependent biases, be reduced. In order to tackle this challenge, all ambiguity resolution techniques, and bias elimination and mitigation methods have been investigated and compared. Based on these current techniques, and some new innovations to these developed by the author, three techniques are suggested for achieving centimetre, or sub-decimetre, accuracy for long-range kinematic positioning in the data post-processing or real-time processing modes.

The first suggested technique is to resolve integer ambiguity directly using multiple reference stations. Although this idea is suggested by research into WADGPS or WAAS, the current bias mitigation procedure is not accurate enough, and a new method need to be developed. Based on the method suggested by Wu (1994) and Han & Rizos (1996e), the linear combination of the single-differenced observations between the roving receiver and every reference stations will eliminate orbit bias. The ionospheric delay can be interpolated by using the epoch-by-epoch and satellite-by-satellite model within a medium-sized area. An impressive result that was obtained is that the linear combination suggested for elimination of the orbit bias, can also *eliminate* ionospheric delay, and *reduce* tropospheric delay, multipath and observation noise. The functional model, which is very similar to the short-range kinematic positioning functional model, has been developed. An integrated method, with improvements to the real-time stochastic model, new criteria to verify the correct ambiguity set, and a fault detection and adaptive

procedure, is proposed for use with this functional model. Instantaneous ambiguity resolution or AR on-the-fly is possible.

The second suggested technique is to resolve cycle slips and recover integer ambiguity, using a search procedure in the observation domain. However what is resolved is the "relative" ambiguity, rather than the "absolute" ambiguity. This method uses full wavelength carrier phase, and precise pseudo-range observations on L1 and L2. The orbit bias, receiver and satellite clock biases can be eliminated, and the ionospheric delay can be predicted from the previous data epochs for which it is assumed that the integer ambiguity has been resolved. It is found that the widelane (0.86 m) and $\varphi_{-7,9}$ (wavelength 14.65 m) combinations are best for cycle slip candidate determination. Validation criteria for the search procedures in the estimated ambiguity domain, and in the coordinate domain, can be used here to verify the correct cycle slip set. If precise pseudo-range observations are not available, the AFM with Kalman filtering is used for cycle slip detection and repair.

If the ambiguity set is fixed, but to the incorrect integer ambiguity values, the baseline from the reference receiver to roving receiver will be biased. The baseline biases are almost linear with time if the ambiguity bias is constant (that is, no cycle slips). From this error behaviour, the third suggested technique is developed for trajectory determination *relative to itself*. If a user receiver, which is far away from the reference receiver, moves around and back to the starting point at the end of a session, the trajectory can be corrected using the misclosure differences. The corrected trajectory will be of sub-decimetre accuracy relative to the trajectory itself, although a few metre bias may result relative to the reference station. This technique can be used for GIS database generation, profile surveying, or other surveying within a smaller area, and where the user simply uses a single receiver and the nearest permanent GPS base station is within a few hundreds of kilometres of the user.

1.8 Outline of the Thesis

This thesis consists of seven chapters and two appendices.

Chapter 1 gives some of the GPS background, state-of-the-art receiver techniques, and typical applications. After the research motivation on carrier phase-based long-range

GPS kinematic positioning is presented, and previous achievements discussed, the methodology and contributions of this research work are outlined.

Chapter 2 reviews and compares all current ambiguity resolution techniques. The four general classes have been classified and reviewed. The search procedures in the observation domain, in the coordinate domain and in the estimated ambiguity domain are related by using the integer least squares estimation technique. A new method to compute the transformation matrix for the LAMBDA method is suggested. The physical correlation and its effect on ambiguity resolution is also discussed.

Chapter 3 describes the orbit bias elimination and the ionospheric delay elimination procedures for medium-range or long-range kinematic positioning. The tropospheric delay correction methods are reviewed. The multipath characteristics have been analysed and a FIR filtering method is suggested to extract and mitigate multipath bias.

Chapter 4 presents a new technique for ambiguity resolution on-the-fly, for medium-range GPS kinematic positioning. The functional model is suggested, in which orbit bias and ionospheric delay have been eliminated and the tropospheric delay, multipath and observation noise have been reduced. A three-step quality control method is then developed to enhance the reliability of ambiguity resolution, which includes real-time improvement of the stochastic model, new criteria to verify the correct ambiguity set, and a fault detection and adaptive procedure. Short-range and medium-range experiments are described.

Chapter 5 presents an ambiguity *recovery* technique for long-range GPS kinematic positioning, which includes cycle slip detection and repair, with and without precise pseudo-range data. The implementation procedure and experiments using this technique are described.

Chapter 6 presents a long-range kinematic positioning algorithm which is biased relative to the reference station, but the trajectory of the user's roving receiver has sub-decimetre accuracy relative to the trajectory itself.

Chapter 7 summarises findings, draws conclusions, and makes recommendation topics for future investigations. Some points related to real-time positioning, limitations, prospects and potential of carrier phase-based long-range GPS kinematic positioning are also presented.

Appendix A derives the ionosphere interpolation formula using the epoch-by-epoch and satellite-by-satellite model, based on the ground Gauss plane coordinate system, from the interpolation based on the intersection point position between the line from the satellite to receiver and the single ionosphere layer. This derivation illustrates how the ionospheric delay term is eliminated in the functional model, using the multiple reference stations method described in Chapter 4.

Appendix B summarises the ambiguity resolution techniques for long-range static positioning, which can be used for data processing between reference stations, or for ambiguity initialisation.

1.9. Contributions of the Research

The three techniques that deal with ambiguity resolution and bias mitigation for carrier phase-based long-range GPS kinematic positioning are the most significant contributions of this research. In addition, the three-step quality control method, improvements to the fast ambiguity search technique using the LAMBDA method, and the new computation procedure for the transformation matrix which can be used for short-range kinematic or rapid static positioning, are also important new findings. A multipath extraction and mitigation method, and some other innovations which are not restricted to long-range methods, are also described. The contributions of this research can therefore be summarised as follows:

- The functional model using multiple reference stations has been developed, in which the orbit bias and ionospheric delay are eliminated, and the tropospheric delay, multipath and observation noise are reduced, for medium-range GPS kinematic positioning.

- The ambiguity recovery technique has been developed for long-range GPS kinematic positioning, using the widelane and $\varphi_{-7,9}$ combinations if the precise pseudo-range observations are available, or using the AFM and Kalman filtering if the precise pseudo-range observations are not available.

- A method of determining a trajectory with sub-decimetre accuracy relative to the trajectory itself, rather than relative to the reference station, has been developed, which makes use of the nearly linear behaviour of the baseline bias caused by fixing

the wrong integer ambiguity set. This technique allows single receiver positioning with the aid of a permanent GPS receiver which may be located hundreds of kilometres away.

- A three-step quality control method has been developed which can be used with the suggested functional model, using multiple reference stations, for medium-range GPS kinematic positioning, but which can also used with a single reference station for short-range GPS kinematic positioning.

- A new method of constructing the multi-satellite ambiguity combination has been suggested, which provides an easy way to obtain the LAMBDA transformation matrix. A comparison of the current ambiguity resolution techniques in the original ambiguity domain and the transformed ambiguity domain has been made, which will be helpful for future research on ambiguity resolution techniques.

- Multipath characteristics in the frequency domain have been investigated, and a Finite Impulse Response (FIR) filter suggested for extracting and eliminating multipath.

- Formulae for ionospheric delay interpolation from an ionosphere single layer to the ground Gauss plane coordinate system have been derived. This will significantly reduce computation effort, and can be used for other applications.

Chapter 2

A STUDY OF AMBIGUITY RESOLUTION TECHNIQUES

2.1 Introduction

Ambiguity resolution is the mathematical process of converting ambiguous ranges (integrated carrier phase) to unambiguous ranges of millimetre measurement precision (Rizos, 1996).

It is very difficult, if not impossible, to determine integer ambiguity for one-way data because it is indistinguishable from other, non-integer, biases such as satellite orbit uncertainties, multipath and atmospheric refraction (ionosphere and troposphere), and is in fact "contaminated" by them. Thus, ambiguity resolution, as it is generally known, is only possible after all biases are eliminated or otherwise accounted for to better than half a cycle of the carrier phase wavelength.

2.1.1 Double-Differenced Carrier Phase Observations

The commonly used method to eliminate non-integer biases is by double-differencing data between satellites and between receivers. The double-differenced observation equation can be derived from equation (1-4):

$$\Delta\nabla\phi = \Delta\nabla\rho + \Delta\nabla d\rho + \lambda \cdot \Delta\nabla N - \Delta\nabla d_{ion} + \Delta\nabla d_{trop} + \Delta\nabla d^{\phi}_{mp} + \varepsilon_{\Delta\nabla\phi} \qquad (2\text{-}1)$$

where $\Delta\nabla$ is the double-differencing operator. From the equation above it is obvious that the satellite clock bias and receiver clock bias have been eliminated. Furthermore, the other biases (orbit bias, ionospheric delay and tropospheric delay, $\Delta\nabla d\rho - \Delta\nabla d_{ion} + \Delta\nabla d_{trop}$) will be reduced, but the degree to which this occurs is

dependent on the distance between the two receivers, and normally the total magnitude of these biases will be less than half a wavelength if the separation between receivers is less than 15km. The double- differencing operator cannot reduce the multipath effect, and most probably increases it compared with the one-way observation. The noise standard deviation of the double-differenced observation will be twice that of the one-way observation. The double-differenced ambiguity remains an integer, and can be determined in some way.

The non-differenced method (e.g. Goad, 1985) or centralized method (Shi & Han, 1992) use carrier phase observations in the non-differenced mode, but define the ambiguities in the double-differenced form in order to make use of their integer characteristic. The equivalence of the methods has been proven in Han (1991).

Although the initial integer ambiguity is unknown, the GPS receiver can keep track of the *changes* to the carrier phase from one epoch to the next if the signal is tracked continuously. Therefore, the integer ambiguity should be the same over a session of tracking if the receiver is locked onto the signal. The triple-differenced observation method implements a differencing operator between epochs, on the double-differenced carrier phase, and results in the integer ambiguity term being eliminated.

2.1.2 Geometric Constraints

An ambiguity resolution procedure should make use of all possible constraints provided by the observations. The main geometric constraints can be categorised as follows (Han & Rizos, 1996g):

Integer Constraint: In theory, the initial ambiguities of the carrier phase observations on L1 and L2 should be integers, and this constraint will play a significant role in the ambiguity resolution process of fixing the ambiguities to known values. In practice many sources of systematic error will bias the observations. If the biases cannot be reduced to a level that is insignificant, relative to the wavelengths of the L1 and L2 carrier phase, the ambiguities cannot be fixed reliably to the correct integer values.

Short-Range Constraint: The ionospheric delay, tropospheric delay and orbital biases can be neglected in double-differenced carrier phase observations as far as the ambiguity resolution process is concerned. This constraint will make the observation equation

much simpler than in the long-range case, and ambiguity resolution will therefore be much easier.

L1 and L2 Carrier Phase Constraint: If the ionospheric delay, multipath and observation noise can be neglected, the L1 and L2 carrier phase observations and the pseudo-range observations are subject to the same bias effects. This constraint has the effect of resulting in a set of dual-frequency observations with only half the number of ambiguities. If the ionospheric delay, multipath and observation noise cannot be neglected, the L1 and L2 carrier phase have very strong correlations, and this correlation may be useful for ambiguity resolution (Frei & Beutler, 1990). The use of this constraint can be applied through the least squares system directly, through linear combinations of dual-frequency carrier phase observations outside of the least squares adjustment system, or via a LAMBDA transformation within the least squares system (Teunissen, 1996a; 1996b).

Instantaneous Satellite Geometry Constraint: The instantaneous satellite geometry has generally been measured by such factors as GDOP, PDOP, etc. These measures were first suggested for point positioning using pseudo-range data. If the reference receiver has known coordinates in the WGS-84 datum, these measures will also be suitable for describing the quality of the instantaneous satellite geometry in the case of relative positioning, as well as for carrier phase observations if the integer ambiguities are determined (or "resolved"). In the case of the ambiguity resolution process itself, these measures will reflect the geometric condition in a different way depending upon the ambiguity resolution technique being used.

Satellite Change Geometry Constraint: If all the satellite positions were not to change, the integer ambiguity resolution process, using carrier phase observations alone, will be impossible to carry out unless very accurate *a priori* receiver and satellite coordinates are available (typically, better than 5cm). Fortunately, the satellite positions change with time and the Doppler observations can be characterised by the *difference* in the distances from receiver to the satellite between epochs. This information can be used for positioning, as in the case of the Transit Doppler System, as well as for the ambiguity resolution process. This constraint will become stronger if longer spans of data are available. BDOP1 defined in Merminod (1990) is one such indicator of satellite change geometry.

2.2 Ambiguity Resolution Techniques

The simplest procedures to account for the ambiguities are to either use triple-differenced observations to remove the ambiguity terms from the observation equation, or to process the double-differenced phase observations with the ambiguities as real-valued estimable parameters (the solution is often referred to as an "ambiguity-free" or "bias-float" solution). Due to the application of only the *satellite change geometry constraint* in these two procedures, the potential accuracy of the carrier phase observations is not fully exploited. The earliest method used to determine the integer ambiguities required the estimated real-valued ambiguities to be "rounded-off" to the nearest integer, but was attempted only if the real-valued ambiguity estimates were precise enough. Typically this required an observation span of at least 0.5 to 1 hour for short baselines (less than 15km), which resulted in GPS high precision positioning being relatively inefficient for most applications, apart from the establishment of first order geodetic control networks. To overcome this inefficiency different AR techniques have been developed over the last decade. Generally speaking, the following classes of AR techniques can be identified, with the exception of the aforementioned triple-differenced solution or double-differenced float solution:

- AR through the use special operational modes, such as antenna swap initialisation, re-occupation and "stop & go" procedures.
- AR using the pseudo-range data directly, in which use is made of linear combinations of L1 and L2 carrier phase (with longer wavelength), and linear combinations of L1 and L2 P-code pseudo-ranges (with lower noise).
- AR through a search in the "Coordinate Domain", such as in the case of the Ambiguity Function Method.
- AR through a search in the "Estimated Ambiguity Domain", by first estimating the ambiguities as real-valued parameters, and then determining the likeliest integer ambiguities through an integer least squares estimation process.

Each of these classes of AR techniques are briefly discussed in the following sub-sections.

2.2.1 Operational Mode

Antenna Swap: The "antenna swap" or "antenna exchange" technique is performed as follows. Place GPS Antenna 1 on Mark A and GPS Antenna 2 on Mark B, several metres apart. When tracking is acquired on at least four satellites (five or more are recommended) move Antenna 1 to Mark B and Antenna 2 to Mark A, taking care that there is no loss of carrier phase tracking (ie., no cycle slips). One can, within seconds, measure the vector between the two unknown points to an accuracy of a couple of millimetres. In this way, the integer ambiguity can be effectively eliminated from the observation equation. This procedure uses the *instantaneous satellite geometry constraint* and the *short-range constraint*. It is not necessary to use *the integer constraint, L1 & L2 carrier phase constraint* or the *satellite change geometry constraint*. GPS receiver types 1-4 are suitable for this operation (Table 1-1). Due to the constraint of requiring the maintenance of satellite signal lock during the exchange of antennas, this technique is mostly used for static ambiguity initialisation for "stop & go" and kinematic surveys (Remondi, 1988).

Stop & Go: If a GPS receiver can maintain lock on the satellite signal, the integer ambiguity does not change, even while the antenna is moving. If the integer ambiguity has been determined at a site, the integer ambiguity will be same at any other site, as long as satellite signal lock has been maintained. The integer ambiguity at the first site can be determined using the antenna swap technique, or any other AR method. *The integer constraint, instantaneous satellite geometry constraint* and the *short-range constraint* are used in this procedure. It is not necessary to use the *L1 & L2 carrier phase constraint* or the *satellite change geometry constraint*. GPS receiver types 1-4 are suitable for this operation (Table 1-1). This technique is efficient for GPS surveys if lock on the satellite signal is easy to maintain during the surveying. The trajectory of the antenna is also determined to a high accuracy if used in the kinematic positioning mode (Ibid, 1988).

Re-occupation: Reliable real-valued ambiguity estimation requires about one hour of observations. The reason for this has been known for many years: what is important is that the receiver-satellite geometry *changes*, not because of the need to suppress the observation noise. So the question naturally arose: "Can anything be done while we are waiting for the receiver-satellite geometry to change?" and "Can we visit other nearby survey marks while we are waiting for the geometry to change?". The answer to both

questions is "YES", and this mode is now referred to as re-occupation or "pseudo-kinematic". This mode requires that each baseline should be occupied at least twice and the interval between occupations should be of the order of a half to one hour (Ibid, 1988). The *integer, short-range* and *satellite change geometry constraints* will be most important for ambiguity resolution. It is not necessary to use the *L1 & L2 carrier phase* or the *instantaneous satellite geometry constraints*. GPS receiver types 1-4 are suitable for this operation (Table 1-1). The operation is normally applied for post-processed, short-range, static positioning.

2.2.2 Search in the Observation Domain

The ambiguities can be determined using pseudo-range and carrier phase data directly. Unfortunately the accuracy of the C/A or P-code pseudo-ranges is not good enough, on their own, to determine the integer ambiguities because the wavelength of the carrier phase observable is only 19.03cm for L1 and 24.42cm for L2. Therefore, integer linear combinations of the L1 and L2 observations which have a relatively long wavelength, low noise behaviour and a reasonably small ionospheric delay, such as the "widelane" ($\phi_1 - \phi_2$, with wavelength 0.86m), "narrowlane" ($\phi_1 + \phi_2$, with wavelength 0.11m) or "extra-widelane" ($-3\cdot\phi_1 + 4\cdot\phi_4$, with wavelength 1.63m), and the longest wavelength combination ($-7\cdot\phi_1 + 9\cdot\phi_2$, with wavelength 14.65m), are used. If the baseline is short enough, the differential ionospheric delay can be ignored and the P-code pseudo-ranges can be used to determine the initial integer ambiguity of the combined observable, and then used to decouple the integer ambiguity of L1 and L2 carrier phase. Some useful linear combination observables are listed in Table 2-1 (Han & Rizos, 1996b). f and λ are frequency and wavelength of the carrier phase combination $i\cdot\phi_1 + j\cdot\phi_2$; α_i, α_ϕ, α_L are the ratio values of the ionospheric delay, noise in cycle and noise in metres, of the carrier phase combination with respect to the L1 carrier phase observation, respectively.

For the many applications, the baseline is not short enough to neglect the differential ionospheric delay and the ionosphere-free combination has been used (Blewitt, 1989):

$$\Delta\nabla N_{1,-1} = \Delta\nabla\phi_1 - \Delta\nabla\phi_2 - \frac{f_1 - f_2}{f_1 + f_2}\left(\frac{\Delta\nabla R_1}{\lambda_1} + \frac{\Delta\nabla R_2}{\lambda_2}\right) \qquad (2\text{-}2)$$

where $\Delta\nabla$ is the double-differencing operator; ϕ_1, ϕ_2, R_1, R_2 and $N_{1,-1}$ are the L1 and L2 carrier phase, L1 and L2 pseudo-ranges, and the widelane integer ambiguity, respectively. This technique uses the *integer constraint*, the *L1 & L2 constraint* and requires precise pseudo-range observations on L1 and L2. GPS receiver type 1 is required (Table 1-1). This technique can be used for widelane ambiguity determination in the post-processed, long-range, static positioning case. The ionosphere-free combination will be used to determine a 10.7cm wavelength integer ambiguity, making use of the *instantaneous satellite geometry* and the *satellite change geometry constraints*. This requires a relatively long observation session, perhaps two or three hours. The orbit bias should be considered during data processing, or a precise ephemeris may be used instead. The accuracy can reach the 0.01 ppm level, if the observation time for each baseline is over several days.

Table 2-1. Characteristics of certain dual-frequency combinations (full- & half-wavelength L2)

i	j	f (MHz)	λ (m)	α_i	L2 full-wavelength		L2 half-wavelength	
					α_ϕ	α_L	α_ϕ	α_L
1	0	1575.42	0.1903	1.0000	1.0000	1.0000	-	-
0	1	1227.60	0.2442	1.6469	1.0000	1.2833	-	-
0	2	2455.20	0.1221	1.6469	2.0000	1.2833	1.0000	0.6417
77	-60	47651.34	0.0063	0.0000	97.6166	3.2273	82.6378	2.7321
1	-1	347.82	0.8619	-1.2833	1.4142	6.4056	-	-
1	1	2803.02	0.1070	1.2833	1.4142	0.7948	-	-
-1	2	879.78	0.3408	2.8054	2.2361	4.0041	1.4142	2.5324
2	-2	695.64	0.4310	-1.2833	2.8284	6.4056	2.2361	5.0640
-3	4	184.14	1.6281	18.2518	5.0000	42.7778	3.6056	30.8475
-7	9	20.46	14.6526	350.3500	11.4018	877.9350	-	-

2.2.3 Search in the Coordinate Domain

If the initial coordinate estimate is accurate enough, the integer ambiguity can be computed using these initial coordinates. This means that if the initial coordinate is a good approximate, the integer ambiguity can be determined using only one epoch, or

perhaps a few epochs, of data. For some applications, such as a deformation survey, this method is quite useful. After the integer ambiguity set is determined, the high precision baseline can be estimated.

However, if the initial coordinate bias is a few decimetres, the integer ambiguity cannot be determined using the coordinates directly. Alternatively, a search procedure in the coordinate domain can be applied. The commonly used method is known as the Ambiguity Function Method (AFM). The ambiguity function is defined as (Remondi, 1984):

$$AF(X) = \sum_{k=1}^{m}\sum_{l=1}^{n}\left|\sum_{j=1}^{m_{kl}} \exp\left(\vec{i}\left(\Delta\phi_{obs}^{jl}(k) - \Delta\phi_{calc}^{jl}(k,X)\right)\right)\right| \tag{2-3}$$

where $\Delta\phi_{obs}^{jl}(k)$ and $\Delta\phi_{calc}^{jl}(k,X)$ are the single-differenced carrier phase observables between receivers and its computation value using the trial baseline vector X with respect to satellite j, frequency l and epoch k. m_{kl} is the number of single-differenced carrier phase observations, while m and n are the number of epochs and frequencies, respectively. Different trial baseline vector X results in a different ambiguity function value. The search seeks to find the baseline vector $\hat{X}$ which causes the ambiguity function value to be a maximum. It can be shown that the ambiguity function value is not affected by the magnitude of the integer ambiguities and cycle slips (Ibid, 1984).

It is preferable to use the linear combination observables in Table 2-1 in the implementation of the AFM (Han & Rizos, 1996b). All combination observables have the same geometric configuration. They have the same distribution of AF maxima, and the distance between these maxima are proportional to their wavelength. The distance between these maxima depends on the satellite geometry, including the instantaneous satellite geometry and satellite change geometry. If the GDOP is bigger for the same number of satellites, the distance between these maxima will be larger, but the positioning accuracy will be lower. This technique uses all the constraints, but the *satellite geometry constraint* is applied in only a weak form because only the fraction of the carrier phase observation is used, not the integer cycle part incremented between epochs. The advantage is that this technique is insensitive to the size of the integer ambiguities or the presence of cycle slips. However, the disadvantage is that the *satellite geometry constraint* is weak. GPS receiver types 1-4 are suitable for this technique

(Table 1-1). The most common application is for post-processed, short-range, static positioning, or other applications in a modified form.

2.2.4 Search in the Estimated Ambiguity Domain

There are two steps within the search procedure. The first step is to obtain the "float" solution, where the ambiguities are obtained from a least squares estimation process: the real-valued ambiguity estimate $\hat{X}_N$ and its co-factor matrix $Q_{\hat{X}_N}$. The second step is to search for the integer ambiguity set which satisfies the following relation:

$$R_k = \left(\hat{X}_N - N_k\right)^T Q_{\hat{X}_N}^{-1} \left(\hat{X}_N - N_k\right) = \min \tag{2-4}$$

The derivation of the above relation, and also the validation criteria derived from it, is presented in Section 2.3.

Several fast ambiguity search methods have been suggested based on the above relation. On the other hand, the transformed form of the integer ambiguities has been introduced in order to reduce the computation, in the so-called Least-squares AMBiguity Decorrelation Adjustment (LAMBDA) method. This will be discussed further in Section 2.4.

This technique uses all the constraints for short-range applications. This technique can also be used for long-range applications, but the *short-range constraint* cannot be applied. GPS receiver types 1-4 are suitable for this technique (Table 1-1). The applications of this technique cover almost all applications of GPS precise positioning, including attitude determination (which has some special constraints due to the fixed configuration of the GPS antenna array). However, ambiguity resolution for long-range kinematic positioning is very difficult using this technique.

2.3 Integer Least Squares Estimation

Integer least squares estimation includes both least squares estimation with integer conditions, and the validation and rejection criteria.

2.3.1 Least Squares Estimation with Integer Constraints

Linearization of the double-differenced carrier phase observations leads to the following system of equations:

$$V = AX - L \tag{2-5a}$$

where

$$A = [A_C \quad A_N] \tag{2-5b}$$

$$X = \begin{bmatrix} X_C \\ X_N \end{bmatrix} \tag{2-5c}$$

and the weight matrix of the observations P with respect to the unit weight variance factor σ_0^2. The integer least squares criteria for solving this linearized system of observation equations are:

$$V^T PV = \min \tag{2-6a}$$

$$X_C \in R^t \tag{2-6b}$$

$$X_N \in Z^m \tag{2-6c}$$

where X_C is the $t \times 1$ real-valued parameter vector which includes coordinate parameters (and any other real-valued parameter that may be estimated); X_N is the $m \times 1$ integer-valued parameter vector; L is the $n \times 1$ residual vector between the double-differenced carrier phase and/or pseudo-range observations and their computed value vectors; R^t refers to t-dimensional real space and Z^m refers to m-dimensional integer space.

The above integer least squares problem may be solved in two steps. The first step consists of solving the problem with R^m replacing Z^m using the traditional least squares theory. That is (Cross, 1983, 1996; Harvey, 1995):

$$\hat{X} = (A^T P A)^{-1} A^T P L \tag{2-7}$$

$$Q_{\hat{X}} = (A^T P A)^{-1} = \begin{bmatrix} Q_{\hat{X}_C} & Q_{\hat{X}_C \hat{X}_N} \\ Q_{\hat{X}_N \hat{X}_C} & Q_{\hat{X}_N} \end{bmatrix} \tag{2-8}$$

$$\Omega = V_0^T P V_0 \tag{2-9}$$

$$m_0^2 = \frac{\Omega}{n - t - m} \tag{2-10}$$

In this step, the accuracy estimation is always over-optimistic. In order to obtain more reliable accuracy estimations, the observation correlations between epochs should be considered (El-Rabbany, 1994), or the standardization procedure for the co-factor matrix and *a posteriori* unit weight variance factor should be used (Han & Rizos, 1995c). On the other hand, the following test should be employed in order to check the fidelity of the stochastic and functional models.

The null hypothesis H_0 and the alternative hypothesis H_1 are:

$$H_0 : m_0^2 = \sigma_0^2 \tag{2-11a}$$

$$H_1 : m_0^2 \neq \sigma_0^2 \tag{2-11b}$$

and the corresponding test statistic is:

$$\frac{\Omega}{\sigma_0^2} = \frac{(n - t - m) \cdot m_0^2}{\sigma_0^2} \sim \chi^2_{n-t-m} \tag{2-12}$$

The rejection regions of H_0 are:

$$\frac{(n - t - m) \cdot m_0^2}{\sigma_0^2} > \xi_{\chi^2_{n-t-m};1-\alpha/2} \tag{2-13a}$$

$$\frac{(n-t-m)\cdot m_0^2}{\sigma_0^2} < \xi_{\chi^2_{n-t-m};\alpha/2} \tag{2-13b}$$

where $\xi_{\chi^2_{n-t-m};\alpha/2}$ and $\xi_{\chi^2_{n-t-m};1-\alpha/2}$ are the lower and upper boundary of the $1-\alpha$ confidence interval for the χ^2-distribution statistic with n-t-m degrees of freedom.

If the *a posteriori* unit weight variance factor is rejected by equation (2-13a), a check should be made for outliers in the observations, such as cycle slips, multipath, system biases (eg., the ionospheric or tropospheric delay effects not eliminated in double-differencing), or the *a priori* standard deviations of the observations do not reflect the accuracies of these observations. If the *a posteriori* unit weight variance factor is rejected by equation (2-13b), a check should be made as to whether there are too many parameters (eg., the ionospheric or tropospheric delay parameters are included in the functional model, even though the ionospheric/tropospheric delay effects are insignificant), or the *a priori* standard deviations of the observations do not reflect the accuracies of these observations.

The second step requires a constraint to be added:

$$X_N = N_k \tag{2-14}$$

where N_k is an integer vector. The results can then be obtained as follows:

$$\tilde{X}_{C,k} = \hat{X}_C - Q_{\hat{X}_C\hat{X}_N} Q^{-1}_{\hat{X}_N} \left(\hat{X}_N - N_k\right) \tag{2-15}$$

$$Q_{\tilde{X}_{C,k}} = Q_{\hat{X}_C} - Q_{\hat{X}_C\hat{X}_N} Q^{-1}_{\hat{X}_N} Q_{\hat{X}_N\hat{X}_C} \tag{2-16}$$

$$V_k^T P V_k = \Omega + R_k \tag{2-17}$$

where

$$R_k = \left(\hat{X}_N - N_k\right)^T Q^{-1}_{\hat{X}_N} \left(\hat{X}_N - N_k\right) \tag{2-18}$$

and the standard deviation m_{0k} can be represented as:

$$m_{0k} = \sqrt{\frac{V_k^T P V_k}{n-t}} \tag{2-19}$$

The equivalent relations can be obtained:

$$V_k^T P V_k = \min \tag{2-20}$$

$$\left(\hat{X}_N - N_k\right)^T Q_{\hat{X}_N}^{-1} \left(\hat{X}_N - N_k\right) = \min \tag{2-21}$$

For a different integer set N_k, a different value of R_k, and associated $V_k^T P V_k$ and m_{0k}, will be obtained. Then the optimal integer set, which satisfies the following validation and rejection criteria, should be searched for.

2.3.2 Validation and Rejection Criteria

The correct integer vector N_k in the constraint equation (2-14) should satisfy the following conditions:

N_k should be within the confidence region of $\hat{X}_N$

This condition for the integer vector N_k can be expressed as:

$$\frac{(\hat{X}_N - N_k)^T Q_{\hat{X}_N}^{-1} (\hat{X}_N - N_k)}{m \cdot m_0^2} \le \xi_{F_{m,n-t-m};1-\alpha} \tag{2-22}$$

where $\xi_{F_{m,n-t-m};1-\alpha}$ is the one-tailed boundary of the $1-\alpha$ confidence interval for the Fisher's distribution statistic with m and n-t-m degrees of freedom.

This condition, for each element $(n_i)_k$ (i=1,2, ..., m) in the integer vector N_k, can be represented as:

$$\frac{\left|\hat{x}_{n_i} - (n_i)_k\right|}{m_0 \cdot Q_{\hat{x}_{n_i}}^{1/2}} \le \xi_{t_{n-t-m};1-\alpha} \tag{2-23}$$

where $\hat{x}_{n_i}$ and $m_0 \cdot Q_{\hat{x}_{n_i}}^{1/2}$ are the i-th element of the vector $\hat{X}_N$ and its standard deviation; $(n_i)_k$ is the i-th element of the integer vector N_k; i=1,2,...,m; $\xi_{t_{n-t-m};1-\alpha}$ is

the one-tailed boundary of the $1-\alpha$ confidence interval for the Student's distribution statistic with n-t-m degrees of freedom.

This condition, for a linear combination $f((n_1)_k,\cdots,(n_m)_k)$ of the elements in the integer vector N_k, can be represented as:

$$\frac{\left|f(\hat{x}_{n_1},\cdots,\hat{x}_{n_m})-f((n_1)_k,\cdots,(n_m)_k)\right|}{m_0\cdot Q_f^{1/2}}\le \xi_{t_{n-t-m};1-\alpha} \tag{2-24}$$

where $m_0\cdot Q_f^{1/2}$ is the standard deviation of the linear combination $f(\hat{x}_{n_1},\cdots,\hat{x}_{n_m})$.

$\tilde{X}_{C,k}$ *should be within the confidence region of* $\hat{X}_C$

This condition for the vector $\tilde{X}_{C,k}$ can be expressed as (Frei & Beutler, 1990):

$$\frac{(\hat{X}_C-\tilde{X}_{C,k})^T Q_{\hat{X}_C}^{-1}(\hat{X}_C-\tilde{X}_{C,k})}{t\cdot m_0^2}\le \xi_{F_{t,n-t-m};1-\alpha} \tag{2-25}$$

and for each element in the vector can be represented as:

$$\frac{\left|(\hat{x}_i)_C-(\tilde{x}_i)_{C,k}\right|}{m_0\cdot Q_{(\hat{x}_i)_C}^{1/2}}\le \xi_{t_{n-t-m};1-\alpha} \tag{2-26}$$

where $(\hat{x}_i)_C$ and $m_0\cdot Q_{(\hat{x}_i)_C}^{1/2}$ are the i-th element of the vector $\hat{X}_C$ and its standard deviation; $(\tilde{x}_i)_{C,k}$ is the i-th element of the vector $\tilde{X}_{C,k}$; i=1,2,...,t; $\xi_{F_{t,n-t-m};1-\alpha}$ is the one-tailed boundary of the $1-\alpha$ confidence interval for the Fisher's distribution statistic with t and n-t-m degrees of freedom.

m_{0k}^2 *should be compatible with* σ_0^2

This condition can be expressed as:

$$\xi_{\chi^2_{n-t};\alpha/2} \le \frac{(n-t)\cdot m_{0k}^2}{\sigma_0^2} \le \xi_{\chi^2_{n-t};1-\alpha/2} \tag{2-27}$$

where $\xi_{\chi^2_{n-t};\alpha/2}$ and $\xi_{\chi^2_{n-t};1-\alpha/2}$ are the lower and upper boundary of the $1-\alpha$ confidence interval for the χ^2-distribution statistic with n-t degrees of freedom.

If m_{0k}^2 is rejected, the corresponding integer vector will be rejected.

R_k = min in order to obtain $V_k^T PV_k$ = min

All integer vectors which are consistent with the above conditions should be selected as integer vector candidates and the two integer vectors which make R_k a minimum and the second minimum should be found.

Contrast test between sec(R_k) and min(R_k)

All other candidates, especially the second smallest sec(R_k), should be significantly larger than the min(R_k) to ensure that a reliable unique result can be obtained. This condition can be expressed as the test:

$$\frac{\sec(m_{0k}^2)}{\min(m_{0k}^2)} > F \tag{2-28}$$

where F is an empirical value. Frei & Beutler (1990) assume that the ratio value is a F-distribution statistic, and F can be chosen as the boundary of the $1-\alpha$ confidence interval for the Fisher's distribution statistic with degrees of freedom n-t and n-t. Landau & Euler (1992) suggest 2 as the critical value.

Several search procedures based on all or some of the abovementioned validation and rejection criteria have been developed in the past few years. The next section will discuss these techniques and make some comparisons.

2.4 Fast Integer Ambiguity Search Techniques

2.4.1 Fast Integer Search in the Original Ambiguity Domain

The ambiguity search problem has been investigated over the past decade. The earliest and simplest method is to round off the real-valued ambiguities to the nearest integer. A long observation session is normally required in order to ensure that even one integer is in the confidence region of the real-valued ambiguities.

Frei & Beutler (1990) suggested the Fast Ambiguity Resolution Approach (FARA), which uses equation (2-23) to define the initial search region and then reduce the number of candidate sets by making use of the correlations through all combinations of the difference between two ambiguities and the relations between two ambiguities on L1 and L2 to create the candidates (equation (2-24)). The linear functions in equation (2-24) are selected as:

$$f(\hat{x}_{n_1},\cdots,\hat{x}_{n_m}) = \hat{x}_{n_i} - \hat{x}_{n_j} \tag{2-29}$$

for any combinations of i=1,2,...,m-1 and j=i+1,...,m and

$$f(\hat{x}_{n_1},\cdots,\hat{x}_{n_m}) = \hat{x}_{n_i} - \frac{\lambda_2}{\lambda_1}\cdot\hat{x}_{n_j} \tag{2-30}$$

for dual-frequency observations, where $\hat{x}_{n_i}$ and $\hat{x}_{n_j}$ are the real-valued ambiguities for L1 and L2 carrier phase observations for the same pair of satellites.

The tests of equations (2-26), (2-27) and (2-28) can be used to determine the final unique solution from the candidate sets.

Hatch (1990) has suggested the Least Squares Ambiguity Search Technique (LSAST), which makes use of the fact that four satellites are sufficient for positioning and for determining the other satellites' ambiguities if the three double-differenced ambiguities for these four satellites have been resolved. This technique separates the satellites into two groups. The first or primary group consists of a set of four satellites which are used

to generate a set of potential solutions that lie within some uncertainty region. After one set of three ambiguities is fixed, the remaining ambiguities can be estimated (real-values) and then rounded to the nearest integer to form the ambiguity candidate sets.

Euler & Landau (1992) have suggested Cholesky decomposition of the $Q_{\hat{X}_N}^{-1}$ matrix (the computation of R_k will be very efficient) and then form the vector which derives R_k by squaring and adding the vector elements. The rejection can be performed for some integer combinations at a very early computation state when the partly summed squaring elements exceed a previously found second minimum. The candidates are constructed using equation (2-23). The ratio test will be employed to determine the final solution.

Chen (1993) and Chen & Lachapelle (1994, 1995) have suggested the Fast Ambiguity Search Filter (FASF), which uses a Kalman filter and a recursive computation of the search range for the ambiguities (RCSR). The concept of RCSR is described as follows. Assuming the ambiguity series is $n_1, n_2, \cdots, n_m$, the search range of the ambiguities is computed from n_1 to n_m. The search range of the possible integers for ambiguity parameter n_i are computed for each specific integer set of the ambiguities on the left of n_i, ie., $n_1, n_2, \cdots, n_{i-1}$, which is treated as being known, while $n_i, n_{i+1}, \cdots n_m$ are the estimated parameters. The search range for n_i can be expressed as:

$$\left|\hat{x}_{n_i/n_1,n_2,\cdots,n_{i-1}} - n_i\right| \le \xi_{t_{f_i};1-\alpha/2} \cdot m_0 \cdot \sqrt{q_i} \qquad (2\text{-}31)$$

where $m_0 \cdot \sqrt{q_i}$ is the standard deviation of $\hat{x}_{n_i/n_1,n_2,\cdots,n_{i-1}}$ for the fixed $n_1, n_2, \cdots, n_{i-1}$; $\hat{x}_{n_i/n_1,n_2,\cdots,n_{i-1}}$ is the float estimation of n_i corresponding to a specific integer set for $n_1, n_2, \cdots, n_{i-1}$; $\xi_{t_{f_i};1-\alpha}$ has the same meaning as in equation (2-23) but with f_i degrees of freedom.

Teunissen (1994) has suggested the LDL^T decomposition method to search the transformed ambiguities (now generally referred to as the LAMBDA method). But it can be used to search the original ambiguities as well. $Q_{\hat{X}_N}$ can be decomposed as:

$$Q_{\hat{X}_N} = LDL^T \qquad (2\text{-}32)$$

where

$$L = \begin{bmatrix} 1 & 0 & 0 & \cdots & 0 \\ L_{21} & 1 & 0 & \cdots & 0 \\ L_{31} & L_{32} & 1 & \cdots & 0 \\ \vdots & \vdots & \vdots & \ddots & \vdots \\ L_{m1} & L_{m2} & L_{m3} & \cdots & 1 \end{bmatrix} \tag{2-33}$$

$$D = \mathrm{diag}(q_1, q_2, \cdots, q_m) \tag{2-34}$$

$\hat{x}_{n_1}$ is not changed and $\hat{x}_{n_i/n_1,n_2,\cdots,n_{i-1}}$ can be represented as follows, for i>1:

$$\hat{x}_{n_i/n_1,n_2,\cdots,n_{i-1}} = \hat{x}_{n_i} - \sum_{j=1}^{i-1}\left[L_{ij}(\hat{x}_{n_j/n_1,n_2,\cdots,n_{j-1}} - n_j)\right] \tag{2-35}$$

Equations (2-32 to 2-35) define the other computation method of $\hat{x}_{n_i/n_1,n_2,\cdots,n_{i-1}}$ and q_i for the FASF method. The following relation should hold from equation (2-22):

$$\sum_{i=1}^{m}\left[\left(\hat{x}_{n_i/n_1,n_2,\cdots,n_{i-1}} - n_i\right)^2 \Big/ q_i\right] < m \cdot m_0^2 \cdot \xi_{F_{m,n-t-m};1-\alpha} \tag{2-36}$$

The search region is defined as:

$$\left|\hat{x}_{n_i/n_1,n_2,\cdots,n_{i-1}} - n_i\right| < m \cdot m_0^2 \cdot \xi_{F_{m,n-t-m};1-\alpha} - \sum_{j=1}^{i-1}\left[\left(\hat{x}_{n_j/n_1,n_2,\cdots,n_{j-1}} - n_j\right)^2 \Big/ q_j\right] \tag{2-37}$$

2.4.2 Fast Integer Search in the Transformed Ambiguity Domain

The abovementioned search procedures are directly or indirectly dependent on the diagonal elements of the variance-covariance matrix obtained from the real-valued ambiguity estimation. If the invertible integer transformation matrix can be obtained and the diagonal elements of the variance-covariance matrix of the transformed integer parameters are much smaller than the original ones, the search methods will become

much more efficient. This idea was first suggested by Teunissen (1994) as the Least-squares AMBiguity Decorrelation Adjustment (LAMBDA) method, which uses an ambiguity transformation matrix Z that reformulates the original ambiguity vector $\hat{X}_N$ into the transformed ambiguity vector $\hat{Z}_N$, whose variance-covariance matrix has much smaller diagonal elements:

$$\hat{Z}_N = Z \cdot \hat{X}_N \tag{2-38}$$

$$Q_{\hat{Z}_N} = Z Q_{\hat{X}_N} Z^T \tag{2-39}$$

and equation (2-18) can be rewritten as:

$$R_k = \left(\hat{Z}_N - N_k^Z\right)^T Q_{\hat{Z}_N}^{-1} \left(\hat{Z}_N - N_k^Z\right) \tag{2-40}$$

The original ambiguity estimation problem has therefore been changed. The new problem is to search N_k^Z for an integer set that makes $R_k = \min$, and passes the validation and rejection criteria tests.

In order to ensure that the transformed ambiguity has integer characteristics, the transformation matrix Z has to have integer elements. In order to ensure that the original ambiguity can be determined from the transformed ambiguity, the inverse of the transformation matrix also has to have integer elements. Therefore, *matrix Z is an admissible ambiguity transformation if and only if matrix Z has integer elements and its determinant equals ±1* (Ibid, 1994). The original ambiguities are transformed:

$$N_k = Z^{-1} \cdot N_k^Z \tag{2-41}$$

The key to the LAMBDA method is to find the admissible ambiguity transformation which makes $Q_{\hat{Z}_N}$ have almost the same diagonal values and $\det\left[\mathrm{diag}\left(Q_{\hat{Z}_N}\right)\right]$ as small as possible, and then search the optimal integer solution.

The number of integer ambiguity candidate sets is dependent on the variance-covariance matrix, especially the determinant of the diagonal matrix of the variance-covariance matrix of the real-valued ambiguity estimates, $\det\left[\mathrm{diag}\left(R_{\hat{X}_N}\right)\right]$. The transformation matrix, which has integer elements and determinant equal to ±1, should make the diagonal elements as small as possible. In order to quantify the extent of the decorrelation, the correlation matrix and decorrelation number are introduced.

The correlation matrix for the co-factor matrix $Q_{\hat{X}_N}$ is defined as:

$$R_{\hat{X}_N} = \left[\mathrm{diag}\left(Q_{\hat{X}_N}\right)\right]^{-1/2} Q_{\hat{X}_N} \left[\mathrm{diag}\left(Q_{\hat{X}_N}\right)\right]^{-1/2} \tag{2-42}$$

and its determinant is defined as the decorrelation number (Ibid, 1994):

$$r_{\hat{X}_N} = \sqrt{\det\left(R_{\hat{X}_N}\right)} \tag{2-43}$$

Due to the fact that $Q_{\hat{X}_N}$ and $Q_{\hat{Z}_N}$ have the same determinant, the following relation can be obtained:

$$r_{\hat{Z}_N}^2 \cdot \det\left[\mathrm{diag}\left(Q_{\hat{Z}_N}\right)\right] = r_{\hat{X}_N}^2 \cdot \det\left[\mathrm{diag}\left(Q_{\hat{X}_N}\right)\right] = \text{const.} \tag{2-44}$$

In order to make $\det\left[\mathrm{diag}\left(Q_{\hat{Z}_N}\right)\right]$ as small as possible, $r_{\hat{Z}_N}$ should be made as large as possible.

This can be easily achieved using the following procedure to compute the integer transformation matrix Z, which is used to construct multi-satellite ambiguity combination (Han & Rizos, 1995b).

The first step is the unit upper triangular factorization (UDU^T) for $Q_{\hat{X}_N}$:

$$Q_{\hat{X}_N} = U_1 D_{U_1} U_1^T \tag{2-45}$$

and compute the integer matrix Z_{U_1} :

$$Z_{U_1} = \left[\mathrm{Int}(U_1)\right]^{-1} \tag{2-46}$$

where Int is an operator to round all elements in U_1 to the nearest integer, and then

$$Q_{\hat{Z}_{N,U_1}} = Z_{U_1} Q_{\hat{X}_N} Z_{U_1}^T \tag{2-47}$$

The second step is the unit lower triangular factorization (LDL^T) for $Q_{\hat{Z}_{N,U_1}}$:

$$Q_{\hat{Z}_{N,U_1}} = L_1 D_{L_1} L_1^T \tag{2-48}$$

and compute the integer matrix Z_{L_1} :

$$Z_{L_1} = \left[\mathrm{Int}(L_1)\right]^{-1} \tag{2-49}$$

and

$$Q_{\hat{Z}_{N,L_1}} = Z_{L_1} Q_{\hat{Z}_{N,U_1}} Z_{L_1}^T \tag{2-50}$$

An iterative procedure is used for the first and second steps to create Z_{U_i} from $Q_{\hat{Z}_{N,L_{i-1}}}$ (or $Q_{\hat{X}_N}$ when i=1) and Z_{L_i} from $Q_{\hat{Z}_{N,U_i}}$ until both integer matrices $\mathrm{Int}(U_k)$ and $\mathrm{Int}(L_k)$ become unit matrices. The integer transformation matrix can be obtained using the following relation:

$$Z = Z_{L_{k-1}} \cdot Z_{U_{k-1}} \cdots Z_{L_1} \cdot Z_{U_1} \tag{2-51}$$

Z can be used to transform the original ambiguities to the transformed ambiguities and to cause the variance-covariance matrix to have a large decorrelation number in order to carry out the search in an efficient way. The suggested procedure therefore provides an easy way to implement the LAMBDA approach.

Four examples are given in Table 2-2 to compare the original variance-covariance (VCV) matrix and the transformed VCV matrix. $e_{\hat{X}_N}$ and $e_{\hat{Z}_N}$ are the ratios of the length of the largest principal axis with respect to the length of the smallest principal axis of the confidence ellipsoids for the original VCV matrix and the transformed VCV matrix, respectively; $\min(\sigma_{\hat{X}_N})$ and $\max(\sigma_{\hat{X}_N})$ are the minimum and maximum values of the standard deviations of the original ambiguity estimates; $\min(\sigma_{\hat{Z}_N})$ and $\max(\sigma_{\hat{Z}_N})$ are the minimum and maximum values of the standard deviations of the transformed ambiguities. Comparing the original and transformed ellipsoid it is obvious that the transformed ellipsoid is much more like a sphere, the decorrelation number is much larger and the maximum value of the standard deviation of the transformed ambiguities is much smaller. The transformation time is from a few milliseconds to a few tens of milliseconds using a 486 DX4-100MHz PC. Note that the variance-covariance matrices in the examples have been standardized using the procedure suggested by Han & Rizos (1995c).

Table 2-2. Comparison of the original VCV matrix and the transformed VCV matrix

	Original VCV Matrix				Transformed VCV Matrix				Time
	$r_{\hat{X}_N}$	$e_{\hat{X}_N}$	$\min(\sigma_{\hat{X}_N})$	$\max(\sigma_{\hat{X}_N})$	$r_{\hat{Z}_N}$	$e_{\hat{Z}_N}$	$\min(\sigma_{\hat{Z}_N})$	$\max(\sigma_{\hat{Z}_N})$	(ms)
Ex 1	5.26×10^{-14}	2069.1	5.88	14.11	0.33	3.86	0.18	0.26	58.8
Ex 2	1.14×10^{-10}	468.54	0.88	2.39	0.29	3.92	0.08	0.12	32.5
Ex 3	6.99×10^{-7}	2936.4	2.02	21.93	0.80	3.65	0.26	0.81	11.5
Ex 4	2.16×10^{-5}	448.19	0.04	3.65	0.72	3.08	0.12	0.31	9.3

Example 1: Dual-frequency phase data, 5 satellites, 30 sec session with 1 sec data rate.
Example 2: Dual-frequency phase data, 5 satellites, 4 min session with 1 sec data rate.
Example 3: Single frequency phase data, 6 satellites, 1 min session with 1 sec data rate.
Example 4: Single frequency phase data, 6 satellites, 5 min session with 1 sec data rate.

2.4.3 Comparison of the Different Search Techniques

All fast search approaches are just different mathematical procedures to find the integer ambiguity set which makes R_k minimum. They do not change the reliability of

ambiguity resolution. The only criterium that can be used to compare these techniques is the computation speed. Therefore, two tests have been carried out using all the suggested AR search techniques, and the results are listed in Table 2-3 for a single frequency experiment, and in Table 2-4 for a dual-frequency experiment. For each test, the AR search techniques have been employed to search the original integer ambiguities directly, and to then search the transformed integer ambiguities. The computation times are listed in the column "Time" in Table 2-3 and Table 2-4. The "Number of Candidates" refers to the number of integer ambiguity sets are considered, from which the minimum R_{min} and second minimum R_{sec} are selected. Although the Fortran software was developed by this author (not the original authors), the implementations are as faithful as possible to the original authors' ideas.

Table 2-3. Test 1: Comparison of the different methods for searching the original ambiguities and for searching the transformed ambiguities

Search Methods	Searching the Original Ambiguities		Searching the Transformed Ambiguities	
	Number of Candidates	Time (sec)	Number of Candidates	Time (ms)
FARA	24095934	1195.46	1051	35.37
LSAST	83720	2.91	N/A	N/A
Cholesky	6.85×10^8	3.41	2250	4.23
FASF	24637	1.15	1906	60.20
LDL^T	978	1.54	977	49.76

Note: Single frequency phase data from 6 satellites, 1 minute session and 1 second data rate are used. The variance-covariance matrix has been standardized using the Han & Rizos (1995c) procedure. The confidence level is selected as 0.997. The volume of the ellipsoid determined by equation (2-22) is 987.44 $cycle^5$. The search time for the transformed ambiguities does not include the transformation time. A 486 DX4-100MHz PC running Fortran code written by this author (not the original authors) has been used.

Table 2-4. Test 2: Comparison of the different methods for searching the original ambiguities and for searching the transformed ambiguities

Search Methods	Searching the Original Ambiguities		Searching the Transformed Ambiguities	
	Number of Candidates	Time (sec)	Number of Candidates	Time (ms)
FARA	788	2.08	88	9.45
LSAST	370175	28.29	N/A	N/A
Cholesky	5.55×10^{13}	5.22	1296	8.68
FASF	85227	7.80	624	44.98
LDL^T	10	0.27	10	4.34

Note: Dual-frequency phase data from 5 satellites, 30 second session and 1 second data rate are used. The variance-covariance matrix has been standardized using the Han & Rizos (1995c) procedure. The confidence level is selected as 0.997. The volume of the ellipsoid determined by equation (2-22) is 10.573 $cycle^8$. The search time for the transformed ambiguities does not include the transformation time. A 486 DX4-100MHz PC running Fortran code written by this author (not the original authors) has been used.

For the LSAST method, if three transformed ambiguities are fixed, the other transformed ambiguities, in general, cannot be rounded to the nearest integer. Therefore, the LSAST method is not used to search the transformed ambiguities.

The performance characteristics are quite different for these two tests. Although the FARA method is not efficient for single frequency data, it is comparatively efficient for use with dual-frequency data, and is implemented within the SKI commercial GPS software. The LSAST and FASF methods are quite good for single frequency data. The Cholesky decomposition method has been significantly improved by searching the transformed ambiguities, and appears to be one of the best methods when combined with the LAMBDA transformation procedure. Although the LDL^T decomposition search method is suggested for searching the transformed ambiguities (Teunissen, 1994), it is

also one of the most efficient methods to search the original ambiguities, especially in cases of a huge search region.

Using the suggested method for constructing the multi-satellite ambiguity combinations and searching the transformed ambiguities, search methods such as FARA, Cholesky, FASF and LDL^T will be significantly improved.

2.5 Stochastic Model Effects on Ambiguity Resolution Techniques

The reliability of ambiguity resolution is mainly affected by unaccounted for biases. If the biases have not been reduced to a small enough level, or the stochastic model does not reflect the error (statistical) characteristics, the estimation results will be biased and therefore lead to the wrong integer ambiguity set being identified (based on the minimum quadratic form of the residuals). Multipath and ionospheric effects are the main sources of these biases, and it is difficult to model them, or correct for them. These biases can be accounted for in the stochastic model.

2.5.1 Spatial Observation Correlation

Least squares estimation requires that the correct functional and stochastic models are specified. The biases in the observations can, in principle, be modelled in the functional model as parameters. Due to the range of complex biases in GPS observations it is often too difficult to incorporate them within the functional model. An alternative is to account for the biases within the stochastic model. If biases affect the GPS observations, a larger standard deviation can be specified for the observations. This procedure will make least squares estimation more reliable. The stochastic model for one-way GPS observations has been investigated by Jin (1995). However, the stochastic model here not only reflects the stochastic characteristics of the observation noise, but also the residual biases due to atmospheric delay and orbit error that remain after double-differencing the data. This will make stochastic model estimation more difficult, and dependent on the baseline length and antenna environments. The definition of a real-time stochastic model with an adaptive improvement feature is an important innovation, and a detailed description is given in Chapter 4.

On the other hand, the variance-covariance-components of the double-differenced observations can be estimated directly using the previous segment of data. The elements of the symmetric variance-covariance matrix of the double-differenced observations can be considered to be the same within a segment (of a few minutes in length), and estimated using the variance-covariance-component estimation method. The estimated variance-covariance matrix can then be applied to the current epoch (Han & Rizos, 1996f).

2.5.2 Temporal Observation Correlation

From an analysis of the biases in GPS carrier phase observations it can be seen that the carrier phase observations between epochs are correlated. The smaller the interval between epochs (i.e., the higher the data rate), the stronger the correlation. Not accounting for this correlation, known as temporal physical correlation, usually leads to an over-optimistic estimate of the accuracy of the baseline results (Cross & Roberts, 1992). Hence, in order to obtain realistic results it is necessary to consider the between-epoch correlations in all cases (with exception of instantaneous ambiguity resolution). El-Rabbany (1994) has studied the temporal physical correlation in time and concludes that an exponential function of time is the best approximation for the covariance function for the GPS carrier phase errors, in the least squares sense. Roberts & Cross (1993) investigated DGPS temporal correlation and account for the effects within a Kalman filter. Although these procedures for accounting for the unmodelled biases yields a fully populated variance covariance (VCV) matrix for the GPS double-differenced carrier phase observations, Han & Rizos (1995c) have derived a simple technique to account for this correlation by scaling the co-factor matrix (which neglects the correlations) and re-computing the unit variance factor (using the residuals, obtained from neglecting the correlations). This method has been successfully used for GPS network adjustment and baseline outlier detection (Han & Rizos, 1995e; 1995f). Although the temporal correlation will have a significant effect on the *a posteriori* VCV matrix, rather than on the parameter estimation results, this will affect the size of the search region for ambiguity resolution, and hence impact on the reliability of the ambiguity resolution process.

Chapter 3

ERROR ANALYSIS FOR LONG-RANGE GPS KINEMATIC POSITIONING

3.1 Introduction

In equation (2-1), note that there are four bias terms (orbit bias, ionospheric delay, tropospheric delay and multipath) remaining in the functional model after application of the double-differencing operator. If the separation between receivers is small enough (e.g. <15km) and there is no serious multipath effect, all of these biases can be neglected. But the use of GPS kinematic positioning has been growing for precise marine and airborne positioning applications, circumstances where the GPS reference receiver(s) cannot be set up near the survey area. The distance from the fixed reference receiver(s) to the roving receiver(s) may range from tens to many of hundreds of kilometres. Although the pseudo-range-based systems such as the Wide Area Differential GPS (WADGPS) or Wide Area Augmentation Systems (WAAS) are intended to deliver accuracies at the few metre level, further bias mitigation will become a serious problem for sub-decimetre accuracy long-range applications. In this chapter, error analysis and error mitigation for long-range kinematic positioning will be studied.

3.2 Orbit Bias

The orbit bias is a baseline length dependent bias which must be reduced before implementing any ambiguity resolution procedure for long-range positioning. There are two ways to resolve orbit bias. One is to use precise satellite ephemerides, estimated to be of 10 cm accuracy with 10 day delay, or 25 cm accuracy with 1 day delay (Neilan, 1996). This method is suitable for post-processed, long-range positioning. The other way is to *estimate* the ephemeris bias using multiple reference stations and then correct the effect of orbit bias on user receiver positioning, similar to the approach used in WADGPS or WAAS. Colombo et al. (1995) propose a two-step Kalman filter

procedure to reduce the effect of orbit bias. The first step is to estimate the orbit bias using compressed observation data, and the second step is to hold fixed the corrected ephemeris while estimating the roving receiver's trajectory on an epoch-by-epoch basis. This method is difficult to implement in real-time. On the other hand, using multiple reference station GPS data, the parameters of an appropriate error model which describes the distance dependent errors, including orbit bias, can be estimated and then disseminated to users in real-time (Wübbena et al., 1996). Wu (1994) has suggested that a linear combination of single-differenced observations between different reference stations and the roving receiver can reduce the orbit bias. Han & Rizos (1996e) have proposed this method for reducing the effect of orbit bias for medium-range ambiguity resolution. This section will give further details of this techniques

3.2.1 Effects of the Orbit Bias on Single-Differenced Observations

As first step it is necessary to derive the effect of an orbit bias on single-differenced observations. Let's assume that a few reference stations ($\mathrm{Ref_i}$) have coordinates that have been determined very precisely from standard post-processing, using the precise ephemeris and appropriate geodetic software. In the case of a user receiver (U), the single-differenced observation between the reference station ($\mathrm{Ref_i}$) and the user receiver will be affected by any orbit bias. Assume that the orbit bias in the direction from the GPS satellite to the user receiver is $\vec{\xi}$, and the other component in the plane (O) that is perpendicular to the direction from the satellite (S) to the user receiver (U) is $\vec{\eta}$. $\vec{\eta}$ can be further partitioned into $\vec{\eta}_1$, in the direction of the section line between the two perpendicular planes of RSU and O, and $\vec{\eta}_2$ in the direction perpendicular to $\vec{\eta}_1$ in the plane (O). Figure 3-1 illustrates the geometric relations.

If the orbit bias is known, the computed range ρ with orbit bias can be represented by the range without orbit bias ρ', which is represented as $\rho + d\rho$ in equations (1-3) and (1-4), and the orbit bias term can be represented as follows, from Figure 3-1:

$$d\rho = \rho' - \rho = \left|\vec{\xi}\right| \tag{3-1}$$

for the user receiver, and

$$d\rho_i = \rho'_i - \rho_i = \left|\vec{\xi}\right| \cdot \cos\beta - \left|\vec{\eta}_1\right| \cdot \sin\beta \tag{3-2}$$

for the reference station Ref_i. Considering the relation:

$$\rho'_i \cdot \sin\beta = \left|\Delta\vec{X}_i\right| \cdot \cos\theta \tag{3-3}$$

the following relation can be derived:

$$d\rho_i - d\rho = -\left|\vec{\xi}\right|(1-\cos\beta) - \frac{1}{\rho}\cdot\left|\vec{\eta}_1\right|\cdot\left|\Delta\vec{X}_i\right|\cdot\cos\theta \tag{3-4}$$

where ρ'_i, in the last term of the right hand of equation (3-4), has been approximated by a constant ρ. Within a region of 100 km radius, the angle β should be less than 1/100 radian and therefore

$$\left|\vec{\xi}\right|\cdot(1-\cos\beta) < 5.0\times10^{-5}\cdot\left|\vec{\xi}\right| \tag{3-5}$$

Hence a 20 m orbit bias in the direction from the satellite to the receiver will result in less than a 1.0 mm bias from the first term on the right hand of equation (3-4), in the single-differenced range between receivers separated less than 200 km. Therefore, this term can be ignored. The maximum value that the second term can reach is 0.2 m, if the orbit bias is 20 m and the baseline length is 200 km:

$$\max\left(\frac{1}{\rho}\cdot\left|\vec{\eta}_1\right|\cdot\left|\Delta\vec{X}_i\right|\cdot\cos\theta\right) = \frac{1}{20000\text{km}}\cdot 20\text{m}\cdot 200\text{km} = 0.2\text{m}$$

For the second term, θ is the angle between the two vectors $\vec{\eta}_1$ and $\Delta\vec{X}_i$, and as $\vec{\eta}_2$ and $\Delta\vec{X}_i$ are orthogonal:

$$\frac{1}{\rho}\cdot\left|\vec{\eta}_1\right|\cdot\left|\Delta\vec{X}_i\right|\cdot\cos\theta = \frac{1}{\rho}\cdot\vec{\eta}_1\cdot\Delta\vec{X}_i = \frac{1}{\rho}\cdot\vec{\eta}\cdot\Delta\vec{X}_i \tag{3-6}$$

and finally

$$d\rho_i - d\rho = -\frac{1}{\rho}\cdot\vec{\eta}\cdot\Delta\vec{X}_i \tag{3-7}$$

The orbit bias effect on the single-differenced range is the product of the baseline vector and the orbit bias component in the plane (O), orthogonal to the direction from the

satellite to the user receiver. If there are several reference stations whose positions are known with high precision, the orbit bias term in the single-differenced range will be eliminated through a particular linear combination. This idea was suggested by Wu (1994).

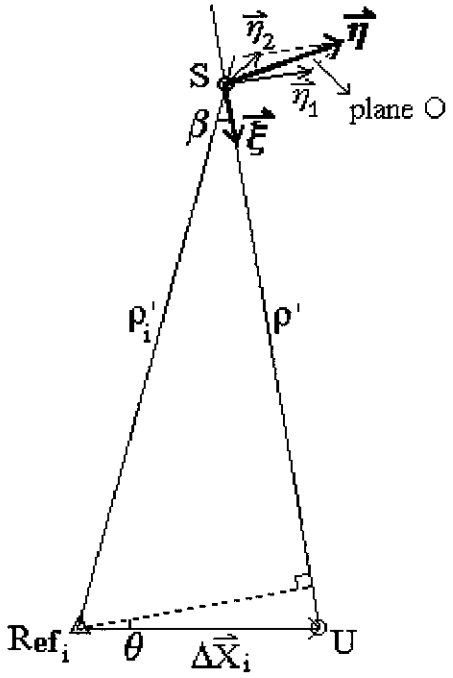

Figure 3-1. Geometric representation of the orbit bias

3.2.2 Elimination Procedure for the Orbit Bias

If the parameters α_i can be found which satisfy the conditions:

$$\sum_i \alpha_i \cdot \Delta\vec{X}_i = 0 \tag{3-8}$$

and

$$\sum_i \alpha_i = 1 \tag{3-9}$$

the linear combination of the single-differenced range can be formed as:

$$\sum_i \alpha_i \cdot (d\rho_i - d\rho) = \sum_i \alpha_i \cdot \left(-\frac{1}{\rho} \cdot \vec{\eta} \cdot \Delta \vec{X}_i \right) = 0 \tag{3-10}$$

Therefore, the single-differenced observation $\sum_i \alpha_i \cdot (\phi_i - \phi)$ will not be affected by ephemeris bias, and the standard deviation of the linear combination of single-differenced observations is

$$\sigma_\Sigma = \sigma_0 \cdot \sqrt{\sum_i \alpha_i^2 + 1} \tag{3-11}$$

where σ_0 is the standard deviation of one-way carrier phase observations. In order to minimize σ_Σ, another constraint should be added:

$$\sum_i \alpha_i^2 = \min \tag{3-12}$$

In order to satisfy equations (3-8) and (3-9), the minimum number of reference stations is two if a user receiver is on a line joining the two reference stations; the minimum number of reference stations is three if a user receiver is on the plane defined by three reference stations; and the minimum number of reference stations is four if a user receiver is arbitrarily located. If more reference stations are available, equation (3-12) should be used to uniquely determine the linear coefficient parameters which make the standard deviation of the linear combination of single-differenced observations a minimum.

Three examples of a three reference station network are discussed below, all assume that the user receiver is on the plane defined by the three reference stations. Example 1: The three reference stations form an equilateral-triangle, with the user receiver located at the centroid (Figure 3-2a). Example 2: Using the same reference stations, the user receiver is located midway along one baseline (Figure 3-2b). Example 3: Using the same reference stations, the user receiver is located outside the triangle (Figure 3-2c). The results for α_i and the standard deviations of the linear combination of single-differenced observations are given in Table 3-1.

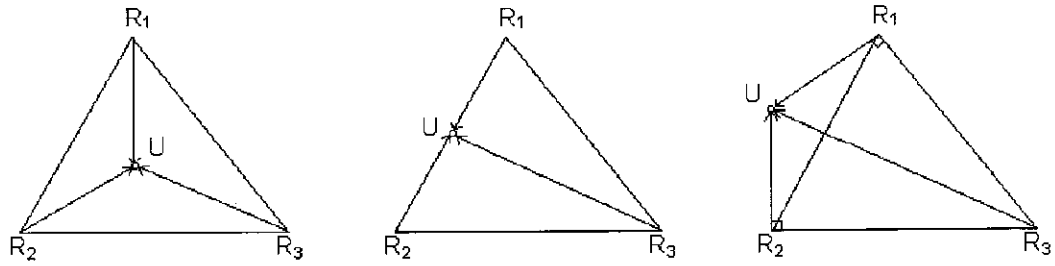

(a) Example 1 (b) Example 2 (c) Example 3

Figure 3-2. Three cases of network configurations

Table 3-1. Linear combination coefficients resulting from the network examples in Figure 3-2

	α_1	α_2	α_3	σ_Σ
Ex 1	0.3333	0.3333	0.3333	$1.15\sigma_0$
Ex 2	0.5000	0.5000	0.	$1.22\sigma_0$
Ex 3	1.0000	1.0000	-1.000	$2.00\sigma_0$

From these examples, it is obvious that the user receiver should be located within the triangle formed by the reference stations. It is easy to generalise this to four reference stations, that is, the user receiver should be located within the tetrahedron formed by the four reference stations. Because the earth is approximately an ellipsoid and the active area may be in a mountainous region, it could be difficult to set up a user receiver within the tetrahedron. Therefore, it is necessary to investigate whether the height component should be neglected, and to determine how much effect it has on the linear combination of single-differenced ranges.

The baseline vector $\Delta\bar{X}_i$ can be separated into two components, $\Delta\bar{X}_i^P$ which is on the Gauss plane coordinate system, and the other component $\Delta\bar{X}^H$ which is orthogonal to this plane. The constraint of equation (3-8) is relaxed as:

$$\sum_i \alpha_i \cdot \Delta\bar{X}_i^P = 0 \tag{3-13}$$

and the orbit bias component η can also be partitioned into two components (η^P, η^H) in the same way. Equation (3-10) becomes:

$$\sum_i \alpha_i \cdot (d\rho_i - d\rho) = \sum_i \alpha_i \cdot \left(-\frac{1}{\rho} \cdot \vec{\eta} \cdot \Delta\vec{X}_i \right) = -\frac{1}{\rho} \cdot \eta^H \cdot \Delta X_i^H \tag{3-14}$$

The maximum magnitude of $\frac{1}{\rho} \cdot \eta^H \cdot \Delta X_i^H$ can be computed by

$$\max\left(\frac{1}{\rho} \cdot \eta^H \cdot \Delta X_i^H \right) = \frac{1}{20000\text{km}} \cdot 20\text{m} \cdot 1785\text{m} = 1.8\text{mm}$$

if the orbit bias is assumed to be 20 m, the height of the receiver above the ellipsoid is 1000 m, and there is a 785 m height difference caused by the curvature of the earth across an area with radius 100 km. Therefore, for most cases, the user receiver can be assumed to lie on the plane formed by the reference stations, and the height component can be ignored.

If a data gap occurred at one of the external reference stations, the linear coefficient parameters can be redetermined using the other reference stations. Therefore, the linear coefficient parameters should be determined for each epoch. If there are no data gaps for all reference stations, or a few short data gaps which can be ignored, the linear combination can be determined from the estimated coordinate correction vectors:

$$\delta\Delta\vec{X} = \sum_i \alpha_i \, \delta\Delta\vec{X}_i \tag{3-15}$$

The estimated coordinates of the user roving receiver are:

$$\vec{X} = \vec{X}_0 + \sum_i (\alpha_i \cdot \delta\Delta\vec{X}_i) \tag{3-16}$$

3.3 Ionospheric delay

3.3.1 Ionospheric Delay and Interpolation

The ionosphere is that region of the earth's atmosphere in which ionising radiation causes electrons to exist in sufficient quantities to affect the propagation of radio waves. The height at which the ionosphere starts is about 50 km and stretches to heights of 1000 km

or more. The ionosphere is a dispersive medium for radio waves, that is, its refractive index is a function of the frequency. By ignoring the effect of the longitudinal components of the earth's magnetic field and the higher order terms, the phase refractive index of the ionosphere, appropriate for carrier phase observations, is approximated by (Langley, 1996):

$$n_\phi = 1 - \frac{\alpha N_e}{f^2} \tag{3-17}$$

and the ionospheric group refractive index, appropriate for pseudo-range observations, is approximated by (ibid, 1996)

$$n_R = 1 + \frac{\alpha N_e}{f^2} \tag{3-18}$$

where α is a constant; N_e is the electron density and f is the frequency of the radio wave. If N_e has units of reciprocal metres cubed and f is given in Hz, then $\alpha = 40.28$.

The integration of the expressions for n_ϕ and n_R along the path followed by a radio signal yields the electromagnetic path lengths:

$$\int_S n_\phi dS = \int_S \left(1 - \frac{\alpha N_e}{f^2}\right) dS = \rho - d_{ion} \tag{3-19}$$

and

$$\int_S n_R dS = \int_S \left(1 + \frac{\alpha N_e}{f^2}\right) dS = \rho + d_{ion} \tag{3-20}$$

where ρ is the true geometric range and d_{ion} is the ionospheric range error which (ignoring path bending) is given by:

$$d_{ion} = \frac{\alpha}{f^2} \int_S N_e dS = \frac{\alpha TEC}{f^2} \tag{3-21}$$

with TEC (total electron content) being the integrated electron density along the signal path. The VEC (vertical electron content) at the ionospheric intercept point to the line-of-sight at the receiver location can be approximated as (Klobuchar, 1987):

$$VEC = TEC \cdot \cos\left[\sin^{-1}(0.94792\cos E)\right] \tag{3-22}$$

where the height of the ionospheric layer is assumed to be 350 km.

For a dual-frequency GPS receiver, which outputs pseudo-ranges R^{L1} and R^{L2}, or carrier phase observations ϕ_1 and ϕ_2 in metres, TEC can be estimated by:

$$TEC = \frac{1}{\alpha}\frac{f_1^2 f_2^2}{f_1^2 - f_2^2}\left(R^{L2} - R^{L1}\right) \tag{3-23}$$

or

$$TEC = \frac{1}{\alpha}\frac{f_1^2 f_2^2}{f_1^2 - f_2^2}\left(\left(\phi^{L1} - \lambda_1 N^{L1}\right) - \left(\phi^{L2} - \lambda_2 N^{L2}\right)\right) \tag{3-24}$$

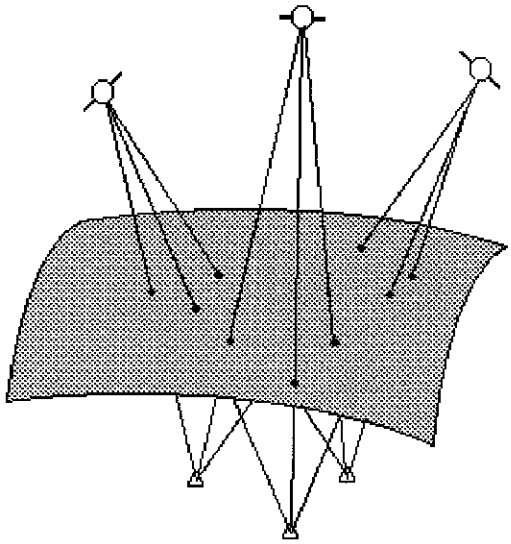

Figure 3-3. An ionospheric model for all satellites and for an observation session of several hours

Models of the absolute TEC have been suggested using one set of coefficients derived from dual-frequency GPS observations at one or several receivers, as shown in Figure 3-

3. Such a model can be used to reduce single frequency baseline coordinate errors (Georgiadou & Kleusberg, 1988a; Wild et al., 1989), and to improve ambiguity resolution on long baselines and for observation sessions of several hours (Mervert et al., 1994). Many functions can serve this purpose. First order spherical harmonic functions were used by Cohen et al. (1992) to model the vertical electron content. A third order polynomial was found to produce satisfactory results for periods of three to four hours by Qiu et al. (1995).

These models are used for WADGPS or WAAS, or other pseudo-range-based applications. However, the accuracies are not good enough to estimate integer ambiguities in carrier phase-based applications because the ionosphere fitting area at the ionospheric layer is much larger than the ground station network and the model with a few coefficients, e.g. the first order spherical harmonic functions or a third order polynomial, can only represent the large-scale structure of the ionospheric electron content, and cannot reproduce the small-scale or medium-scale structure of the ionospheric electron content.

An example can illustrates this. Assume a ground area with radius r_g, the ionosphere fitting area can be derived from the following relations, according to Figure 3-4:

$$\sin(180-90-E-\theta)=\frac{R_e}{R_e+H}\cdot\sin(90+E) \tag{3-25}$$

where E is the cutoff elevation angle in degrees. The radius of the ionospheric area can be expressed as:

$$r_{ion}=\left(\frac{r_g}{R_e}+\frac{\theta}{180}\cdot\pi\right)\cdot(R_e+H) \tag{3-26}$$

For an area with $r_g = 100\,\text{km}$ radius, the ionosphere fitting area at the ionospheric layer is the area with radius $r_{ion} = 1397\,\text{km}$ if the height of the ionospheric layer is assumed to be 350 km and the cutoff elevation angle is selected as 10 degrees. This means that the radius of the ionosphere fitting area is 14 times that of the radius of the ground area !

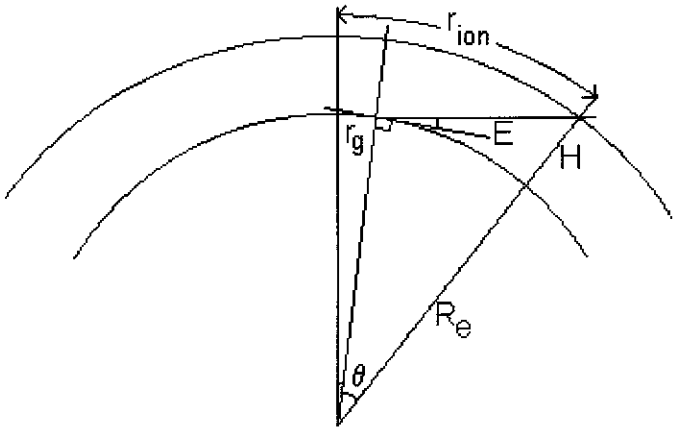

Figure 3-4. Fitting region on the ionospheric layer for a certain area on the ground

3.3.2 Epoch-by-Epoch and Satellite-by-Satellite Ionospheric Model

The epoch-by-epoch and satellite-by-satellite ionospheric model has been suggested as a candidate for a high accuracy ionospheric model (Webster & Kleusberg, 1992; Wanninger, 1995; Han & Rizos, 1996e). The ionospheric delay at a user receiver is estimated from the interpolation of ionospheric delays at three or more surrounding reference stations, using the intersection points of the GPS signal paths with an ionospheric single-layer model at a height of 350 km (Figure 3-5). In this case, for the area with $r_g = 100\text{km}$ radius, the ionosphere fitting area at the ionospheric layer is an area with radius $r_{ion} < 100$ km. The lower the satellite elevation, the smaller the ionosphere fitting area, if the height of the ionospheric layer is assumed to be 350 km and the satellite height is about 20,000 km.

The actual implementation of this will require the computation of the intersection points, and the transformation from TEC to VEC and from VEC to TEC. As precise TEC can only be computed in the double-differenced form, an approximation will also be necessary in the computation. For an area of 200×200 km^2, the computation procedure reduces simply to the interpolation of the single-differenced TEC between receivers, or double-differenced TEC, based on the receiver positions in the Gauss plane coordinate system. The proof is given in Appendix A.

If there are three reference stations set up surrounding the survey area, the TEC values for a satellite at reference stations 1 and 2, relative to the TEC value at reference station 3, can be represented by (equation (3-24)):

$$\Delta TEC_{i,3}(k) = \frac{1}{\alpha} \cdot \frac{f_2^2}{f_1^2 - f_2^2} \cdot \left(\left(\Delta\phi_{i,3}^{L1}(k) - \lambda_1 \cdot \Delta N_{i,3}^{L1} \right) - \left(\Delta\phi_{i,3}^{L2}(k) - \lambda_2 \cdot \Delta N_{i,3}^{L2} \right) \right) \tag{3-27}$$

where i=1,2. The TEC value at the user receiver, relative to reference station 3, can be interpolated as (see equation (A-14)):

$$\Delta TEC_{u,3} = \begin{bmatrix} x_u & y_u \end{bmatrix} \cdot \begin{bmatrix} x_1 & y_1 \\ x_2 & y_2 \end{bmatrix}^{-1} \cdot \begin{bmatrix} \Delta TEC_{1,3} \\ \Delta TEC_{2,3} \end{bmatrix} \tag{3-28}$$

where (x_1,y_1), (x_2,y_2) and (x_u,y_u) are coordinates of the reference stations 1 and 2, and the user receiver, respectively, in the Gauss plane coordinate system, relative to reference station 3. From equation (3-21), the single-differenced ionospheric delay on L1 or L2 can be derived as:

$$d_{ion,u} - d_{ion,3} = \begin{bmatrix} x_u & y_u \end{bmatrix} \cdot \begin{bmatrix} x_1 & y_1 \\ x_2 & y_2 \end{bmatrix}^{-1} \cdot \begin{bmatrix} d_{ion,1} - d_{ion,3} \\ d_{ion,2} - d_{ion,3} \end{bmatrix} \tag{3-29}$$

Note that the single-differenced TEC interpolation coefficients are not dependent on the satellite, and only dependent on the user receiver and reference stations positions. Therefore, for any two satellites, the double-differenced TEC can be derived from the interpolated single-differenced TEC (equation (3-28)) as:

$$\nabla\Delta TEC_{u,3} = \begin{bmatrix} x_u & y_u \end{bmatrix} \cdot \begin{bmatrix} x_1 & y_1 \\ x_2 & y_2 \end{bmatrix}^{-1} \cdot \begin{bmatrix} \nabla\Delta TEC_{1,3} \\ \nabla\Delta TEC_{2,3} \end{bmatrix} \tag{3-30}$$

where $\nabla\Delta TEC_{1,3}$ and $\nabla\Delta TEC_{2,3}$ can be determined by:

$$\nabla\Delta TEC_{i,3}(k) = \frac{1}{\alpha} \cdot \frac{f_2^2}{f_1^2 - f_2^2} \cdot \left(\left(\nabla\Delta\phi_{i,3}^{L1}(k) - \lambda_1 \cdot \nabla\Delta N_{i,3}^{L1} \right) - \left(\nabla\Delta\phi_{i,3}^{L2}(k) - \lambda_2 \cdot \nabla\Delta N_{i,3}^{L2} \right) \right) \tag{3-31}$$

if the double-differenced integer ambiguities for reference stations 1 and 3, and for reference stations 2 and 3 are known.

The data from reference stations should be processed first in order to determine the integer ambiguity set and subsequently for the ionospheric model determination. The initial ambiguity set for dual-frequency data can be determined when the system is initially set up, and then real-time ambiguity recovery techniques can be employed to maintain ambiguity continuity (Blewitt, 1990; Han, 1995b). The double-differenced TEC can be determined relative to the reference station and the reference satellite at each epoch. The reliable fixing of the double-differenced ambiguities of a newly risen satellite may require a half hour, or longer, period of observations. As long as the ambiguities of a particular satellite cannot be fixed, no ionospheric corrections can be applied to determine the ionospheric model for this satellite. This procedure can be implemented in real-time, or near real-time.

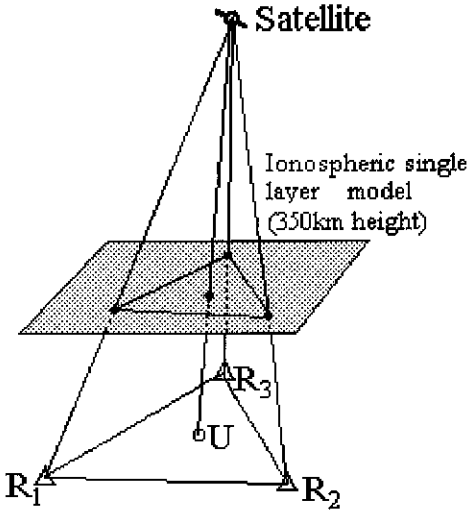

Figure 3-5. Differential model of the ionospheric delays

3.3.3 An Example of Ionospheric Delay Interpolation

An experiment was carried out on the 2nd July, 1996, using two stationary dual-frequency GPS receivers and a receiver on a car (a dual-frequency receiver which can be used to check the accuracy of the ionospheric delay interpolation). The trajectory was almost a straight line and is shown in Figure 3-6. If the roving receiver offsets from the line joining the two reference receivers are ignored, the ionospheric delay for the moving receiver can be interpolated using the ionospheric delay of one fixed receiver relative to the reference receiver.

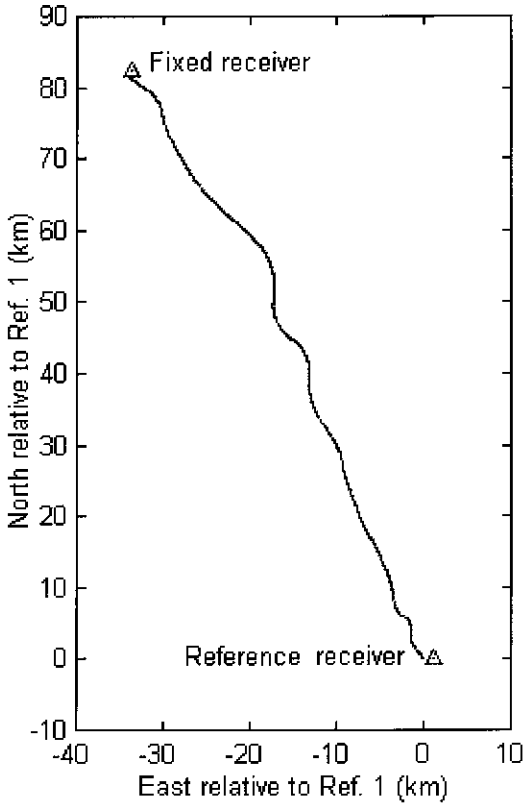

Figure 3-6. Trajectory of the moving receiver on 2 July, 1996, Sydney, Australia

The double-differenced ionospheric delay on L1 for the fixed receiver and satellite PRN18 can be computed using equations (3-31) and (3-21) relative to the reference receiver and reference satellite PRN14. This is plotted in Figure 3-7a. The elevations of the two satellites are also plotted in Figure 3-7a. Linear interpolation was used to estimate the ionospheric delay on L1 for the roving receiver and satellite PRN18 at each epoch, and the results are also plotted in Figure 3-7b. The distances from the roving receiver to the reference receiver are plotted in Figure 3-7b. Since the roving receiver is a dual-frequency receiver, the ionospheric delay on L1 can be computed directly, and this is plotted in Figure 3-7c, if the integer ambiguity set for the roving receiver is determined. It can be seen that the ionospheric delay on L1 increases with increasing distance between the roving receiver and the reference receiver. The difference between the measured ionospheric delays and the interpolated values are plotted in Figure 3-7d. The ionospheric delay residuals do not depend on distance, and most likely reflect multipath and random noise. The mean value of the offset is about 4mm.

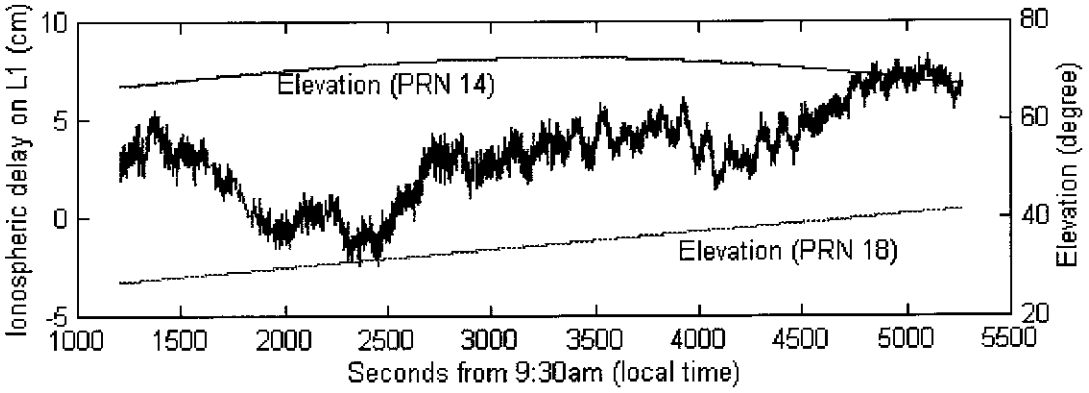

Figure 3-7a. Measured double-differenced ionospheric delays on L1 for the fixed and reference receivers (baseline length 85.378km), and elevation of the reference satellite (PRN14) and the satellite PRN18

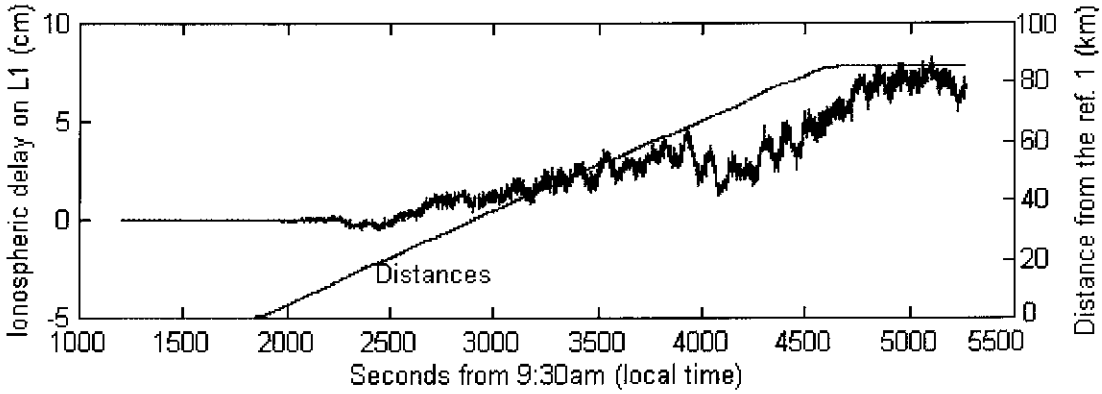

Figure 3-7b. The interpolated double-differenced ionospheric delays on L1 for the roving receiver relative to the reference receiver, and the distances between two receivers

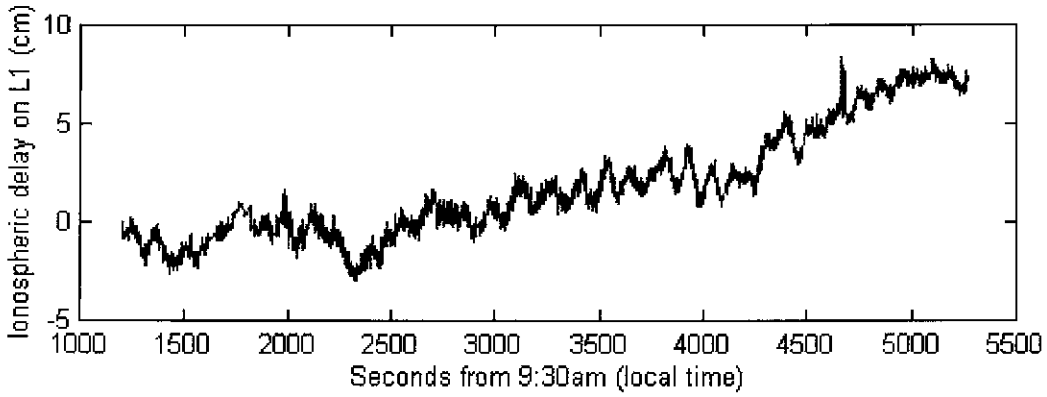

Figure 3-7c. The measured double-differenced ionospheric delays on L1 of the same satellites for the roving receiver relative to the reference receiver derived from dual-frequency observations

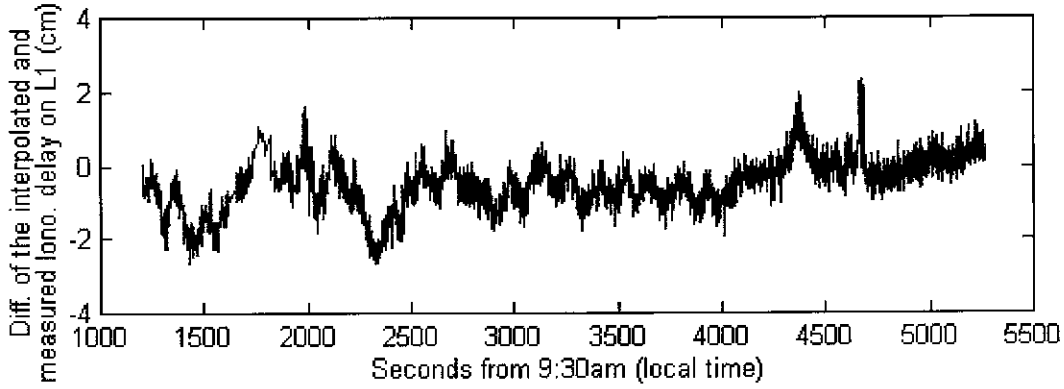

Figure 3-7d. Differences between the interpolated double-differenced ionospheric delays and the measured values

3.4 Tropospheric Delay

The neutral atmosphere is a non-dispersive medium at microwave frequencies. The effect of the neutral atmosphere is represented by the tropospheric refraction, which also includes stratospheric refraction (Brunner & Welsch, 1993). The delay therefore has to be measured, or estimated, from one of a number of models. The requirement of the model is the ability to estimate the integral of refractivity along the line-of-sight. The refractivity can be represented as:

$$N = N_d + N_w \tag{3-32}$$

N_d is a dry component of refractivity which is proportional to the total density of air, and its variability is very small. The height can be extended to 40 km, which is in the stratosphere region. N_w is the wet component of refractivity which is mainly dependent on the density of the water vapour contained in the air. Wet refractivity profiles show quite strong variations with height, time, and location. Hence the wet component of refractivity is very difficult to predict.

The range bias experienced by a signal propagating from a GPS satellite to the ground may be expressed by an integration of refractivity along the line-of-sight:

$$d_{trop} = d_{trop,d} + d_{trop,w} \tag{3-33}$$

where

$$d_{trop,d} = 10^{-6} \cdot \int N_d ds \tag{3-34}$$

$$d_{trop,w} = 10^{-6} \cdot \int N_w ds \tag{3-35}$$

Approximate models for the dry and wet refractivity at the earth's surface are expressed as:

$$N_d(0) = 77.64 \cdot \frac{p}{T} \tag{3-36}$$

$$N_w(0) = -12.96 \cdot \frac{e}{T} + 3.718 \times 10^5 \cdot \frac{e}{T^2} \tag{3-37}$$

where p is the atmospheric pressure in millibar (mbars), T is the temperature in Kelvin (K) and e is the partial pressure of water vapour in mbars.

The Hopfield model assumes that the dry and wet refractivity can be represented as functions of the height h above the surface (Hopfield, 1969):

$$N_d(h) = N_d(0) \cdot \left(\frac{h_d - h}{h_d} \right)^4 \tag{3-38}$$

and

$$N_w(h) = N_w(0) \cdot \left(\frac{h_w - h}{h_w} \right)^4 \tag{3-39}$$

respectively, and the heights associated with the dry and wet refractivities is approximated by (in metres):

$$h_d = 40136 + 148.72(T - 273.16) \tag{3-40}$$

$$h_w = 11000 \tag{3-41}$$

The integral can be solved if the delay is calculated along the vertical direction.

$$d_{trop,d}(90) = 10^{-6} \cdot \int_0^{h_d} N_d(h)dh = \frac{10^{-6}}{5} \cdot N_d(0) \cdot h_d \tag{3-42}$$

$$d_{trop,w}(90) = 10^{-6} \cdot \int_0^{h_w} N_w(h)dh = \frac{10^{-6}}{5} \cdot N_w(0) \cdot h_w \tag{3-43}$$

For an arbitrary elevation angle E (in degrees) at the observing site, the following mapping functions for dry and wet components are used by Hopfield model:

$$m_d(E) = \frac{1}{\sin\sqrt{E^2 + 6.25}} \tag{3-44}$$

$$m_w(E) = \frac{1}{\sin\sqrt{E^2 + 2.25}} \tag{3-45}$$

The troposphere delay at an elevation angle E can be expressed (in metres) as:

$$d_{trop}(E) = d_{trop,d}(90) \cdot m_d(E) + d_{trop,w}(90) \cdot m_w(E) \tag{3-46}$$

The dry component delay accounts for about 90% of the total tropospheric delay and can be modelled with sub-millimetre accuracy, provided accurate pressure measurements are available (Davis et al., 1985). The accuracy of the zenith wet delay as computed by models using surface meteorological measurements is typically no better than a few centimetres (Mendes & Langley, 1995). Many other tropospheric delay models, such as the modified Hopfield model (Goad & Goodman, 1974), Saastamoinen model (1973), Black model (Black, 1978), Shi model (1988) have also been proposed.

For high precision, static applications, the tropospheric delay can be accounted for by measurement correction using a meteorological model, such as the Hopfield model, plus the estimation of local tropospheric scale factors. Local tropospheric scale factors can be modelled as first order Gauss-Markov or random walk processes with temporal correlations (Dodson et al., 1996; Chen, 1994).

For precise airborne GPS navigation, the Altshuler model, NATO model and UNB1 model are preferred, which do not need input of surface meteorological data. The UNB1 model is derived from the Saastamoinen zenith delay model and uses the Niell mapping function, and has demonstrated good performance (Collins & Langley, 1996).

3.5 Multipath and Antenna Phase Centre Biases

3.5.1 Characteristics of Multipath

Multipath is a phenomenon whereby a signal arrives at a receiver site via two or more different paths due to reflections from nearby objects such as buildings, the ground, vehicles, etc. These effects are periodic features and are repeated if the antenna environment is constant. For example, flat ground reflection will cause multipath, with a particular frequency characteristic (Johnson et al., 1995), and the multipath effect will repeat every sidereal day for a static GPS receiver if the environment is unchanged.

If the direct and indirect signals interfere at the antenna electrical centre, they may be represented by (Leick, 1995):

$$V_d = A\cos\varphi \tag{3-47}$$

$$V_i = \alpha A\cos(\varphi + \Delta\varphi) \tag{3-48}$$

the measured signal is:

$$V_m = V_d + V_i = A_m\cos(\varphi + \Delta\varphi_m) \tag{3-49}$$

where A and φ denote the amplitude and phase of the direct signal; α is the attenuation factor of the indirect signal, which is dependent on the reflected surface and ranges from 0 to 1, and $\Delta\varphi$ is the phase shift, which is a function of the geometric configuration. A_m and $\Delta\varphi_m$ can be represented by:

$$A_m = A\cdot\sqrt{1+\alpha^2+2\alpha\cos(\Delta\varphi)} \tag{3-50}$$

$$\Delta\varphi_m = \tan^{-1}\left(\frac{\alpha\sin(\Delta\varphi)}{1+\alpha\cos(\Delta\varphi)}\right) \tag{3-51}$$

It can be shown that there is no multipath effect if $\alpha = 0$, but there is a maximum effect on phase measurements when $\Delta\varphi_m = 90^0 = \frac{1}{4}$cycle if $\alpha = 1$ and $\Delta\varphi = 180^0$.

The different reflecting surfaces and geometry will cause different indirect signals. If the only reflected signals come from the ground, as shown in Figure 3-8, the phase shift can be derived as:

$$\Delta\varphi = \frac{\Delta R}{\lambda} \cdot 2\pi + \pi = \frac{4\pi H \sin E}{\lambda} + \pi \tag{3-52}$$

where H is the height of the antenna above the ground, and E is the satellite elevation angle. The reflection will cause 180^0 phase shift.

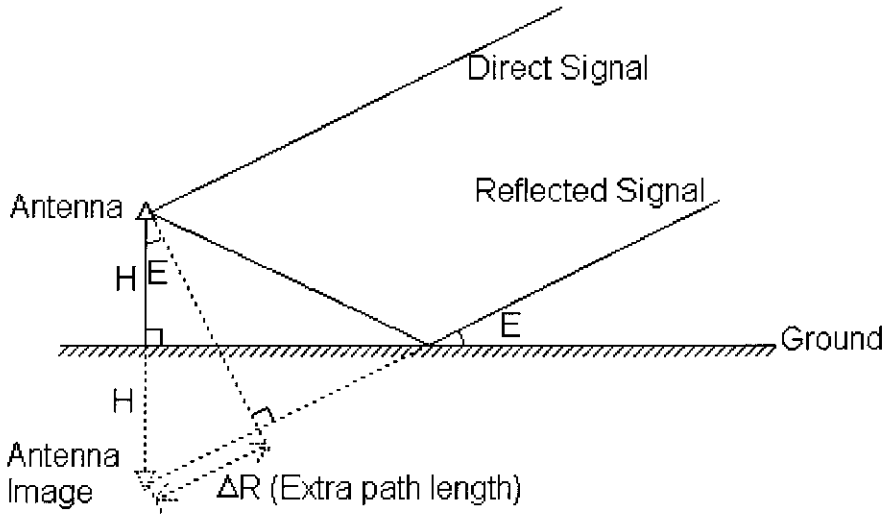

Figure 3-8. Multipath caused by ground surface

If it is assumed that H=1.7 m, A=1.0 and $\alpha = 0.1$, the multipath on L2 carrier phase can be computed by equations (3-51) and (3-52), and plotted in Figure 3-9a. The frequency representation is shown in Figure 3-9b using discrete Fourier transformation (DFT). In a similar way, the amplitude of the measured signal is plotted in Figure 3-10a, and the spectrum in Figure 3-10b. The main frequency component is in the band from 1/300Hz to 1/2000Hz, and is almost the same for amplitude and phase shift.

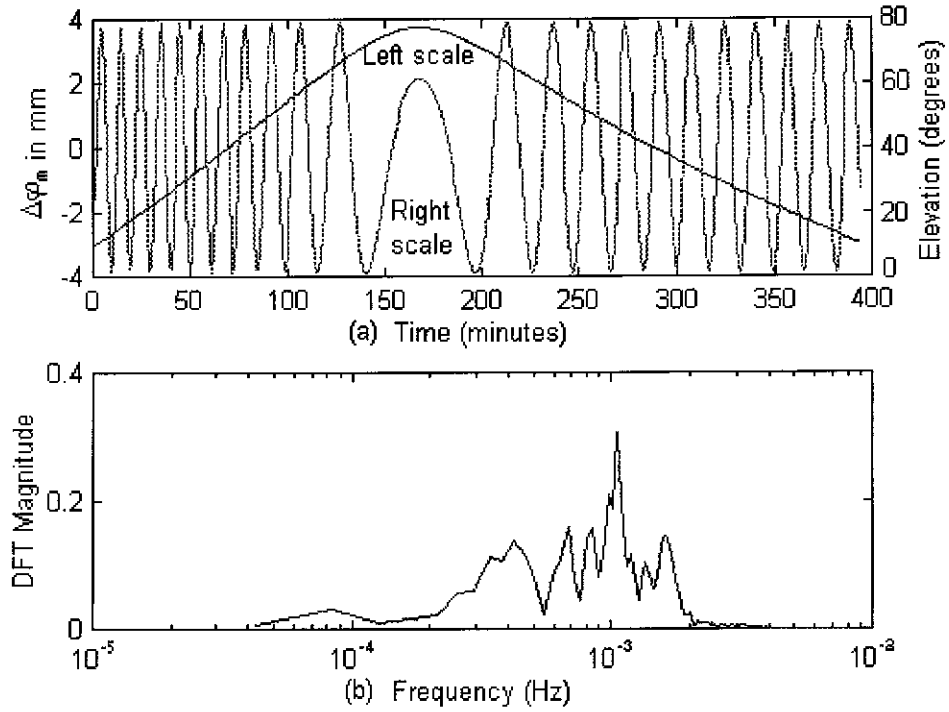

Figure 3-9. Simulated multipath on L2

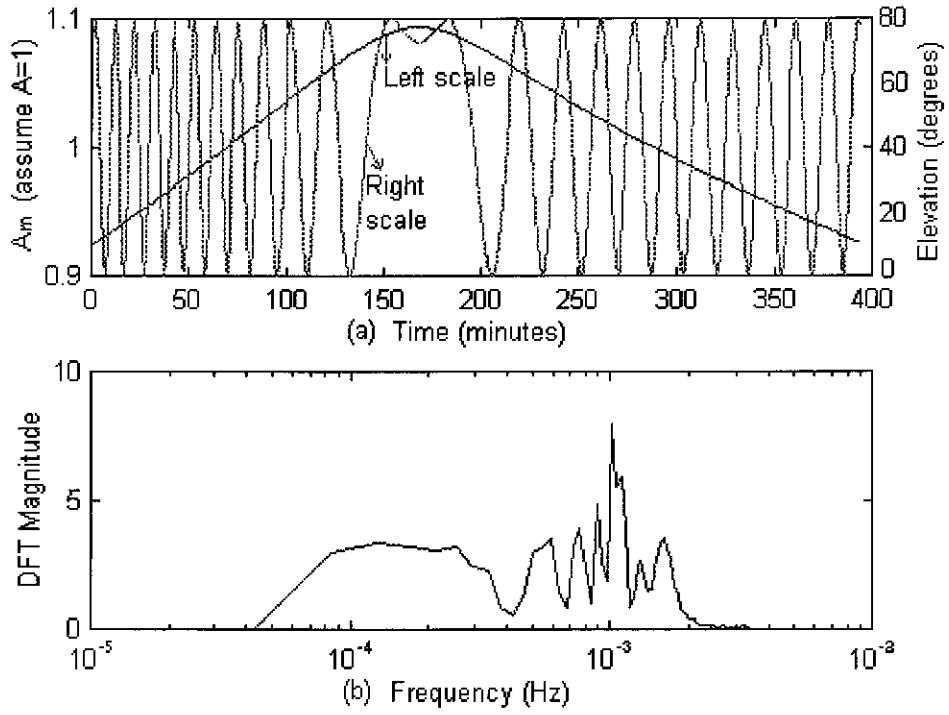

Figure 3-10. Amplitude of the measured signal affected by simulated multipath

3.5.2 Multipath Mitigation Methods

Several methods to mitigate multipath have been suggested in the last few years. Preparing maps of the multipath environment surrounding an antenna has been suggested, to determine multipath corrections for each satellite signal as a function of its azimuth and elevation (Haji, 1990; Cohen & Parkinson, 1991; Clark, 1992). The limitation of such methods is that they only work well if the antenna environment remains constant. Georgiadou & Kleusberg (1988b) describe methods for identifying the presence of multipath by looking at the difference between L1 and L2 phase observation. Axelrad et al. (1994) suggest that it may be possible to identify and eliminate multipath sources by analysing SNR values of the GPS signals. They propose to identify multipath reflectors by isolating sections of the SNR data with strong spectral peaks. From the frequency of these peaks, it would then be possible to generate a model of the phase errors introduced. Due to the periodic feature of the multipath, if the observation span is one hour or more, the multipath effect can be significantly reduced for static positioning. But the multipath will affect the positioning results by up to a few centimetres for rapid static positioning (observation span of the order of a few minutes) and kinematic positioning.

Multipath can be reduced significantly by using a Finite Impulse Response (FIR) bandstop filter for a particular frequency band, or extracted using a FIR bandpass filter. For example, the multipath model can be determined by analysing residual sequences from the data collected over the previous days using a FIR bandpass filter, and applying this multipath correction to the current day's data. The ionospheric delay in Figure 3-7a has been filtered using a FIR filter. Since the high frequency terms are expected to be filtered out, the FIR lowpass filter is designed using the Parks-McClellan method, with a cutoff frequency of 1/600 Hz, a stop frequency of 1/300 Hz, a passband ripple of 0.01 and a stopband ripple of 0.1 (Kraus et al., 1994). The length of the filter is 810, and hence the filter delay is 405 seconds. The magnitude of the response is shown in Figure 3-11. The filtered double-differenced ionospheric delays on L1 for the fixed and reference receivers are plotted in Figure 3-12. It can be seen that although the high frequency (multipath and noise) effects have been removed, the low frequency ionospheric delay signal is preserved.

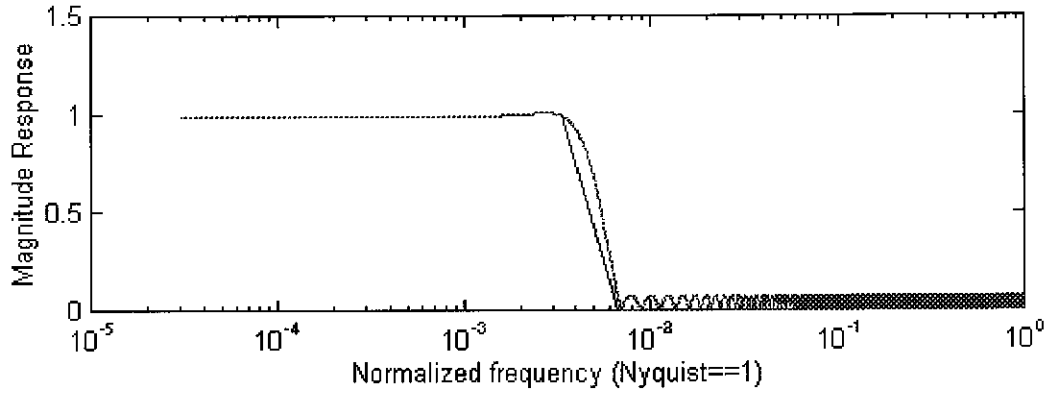

Figure 3-11. Magnitude response of FIR lowpass filter

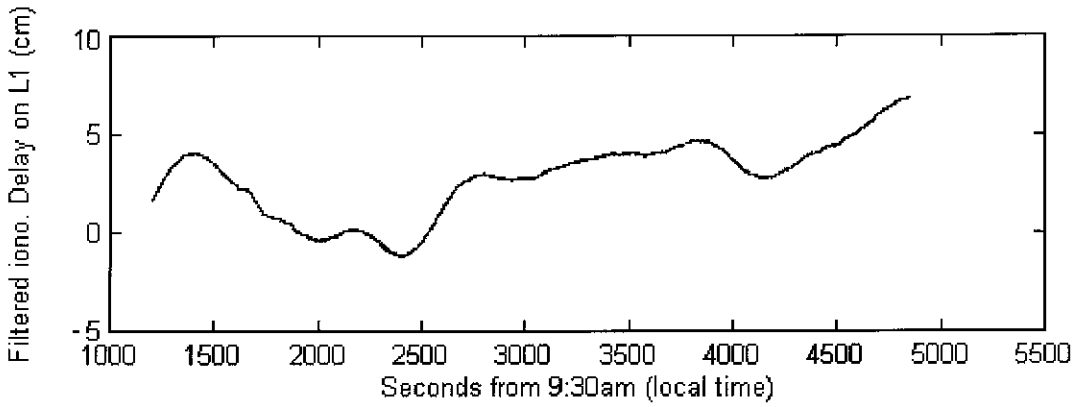

Figure 3-12. Filtered sequences of Figure 3-7a

Multipath can also be *extracted* by assuming that the multipath should be within the frequency band from 1/600 Hz to 1/60 Hz, and that only multipath influences are located in this band. The FIR bandpass filter can be designed using the Parks-McClellan method, with the passband from 1/600 Hz to 1/60 Hz, with a 1/1200 Hz transition band, passband and stopband ripples of 0.1. The magnitude of the response is shown in Figure 3-13. The length of the filter is 848, and hence the filter will have a 424 second delay. The filtered sequence is plotted in Figure 3-14 (which is assumed to be the multipath, under the assumptions made above). In practice, the multipath numerical model would be extracted from the residual sequences of the previous days' data, and then used to correct the current day's data. For kinematic positioning, the multipath can be extracted from the residuals and then the trajectory can be computed using the corrected observations to improve the trajectory accuracy. However, the FIR filter will have a delay (half the length of the FIR filter delay - normally a few minutes) for the estimated ionospheric delay and therefore can only be used for *near* real-time applications. The cutoff

frequency can be determined from the spectral analysis of the signal-to-noise ratio output by GPS receiver (Axelrad et al., 1994).

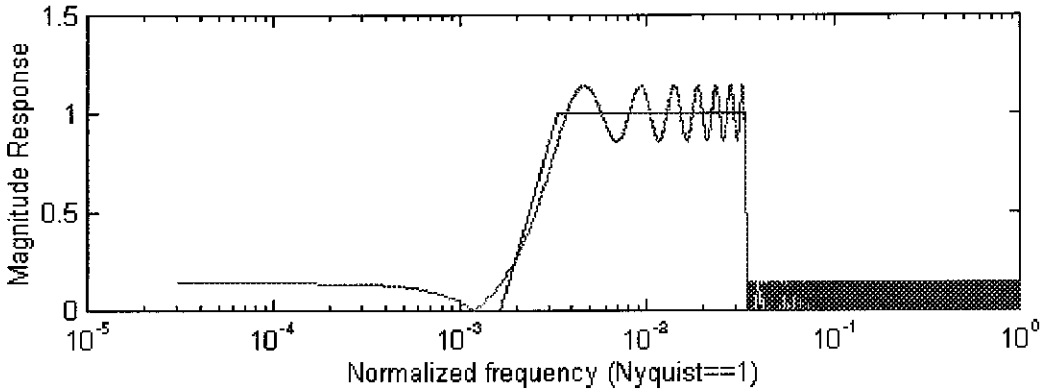

Figure 3-13. Magnitude response of FIR bandpass filter

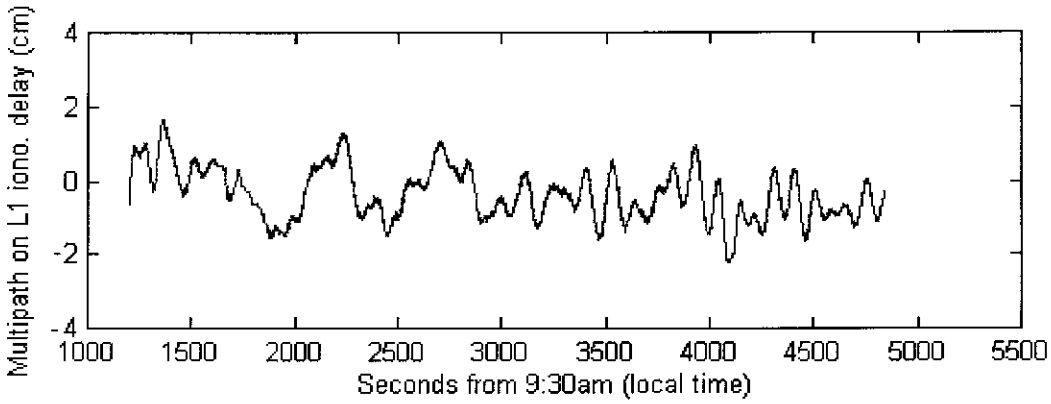

Figure 3-14. Multipath extraction by FIR bandpass filter from Figure 3-7a

3.5.2 Offset Biases Dependent on Receivers and Antennas

The offset bias which is dependent on the antenna is the antenna phase centre offset and variation. The phase centre of the antenna is the point to which the radio signal measurement is referred and generally is not coincident with the physical antenna centre. The offset depends on the elevation, azimuth, and intensity of the satellite signal, and is different for L1 and L2. The antenna phase centre offsets for different kinds of GPS receivers relative to the Turbo Rogue receiver with the Dorne Margolin T antenna have been determined by the International GPS Service for Geodynamics (IGS report on http://igscb.jpl.nasa.gov/, 1996). The offset components in the north and east direction

can reach 5mm. The antenna component in height can reach 3cm, and changes significantly with elevation angle. Figure 3-15 is an example of the antenna offset component in height as a function of satellite elevation from IGS report referred to earlier. The north, east and height (90 degree) components are 1.5mm, -1.2mm and 5.1mm for L1 and -1.1mm, 1.7mm and 1.2mm for L2 (ibid, 1996).

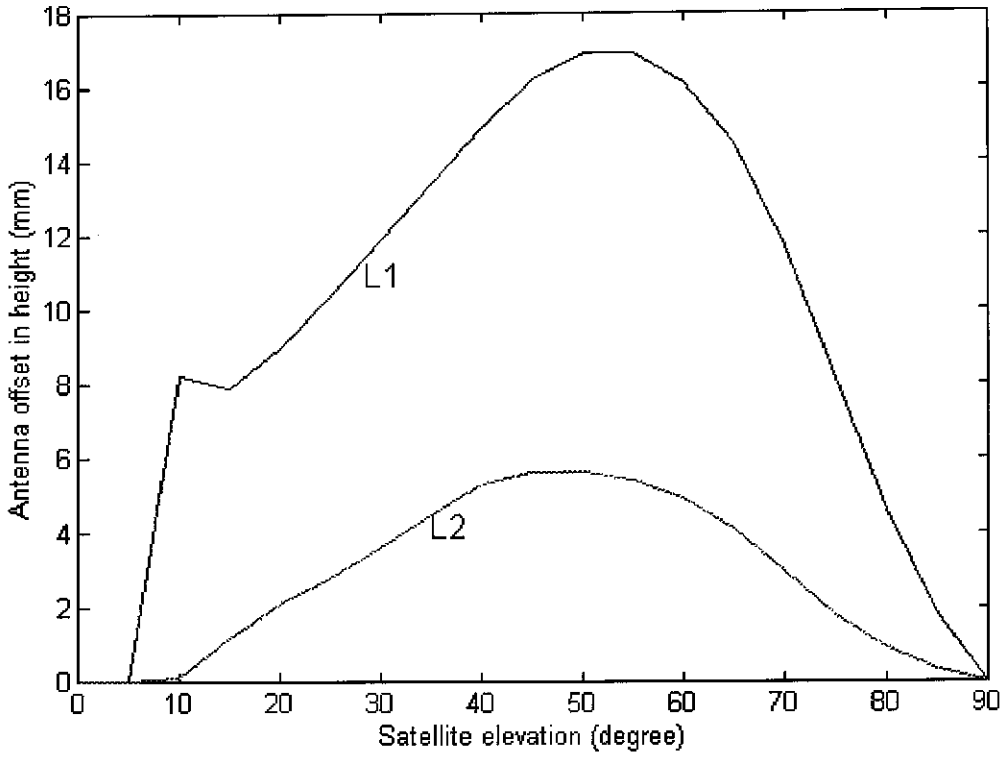

Figure 3-15. Antenna offset change in height component with satellite elevation

If the same kind of GPS receivers and antennas are assumed to have the same antenna offset characteristics, and the antennas are oriented in the same direction, the antenna offset can be ignored for baseline determination using the data double-differencing algorithm. But if different kinds of GPS antennas are used for baseline determination, antenna offsets should be considered carefully in order to achieve millimetre accuracy. Therefore, GPS antenna offset determination and correction will become necessary for precise GPS positioning.

The bias which is dependent on the type of GPS receiver is due to the manner in which different receivers internally process the carrier phase signals. A zero baseline experiment has been performed by Braun & Rocken (1995) using the same antenna

(Trimble 4000ST L1/L2 Geod antenna) and two different types of GPS receivers from the same manufacturer (Trimble 4000SST and Trimble 4000SSE). The results indicate that vertical height error can be up to five centimetres, even when using one hour observation spans! The mixed receiver problem seems to average out over 16 hour observation sessions. Intensive research on this bias is required if millimetre accuracy positioning using mixed GPS receivers is to be routine. Long-range kinematic positioning should also avoid using different GPS receivers.

Chapter 4

AMBIGUITY RESOLUTION ON-THE-FLY FOR MEDIUM-RANGE GPS KINEMATIC POSITIONING

4.1 Introduction

Ambiguity resolution on-the-fly for short-range kinematic positioning assumes that the orbit bias and differential ionospheric delay can be ignored, and the integer ambiguities can be resolved easily. For medium-range or long-range static positioning, the widelane integer ambiguities can be resolved if precise pseudo-ranges on L1 and L2 are available. Then the ionosphere-free combination can be used to resolve the integer ambiguity with wavelength 10.7 cm. Using dual-frequency data sessions of half to one hour in length, with no cycle slips, the integer ambiguities can be resolved (see Appendix B). For long-range kinematic positioning, however, much longer observation spans with no cycle slips will be needed, something which is very difficult in practice (if not impossible) to achieve. Furthermore, this algorithm requires precise ephemeris information, and therefore cannot be used for real-time applications.

A bias analysis has been described in Chapter 3. It was shown that using more than three reference stations with known coordinates, the orbit bias can be eliminated for medium-range applications (less than 100 km to the nearest reference station) through the use of a linear combinations of single-differenced observations. The ionospheric delay relative to one reference station can also be interpolated if the relative ionospheric delay for three or more reference stations are known. Although the bias modelling using multiple reference stations has been developed for pseudo-range based system such as WADGPS (Kee, 1996), the accuracy is not good enough for ambiguity resolution. Even when this concept is used for carrier phase-based systems, the accuracy of the corrected observations will be degraded. In this chapter, a linear combination method has been used to account orbit bias and ionospheric delay. The tropospheric delay, multipath, and observation noise will also be mitigated using this method.

After the distance-dependent biases are eliminated or mitigated, an integrated method which incorporates a three-step quality control procedure is proposed. The integrated method combines the search procedures in the coordinate domain, the observation domain and the estimated ambiguity domain, and uses data from the latest generation of GPS receivers. The three-step procedure for enhancing the quality of ambiguity resolution is as follows. The first step is to improve the stochastic model for the double-differenced functional model *in real-time*. A default model is used at the beginning of a kinematic survey, and then adjusted adaptively by the data. This feature will lead to an improvement in the fidelity of the stochastic model for a specified functional model. The second step is to discriminate between the integer ambiguity sets which generate the minimum quadratic form of the residuals and the second minimum one. The proposed procedure has a rigorous mathematical definition and is more reliable and practical than the standard tests. Numerical comparisons will further support this conclusion. The third step is the fault Detection, Identification and Adaptation (DIA) procedure. In this step a global measure, the TEC value test, using the current and previous results, will be employed. If the ambiguity resolution is unsuccessful, the adaptation procedure will eliminate the identified outlier observations and improve the functional model. Experimental results will demonstrate the utility of the proposed procedure.

4.2 Functional Model for Ambiguity Resolution On-The-Fly using Multiple Reference Receivers

From the earlier analysis of the nature of the orbit bias and its effect on baseline results, it was concluded that the reference stations should be placed outside the survey area. However, for the interpolation of the ionospheric delay, the reference stations should be as close as possible. Figure 4-1 shows a three reference station network with one roving receiver. (▲ denotes the reference stations and ● denotes the local monitoring stations.) It is preferable that one of the reference stations is connected to the IGS network in order to obtain precise positions in the global ITRF frame. Data processing for the reference stations is necessary in order to determine the double-differenced integer ambiguities between them. The methods are described in Appendix B.

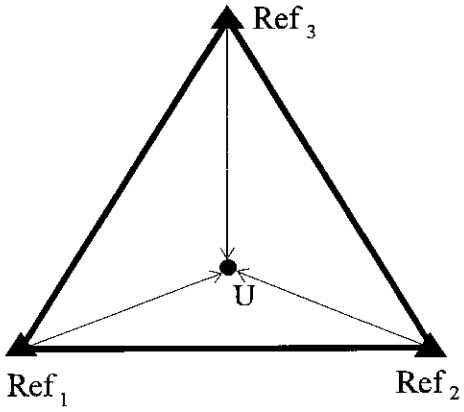

Figure 4-1. Configuration of the reference stations and the roving station

4.2.1 Single-Differenced Functional Model

The single-differenced carrier phase observation can be derived from equation (1-4):

$$\Delta\phi_i = \Delta\rho_i + \Delta d\rho_i - c\cdot\Delta dT_i + \lambda\cdot\Delta N_i - \Delta d_{ion,i} + \Delta d_{trop,i} + \Delta d^{\phi}_{mp,i} + \varepsilon_{\Delta\phi_i} \tag{4-1}$$

where $\Delta(\cdot)_i = (\cdot)_u - (\cdot)_i$, i indicates the reference station i, and u the user station. A set of parameters α_i can be determined, based on the conditions in equations (3-9) and (3-13), that is:

$$\sum_{i=1}^{3}\alpha_i = 1 \tag{4-2}$$

$$\sum_{i=1}^{3}\alpha_i\cdot\Delta\vec{X}_{i,u} = \vec{X}_u - \alpha_1\cdot\vec{X}_1 - \alpha_2\cdot\vec{X}_2 = 0 \tag{4-3}$$

where $\vec{X}_u$ and $\vec{X}_i$ (i=1,2,3) are the coordinates in the Gauss plane coordinate system. (The original point is set up at the reference station 3 in order to simplify the derivation.) Equation (4-3) can be represented as:

$$\begin{bmatrix} x_u \\ y_u \end{bmatrix} = \begin{bmatrix} x_1 & x_2 \\ y_1 & y_2 \end{bmatrix}\begin{bmatrix} \alpha_1 \\ \alpha_2 \end{bmatrix} \tag{4-4}$$

and then α_1 and α_2 can be computed as:

$$\begin{bmatrix}\alpha_1\\ \alpha_2\end{bmatrix}=\begin{bmatrix}x_1 & x_2\\ y_1 & y_2\end{bmatrix}^{-1}\begin{bmatrix}x_u\\ y_u\end{bmatrix} \tag{4-5}$$

The linear combination of the single-differenced observations can be formed as:

$$\sum_{i=1}^{3}\alpha_i\cdot\Delta\phi_i=\sum_{i=1}^{3}\alpha_i\cdot\Delta\rho_i+\sum_{i=1}^{3}\alpha_i\cdot\Delta d\rho_i-c\cdot\sum_{i=1}^{3}\alpha_i\cdot\Delta dT_i+\lambda\cdot\sum_{i=1}^{3}\alpha_i\cdot\Delta N_i-$$

$$-\sum_{i=1}^{3}\alpha_i\cdot\Delta d_{ion,i}+\sum_{i=1}^{3}\alpha_i\cdot\Delta d_{trop,i}+\sum_{i=1}^{3}\alpha_i\cdot\Delta d^{\phi}_{mp,i}+\varepsilon_{\sum_{i=1}^{3}\alpha_i\cdot\Delta\phi_i} \tag{4-6}$$

Orbit bias elimination

The orbit bias term can be easily seen to be:

$$\sum_{i=1}^{3}\alpha_i\cdot\Delta d\rho_i\approx 0 \tag{4-7}$$

from equation (3-14).

Ionospheric delay elimination

The ionospheric delay term can be deduced as:

$$\sum_{i=1}^{3}\alpha_i\cdot\Delta d_{ion,i}=d_{ion,u}-d_{ion,3}-\begin{bmatrix}\alpha_1\\ \alpha_2\end{bmatrix}^{T}\begin{bmatrix}d_{ion,1}-d_{ion,3}\\ d_{ion,1}-d_{ion,3}\end{bmatrix} \tag{4-8}$$

Considering equations (4-5) and (3-29), the above equation can be written as:

$$\sum_{i=1}^{3}\alpha_i\cdot\Delta d_{ion,i}=d_{ion,u}-d_{ion,3}-\begin{bmatrix}x_u & y_u\end{bmatrix}\begin{bmatrix}x_1 & y_1\\ x_2 & y_2\end{bmatrix}^{-1}\begin{bmatrix}d_{ion,1}-d_{ion,3}\\ d_{ion,1}-d_{ion,3}\end{bmatrix}=0 \tag{4-9}$$

Tropospheric delay

The tropospheric delay should be corrected using a tropospheric delay model such as the Hopfield model. The residual part of the tropospheric delay is denoted by d_{trop}. In a

similar manner to the ionospheric delay, the residual part of the tropospheric delay can be expressed as:

$$\sum_{i=1}^{3}\alpha_i \cdot \Delta d_{trop,i} = d_{trop,u} - d_{trop,3} - \begin{bmatrix} x_u & y_u \end{bmatrix} \begin{bmatrix} x_1 & y_1 \\ x_2 & y_2 \end{bmatrix}^{-1} \begin{bmatrix} d_{trop,1} - d_{trop,3} \\ d_{trop,1} - d_{trop,3} \end{bmatrix} \tag{4-10}$$

If it can be assumed that the residual tropospheric delay can be interpolated by the residual tropospheric delay at the reference stations, the residual tropospheric delay should be close to zero. The problem is that the residual tropospheric delay is mostly contributed to by the wet component of the troposphere, which shows strong variation with height, time and location. Geiger et al. (1995) suggest a mitigation method suitable for local and regional GPS networks. From the spatial distribution of water vapour over Ireland (25-28 April, 1995), described by Dodson and Shardlow (1995), a strong spatial correlation still exists and a linear interpolation procedure can be used to predict the wet vapour over an area with 100 km radius with reasonable accuracy. Therefore, the term $\sum_{i=1}^{3}\alpha_i \cdot \Delta d_{trop,i}$ should be mitigated to some extent.

Multipath mitigation

The multipath term can be rewritten as:

$$\sum_{i=1}^{3}\alpha_i \cdot \Delta d^{\phi}_{mp,i} = d^{\phi}_{mp,u} - \sum_{i=1}^{3}\alpha_i \cdot d^{\phi}_{mp,i} \tag{4-11}$$

The last term $\sum_{i=1}^{3}\alpha_i \cdot d^{\phi}_{mp,i}$ on the right hand side of equation (4-11) is the weighted mean value of the multipath values at the three reference stations for this satellite. Due to the random nature of the multipaths at the different stations, the weighted mean value will be significantly reduced if all α_i (i=1,2,3) are positive and less than 1, although the weight α_i is not derived from its standard deviation. On the other hand, the multipath at the roving station will become a high frequency bias, and mostly close to random noise (Zhang & Schwarz, 1996). Therefore, the multipath term has been significantly reduced and will be ignored in the functional model. The residual part of the multipath can be accounted for in the stochastic model.

Observation noise

The standard deviation of the one-way carrier phase observation can be approximated as a function of the elevation angle. Because all stations are located within a region of about 100km radius, the elevation of a satellite is approximately the same. The standard deviation of the one-way carrier phase observation can also be approximated as σ^j and then the standard deviation of the linear combination of single-differenced observations $\varepsilon_{\sum_{i=1}^{3}\alpha_i\cdot\Delta\phi_i}$ can be expressed as:

$$\sigma_{\sum_{i=1}^{3}\alpha_i\cdot\Delta\phi_i} = \sqrt{1+\alpha_1^2+\alpha_2^2+\alpha_3^2}\cdot\sigma^j \tag{4-12}$$

Comparing the standard deviation of the single-differenced carrier phase observation $\sqrt{2}\cdot\sigma^j$, the standard deviation will become smaller if the roving station is located within the triangle formed by the reference stations (Table (3-1)).

The single-differenced carrier phase observation functional model can be simplified as:

$$\sum_{i=1}^{3}\alpha_i\cdot\Delta\phi_i = \sum_{i=1}^{3}\alpha_i\cdot\Delta\rho_i - c\cdot\sum_{i=1}^{3}\alpha_i\cdot\Delta dT_i + \lambda\cdot\sum_{i=1}^{3}\alpha_i\cdot\Delta N_i + \varepsilon_{\sum_{i=1}^{3}\alpha_i\cdot\Delta\phi_i} \tag{4-13}$$

The single-differenced pseudo-range can be derived in the similar way:

$$\sum_{i=1}^{3}\alpha_i\cdot\Delta R_i = \sum_{i=1}^{3}\alpha_i\cdot\Delta\rho_i - c\cdot\sum_{i=1}^{3}\alpha_i\cdot\Delta dT_i + \varepsilon_{\sum_{i=1}^{3}\alpha_i\cdot\Delta R_i} \tag{4-14}$$

4.2.2 Double-Differenced Functional Model

Considering the relation:

$$\sum_{i=1}^{3}\alpha_i\cdot\Delta\phi_i = (\phi_u-\phi_3)-[\alpha_1\cdot(\phi_1-\phi_3)+\alpha_2\cdot(\phi_2-\phi_3)] = \Delta\phi_{u,3}-[\alpha_1\cdot\Delta\phi_{1,3}+\alpha_2\cdot\Delta\phi_{2,3}] \tag{4-15}$$

equation (4-13) can be written as:

$$\Delta\phi_{u,3}-\left[\alpha_1\cdot\Delta\phi_{1,3}+\alpha_2\cdot\Delta\phi_{2,3}\right]=\Delta\rho_{u,3}-\left[\alpha_1\cdot\Delta\rho_{1,3}+\alpha_2\cdot\Delta\rho_{2,3}\right]-c\cdot\sum_{i=1}^{3}\alpha_i\cdot\Delta dT_i+$$

$$+\lambda\cdot\Delta N_{u,3}-\left[\alpha_1\cdot\Delta N_{1,3}+\alpha_2\cdot\Delta N_{2,3}\right]+\varepsilon_{\sum_{i=1}^{3}\alpha_i\cdot\Delta\phi_i} \tag{4-16}$$

The double-differenced observation model can be written as:

$$\nabla\Delta\phi_{u,3}-\left[\alpha_1\cdot\nabla\Delta\phi_{1,3}+\alpha_2\cdot\nabla\Delta\phi_{2,3}\right]=\nabla\Delta\rho_{u,3}-\left[\alpha_1\cdot\nabla\Delta\rho_{1,3}+\alpha_2\cdot\nabla\Delta\rho_{2,3}\right]+$$

$$+\lambda\cdot\nabla\Delta N_{u,3}-\left[\alpha_1\cdot\nabla\Delta N_{1,3}+\alpha_2\cdot\nabla\Delta N_{2,3}\right]+\varepsilon_{\sum_{i=1}^{3}\alpha_i\cdot\nabla\Delta\phi_i} \tag{4-17}$$

Define the residual vectors:

$$V_{1,3}=\nabla\Delta\phi_{1,3}-\nabla\Delta N_{1,3}-\nabla\Delta\rho_{1,3} \tag{4-18}$$

$$V_{2,3}=\nabla\Delta\phi_{2,3}-\nabla\Delta N_{2,3}-\nabla\Delta\rho_{2,3} \tag{4-19}$$

The double-differenced observation model can then be written as:

$$\nabla\Delta\phi_{u,3}-\left[\alpha_1\cdot V_{1,3}+\alpha_2\cdot V_{2,3}\right]=\nabla\Delta\rho_{u,3}+\lambda\cdot\nabla\Delta N_{u,3}+\varepsilon_{\sum_{i=1}^{3}\alpha_i\cdot\nabla\Delta\phi_i} \tag{4-20}$$

The data processing techniques applicable for the reference stations, and the more dispersed continuous GPS stations (e.g. IGS stations) are well known (Dong & Bock, 1989; Blewitt, 1989; Chen, 1994). This mode of data processing is implemented in post-processed mode and the precise ephemeris is used. The first step in the data processing is the detection and repair of cycle slips in the carrier phase data. The procedure for repairing cycle slips is to compute the widelane slip at each observation epoch formed by the widelane carrier phase and the narrowlane precise pseudo-range data, which is also an ionosphere-free combination. Once the wide lane slip is resolved, polynomial fitting to the ionospheric combination is used to extract the cycle slips in the L1 and L2 carrier phase data (e.g. Blewitt, 1990), or by polynomial fitting to the carrier phase combination with the maximum wavelength (14.65m), and using the even-odd relationship to decouple the cycle slips on L1 and L2 (Han, 1995b). The second step is to resolve the integer ambiguities. Since the baseline lengths are typically from tens to hundreds of kilometres (between the reference stations and the wider area continuous GPS stations),

the ambiguity resolution process is not trivial due to the presence of ionospheric and tropospheric delays, even though the external station coordinates are well known and the precise ephemeris is available. A long observation span (at least one hour) will be necessary to determine the integer ambiguities, and then the integer ambiguity set should remain valid for the whole observation span. For rising satellites, new integer ambiguity parameters will have to be estimated, again requiring a sufficiently long observation span. The coordinates of the reference stations should be derived using the ionosphere-free phase combination, and the integer ambiguities should be fixed. Using these positions and the known integer ambiguities, the correction vectors $V_{1,3}^{L1}$, $V_{1,3}^{L2}$, $V_{1,3}^{R_1}$ and $V_{1,3}^{R_2}$ for the double-differenced carrier phase observations and pseudo-ranges on L1 and L2 can be computed for reference stations 1 and 3. $V_{2,3}^{L1}$, $V_{2,3}^{L2}$, $V_{2,3}^{R_1}$ and $V_{2,3}^{R_2}$ are computed in the same way for reference stations 2 and 3.

For real-time applications, the precise positions should be determined in a previous step. The real-time ambiguity recovery technique should be implemented to ensure that the integer ambiguities remain known, and the correction vectors can then be computed in real-time. The correction vectors, together with the carrier phase and pseudo-range data at reference station 3, can be sent to the roving receiver in real-time.

In summary, the double-differenced functional model for carrier phase observations and pseudo-ranges on L1 and L2 can be written as:

$$\nabla\Delta\phi_{u,3}^{L1} - \left[\alpha_1 \cdot V_{1,3}^{L1} + \alpha_2 \cdot V_{2,3}^{L1}\right] = \nabla\Delta\rho_{u,3} + \lambda_1 \cdot \nabla\Delta N_{u,3}^{L1} + \varepsilon_{\sum_{i=1}^{3}\alpha_i \cdot \nabla\Delta\phi_i^{L1}} \tag{4-21a}$$

$$\nabla\Delta\phi_{u,3}^{L2} - \left[\alpha_1 \cdot V_{1,3}^{L2} + \alpha_2 \cdot V_{2,3}^{L2}\right] = \nabla\Delta\rho_{u,3} + \lambda_2 \cdot \nabla\Delta N_{u,3}^{L2} + \varepsilon_{\sum_{i=1}^{3}\alpha_i \cdot \nabla\Delta\phi_i^{L2}} \tag{4-21b}$$

$$\nabla\Delta R_{u,3}^{L1} - \left[\alpha_1 \cdot V_{1,3}^{R_1} + \alpha_2 \cdot V_{2,3}^{R_2}\right] = \nabla\Delta\rho_{u,3} + \varepsilon_{\sum_{i=1}^{3}\alpha_i \cdot \nabla\Delta R_i^{L1}} \tag{4-21c}$$

$$\nabla\Delta R_{u,3}^{L2} - \left[\alpha_1 \cdot V_{1,3}^{R_2} + \alpha_2 \cdot V_{2,3}^{R_2}\right] = \nabla\Delta\rho_{u,3} + \varepsilon_{\sum_{i=1}^{3}\alpha_i \cdot \nabla\Delta R_i^{L2}} \tag{4-21d}$$

In order to efficiently remove orbit bias and ionospheric delay, and reduce tropospheric delay, the distance from roving receiver to the nearest reference GPS should be less than 100 km.

4.3 Integrated Method for Ambiguity Resolution

Centimetre accuracy GPS kinematic positioning applications are most appropriately addressed if the estimation of the integer ambiguity parameters can be carried out either instantaneously (on a single epoch basis), or on-the-fly. Three general classes of ambiguity resolution techniques have been developed in the last decade: search techniques in the *measurement domain* (Abidin & Wells, 1990; Goad, 1992; Han, 1995b; Han & Rizos, 1995a; Teunissen, 1996b; Wübbena, 1989); search techniques in the *coordinate domain* (Han, 1994b; Han & Rizos, 1996b; Lachapelle et al., 1992; Mader, 1992; Mok, 1996; Mok & Cross, 1996; Remondi, 1989; Remondi & Hilla, 1993), and; search techniques in the *estimated ambiguity domain* using least squares estimation (Chen & Lachapelle, 1995; Frei et al., 1993; Han, 1995a; Han & Rizos 1995b; Hatch, 1990; Landau & Euler, 1992; Teunissen, 1994). New generation GPS receivers such as the Ashtech Z12, the Leica System 300 and the Trimble 4000SSi output precise pseudo-range and full wavelength carrier phase observations on both frequencies, even with Anti-Spoofing on. All three general classes of ambiguity resolution techniques can be integrated so as to take advantage of their most positive characteristics, such as search efficiency or reliability, and hence make ambiguity resolution more certain (Han & Rizos, 1996c).

4.3.1 The Integrated Method

The traditional functional model for ambiguity resolution used carrier phase observations only because the C/A pseudo-range data was not precise enough to contribute very much to improving the ambiguity-float solution. This meant that quite a long observation session (a few minutes in the case of dual-frequency receivers, or more than 15 minutes for single frequency GPS receivers) was typically required to obtain an ambiguity-float solution which was accurate enough for the reliable resolution of the integer ambiguities (Han, 1994c). However, the new generation GPS receivers output precise pseudo-range data on L1 and L2, and these observations will significantly improve the ambiguity-float solution using only a short period of data or, at an extreme, even using only a single epoch of data (Han, 1996; Han & Rizos, 1996c).

If only one epoch of data is used, the float solution (using precise pseudo-range and carrier phase measurements) will have no contribution from carrier phase measurements. Hence, relative positioning using pseudo-range data on L1 and L2 will be used to

estimate the coordinate parameters $\hat{X}_C$ and the co-factor matrix $Q_{\hat{X}_C}$. The float solution for $\hat{X}_N$ can then be computed, with variance-covariance matrix:

$$Q_{\hat{X}_N} = \begin{bmatrix} \frac{1}{\lambda_1^2}\left(Q_{L_1} + A_1 Q_{\hat{X}_C} A_1^T\right) & \frac{1}{\lambda_1\lambda_2} A_1 Q_{\hat{X}_C} A_2^T \\ \frac{1}{\lambda_1\lambda_2} A_2 Q_{\hat{X}_C} A_1^T & \frac{1}{\lambda_2^2}\left(Q_{L_2} + A_2 Q_{\hat{X}_C} A_2^T\right) \end{bmatrix} \tag{4-22}$$

$$Q_{\hat{X}_C\hat{X}_N} = \begin{bmatrix} \frac{1}{\lambda_1} Q_{\hat{X}_C} A_1^T & \frac{1}{\lambda_2} Q_{\hat{X}_C} A_2^T \end{bmatrix} \tag{4-23}$$

Where Q_{L_1} and Q_{L_2} are the co-factor matrices for the L1 and L2 carrier phase observations respectively; A_1 and A_2 are the design matrices for the L1 and L2 carrier phase observations; and λ_1 and λ_2 are the wavelengths of the L1 and L2 carrier waves.

If more than one epoch of data are used, $\hat{X}_C$, $\hat{X}_N$ and the covariance matrices $Q_{\hat{X}_C}$, $Q_{\hat{X}_N}$ and $Q_{\hat{X}_C\hat{X}_N}$ should be estimated using all the available observations, and the number of coordinate parameters will become three times the number of epochs.

In order to simplify the computation for the test at equation (2-25), the Cholesky decomposition of $Q_{\hat{X}_C}^{-1}$:

$$Q_{\hat{X}_C}^{-1} = C \cdot C^T \tag{4-24}$$

is used and then yields (see equation (2-380 and (2-39)):

$$f_k = C^T Q_{\hat{X}_C,\hat{X}_N} Q_{\hat{X}_N}^{-1} Z^{-1}\left(\hat{X}_N^Z - N_k^Z\right) \tag{4-25}$$

which can be used to simplify equation (2-25) as:

$$f_k^T f_k \le t \cdot m_0^2 \cdot \xi_{F_{t,n-t-m};1-\alpha} \tag{4-26}$$

where $C^T Q_{\hat{X}_C,\hat{X}_N} Q_{\hat{X}_N}^{-1} Z^{-1}$ is computed outside the search loop. After the integer ambiguities are fixed, equations (2-15, 2-16 and 2-17) can be used to compute the ambiguity fixed solution.

4.3.2. Comparison with Existing Methods

Search procedure in the coordinate domain

The usual search procedure in the coordinate domain is the Ambiguity Function Method (Han, 1994b; Remondi & Hilla, 1993; Mader, 1992). The relationship between the AFM and the least squares method has been discussed in Lachapelle et al. (1992), Han (1993 & 1994a). The $\hat{X}_C$ makes the Ambiguity Function's value a maximum if and only if $\hat{X}_C$ causes the quadratic form of the residuals V^TPV to be a minimum. The initial search region for the AFM is formed using equation (2-25), and the criterium for the optimal solution is that which makes the ambiguity function value a maximum. This means that the optimal solution should satisfy equation (2-25) with V^TPV as minimum. These two criteria have been included in the integrated procedure. The problem for the AFM is that it requires a comparatively long computation time, and it is not easy to consider the stochastic model of the observations.

Search procedure in the observation domain

Ambiguities can be determined directly using pseudo-range and carrier phase observations (Abidin & Wells, 1990; Goad, 1992; Han, 1995b; Han & Rizos, 1995a; Wübbena, 1989). The problem is that the noise of the pseudo-range data is generally very large, compared to the carrier phase wavelength, to effectively determine the integer ambiguities using pseudo-range data alone. Therefore, integer linear combinations of the L1 and L2 observations which have a relatively long wavelength, low noise characteristics and a reasonably small ionospheric delay, such as the so-called widelane, extra-widelane combinations, and others, have generally been used. However, these techniques are all restricted to integer linear combinations of the single-channel variety. This implies that the relative receiver-satellite geometry, which is so emphatically present in the ambiguity variance-covariance matrix, is not taken into account in the linear combinations (Teunissen, 1994). All combinations of L1 and L2 carrier phase can be considered as special cases of LAMBDA (Teunissen, 1996b). The integrated method uses multi-channel integer linear combinations formed by the LAMBDA transformation, rather than single-channel integer linear combinations which is the general case of the traditional search procedure in the observation domain (ibid, 1996b).

Search procedure in the estimated ambiguity domain

The proposed integrated method is based on the search procedure in the estimated ambiguity domain. The first difference is that the search procedure in the estimated ambiguity domain normally uses the carrier phase observations only, due to the low accuracy of C/A pseudo-range data output by the older generation GPS receivers. The second difference is that the test (2-25) is added as a criteria, as is used in the AFM. The third difference is that the LAMBDA method is used in the search procedure, which is the generalised form of the search procedure in the observation domain when the carrier phase and pseudo-range observations are used together. Therefore, it is possible for the integrated method to resolve integer ambiguity using a single epoch of data. In addition to the above improvements, the integrated method will use a more precise stochastic model, which makes the ambiguity-float solution more reliable.

4.4 Real-Time Stochastic Model Improvement

4.4.1 Characteristics of the "Noise"

Least squares estimation requires that the correct functional model and stochastic model be specified. The biases in observations can be modelled in the functional model as parameters. Due to the range of complex biases in GPS observations, it is often too difficult to incorporate them within the functional model. An alternative is to account for the biases within the stochastic model. If biases affect the GPS observations, a larger standard deviation for the observations can be specified so as to ensure they still have normal distribution characteristics (albeit with a larger uncertainty). This procedure will make the precision of the least squares estimation results more realistic. The stochastic model for one-way GPS pseudo-range observations has been investigated by Jin (1995). However, the stochastic model in this paper not only reflects the stochastic characteristics of the observation noise, but also the residual biases in the functional model of equation (4-21). This will make stochastic model estimation more difficult. The definition of a real-time stochastic model with an adaptive improvement capability is therefore an important innovation.

The functional model has been defined in equation (4-21), which eliminates or mitigates the biases due to orbit error, ionosphere, troposphere, and multipath effects. However, the residual biases from these sources still exist, and contribute to the noise terms. This

makes the noise characteristics more complicated. It is well known that most of the residual biases are dependent on the satellite elevation, and expressed by several models, such as an exponential function of the elevation, or the inverse of the sine of the elevation, and can be used to model the standard deviation of the noise. Here, an exponential function of the elevation is used to represent the standard deviation of the one-way L1 observations for satellite j:

$$\sigma^j = s\cdot\left(a_0 + a_1\cdot\exp(-E^j / E_0)\right) \tag{4-27}$$

where σ^j is the standard deviation of the L1 observations for satellite j with elevation angle E^j; a_0, a_1 and E_0 are approximated by constants, which may be experimentally determined for both carrier phase and pseudo-range observations using different kinds of GPS receivers. Table 4-4 gives some values for one-way carrier phase and pseudo-range observations. The s is a scale factor which is determined from an analysis of real data under the assumption that it is the same for all carrier phase observations (or pseudo-range observations) over a short period. The estimation is carried out using the double-differenced observations in which error propagation is applied to account for the correlations. The standard deviation for one-way L2 carrier phase observations can be roughly approximated by $\sigma\cdot\lambda_2/\lambda_1$, and the standard deviation for one-way L2 pseudo-range observations can be assumed to be the same as for L1 pseudo-range observations for receivers such as the Leica System 300 or Ashtech Z12.

Note that the stochastic model will be influenced by such factors as environmental conditions within the troposphere, the volatility of the ionosphere, multipath effects and receiver type. This model is appropriate for instantaneous ambiguity resolution. For ambiguity resolution on-the-fly however, which seek to determine ambiguities using several minutes of data before the current epoch, the improvement of the stochastic model should include the temporal correlation. The simplified model has been given in Han & Rizos (1995c). Although the temporal correlation will have a significant effect on the *a posteriori* VCV matrix, rather than the parameter estimation results, this will affect the size and shape of the search region for ambiguity resolution, and hence further impact on the reliability of ambiguity resolution.

4.4.2 Geometric Correlations

From the linear combination of the single-differenced observation model for satellite j, the standard deviation of this combination has been derived in equation (4-12). For the

other satellites, similar linear combinations can also be formed and they are independent if their spatial correlation are ignored:

$$VCV_{\sum_{i=1}^{3}\alpha_i\cdot\Delta\phi_i}=\begin{bmatrix}(\sigma^1)^2 & 0 & \cdots & 0\\ 0 & (\sigma^2)^2 & \cdots & 0\\ \vdots & \vdots & \ddots & \vdots\\ 0 & 0 & \cdots & (\sigma^m)^2\end{bmatrix}\cdot\left(1+\alpha_1^2+\alpha_2^2+\alpha_2^2\right) \tag{4-28}$$

m is the number of satellites. The double-difference operator is:

$$\nabla_m=\begin{bmatrix}1 & -1 & 0 & \cdots & 0\\ 1 & 0 & -1 & \cdots & 0\\ \vdots & \vdots & \vdots & \ddots & \vdots\\ 1 & 0 & 0 & \cdots & -1\end{bmatrix}_{(m-1)\times m} \tag{4-29}$$

for a fixed satellite as reference satellite, or

$$\nabla_m=\begin{bmatrix}1 & -1 & 0 & \cdots & 0\\ 0 & 1 & -1 & \cdots & 0\\ \vdots & \vdots & \vdots & \ddots & \vdots\\ 0 & 0 & 0 & \cdots & -1\end{bmatrix}_{(m-1)\times m} \tag{4-30}$$

for sequential satellite differencing. The variance-covariance matrix of the double-differenced observations can be derived as:

$$VCV_{\sum_{i=1}^{3}\alpha_i\cdot\nabla\Delta\phi_i}=\nabla_m\cdot VCV_{\sum_{i=1}^{3}\alpha_i\cdot\Delta\phi_i}\cdot\nabla_m^T \tag{4-31}$$

If the variance-covariance matrix for one reference station can be formed as $VCV_{\nabla\Delta\phi_{u,3}}$, the variance-covariance matrix $VCV_{\sum_{i=1}^{3}\alpha_i\cdot\nabla\Delta\phi_i}$ can be derived from $VCV_{\nabla\Delta\phi_{u,3}}$:

$$VCV_{\sum_{i=1}^{3}\alpha_i\cdot\nabla\Delta\phi_i}=VCV_{\nabla\Delta\phi_{u,3}}\cdot\frac{1+\alpha_1^2+\alpha_2^2+\alpha_3^2}{2} \tag{4-32}$$

4.4.3 Temporal Correlations

The temporal correlation is normally ignored in GPS data processing. However, it really affects the variance-covariance matrix of the estimated real-valued ambiguities and subsequently affects the ambiguity search region and the reliability of ambiguity resolution. If the temporal correlation is ignored, the variance-covariance matrix of the estimated real-valued ambiguities is estimated as $Q_{\hat{X}_N}$. The effect on the co-factor matrix of the estimated real-valued ambiguities by considering the temporal correlation can be approximated by a scale factor s_{temp}, where s_{temp} can be represented (Han & Rizos , 1995c) for the static case by:

$$s_{temp} = \frac{m(1+f)}{m(1-f)+2f} \tag{4-33}$$

where m is the number of the epochs which are used to estimate real-valued ambiguities, f is the temporal correlation coefficient between epochs. The unit weight standard deviation can be re-computed using the residuals ignoring the temporal correlation (ibid, 1995c). On the basis of experimental data, El-Rabbany (1994) derived an exponential covariance function that describes the temporal physical correlations for at a stationary receiver:

$$f(\tau) = \exp(-\frac{\tau}{T}) \tag{4-34}$$

where τ is the time period between epochs in seconds and T is the correlation length in seconds, with a typical value of about 250-350 seconds, for the static case (ibid, 1994). Table 4-1 gives the correlation coefficient for different data rates.

Table 4-1. The correlation coefficient for different data rates (T=260 seconds)

τ_i (sec)	1	5	15	30	60	300	600	900
$f(\tau_i)$	0.996	0.981	0.944	0.891	0.794	0.315	0.099	0.031

4.4.4 Real-Time Stochastic Model Estimation

Although the standard deviations for carrier phase observations and pseudo-range observations are defined by equation (4-27), the magnitudes of the scale factors for

carrier phase and pseudo-range observations have not been determined. The scale factors will weight the contribution of the carrier phase and pseudo-range observations, and also affect the tests in equations (2-22, 2-25 and 2-27). These values are sensitive to the real data (both receiver type and measurement circumstances), and cannot be considered constants.

The scale factor for pseudo-range observations can be estimated using different sections of data. For the first section, $s = s_P^1 = 1$, the default stochastic model is used. For the Lth section, s can be estimated as s_P^L, using the following relation based on the (L-1)th section of data:

$$s_P^L = \frac{\sum_{k=K_{L-1}}^{K_L-1} \Omega_{Float}^k}{\sum_{k=K_{L-1}}^{K_L-1} \left(n_P^k - t^k\right)} \tag{4-35}$$

where K_{L-1} and $K_L - 1$ are the first and last epoch number for section L-1; k is the epoch number; n_P^k, t^k and Ω_{Float}^k are the number of pseudo-range observations, the number of real-valued parameters and the quadratic form of the residuals for the ambiguity-float solution at epoch k, respectively. The section length is selected as 2-5 minutes.

The scale factor for carrier phase observations is derived as:

$$s_\phi^L = \frac{\sum_{k=K_{L-1}}^{K_L-1} \overline{\Omega}_{Fix}^k}{\sum_{k=K_{L-1}}^{K_L-1} \left(n_\phi^k - t^k\right)} \tag{4-36}$$

where n_ϕ^k is the number of carrier phase observations; $\overline{\Omega}_{Fix}^k$ is the quadratic form of the residuals using carrier phase observations only and the fixed integer ambiguities at epoch k.

4.5 Criteria to Validate the Integer Ambiguity Set

Based on the results of the ambiguity-float solution, a large number of integer ambiguity sets will be included within the search region in the estimated ambiguity domain. In

principle, the ambiguity set corresponding to the minimum quadratic form of the residuals should be the correct one. However, due to the presence of noise and unmodelled biases, the quadratic form of the residuals will be biased as well. This will make the discrimination of the integer ambiguity sets more difficult. The standard procedure is to use the ratio test, defined as the ratio of the second minimum quadratic form of the residuals to the minimum quadratic form of the residuals. The critical value is empirically derived or chosen arbitrarily. Although this ratio value is assumed to be an F-distributed statistic (Frei & Beutler, 1990), in reality it is not an F-distributed statistic and, furthermore, the upper boundary defined by the F-distribution is too conservative. Euler & Schaffrin (1990) have derived another ratio test, but the critical value is still too conservative and is often experimentally specified as being the value 2 (Wei & Schwarz, 1995), or 1.5 (Han & Rizos, 1996c). Tiberius & de Jonge (1995) suggest another test to discriminate between the integer ambiguity sets which give the minimum and second minimum quadratic form of the residuals, but the critical value is also experimentally specified.

After the search procedure has been performed using the conditions (equations (2-22, 2-25 and 2-27)), there are three resultant cases: (1) no integer ambiguity set satisfied the above tests and hence ambiguity resolution has failed; (2) only one integer ambiguity set satisfied the above tests, assumed to be the correct integer ambiguity set and used to derive the positioning result; or (3) two or more integer ambiguity sets satisfied the above tests, requiring the application of another test to discriminate the correct set from the others.

4.5.1 Current Procedures

Frei & Beutler (1990) assume that $\Omega_{\text{Fix,sec}}$ and $\Omega_{\text{Fix,min}}$ are χ^2 – distributed and independent statistics, and the F-distribution statistic can then be derived. The following test was employed to distinguish the ambiguity sets:

$$\frac{\Omega_{\text{Fix,sec}}}{\Omega_{\text{Fix,min}}} > \xi_{F_{n-t,n-t};1-\alpha} \tag{4-37}$$

If the above test is passed, the integer ambiguity set which causes the minimum quadratic form of the residuals will be selected as the correct one. Otherwise ambiguity resolution has failed. This test has been extensively used by Abidin (1993), Corbett & Cross (1995), and others. The comparison between equation (4-37) and equation (2-22) has

been discussed in Han & Rizos (1996d). If there are two or more integer ambiguity sets which satisfy equation (2-22), equation (4-37) will automatically not be satisfied under certain conditions (ibid, 1996d). This means that this test is too conservative and sometimes the correct ambiguity resolution is considered to have failed. The reason for this is that $\Omega_{Fix,sec}$ and $\Omega_{Fix,min}$ are dependent. A modified ratio test has been suggested by Landau & Euler (1992), using the critical value of 2.

A rigorous ratio test has been suggested by Euler & Schaffrin (1990):

$$\frac{R_{sec}}{R_{min}} > \gamma(\alpha,\beta_1,\beta_2) \tag{4-38}$$

However, the critical value $\gamma(\alpha,\beta_1,\beta_2)$ is also too conservative to ensure higher success rates. A modified ratio test has been suggested by Wei & Schwarz (1995), using an experimental critical value of 2. If the more accurate stochastic model is used, the critical value can be chosen as small as 1.5 (Han & Rizos, 1996c).

An alternative to the ratio test has been suggested by Tiberius & de Jonge (1995):

$$R_{sec} - R_{min} > \sigma_0^2 \cdot K_2 \tag{4-39}$$

where K_2 is selected as 15, based on experimental data. However, the theoretical basis for K_2 has not been presented.

4.5.2 New Criteria for Discrimination

After the integer ambiguity set N_m giving $\Omega_{Fix,min}$ has been identified, the observation model with the fixed integer ambiguity set is:

$$L - A_N N_m + V = A_C \hat{X} \tag{4-40}$$

The null hypothesis is:

$$H_0 : E\left((L - A_N N_m)/H_0\right) = A_C \tilde{X} \tag{4-41}$$

and the alternative hypothesis is:

$$H_a : E\left((L - A_N N_m)/H_a\right) = A_C \tilde{X} + A_N \tilde{V} \tag{4-42}$$

where ∇ is an outlier parameter vector; and ~ denotes the expectation of the quantity. In order to find the outlier in the direction of $(N_s - N_m)$ and therefore discriminate N_m from N_s, assume that:

$$\nabla = \gamma \cdot (N_s - N_m) \tag{4-43}$$

where γ is a real-valued parameter and equation (4-40) becomes:

$$L - A_N N_m + V = A_C \hat{X}_C + A_N (N_s - N_m)\hat{\gamma} \tag{4-44}$$

where N_s is the integer ambiguity set which corresponds to $\Omega_{Fix,sec}$. If the alternative hypothesis is assumed to be true:

$$\hat{\gamma} = \frac{(N_s - N_m)^T Q_{X_N}^{-1} (\hat{X}_N - N_m)}{(N_s - N_m)^T Q_{X_N}^{-1} (N_s - N_m)} \tag{4-45}$$

and the inverse of the co-factor matrix is:

$$P_\gamma = (N_s - N_m)^T Q_{X_N}^{-1} (N_s - N_m) \tag{4-46}$$

The *a posteriori* variance factor can be estimated as:

$$\hat{\sigma}_0' = \sqrt{\frac{\Omega_{Fix,min} - \hat{\gamma}^2 P_\gamma}{n - t - 1}} \tag{4-47}$$

and the standard deviation of $\hat{\gamma}$ will be:

$$\hat{\sigma}_\gamma = \hat{\sigma}_0' \cdot P_\gamma^{-1/2} \tag{4-48}$$

Constructing a t-distribution statistic τ under H_0:

$$\tau = \frac{\gamma}{\hat{\sigma}_\gamma} \sim t(n - t - 1) \tag{4-49}$$

If the integer set corresponding to $\Omega_{Fix,min}$ is selected, it is equivalent to $\gamma < 0.5$. The probability of the selection of H_0 will be:

$$P\left((\gamma < 0.5)|H_0\right) = \int_{-\infty}^{0.5/\hat{\sigma}_\gamma} f_{t_{n-t-1}}(\tau)d\tau = 1-\alpha_0 \tag{4-50}$$

If H_a is assumed to be true, τ will become the non-central t-distributed statistic $t'(n-t-1,\delta)$. Although H_a is assumed to be true with non-centrality parameter $\frac{\hat{\gamma}}{\hat{\sigma}_\gamma}$, the probability of the selection of H_0 is required to be larger than β_1 (Figure 4-2):

$$P\left((\gamma < 0.5)|H_a\right) = \int_{-\infty}^{0.5/\hat{\sigma}_\gamma} f_{t_{n-t-1}}(\tau,\frac{\hat{\gamma}}{\hat{\sigma}_\gamma})d\tau > \beta_1 = \int_{-\infty}^{0.5/\hat{\sigma}_\gamma} f_{t_{n-t-1}}(\tau,\delta_1)d\tau \tag{4-51}$$

Therefore, $\delta_1 = \frac{0.5}{\hat{\sigma}_\gamma} - \xi_{t_{n-t-1};\beta_1}$, $\frac{\hat{\gamma}}{\hat{\sigma}_\gamma} < \delta_1$, and subsequently the discrimination test will be derived as follows:

$$\left(0.5-\hat{\gamma}\right) > \xi_{t_{n-t-1};\beta_1}\cdot\hat{\sigma}_\gamma \tag{4-52}$$

Note that the selection of β_1 should be less than $1-\alpha_0$ and is normally suggested as being 0.8.

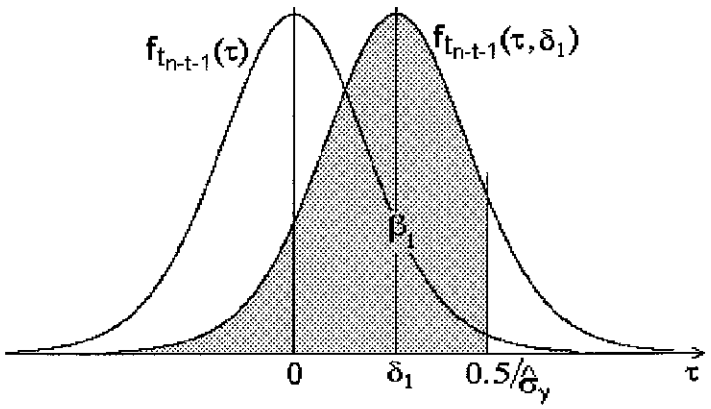

Figure 4-2. Maximum non-centrality in acceptance region

On the other hand, if H_a is assumed to be true with non-centrality parameter $\frac{\hat{\gamma}}{\hat{\sigma}_\gamma}$, the probability of the selection H_0 is required to be smaller than $1-\beta_2$ (Figure 4-3):

$$P\left((\gamma < 0.5)|H_a\right) = \int_{-\infty}^{(0.5-\hat{\gamma})/\hat{\sigma}_\gamma} f_{t_{n-t-1}}(\tau, \frac{\hat{\gamma}}{\hat{\sigma}_\gamma})d\tau < 1-\beta_2 = \int_{-\infty}^{(0.5-\hat{\gamma})/\hat{\sigma}_\gamma} f_{t_{n-t-1}}(\tau, \delta_2)d\tau \quad (4\text{-}53)$$

Therefore, $\delta_2 = \frac{0.5}{\hat{\sigma}_\gamma} + \xi_{t_{n-t-1};\beta_2}$, $\frac{\hat{\gamma}}{\hat{\sigma}_\gamma} > \delta_2$, and subsequently the following relation will be derived:

$$\hat{\gamma} > 0.5 + \xi_{t_{n-t-1};\beta_2} \cdot \hat{\sigma}_\gamma \quad (4\text{-}54)$$

$0.5 + \xi_{t_{n-t-1};\beta_2} \cdot \hat{\sigma}_\gamma$ is the minimal bias which can be detected by means of hypothesis testing (referred to as internal reliability, with significance level α_0 and the power of the test β_2). In order to find the outlier $\hat{\gamma} = 1$, which means $\nabla = N_s - N_m$, another discrimination test will be derived, from equations (4-46, 4-48 and 4-54):

$$(N_s - N_m)^T Q_{X_N}^{-1} (N_s - N_m) > 4 \cdot \xi^2_{t_{n-t-1};\beta_2} \cdot \hat{\sigma}'^2_0 \quad (4\text{-}55)$$

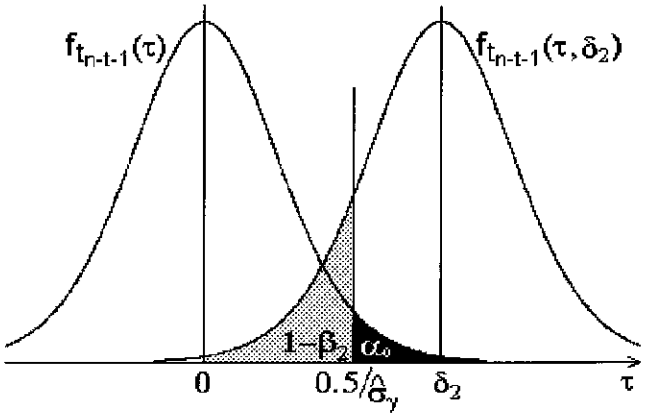

Figure 4-3. Minimum non-centrality in rejection region

4.5.3 Comparisons

The relationship to the existing criteria can be derived (Figure 4-4):

$$R_{sec} - R_{min} = (1 - 2\hat{\gamma}) \cdot (N_s - N_m)^T Q_{X_N}^{-1} (N_s - N_m) \quad (4\text{-}56)$$

and considering the discrimination test equation (4-52), test equation (4-39) will be:

$$R_{sec} - R_{min} < 2\hat{\sigma}_\gamma \cdot \xi_{t_{n-t-1};\beta_1} \cdot (N_s - N_m)^T Q_{X_N}^{-1} (N_s - N_m) \tag{4-57}$$

The relationship to the other criteria (equations (4-37) and (4-38)) can be derived in the same way:

$$\frac{R_{sec}}{R_{min}} > \frac{2\hat{\sigma}_\gamma \cdot \xi_{t_{n-t-1};\beta_1} \cdot (N_s - N_m)^T Q_{X_N}^{-1} (N_s - N_m)}{R_{min}} + 1 \tag{4-58}$$

$$\frac{\Omega_{Fix,sec}}{\Omega_{Fix,min}} > \frac{2\hat{\sigma}_\gamma \cdot \xi_{t_{n-t-1};\beta_1} \cdot (N_s - N_m)^T Q_{X_N}^{-1} (N_s - N_m)}{\Omega_{Fix,min}} + 1 \tag{4-59}$$

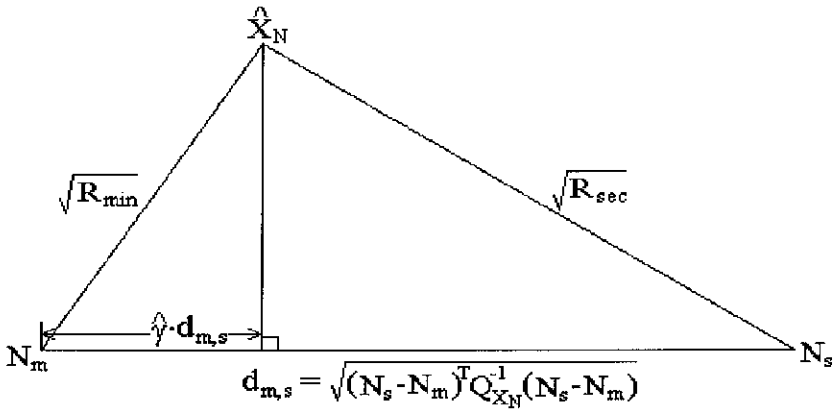

Figure 4-4. Geometrical relations

4.6 Adaptive Procedure to Improve Reliability

The third problem is the definition of the Fault Detection, Identification and Adaptation procedure which must guard against wrong integer ambiguity determination. This is an increasingly important aspect of instantaneous ambiguity resolution for centimetre accuracy real-time GPS positioning due to the small number of degrees-of-freedom.

4.6.1 Fault Detection Using TEC Values

If the above procedure uses only one epoch of data, the relational information between epochs has not been used. In order to further ensure that the final solution is correct, global information should be used. As is well known, the Total Electron Content (TEC)

of the path through the ionosphere has very strong correlation in space and time. The TEC value for the neighbouring epoch should therefore be very close and this information will be considered as the basis for a global test. The difference between the double-differenced ionospheric delay on L1 and L2 carrier phase observations is defined as Δ_{ion}, which can be represented as follows (assuming known integer ambiguities):

$$\Delta_{ion} = \lambda_1 \Delta\nabla\phi_{L1} - \lambda_2 \Delta\nabla\phi_{L2} - \lambda_1 \Delta\nabla N_{L1} + \lambda_2 \Delta\nabla N_{L2} \tag{4-60}$$

If the integer ambiguities are resolved correctly, the Δ_{ion} sequence should change smoothly. Otherwise, a jump will occur due to wrong ambiguity resolution at an epoch. The jump can be found from the difference $\delta\Delta_{ion}$, between Δ_{ion} at the current epoch and at the previous epoch. If wrong ambiguity resolution at the current epoch occurs, $\delta\Delta_{ion}$ can be represented as:

$$\delta\Delta_{ion} = -\lambda_1 \delta\Delta\nabla N_{L1} + \lambda_2 \delta\Delta\nabla N_{L2} \tag{4-61}$$

where $\delta\Delta\nabla N_{L1}$ and $\delta\Delta\nabla N_{L2}$ are the magnitudes of the integer biases caused by wrong ambiguity resolution. Note that $\delta\Delta_{ion}$ is not affected by cycle slips. If the instantaneous ambiguity resolution is correct at the current epoch and the previous epoch, $\delta\Delta_{ion}$ will be small, even though cycle slips occurred between these two epochs. If the integer biases of the resolved ambiguities are assumed to be within ±20cycles and the criterium

$$\delta\Delta_{ion} < 5.0 \text{ cm} \tag{4-62}$$

is used for fault detection, the integer biases which cannot be discriminated are listed in Table 4-2. Obviously, if ambiguity resolution is correct, equation (4-62) will be satisfied. However if equation (4-62) is satisfied, the ambiguity resolution cannot be assured as being correct. Therefore the TEC test is a necessary condition, but not a sufficient condition. The critical value is selected as 5 cm for the experiments described in this report. If the critical value is selected too large, more ambiguity biases will not be found. If the critical value is selected too small, the ionospheric change will possibly be considered as the ambiguity biases, and the magnitude of ionospheric change between epochs depends on the sampling rate.

The last column of Table 4-2 gives the effect of the integer biases on the mean value of L1 and L2 carrier phase ranges, which has been used to verify the successful results in Section 4.7.2.

Table 4-2. Ambiguity biases causing $\delta\Delta_{ion} < 5.0$ cm

δN_{L1} (cycle)	δN_{L2} (cycle)	$\delta\Delta_{ion}$ (cm)	$\frac{1}{2}(\lambda_1\delta\Delta\nabla N_{L1} + \lambda_2\delta\Delta\nabla N_{L2})$ (cm)
± 4	± 3	∓ 2.85	$\pm$ 74.69
± 5	± 4	± 2.54	$\pm$ 96.42
± 9	± 7	∓ 0.31	± 171.11
± 13	± 10	∓ 3.17	± 245.80
± 14	± 11	± 2.23	± 267.52
± 18	± 14	∓ 0.63	± 342.21
± 19	± 15	± 4.76	± 363.94

4.6.2 Adaptation

If the resolved integer ambiguities are incorrect, in general the wrong integer ambiguities will refer to more than one satellite, and it is almost impossible to identify which ambiguity is incorrect. But one thing can be confirmed, and that is that some biases are present in the observations.

If instantaneous ambiguity resolution is to be attempted, the minimum number of satellites should be five. If six or more satellites are observed, some of these observations could be eliminated. All combinations of five or more satellites from all observed satellites should be tested. This procedure has been implemented in software if the ambiguity resolution has failed by eliminating one (or more) satellite (at least five satellites are kept), starting with the one with the lowest elevation, and the procedure repeated until ambiguity resolution is successful. If all possible sets of five or more satellites are combined and the ambiguity test still fails, the ambiguity resolution procedure is considered to have failed. This procedure ensures that the ambiguity resolution success rate increases significantly.

4.7 Experiments

The results of short-range experiments are presented in order to test the improvements due to the real-time stochastic model, new criteria, and the fault detection and adaptation procedure, which can be used for medium-range positioning as well. The functional model using multiple reference station to eliminate or mitigate the biases due to orbit errors, ionosphere, troposphere, and multipath will be tested in the medium-range experiment.

4.7.1 Short-Range Experiments

The suggested functional model for multiple reference stations can be easily simplified to the one reference station case, for which orbit bias and ionospheric delay cannot be eliminated, but they can be ignored due to the short-range mode being tested.

Three experiments have been carried out to test the proposed technique. The first one is a static experiment using data collected between 8:00am-11:00am on 21 August, 1995, in Bandung, Indonesia, using two Ashtech Z12 GPS receivers. The data rate is 15 seconds and a total of 720 epochs were observed. The baseline length is 11287.450 metres. The instantaneous ambiguity resolution results can be easily checked by studying the repeatability of the baseline results determined at each epoch.

The second experiment was carried out on 17 January, 1996, using an Ashtech Z12 GPS receiver mounted on a car. A permanent GPS station on the Mather Pillar, on the roof of the Geography & Surveying Building, at The University of New South Wales, equipped with an Ashtech Z12 GPS receiver, was selected as the reference station. The data rate was 1 Hz. After about 20 minutes of static occupation (approximately 5.2km away from the reference station), the roving receiver started to move along Foreshore Road, Sydney, and then returned to the starting point. This was done for a total of five runs. The trajectory of the first run is shown in Figure 4-5 (the subsequent four runs are almost identical). The number of satellites observed during the experiment is illustrated in Figure 4-6. The maximum velocity was 27.6m/sec, and the maximum acceleration was 2.9 m/sec^2. The continuity of the integer ambiguity is used to check whether the instantaneous ambiguity resolution is correct or not.

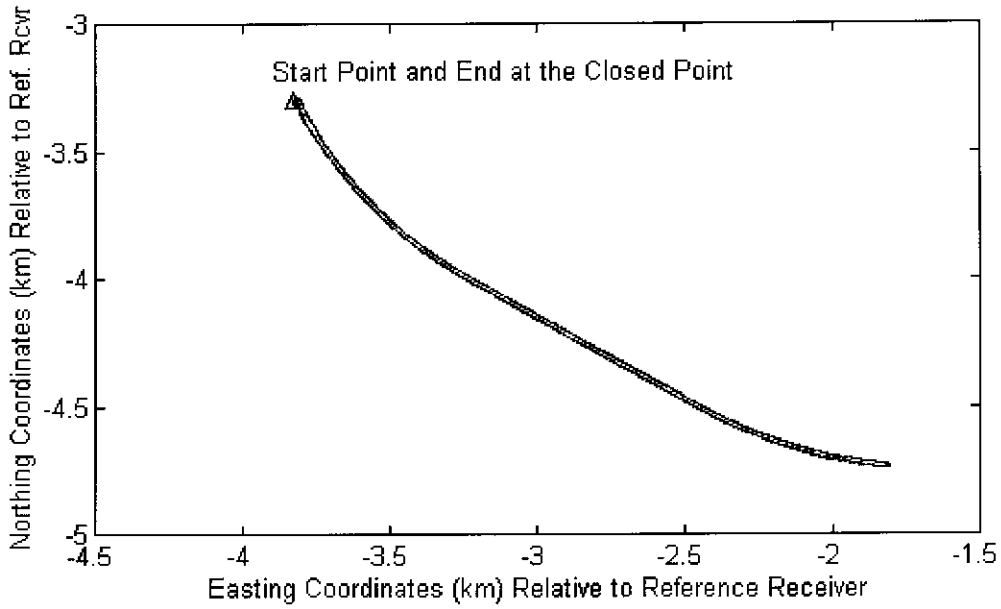

Figure 4-5. Trajectory of Ashtech receiver during run 1 on 17 January, 1996

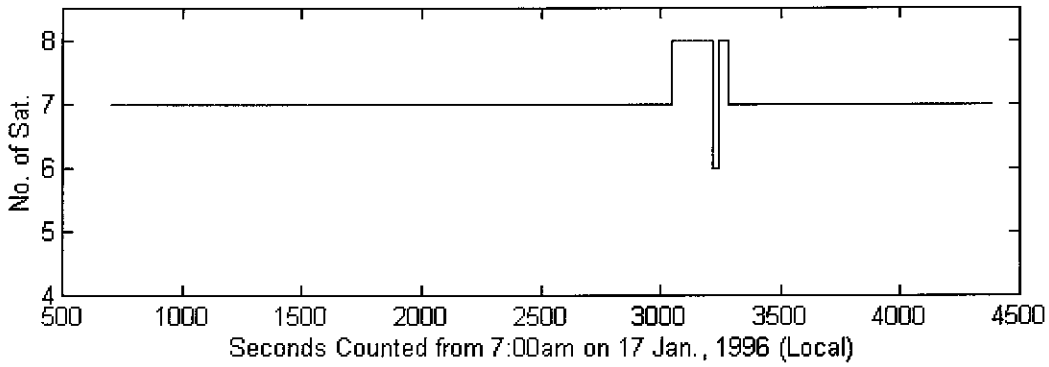

Figure 4-6. Number of satellites observed during experiment on 17 January, 1996

The third experiment was carried out on 7 April, 1996, using one Ashtech Z12 GPS receiver and one Leica System 300 GPS receiver, both mounted on a car with antennas separated by about 60cm. A Leica System 300 GPS receiver was set up at Ollie Webb Reserve, Sydney, and operated as the reference receiver. The data rate was 1 Hz. After about 25 minutes of static occupation (approximately 7.5km away from the reference station at the beginning), the roving receivers started to move along the M3 Freeway, Sydney, then back to the closest point on the other side of the road. The trajectory is shown in Figure 4-7 (the maximum distance from the reference receiver was 13.7km). The number of satellites observed during the experiment is illustrated in Figure 4-8. The maximum velocity was 26.5m/sec, and the maximum acceleration was 2.9m/sec^2. Care was taken to keep satellites locked on during the total observation span, but cycle slips did occur several times. Fortunately the Ashtech Z12 receiver kept tracking at least five

satellites on the L1 frequency throughout the observation span, although PRN 21 and 22 lost a few epochs of data. A reliable trajectory for the Ashtech Z12 antenna can be determined using the L1 carrier phase observations. This is considered to be the true trajectory for checking the instantaneous ambiguity resolution results for the roving Ashtech Z12 receiver. The constant distance (about 60cm) between the Ashtech Z12 and Leica System 300 antennas is used to check whether the instantaneous ambiguity resolution is correct for the roving Leica System 300 receiver.

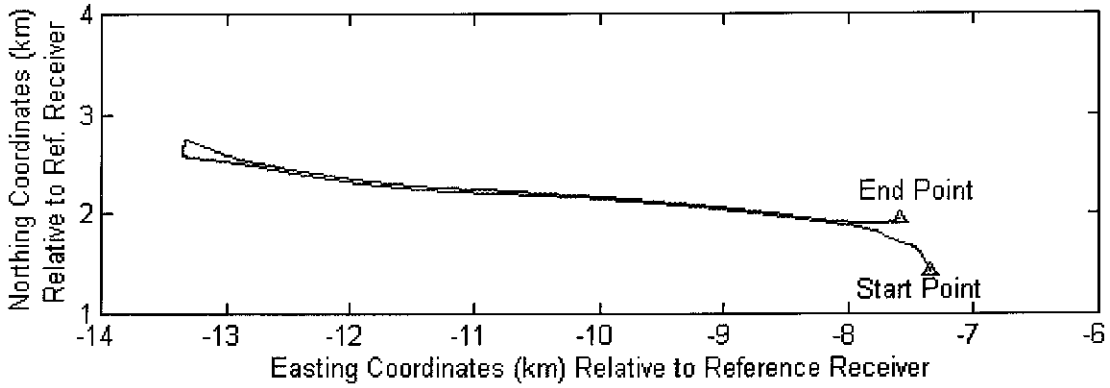

Figure 4-7. Trajectory of the car on 7 April, 1996

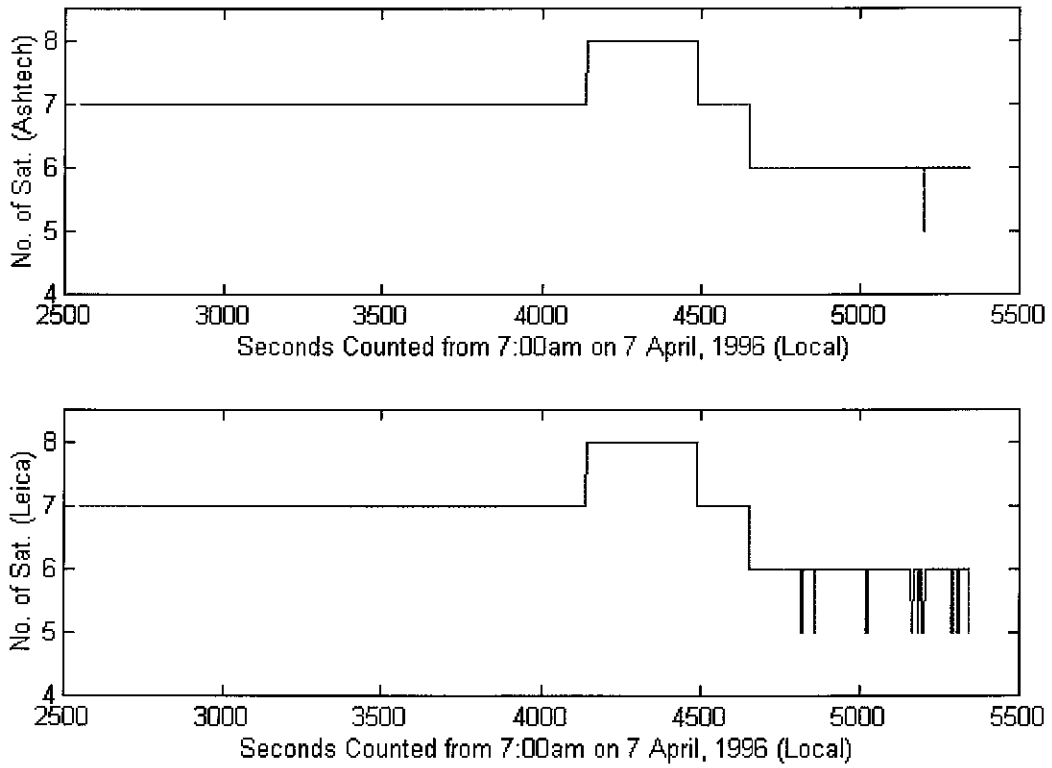

Figure 4-8. Number of satellites observed during experiment on 7 April, 1996 (upper for Ashtech receiver, lower for Leica receiver)

Firstly, all data processing has been carried out using the same observation weights. The *a priori* standard deviations for the carrier phase observations were carefully selected because the tests are sensitive to these values. Six different discrimination tests were used: (1) select the integer ambiguity set which gives $\Omega_{Fix,min}$; (2) test $\frac{\Omega_{Fix,sec}}{\Omega_{Fix,min}} > 2$; (3) test $\frac{R_{sec}}{R_{min}} > 2$; (4) test $\frac{R_{sec}}{R_{min}} > 1.5$; (5) test $R_{sec} - R_{min} > \hat{\sigma}_0^2 \cdot K_2$, and $K_2 = 12$ (because $K_2 = 15$ is too conservative in these experiments); and (6) the new discrimination tests (equations (4-54, 4-57)) with $\beta_1 = 0.8$ and $\beta_2 = 0.8$. The results are listed in Columns 3 to 8 in Table 4-3. For each experiment, three sub-rows are included. The first sub-row is the number (and percentage) of epochs for which ambiguity resolution is successful on an epoch-by-epoch basis; the second sub-row is the number of epochs (and percentage) which pass the validation criteria tests, but for which the result is incorrect, and; the third sub-row is the number of epochs (and percentage) which do not pass the validation criteria tests. Column 9 in Table 4-3 gives the mean computation time for one epoch processing using a 486 DX4-100MHz PC (from input of the raw observation data to the final positioning results), and shows that the integrated method has high computational efficiency. On the other hand, it also shows that quite a large percentage of epochs (2.8%) give the wrong ambiguity for test 1 on the Leica-Leica baseline. If discrimination tests 2 and 5 are used on this baseline, Columns 4 and 7 indicate no wrong ambiguity, but a large percentage of epochs are rejected (maximum values 31.6% and 22.5%, respectively, for all baselines). The other tests result in some wrong integer ambiguity sets being accepted.

Secondly, the real-time stochastic model improvement procedure has been tested. The values of a_0, a_1 and E_0 in equation (4-27) are listed in Table 4-4. The results of the real-time estimation of the scale factors of the pseudo-range and carrier phase observations for the Leica-Ash experiment are plotted in Figure 4-9. (The scale factor for the other experiments has a similar signature.) The positioning performance is shown in Table 4-5. Note that the mean computation time is not much changed. However, the percentage of wrong ambiguity sets being accepted has been significantly reduced. All discrimination tests do not accept any wrong integer ambiguity set, and the percentage of successful single epoch positioning results has increased significantly. Although the test $\frac{R_{sec}}{R_{min}} > 1.5$ and the new discrimination tests both give a higher percentage of success rates than the others, the new discrimination test is more theoretically rigorous. It also shows that false ambiguity resolution for some epochs cannot be avoided by

improvements to the stochastic model. For example, there is still wrong ambiguity resolution 38 times for the Leica-Ash experiment. Functional model improvements, using an adaptive procedure, will therefore still be necessary.

Thirdly, the TEC test, which makes use of the correlation information between neighbouring epochs, has been applied for further testing of the ambiguity resolution results. The TEC value should not change by very much within a short time span (Figure 4-10). This test is a necessary condition, but not a sufficient condition. If the ambiguity resolution cannot pass this test, the ambiguity resolution will also be considered wrong. Figure 4-10 shows that some of the incorrect ambiguity resolution epochs can be identified when test equations (4-62) is used.

Table 4-3. Positioning performance using different discrimination tests (same weight for all carrier phase observations and same weight for all pseudo-range observations)

Baseline Name		Without Test	$\frac{\Omega_{Fix,sec}}{\Omega_{Fix,min}} > 2$	$\frac{R_{sec}}{R_{min}} > 2$	$\frac{R_{sec}}{R_{min}} > 1.5$	$R_{sec} - R_{min} > \sigma_0^2 \cdot K_2$	New Test	Time (ms)
Static	Correct	690 (95.8)	582 (80.8)	597 (82.9)	658 (91.4)	666 (92.5)	685 (95.1)	
Baseline	Wrong	2 (0.3)	0	0	0	0	0	99
(21.8.95)	Reject	28 (3.9)	138 (19.2)	123 (17.1)	62 (8.6)	54 (7.5)	35 (4.9)	
Ash-Ash	Correct	3656 (99.1)	3436 (93.1)	3551 (96.3)	3657 (99.1)	3593 (97.4)	3662 (99.3)	
(17.1.96)	Wrong	25 (0.7)	0	0	0	0	0	80
	Reject	8 (0.2)	253 (6.9)	138 (3.7)	32 (0.9)	96 (2.6)	27 (0.7)	
Leica-Ash	Correct	2761 (98.6)	2503 (89.4)	2534 (90.5)	2738 (97.8)	2542 (90.8)	2751 (98.2)	
(7.4.96)	Wrong	40 (1.4)	0	0	4 (0.1)	0	4 (0.1)	89
	Reject	0	298 (10.6)	267 (9.5)	59 (2.1)	259 (9.2)	46 (1.7)	
Leica-	Correct	2702 (96.5)	1915 (68.4)	2143 (76.5)	2576 (92.0)	2172 (77.5)	2656 (94.8)	
Leica	Wrong	79 (2.8)	0	4 (0.1)	14 (0.5)	0	10 (0.4)	91
(7.4.96)	Reject	20 (0.7)	886 (31.6)	654 (23.4)	211 (7.5)	629 (22.5)	135 (4.8)	

Table 4-4. Standard deviations of the observations

	a_0 (cm)	a_1 (cm)	E_0 (degree)
Carrier Phase Observations	0.3	2.6	20
Pseudo-range Observations	7.0	60.0	20

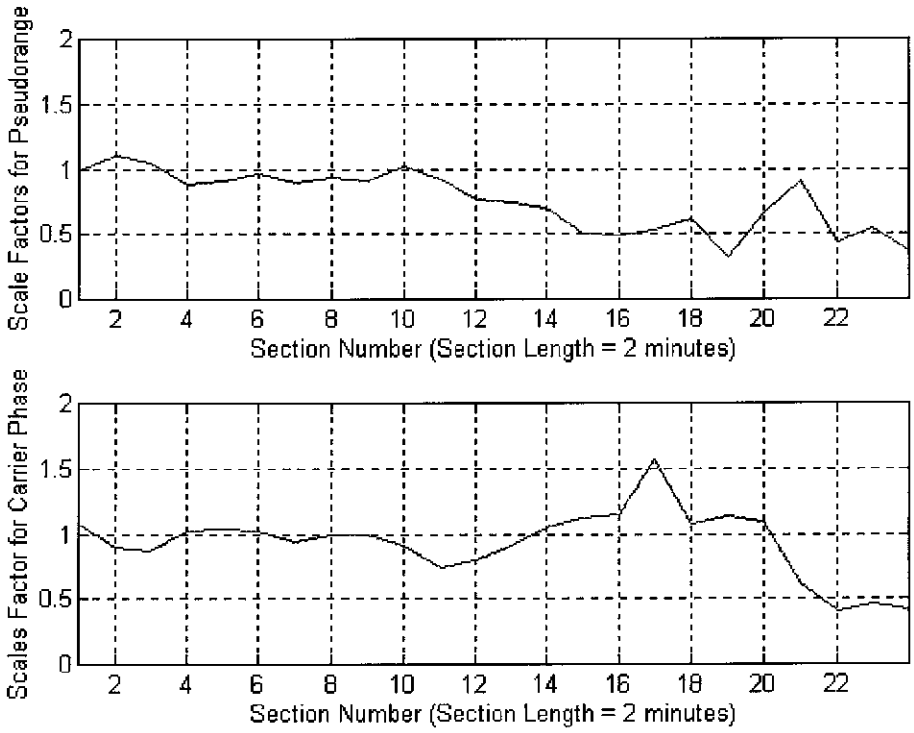

Figure 4-9. Scale factors for pseudo-range observations (Upper) and scale factors for carrier phase observations (Lower) in Leica-Ash (7.4.96) data

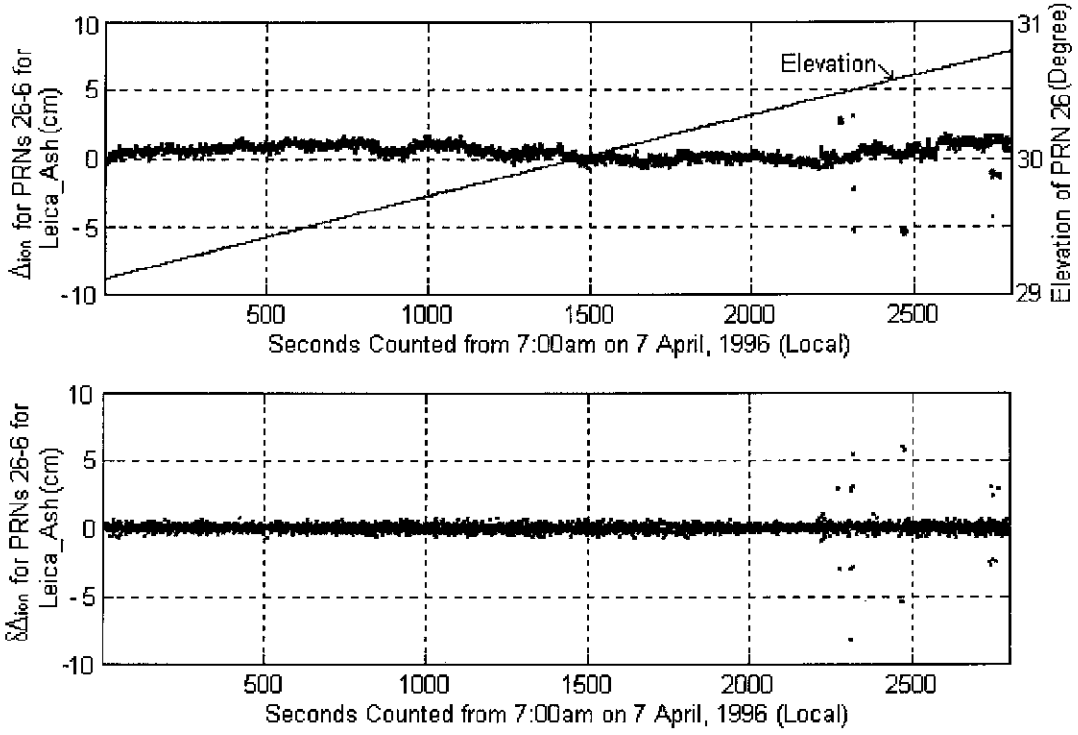

Figure 4-10. Δ_{ion} and $\delta\Delta_{ion}$ values for satellite PRN 26 (reference satellite PRN 6 with highest elevation)

Finally, the adaptive procedure is implemented if ambiguity resolution fails using the new discrimination test and/or fault detection based on the TEC test, and ambiguity resolution is attempted until it is successful or the number satellites is less than 5. The experimental results are listed in Table 4-6. The positioning success rates are now 100%, 100%, 99.7%, 98.4% for the four sets of data considered. Compared with the standard results (Column 4 in Table 4-3), 80.8%, 93.1%, 89.4%, 68.4% for the four sets of data, the improvement in performance is very significant.

Table 4-5. Positioning performance using different discrimination tests (weights are determined using proposed stochastic model)

Baseline Name		Without Test	$\frac{\Omega_{Fix,sec}}{\Omega_{Fix,min}} > 2$	$\frac{R_{sec}}{R_{min}} > 2$	$\frac{R_{sec}}{R_{min}} > 1.5$	$R_{sec} - R_{min} > \sigma_0^2 \cdot K_2$	New Test	Time (ms)
Static Baseline (21.8.95)	Correct	720 (100)	711 (98.8)	715 (99.3)	719 (99.9)	718 (99.7)	719 (99.9)	98
	Wrong	0	0	0	0	0	0	
	Reject	0	9 (1.2)	5 (0.7)	1 (0.1)	2 (0.3)	1 (0.1)	
Ash-Ash (17.1.96)	Correct	3685 (99.9)	3461 (93.8)	3626 (98.3)	3686 (99.9)	3616 (98.0)	3682 (99.8)	79
	Wrong	2 (0.05)	0	0	0	0	0	
	Reject	2 (0.05)	228 (6.2)	63 (1.7)	3 (0.1)	73 (2.0)	7 (0.2)	
Leica-Ash (7.4.96)	Correct	2763 (98.6)	2586 (92.3)	2645 (94.4)	2736 (97.7)	2494 (89.0)	2683 (95.8)	87
	Wrong	38 (1.4)	0	0	0	0	0	
	Reject	0	215 (7.7)	156 (5.6)	65 (2.3)	307 (11.0)	118 (4.2)	
Leica-Leica (7.4.96)	Correct	2794 (99.8)	2340 (83.5)	2469 (88.1)	2703 (96.5)	2399 (85.6)	2619 (93.5)	88
	Wrong	7 (0.2)	0	0	0	0	0	
	Reject	0	461 (16.5)	332 (11.9)	98 (3.5)	402 (14.4)	182 (6.5)	

Table 4-6. Instantaneous ambiguity resolution using adaptive procedure

	Total Number	Fix Ambiguities (Adaptive Procedure)			Mean Time (ms)
		Correct	Wrong	Reject	
Static Baseline (21.8.95)	720	720 (100)	0	0	98
Ash-Ash (17.1.96)	3689	3689 (100)	0	0	80
Leica-Ash (7.4.96)	2801	2794 (99.7)	0	7	90
Leica-Leica (7.4.96)	2801	2757 (98.4)	0	44	93

4.7.2 Medium-Range Experiment

The medium-range experiment is described to test the efficiency of bias elimination in the functional model, using multiple reference stations for ambiguity resolution and precise trajectory determination. The experiment was carried out on 14 December, 1996, using four Ashtech Z12 GPS receivers. A permanent GPS station, the Mather Pillar, on the roof of the Geography & Surveying Building, at The University of New South Wales, was selected as one of the reference stations. The other two reference stations were located at Stanwell Park, to the south of Sydney, and at Springwood, to the west of Sydney. The roving receiver was mounted on a car and the experiment started at the side of the M3 Freeway, 31.44 km, 34.11 km and 46.5 km distant from the Mather Pillar station, Springwood station and Stanwell Park station, respectively. After about 15 minutes of static occupation (although only the data from the last one minute was used because there were not enough visible satellites during the other 14 minutes), the roving receiver started to move along the M3 Freeway, and then back to nearly the same point as the start point, with a further 15 minutes of static occupation. The data rate was 1 Hz and a total of 1903 epochs were used. The locations of the reference stations and the trajectory of the roving receiver are plotted in Figures 4-11a and 4-11b. The skyplot of the observed satellites is shown in Figure 4-12a. The number of observed satellites is plotted in Figure 4-12b.

The Mather Pillar reference station is equipped with a permanent Ashtech Z-12 GPS receiver, managed by the Australian Surveying and Land Information Group as part of their AUSNAV network. This network is being established in all capital cities, and other centres, to satisfy user requirements for real-time DGPS corrections, transmitted by the federal government's Australian Broadcasting Corporation (ABC) on the sidelobe signals of certain of their FM radio stations. The coordinates of this station in the WGS-84 datum are accurate to half a metre or better.

The coordinates of the other two reference stations, Springwood and Stanwell Park, were determined using the traditional long-range static positioning procedure (Appendix B), and are referenced to the known position of the Mather Pillar. After the integer ambiguities for the L1 and L2 carrier phase observations are resolved, the ambiguity-fixed solution is determined using the ionosphere-free phase combination and the IGS precise ephemeris extracted from "igscb.jpl.nasa.gov". As a result, the locations of the reference stations can be considered as being known.

Assume that the Mather Pillar is reference station 3, and Springwood and Stanwell Park are reference stations 1 and 2, respectively. The correction terms $\left[\alpha_1 \cdot V_{1,3}^{L1} + \alpha_2 \cdot V_{2,3}^{L1}\right]$ and $\left[\alpha_1 \cdot V_{1,3}^{L2} + \alpha_2 \cdot V_{2,3}^{L2}\right]$ in equations (4-21a) & (4-21b) for the L1 and L2 carrier phase observations are plotted in Figures 4-13a, 4-13b, 4-13c, 4-13d and 4-13e, for satellite PRNs 4, 5, 9, 10, 30 (PRN 24 is the reference satellite). In a similar way, the correction terms $\left[\alpha_1 \cdot V_{1,3}^{R1} + \alpha_2 \cdot V_{2,3}^{R1}\right]$ and $\left[\alpha_1 \cdot V_{1,3}^{R2} + \alpha_2 \cdot V_{2,3}^{R2}\right]$ can also be determined.

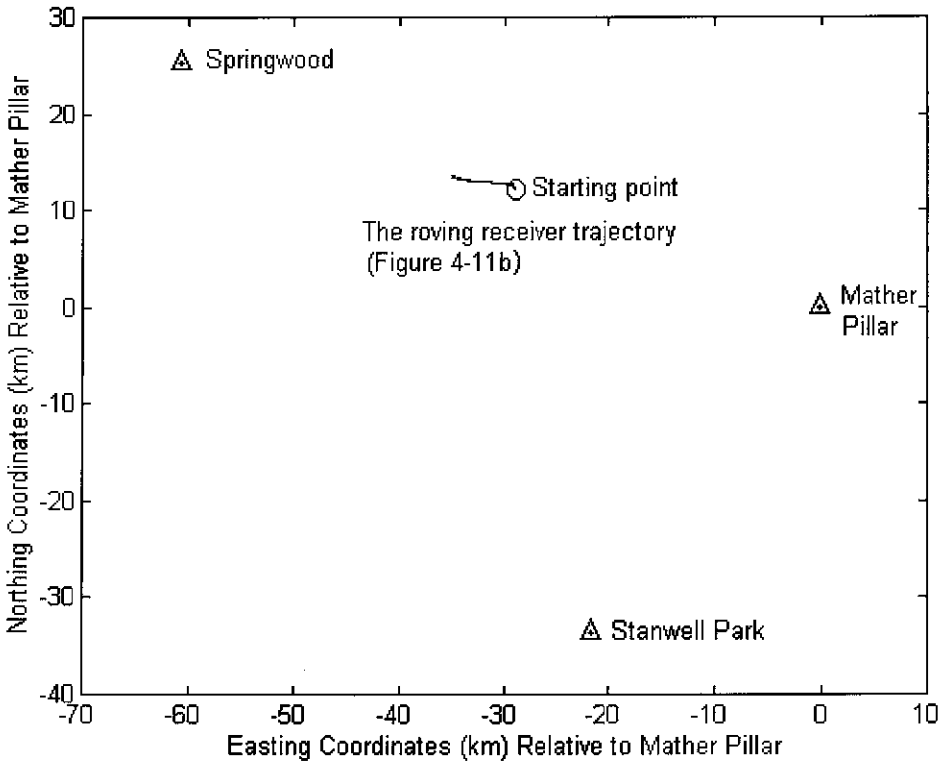

Figure 4-11a. Configuration of the reference GPS stations and the roving GPS receiver trajectory

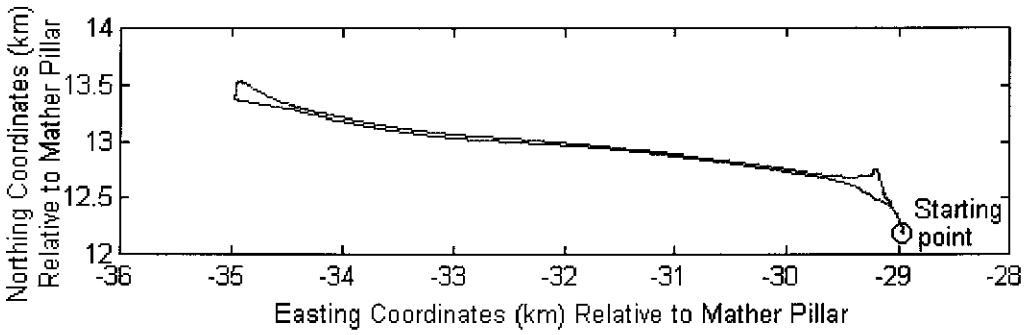

Figure 4-11b. Trajectory of the roving GPS receiver

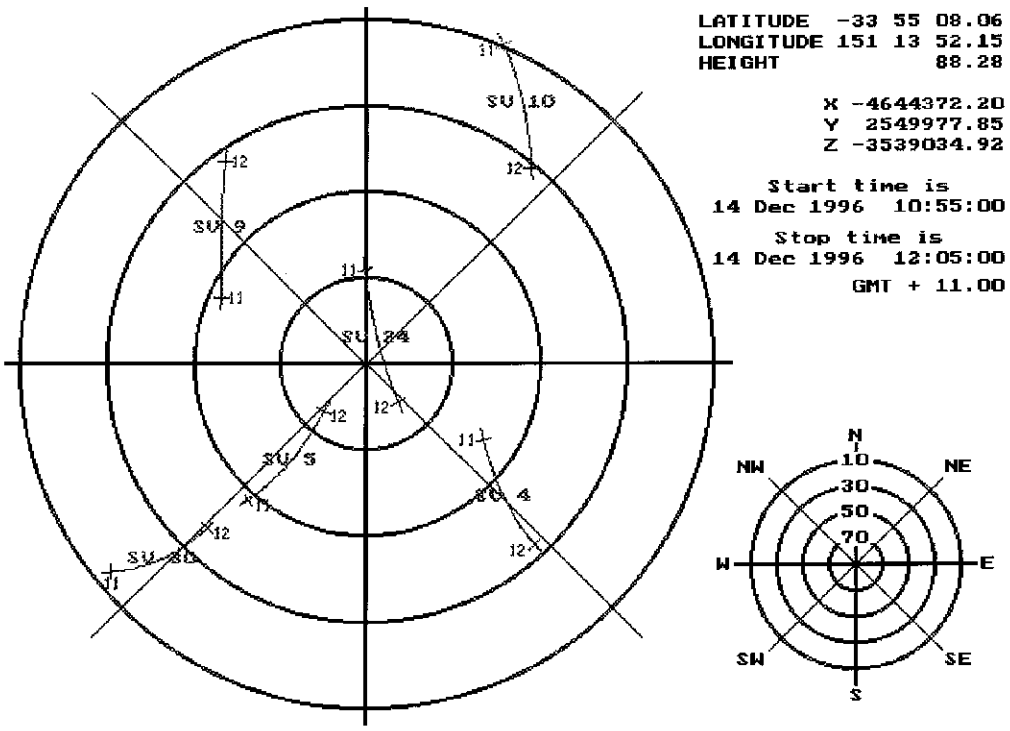

Figure 4-12a. Skyplot for site Mather Pillar

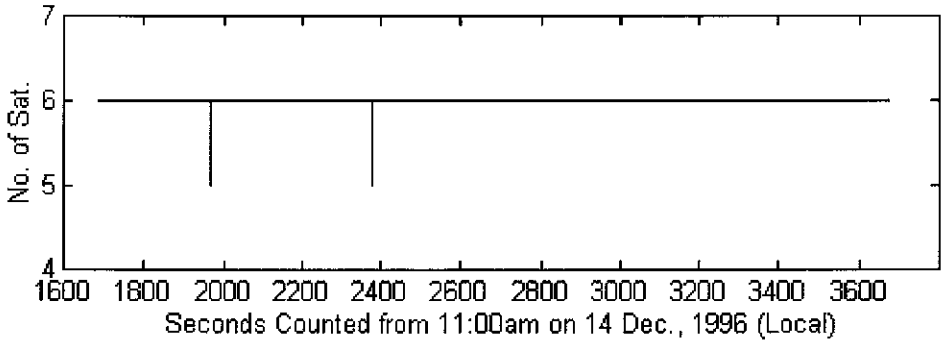

Figure 4-12b. Number of satellites observed

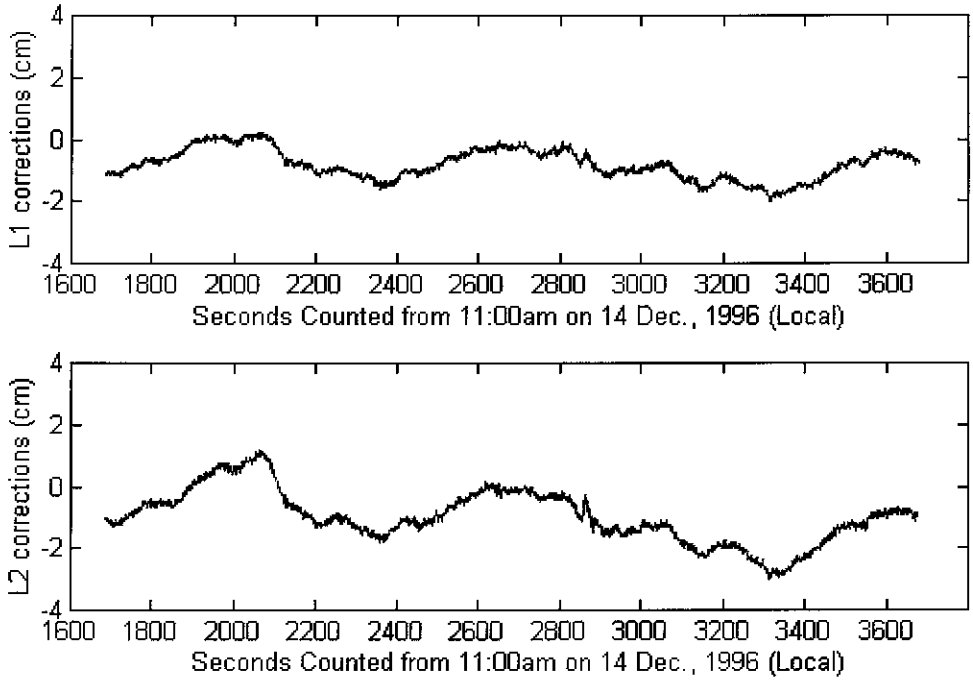

Figure 4-13a. The corrections for double-differenced carrier phase observations for satellite pair PRN 24 and PRN 4

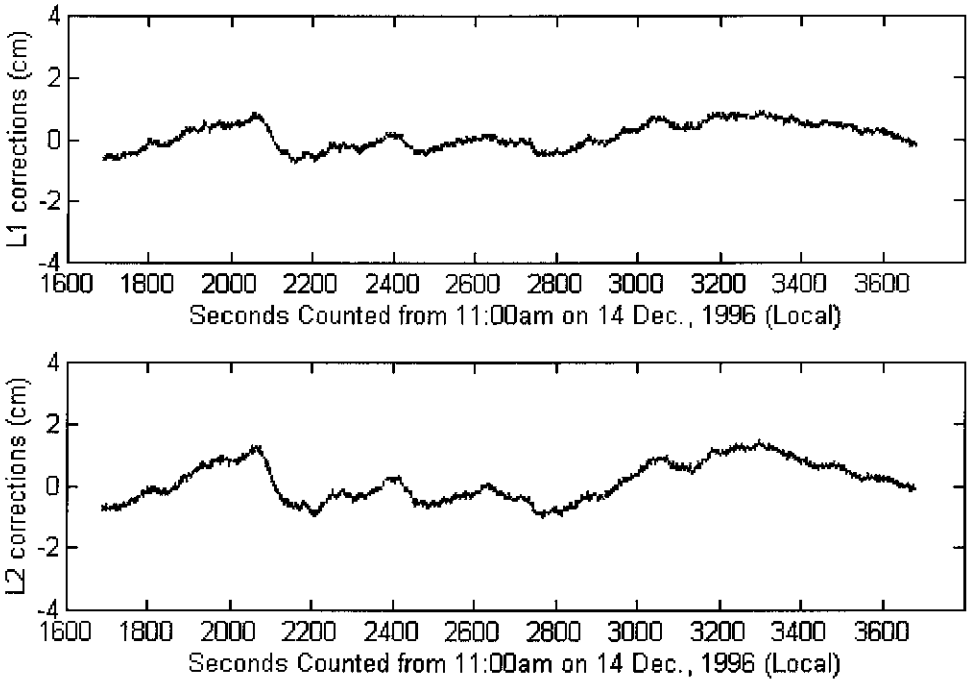

Figure 4-13b. The corrections for double-differenced carrier phase observations for satellite pair PRN 24 and PRN 5

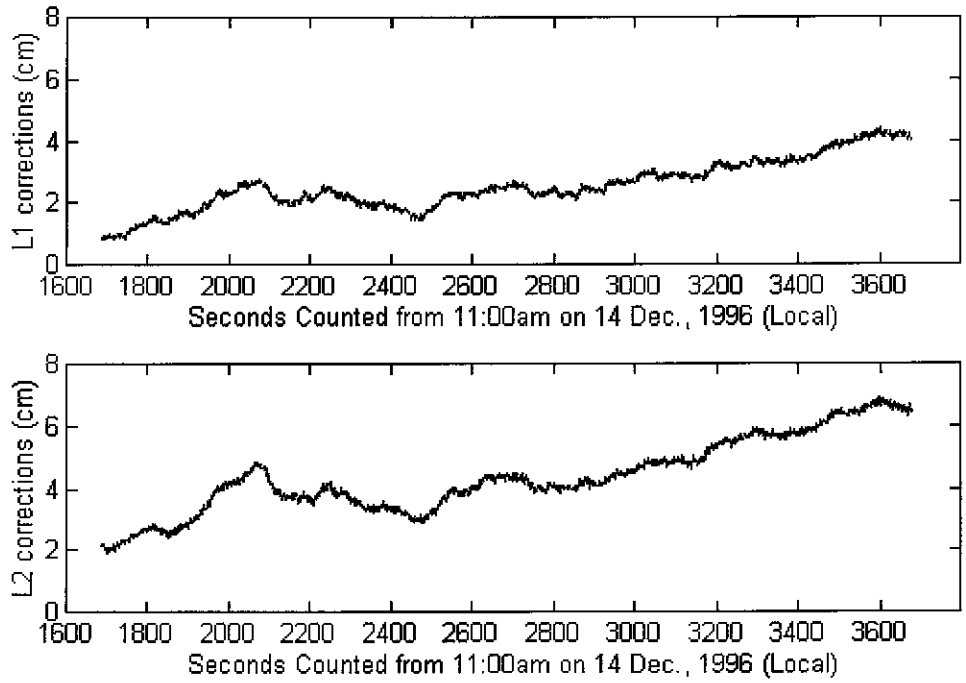

Figure 4-13c. The corrections for double-differenced carrier phase observations for satellite pair PRN 24 and PRN 9

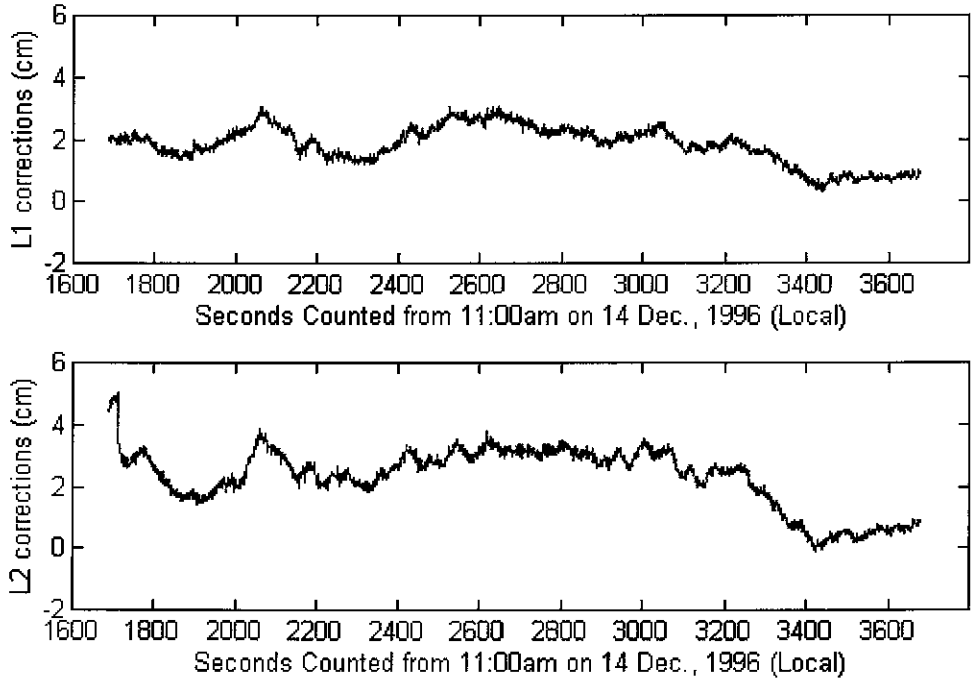

Figure 4-13d. The corrections for double-differenced carrier phase observations for satellite pair PRN 24 and PRN 10

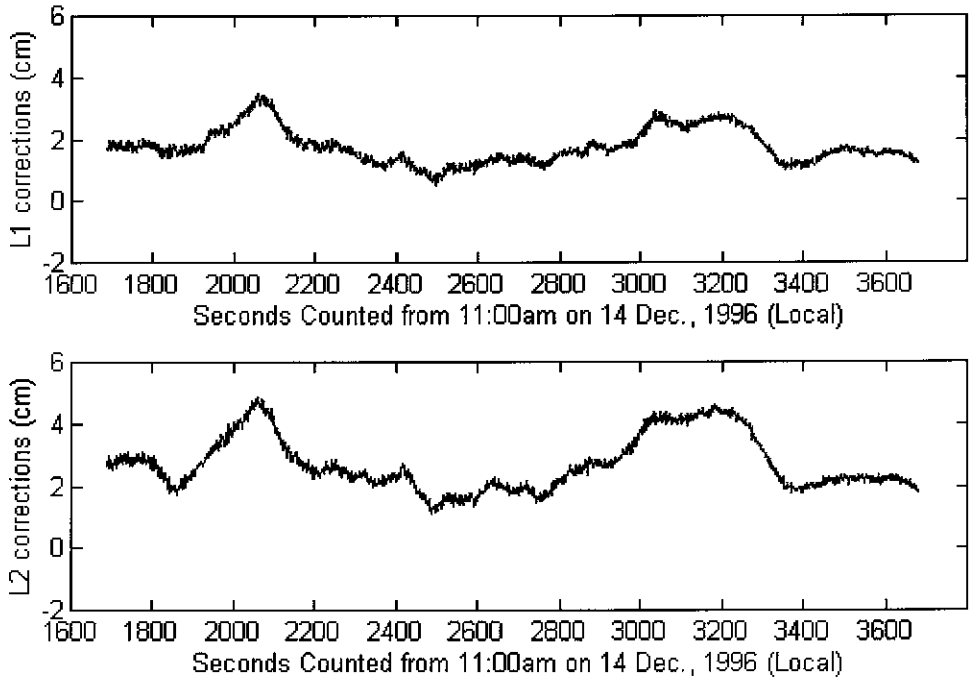

Figure 4-13e. The corrections for double-differenced carrier phase observations for satellite pair PRN 24 and PRN 30

The observation equations (4-21a) to (4-21d) have been formed and the integrated method with three-step improvements has been implemented. The computation procedure for the one-epoch solution can be simplified in the integrated method. The mean value of the corrected pseudo-range observations on L1 and L2 is used to estimate the coordinate parameters $\hat{X}_C$ and the co-factor matrix $Q_{\hat{X}_C}$. The ambiguity-float solution for $\hat{X}_N$, and the associated variance-covariance matrix, can be estimated using equations (4-22) & (4-23), in which the double-differenced carrier phase observations are replaced by the *corrected* double-differenced carrier phase observations.

There are three improvements used within the integrated method: (1) new criteria to validate the integer ambiguity set, (2) the real-time stochastic model and (3) the adaptive procedure (reference to Sections 4.4, 4.5 and 4.6). The results have been separated to illustrate the improvements from these three steps. Firstly, the integrated method with step (1) is used, and the results are presented in Row 2 of Table 4-7. Then, the integrated method with steps (1) and (2) is used and the results are presented in Row 3 of Table 4-7. Finally, the integrated method with all three steps is used and the results are presented in Row 4 of Table 4-7. The adaptive procedure (step (3)) requires the elimination of satellites from the solution. The number of satellites used is plotted in Figure 4-14, and

should be compared with the original set of observed satellites in Figure 4-12b. The last column in Table 4-7 gives the mean computation time for one epoch processing using a 486 DX4-100MHz (from input of the raw observation data to the final positioning results, excluding the computation of the correction sequences illustrated in Figures 4-13a to 4-13e).

Table 4-7. Instantaneous ambiguity resolution for medium-range kinematic positioning using the integrated method with three-step improvements

	Total	Fix Ambiguities			Mean
	Number	Correct	Wrong	Reject	time (ms)
Integrated method with (1)	1903	1840	0	63	62
Integrated method with (1, 2)	1903	1849	0	54	63
Integrated method with (1, 2, 3)	1903	1903	0	0	71

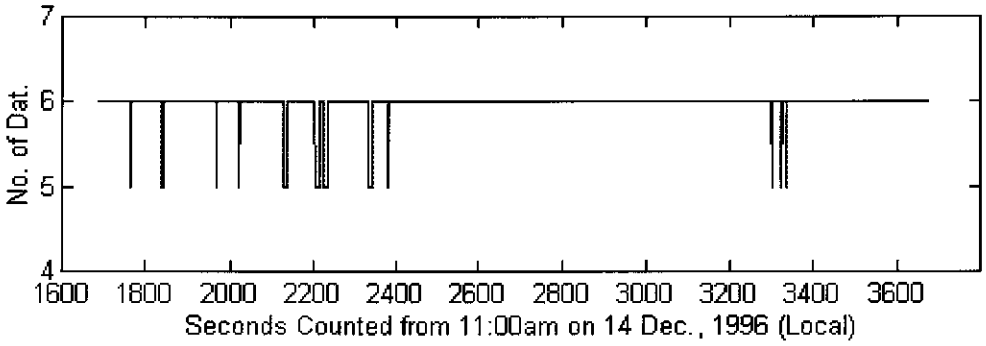

Figure 4-14. Number of the satellites used for ambiguity resolution

Independent verification of the successful ambiguity resolution is difficult to obtain for this experiment. The orginal design of the experiment called for the use two receivers on the car, and the constant distance between the two antennas could be used to verify the results. However, due to a problem with the portable PC computer, the NovAtel Millenium receiver could not be used. In addition, there were not enough GPS receivers to allow for an extra set up at site close to the roving receiver, which would have provided a short-range solution. Fortunately there are four satellites (PRNs 4, 5, 9, 24) tracked during the whole observation session and the *continuity* of the resolved ambiguities for these four satellites can be used to verify the results. The double-

differenced Δ_{ion} and $\delta\Delta_{ion}$ sequences for each pair of satellites, and the two receivers at Mather Pillar reference station and on the car, can also be used as a necessary condition for successful ambiguity resolution. Figures 4-15a to 4-15e illustrate the Δ_{ion} (equation (4-60)) sequence and the change $\delta\Delta_{ion}$ (equation (4-61)) between epochs. From these sequences it can be seen that the resolved ambiguities should be correct or have the values listed in Table 4-2. The residual series of the double-differenced carrier phase observations can also be used as the other necessary condition for sucessful ambiguity resolution. Because the integer ambiguity values for the four satellites (PRNs 4, 5, 9, 24) should be correct, if the ambiguities for the other two satellites (PRNs 10 and 30) are biased by the values listed in Table 4-2, the mean value of the L1 and L2 carrier phase ranges used for positioning will therefore be biased by the values listed in the last column of Table 4-2. Consequently the residuals will be quite large. The residual sequences are plotted in Figures 4-16a to 4-16e, and the sucessful results can be verified because the residuals are very small for all epochs.

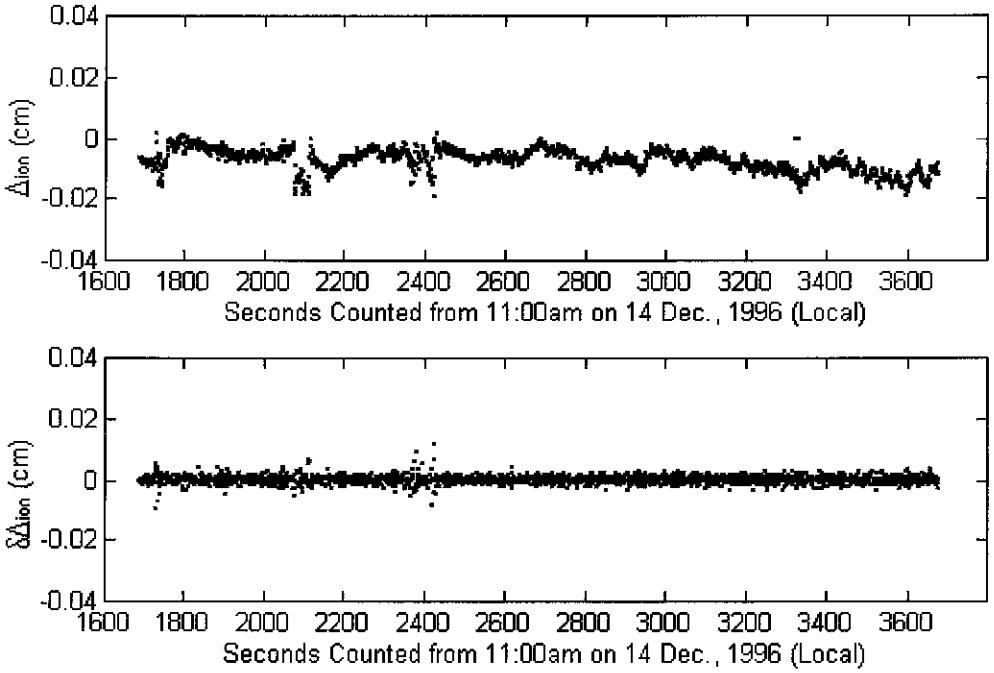

Figure 4-15a. Δ_{ion} and $\delta\Delta_{ion}$ sequences for the satellite pair PRNs 4 and 24

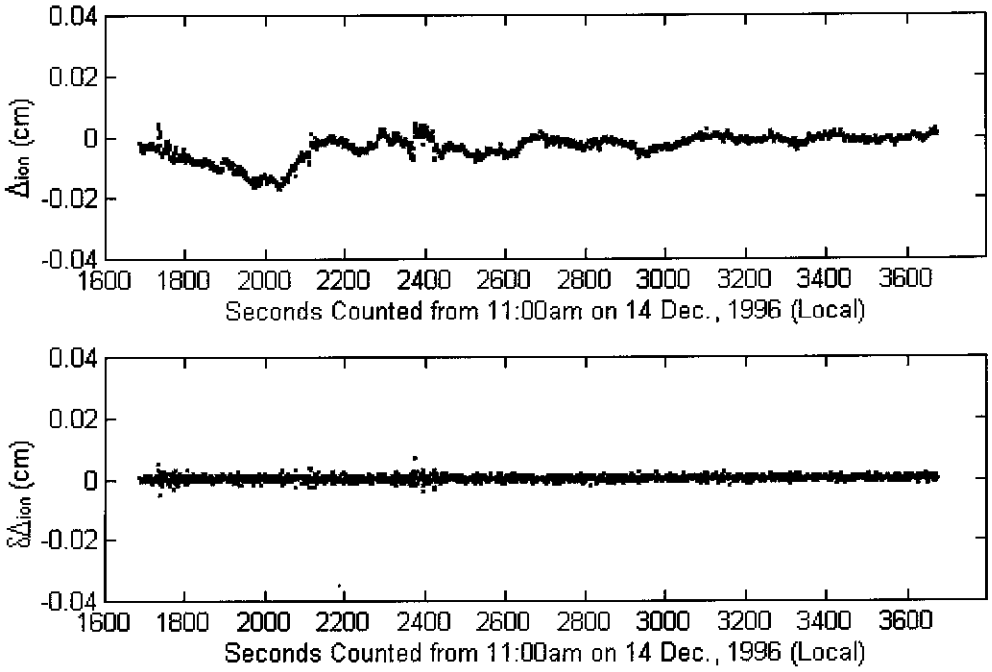

Figure 4-15b. Δ_{ion} and $\delta\Delta_{ion}$ sequences for the satellite pair PRNs 5 and 24

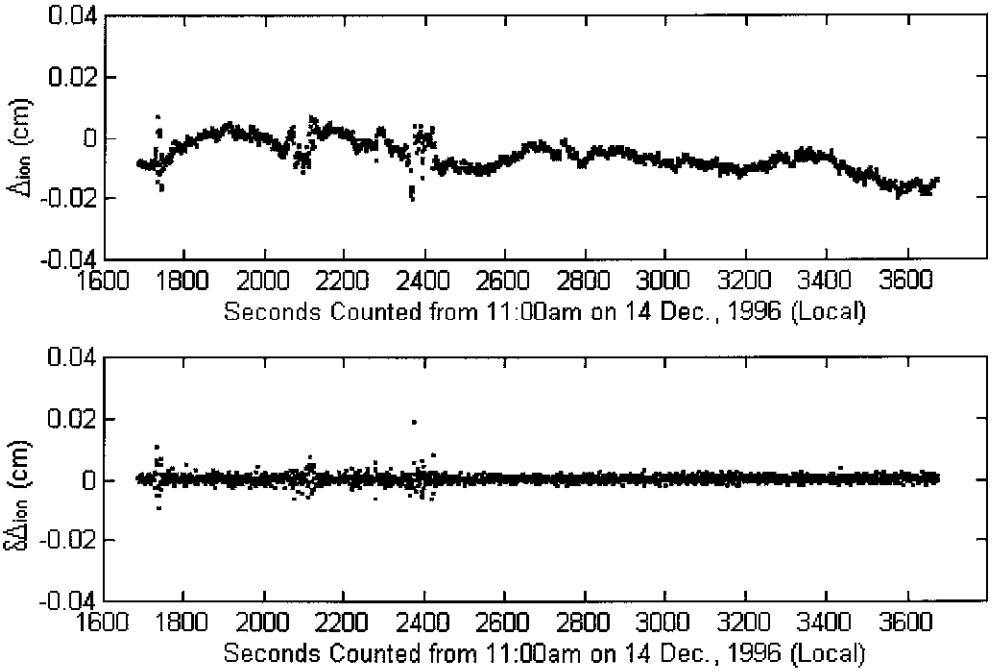

Figure 4-15c. Δ_{ion} and $\delta\Delta_{ion}$ sequences for the satellite pair PRNs 9 and 24

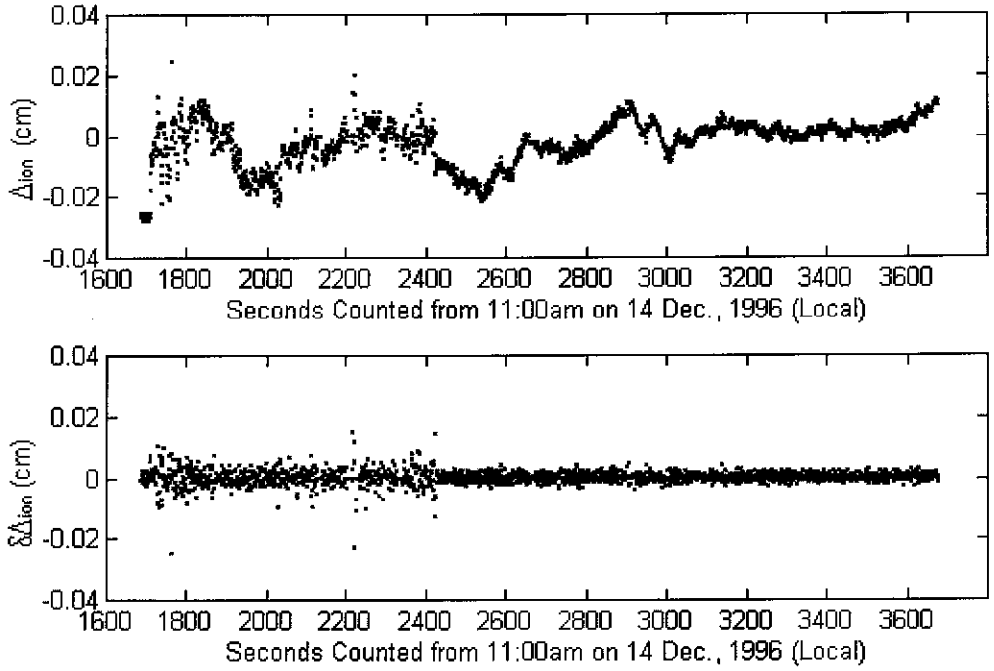

Figure 4-15d. Δ_{ion} and $\delta\Delta_{ion}$ sequences for the satellite pair PRNs 10 and 24

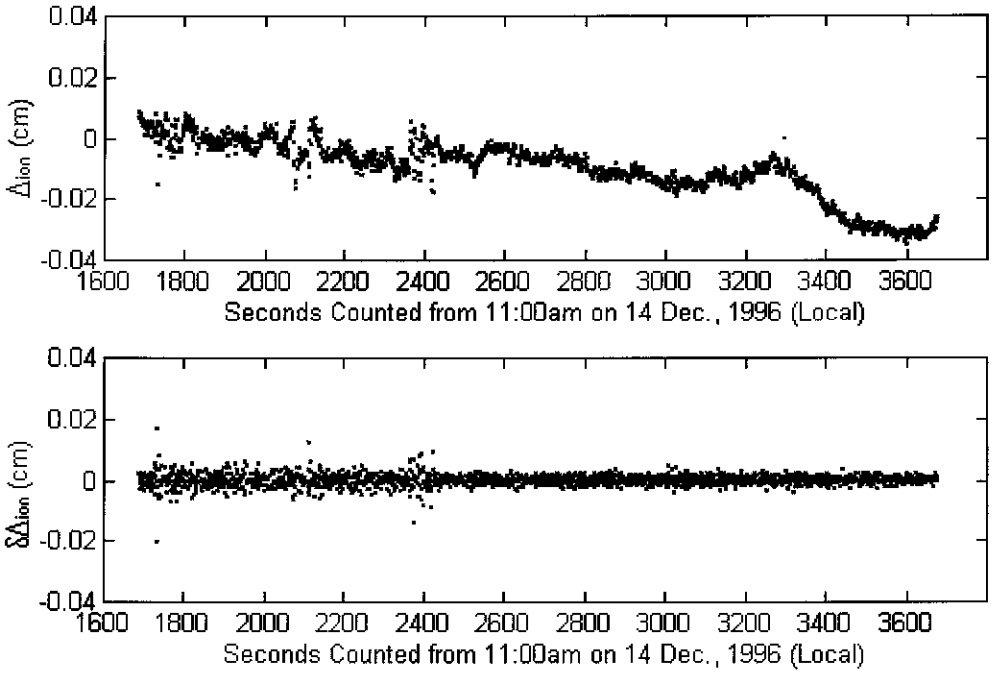

Figure 4-15e. Δ_{ion} and $\delta\Delta_{ion}$ sequences for the satellite pair PRNs 30 and 24

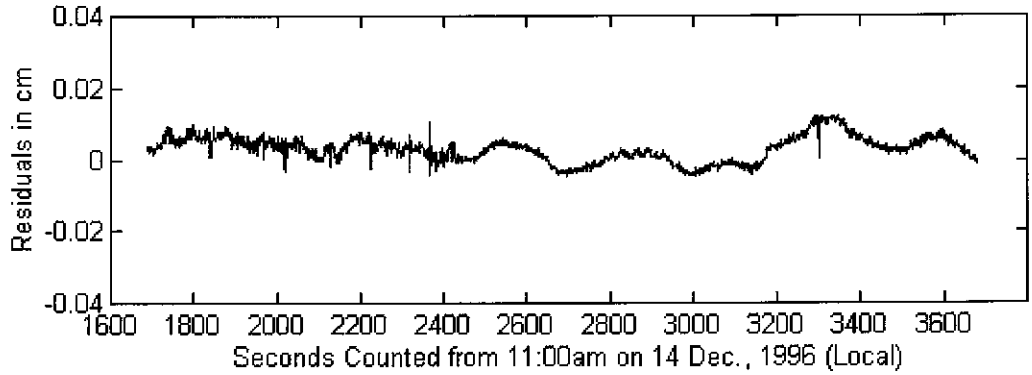

Figure 4-16a. Residuals of the mean values of the corrected carrier phase observations on L1 and L2 (PRNs 4 and 24)

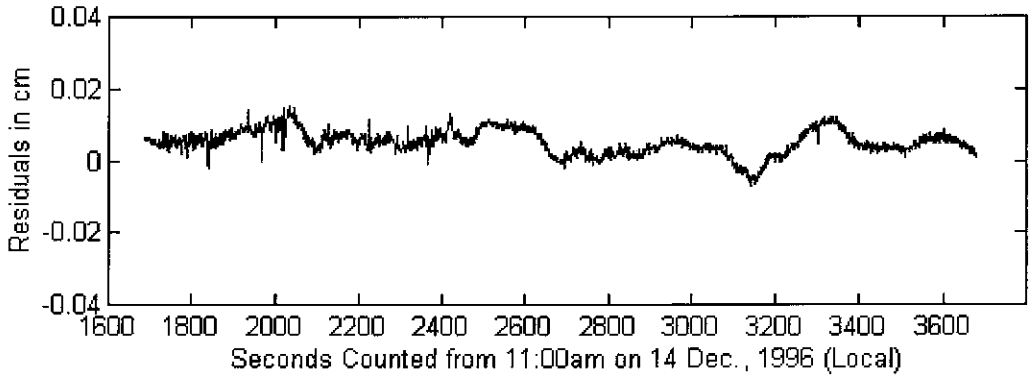

Figure 4-16b. Residuals of the mean values of the corrected carrier phase observations on L1 and L2 (PRNs 5 and 24)

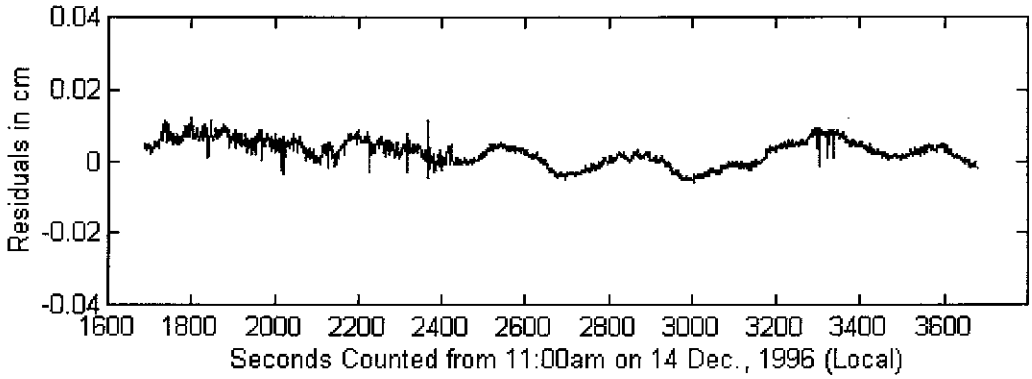

Figure 4-16c. Residuals of the mean values of the corrected carrier phase observations on L1 and L2 (PRNs 9 and 24)

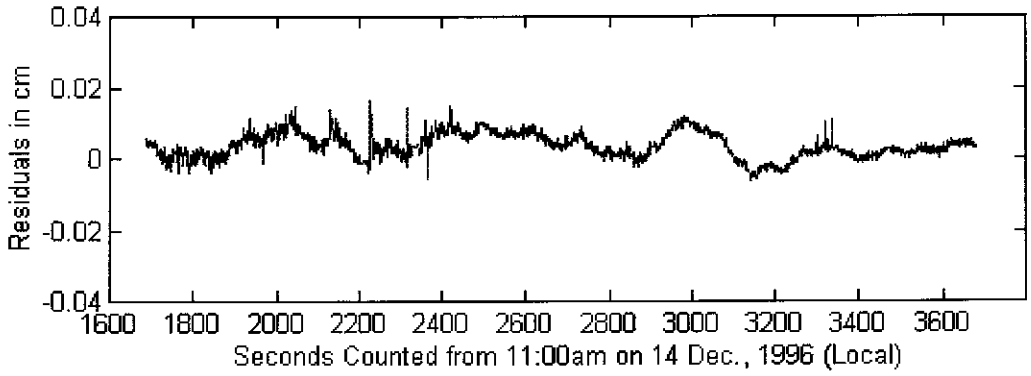

Figure 4-16d. Residuals of the mean values of the corrected carrier phase observations on L1 and L2 (PRNs 10 and 24)

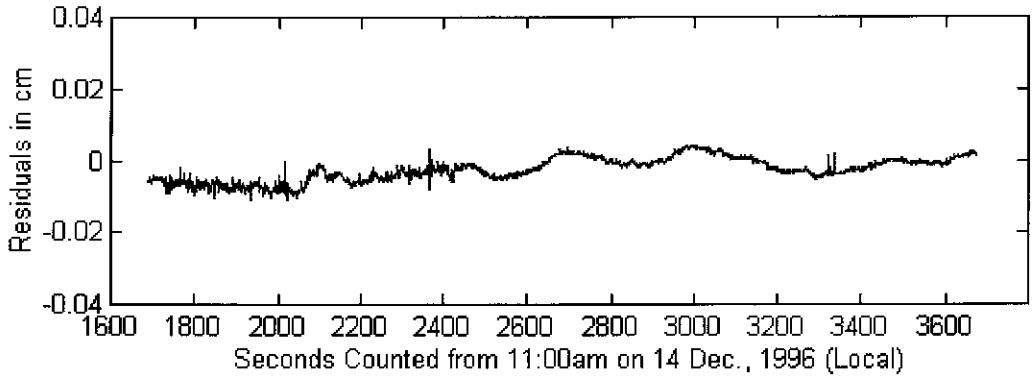

Figure 4-16e. Residuals of the mean values of the corrected carrier phase observations on L1 and L2 (PRNs 30 and 24)

4.8 Concluding Remarks

Based on the error analysis presented in Chapter 3, a linear combination functional model is proposed, formed from the single-differenced functional equation for baselines from the user roving receiver to three or more reference stations. In the functional model the orbit biases and ionospheric delay terms can be eliminated and, in addition, the tropospheric delay, multipath and the observation noise can be reduced. Because the linear ionospheric delay interpolation model has been used in the derivation, the separations between reference stations should be less than about 200 km, a distance that is dependent on the ionospheric conditions even though the satellite-by-satellite and epoch-by-epoch method is used. The roving receiver should be located within the figure formed by the reference stations so that the coefficients are less than 1, and the multipath and observation noise are reduced.

From the computational point of view, the proposed integrated method using pseudo-range and carrier phase observations makes instantaneous ambiguity resolution possible. The computation time is sufficiently short to support real-time applications. With the integrated method, a three-step quality control procedure is used to derive reliable results. The suggested real-time stochastic model estimation procedure is a refinement of the fidelity of the functional and stochastic models and makes the estimation results more reliable. The suggested procedure for discriminating between the integer ambiguity sets which generates the minimum quadratic form of the residuals and the second minimum one has rigorous statistical meaning and is very efficient for practical use. The global measure related to the neighbouring epochs (the variation in the TEC quantity) has been used to define necessary conditions to enhance the reliability of the results. The adaptive procedure is very powerful and leads to maximum positioning success rates. Using the proposed integrated method with the three-step quality control procedure, positioning success rates of 100%, 100%, 99.7% and 98.4% have been obtained for the four sets of data considered. These are a significant improvement on the success rates of 80.8%, 93.1%, 89.4% and 68.4%, obtained using the standard ratio test. In the case of the medium-range experiment the improvement is also significant, there is a 100% success rate.

This algorithm has been designed for real-time applications. Although the data has been post-processed, all calculations were carried out in a simulated real-time processing mode.

Although in the case of the medium-range experiment there were not enough GPS receivers to allow for verification, and the observation session is very short (one hour for the reference stations and 32 minutes for the roving receiver), and the separations between the three reference stations are 40.0 km, 65.6 km and 70.7 km, and the distance from the roving receiver to Mather Pillar reference station ranges from about 31.5 km to 37.5 km, impressive results were nevertheless obtained. This experiment has demonstrated the power of the proposed technique for medium-range kinematic positioning. Greater separation between the roving receiver and reference stations will be tested in the near future.

Chapter 5

AMBIGUITY RECOVERY TECHNIQUE FOR LONG-RANGE GPS KINEMATIC POSITIONING

5.1 Introduction

Long-range GPS kinematic positioning to sub-decimetre accuracy requires that the carrier phase ambiguities be resolved to their integer values. There are many techniques for on-the-fly ambiguity resolution for short baselines (<20km), but none have been proposed explicitly for long-range kinematic applications (100s to 1000s km). Colombo et al. (1995) suggested a two-step procedure. The first step is an initialisation which can fix the initial integer ambiguity using static data at the beginning of a kinematic session. The second step is to compute the trajectory using a Kalman filter and smoothing algorithm. This technique requires a re-initialisation procedure if cycle slips occur during the period the antenna is in motion. This involves a cycle slip repair procedure, or ambiguity resolution on-the-fly, for the long-range kinematic positioning case.

A cycle slip repair algorithm using undifferenced, dual-frequency carrier phase data and P-code pseudo-range data was suggested by Blewitt (1990). This algorithm requires a smoothly varying ionospheric electron content and the algorithm was successfully applied for single static station data when Anti-Spoofing (AS) was off. When AS is on, the precise pseudo-range data output by receivers such as the Ashtech Z12, Leica SR 399 or Trimble 4000SSi is not accurate enough to determine the widelane cycle slips, and subsequently the ionospheric combination does not have an integer ambiguity characteristic. Therefore, another combination of carrier phase observations $(-7\varphi_1 + 9\varphi_2)$, together with the widelane observable, was suggested by Han & Rizos (1995a). However, for a mobile receiver, especially where the satellite elevation is relatively low (< 40 deg), or when a few tens of seconds of data gap exist, the cycle slip cannot be uniquely determined.

Another way of recovering cycle slips is to use ambiguity resolution techniques. Using the search procedure in the measurement domain (Blewitt, 1989; Abidin & Wells, 1990) it is difficult to determine the widelane integer ambiguity using precise pseudo-range data when AS is on. On the other hand, it is also difficult to obtain high precision real-valued ambiguity estimates using the ionosphere-free combination even when the widelane ambiguity is known. In the case of the search techniques in the coordinate domain (Han & Rizos, 1996b; Mader, 1992; Mok, 1996) the ionospheric effect is the main obstacle for long-range kinematic positioning. Using the search technique in the estimated ambiguity domain based on integer least squares estimation (Han, 1995c; Teunissen, 1994), the ionosphere is considered an unknown parameter, which results in the geometry being significantly worse and the resulting large search region makes this technique difficult to apply for long-range GPS positioning.

If the cycle slip repair procedures and ambiguity resolution techniques are combined to resolve the cycle slip, it is found that all of these ambiguity resolution techniques will make contributions to the cycle slip repair process. The problem of cycle slip detection and repair does not involve "absolute" ambiguity determination, but rather "relative" ambiguity determination over time. The concern is only with the biases on phase observations that change with time. It is then possible to carry out cycle slip detection and repair using one-way data within a short time period. If the integer ambiguities at previous epochs are known, the ionospheric delay can be computed and these biases at the current epoch can be predicted with high precision. This means that the Ambiguity Function Method (AFM) can then be used to detect and remove cycle slips, even for the long-range kinematic positioning case. If integer ambiguity candidates are available from the cycle slip repair procedure, the search in the estimated ambiguity domain will become easier and validation criteria can be used to verify that the selected integer ambiguity set is significantly better than others. *In this chapter, an ambiguity recovery procedure that integrates ambiguity resolution and cycle slip repair techniques is proposed.*

5.2 GPS Long-Range Kinematic Positioning using Single Reference Stations

The observation equations and the ambiguity resolution procedure for high precision long-range static positioning were described in Blewitt (1989), and are based on the following equations:

$$R_1 = \rho + \frac{I}{f_1^2} + \varepsilon_{R_1} \tag{5-1}$$

$$\varphi_1\lambda_1 = \rho - \frac{I}{f_1^2} + N_1\lambda_1 + \varepsilon_{\varphi_1} \tag{5-2}$$

$$R_2 = \rho + \frac{I}{f_2^2} + \varepsilon_{R_2} \tag{5-3}$$

$$\varphi_2\lambda_2 = \rho - \frac{I}{f_2^2} + N_2\lambda_2 + \varepsilon_{\varphi_2} \tag{5-4}$$

where R_1 and R_2 are the one-way precise pseudo-ranges on L1 and L2; φ_1 and φ_2 are the one-way carrier phase observations in units of cycles; ρ is the geometric range from station to satellite; I is a function of the Total Electron Content (TEC) of the ionosphere; f_1, f_2 and λ_1, λ_2 are the frequencies and wavelengths of the L1 and L2 carrier waves respectively; N_1 and N_2 are the integer cycle ambiguities of the L1 and L2 carrier phase observations; and ε is the observation noise with respect to the observation type indicated by its subscript. The carrier phase combination (i, j) can be represented as (Han & Rizos, 1996b):

$$\varphi_{i,j} = i \cdot \varphi_1 + j \cdot \varphi_2 \tag{5-5}$$

and its integer ambiguity and wavelength are:

$$N_{i,j} = i \cdot N_1 + j \cdot N_2 \tag{5-6}$$

$$\lambda_{i,j} = c / (i \cdot f_1 + j \cdot f_2) \tag{5-7}$$

where c in equation (5-7) is the speed of light in a vacuum, i and j are arbitrary integer numbers. The double-differenced ionosphere-free combination observation can be represented by the formula:

$$\Delta\nabla\varphi_{77,-60}\lambda_{77,-60} = \Delta\nabla\rho + \Delta\nabla N_{77,-60}\lambda_{77,-60} + \varepsilon_{\Delta\nabla\varphi_{77,-60}\lambda_{77,-60}} \tag{5-8}$$

If the integer ambiguities $\Delta\nabla N_1$ and $\Delta\nabla N_2$ have been determined in an initialisation procedure, the integer ambiguity for the ionosphere-free combination can be determined

as $\Delta\nabla N_{77,-60} = 77 \cdot \Delta\nabla N_1 - 60 \cdot \Delta\nabla N_2$. The double-differenced ionospheric delay can be also computed using the following relation:

$$\Delta\nabla\left(\frac{I}{f_1^2}\right) = \frac{f_2^2}{f_1^2 - f_2^2}\left[(\Delta\nabla\varphi_1 - \Delta\nabla N_1)\lambda_1 - (\Delta\nabla\varphi_2 - \Delta\nabla N_2)\lambda_2\right] \tag{5-9}$$

If there are no cycle slips during the whole observation session the integer ambiguity will remain a constant. If cycle slips do occur, a cycle slip repair or ambiguity recovery technique should be implemented.

5.3 Cycle Slip Detection and Repair using Precise Pseudo-Range Data

Cycle slip detection and repair for one-way data was first suggested by Blewitt (1990) for static environment. For the kinematic environment, especially when AS is on, a more efficient cycle slip detection and repair procedure is suggested by Han & Rizos (1995a), based on the widelane and $\varphi_{-7,9}$ combinations.

5.3.1 Selection of Carrier Phase Combinations for Cycle Slip Detection and Repair

Ionosphere-free combination

Based on equations (5-1) and (5-3), the geometry-free and ionosphere-free combination of pseudo-range observations can be derived:

$$\frac{I}{f_1^2} = -\frac{f_2^2}{f_1^1 - f_2^2}(R_1 - R_2) \tag{5-10}$$

$$\rho = \frac{f_1^2}{f_1^2 - f_2^2}R_1 - \frac{f_2^2}{f_1^2 - f_2^2}R_2 \tag{5-11}$$

Based on equations (5-2) and (5-4), the carrier phase combination $\varphi_{i,j}$ can be expressed as:

$$\varphi_{i,j} = i \cdot \varphi_1 + j \cdot \varphi_2 = \frac{1}{\lambda_{i,j}} \cdot \rho - \left(\frac{i}{\lambda_1} + \frac{j}{\lambda_2} \cdot \frac{f_1^2}{f_2^2} \right) \cdot \frac{I}{f_1^2} + N_{i,j} \tag{5-12}$$

Substituting equations (5-10) and (5-11) into equation (5-12) gives:

$$N_{i,j} = \varphi_{i,j} + a \cdot R_1 + b \cdot R_2 \tag{5-13}$$

where

$$a = -(i \cdot \frac{f_1^2 + f_2^2}{f_1^2 - f_2^2} + j \cdot \frac{2f_1 f_2}{f_1^2 - f_2^2}) \frac{1}{\lambda_1} = -\frac{9240(i+j) + 289 \cdot i}{2329 \cdot \lambda_1} \tag{5-14}$$

$$b = (i \cdot \frac{2f_1 f_2}{f_1^2 - f_2^2} + j \cdot \frac{f_1^2 + f_2^2}{f_1^2 - f_2^2}) \frac{1}{\lambda_2} = \frac{9240(i+j) + 289 \cdot j}{2329 \cdot \lambda_2} \tag{5-15}$$

The standard deviation $m_{N_{i,j}}$ of the computed ambiguities $N_{i,j}$ can be represented as follows:

$$m_{N_{i,j}} = \sqrt{i^2 \cdot m_{\varphi_1}^2 + j^2 \cdot m_{\varphi_2}^2 + a^2 \cdot m_{R_1}^2 + b^2 \cdot m_{R_2}^2} \tag{5-16}$$

Note that for some combinations (i, j) this is dominated by the uncertainty in the pseudo-ranges. Table 5-1 summarises the characteristics of some useful dual-frequency carrier phase combinations suggested by Han & Rizos (1996b). In particular note the range of values of $m_{N_{i,j}}$ in the last column of Table 5-1. The "best" combination, or that with the smallest standard deviation $m_{N_{i,j}}$, is $\varphi_{1,-1}$.

Table 5-1. Standard deviation of real-valued ionosphere-free ambiguities

Obs. Type	λ (m)	a	b	$m_{N_{i,j}}(\lambda)^*$
φ_1	0.190	21.501	16.246	8.085
φ_2	0.244	20.849	16.754	8.024
$\varphi_{77,-60}$	0.006	404.638	245.690	142.020
$\varphi_{1,-1}$	0.862	0.652	-0.508	0.248
$\varphi_{-1,2}$	0.341	20.197	17.262	7.971
$\varphi_{-3,4}$	1.628	18.892	18.278	7.886
$\varphi_{-7,9}$	14.653	37.133	37.065	15.740

* assume that $m_{\varphi_1} = m_{\varphi_2} = 0.01$ cycle and $m_{R_1} = m_{R_2} = 0.3$ metre

Hence, using equation (5-13), it appears that $N_{1,-1}$ can be well determined, but it is difficult to compute any other ambiguities, including the L1 and L2 integer ambiguities. Substituting $i = 1$ and $j = -1$ into equation (5-13), the following relation can be derived:

$$N_{1,-1} = \varphi_{1,-1} - \frac{17}{137 \cdot \lambda_1} \cdot R_1 - \frac{17}{137 \cdot \lambda_2} \cdot R_2 \tag{5-17}$$

which is one combination used for cycle slip detection and repair if precise pseudo-ranges R_1 and R_2 are available.

Ionosphere-biased ambiguity estimation

In order to derive the N_1 and N_2, other combinations should be selected, which will be biased by the ionospheric delay. Another formula that includes the ionospheric delay term and minimises the pseudo-range contribution is:

$$R = \rho + \beta \cdot \frac{I}{f_1^2} \tag{5-18}$$

where R can be chosen as being either R_1 or R_2, or the mean value of R_1 and R_2, and β is defined as:

$$\beta = \begin{cases} 1 & \text{for} \quad R = R_1 \\ 1.647 & \text{for} \quad R = R_2 \\ 1.323 & \text{for} \quad R = (R_1 + R_2)/2 \end{cases} \tag{5-19}$$

Combining equations (5-12) and (5-18), the following relation can be derived:

$$N_{i,j} = \varphi_{i,j} - \frac{R}{\lambda_{i,j}} + \gamma_{i,j} \cdot \frac{I}{f_1^2} \tag{5-20}$$

where

$$\gamma_{i,j} = \left(\frac{i}{\lambda_1} + \frac{j}{\lambda_2} \cdot \frac{f_1^2}{f_2^2} \right) + \frac{\beta}{\lambda_{i,j}} = \left(\frac{4620 \cdot i + 5929 \cdot j}{4620 \cdot i + 3600 \cdot j} + \beta \right) \cdot \frac{1}{\lambda_{i,j}} \tag{5-21}$$

The standard deviation of the computed $N_{i,j}$ (with the ionospheric effect removed) can be expressed as:

$$m_{N_{i,j}} = \sqrt{i^2 \cdot m_{\varphi_1}^2 + j^2 \cdot m_{\varphi_2}^2 + \frac{1}{\lambda_{i,j}^2} \cdot m_R^2} \tag{5-22}$$

The smaller the observation noise of R and the larger the wavelength $\lambda_{i,j}$, the smaller the noise of the computed $N_{i,j}$. For a single pseudo-range, the raw pseudo-range measurement has minimum noise. For two pseudo-range observations, the mean value of R_1 and R_2 has the minimum noise. Table 5-2 gives the noise of the computed $N_{1,-1}$, $N_{-3,4}$ and $N_{-7,9}$ and their ionospheric parameters γ using R_1, R_2 or the mean value of R_1 and R_2.

Table 5-2. Standard deviation of real-valued ionosphere-biased ambiguities

R	$N_{1,-1}$		$N_{-3,4}$		$N_{-7,9}$	
	$m_{N_{1,-1}}$	$\gamma_{1,-1}$	$m_{N_{-3,4}}$	$\gamma_{-3,4}$	$m_{N_{-7,9}}$	$\gamma_{-7,9}$
R_1	0.348	-0.329	0.191	11.825	0.116	23.979
R_2	0.348	0.422	0.191	12.222	0.116	24.023
mean	0.247	0.047	0.140	12.024	0.115	24.001

Note to Column $m_{N_{i,j}}$: assume that $m_{\varphi_1} = m_{\varphi_2} = 0.01$ cycle and $m_{R_1} = m_{R_2} = 0.3$ metre

If the ionospheric bias can be predicted with high precision over a short period, the computed value of $N_{-7,9}$ will be of high precision. If only one precise pseudo-range R_1 or R_2 is available, equation (5-20) should replace equation (5-13) to compute $N_{1,-1}$, but considering the odd-even relationship between $N_{1,-1}$ and $N_{-7,9}$.

Although the ionospheric combination:

$$\begin{aligned} \varphi_1\lambda_1 - \varphi_2\lambda_2 &= -\left(\frac{I}{f_1^2} - \frac{I}{f_2^2}\right) + N_1\lambda_1 - N_2\lambda_2 \\ &= -\left(\frac{I}{f_1^2} - \frac{I}{f_2^2}\right) + N_{1,-1}\lambda_1 - N_2(\lambda_2 - \lambda_1) \end{aligned} \tag{5-23}$$

has no pseudo-range noise effects, it has no integer characteristic. If and only if $N_{1,-1}$ is known, the equivalent wavelength becomes $\lambda_2 - \lambda_1 \approx 5.4$cm. But $N_{1,-1}$ cannot be determined when AS is on and the antenna is moving. Therefore, the best choice is

$N_{-7,9}$ and equation (5-20) can be used to compute $N_{-7,9}$ by substituting i=-7 and j=9. If only one of R_1 and R_2 is available, equation (5-20) is also selected to compute $N_{1,-1}$.

5.3.2 Cycle Slip Detection and Repair for One-Way Data

Real-valued cycle slip estimations

If precise pseudo-ranges on L1 and L2 are available, equation (5-17) can be used to compute the widelane ambiguity sequence $N_{1,-1}(k)$ and equation (5-20) can be used to compute the $N_{-7,9}(k)$ using the mean value of the two precise pseudo-ranges. If only one of the precise pseudo-ranges on L1 and L2 is available, equation (5-20) can be used to compute the sequences $N_{1,-1}(k)$ and $N_{-7,9}(k)$.

The biases caused by the ionospheric delay have very strong correlation between epochs and can be represented as a linear function of time, for short periods of up to a few minutes. If some epochs are used to fit the ionospheric delay as a linear function of time and to predict the value at the next epoch, the differences between the predicted value $N^{-}_{1,-1}(k)$ (or $N^{-}_{-7,9}(k)$) using previous epochs and the computed value $N_{1,-1}(k)$ (or $N_{-7,9}(k)$), using observations at this epoch by equations (5-17) and (5-20), can be obtained:

$$DN_{1,-1}(k) = N_{1,-1}(k) - N^{-}_{1,-1}(k) \tag{5-24}$$

$$DN_{-7,9}(k) = N_{-7,9}(k) - N^{-}_{-7,9}(k) \tag{5-25}$$

The standard deviations of $DN_{1,-1}(k)$ and $DN_{-7,9}(k)$ can also be obtained. If no cycle slip or multipath effect is present, the noises of $DN_{1,-1}(k)$ and $DN_{-7,9}(k)$ are dependent on the correlations of the ionospheric delay and the noise of the observations. If the ionospheric delay changes rapidly, the noises will be larger. This has been verified by the experimental results in Section 5.6.

Determination of the integer cycle slip candidates

Based on the cycle slip estimates (equations (21) and (22)) and their standard deviations, all candidates for integer cycle slips on $\varphi_{1,-1}$ and $\varphi_{-7,9}$, can be formed using the odd-even relationship, which can be derived from the definitions of $N_{1,-1}$ and $N_{-7,9}$:

if $N_{1,-1}$ is even → $N_{-7,9}$ has to be even

if $N_{1,-1}$ is odd → $N_{-7,9}$ has to be odd

This odd-even relation implies that when one of these is resolved, the effective wavelength of the other is doubled, and can therefore be resolved more easily. The cycle slips $CS_{1,-1}$ and $CS_{-7,9}$ are subject to the same conditions:

if $CS_{1,-1}$ is even → $CS_{-7,9}$ has to be even

if $CS_{1,-1}$ is odd → $CS_{-7,9}$ has to be odd

Obviously it is easy to determine $CS_{1,-1}$ when $CS_{-7,9}$ is determined, and vice versa. The cycle slips on φ_1 and φ_2 can then be determined using the following relations:

$$CS_1 = \frac{1}{2}(CS_{-7,9} + 9 \cdot CS_{1,-1}) \tag{5-26}$$

$$CS_2 = \frac{1}{2}(CS_{-7,9} + 7 \cdot CS_{1,-1}) \tag{5-27}$$

For a static receiver, this step can detect and repair almost all cycle slips due to the low noise. However, for a roving receiver, especially where the satellite elevation is relatively low($< 40°$), or when a few tens of seconds data gap exist, the cycle slip cannot be determined as a unique set. Therefore, many cycle slip candidate sets will be formed. The following tests will be necessary.

5.3.3 Cycle Slip Detection and Repair for Double-Differenced Data

If the cycle slip in one-way carrier phase cannot be determined as one set using the above procedure, the geometric constraints and Kalman filter prediction information should be used to create validation and rejection criteria in order to resolve the correct set of cycle slips. Using equations (5-24) and (5-25), the real-valued cycle slip estimates and their standard deviations can be computed. The search regions for $DN_{1,-1}$ and $DN_{-7,9}$ can be formed in the one-way case and then used to create the search region for the double-differenced observable. The satellite with the highest elevation is selected as the

reference satellite. For each double-differenced cycle slips, the following tests should be applied:

Test 1: Tests on the innovation sequences of $\Delta\nabla\hat{\varphi}_{1,-1}$ and $\Delta\nabla\hat{\varphi}_{-7,9}$

The ionospheric delay value for each double-differenced observable can be predicted using the ionospheric delay values computed at the previous epochs (equation (5-9)), and the ionosphere-corrected observable of $\Delta\nabla\hat{\varphi}_{1,-1}$ and $\Delta\nabla\hat{\varphi}_{-7,9}$ can be obtained. The innovation values can be computed using the following equations:

$$\Delta\nabla L_{1,-1} = (\Delta\nabla\hat{\varphi}_{1,-1} - \Delta\nabla CS_{1,-1})\lambda_{1,-1} - HX(-) \tag{5-28}$$

$$\Delta\nabla L_{-7,9} = (\Delta\nabla\hat{\varphi}_{-7,9} - \Delta\nabla CS_{-7,9})\lambda_{-7,9} - HX(-) \tag{5-29}$$

If $\Delta\nabla L_{1,-1} \sim N(0, D_{1,-1} + HP(-)H^T)$ or $\Delta\nabla L_{-7,9} \sim N(0, D_{-7,9} + HP(-)H^T)$, $\Delta\nabla CS_{1,-1}$ or $\Delta\nabla CS_{-7,9}$ will pass the tests, otherwise $\Delta\nabla CS_{1,-1}$ or $\Delta\nabla CS_{-7,9}$ should be rejected. $X(-)$ and $P(-)$ are the Kalman predicted position and its variance matrix; H is the design matrix in the Kalman filter; $D_{1,-1}$ and $D_{-7,9}$ are the variances of $\Delta\nabla\hat{\varphi}_{1,-1}\cdot\lambda_{1,-1}$ and $\Delta\nabla\hat{\varphi}_{-7,9}\cdot\lambda_{-7,9}$.

Test 2: Test on the quadratic form of the residuals of $\Delta\nabla\hat{\varphi}_{1,-1}$

Using the ionosphere-corrected double-differenced widelane observable and the Kalman filter predicted position, the update position and the quadratic form of the residuals $(QF_{1,-1})_i$ with respect to a cycle slip candidate set i can be computed. The following test should then be applied:

$$\left(QF_{1,-1}\right)_i = V_{1,-1}^T D_{1,-1}^{-1} V_{1,-1} + \delta X_{1,-1}^T P^{-1}(-)\delta X_{1,-1} \tag{5-30}$$

$$\frac{\left(QF_{1,-1}\right)_i}{\left(QF_{1,-1}\right)_{min}} < F \tag{5-31}$$

where $V_{1,-1}$ is the residual vector of the widelane observable at this epoch; $\delta X_{1,-1}$ is the correction to $X(-)$ using the widelane observable; F is an empirical value normally chosen as being the value 2. If a cycle slip candidate set does not pass the test (equation (5-31)), this set should be rejected.

Test 3: Contrast tests on quadratic form of the residuals of $\Delta\nabla\hat{\varphi}_{77,-60}$

Using all cycle slip candidate sets that have passed the previous tests, the cycle slip candidates of the ionosphere-free observable can be formed. Table 5-3 gives an example in which $\Delta\nabla N_{1,-1}$ and $\Delta\nabla N_{-7,9}$ are [-2,2], and all possible candidate sets are formed for the ionosphere-free observable. The minimum discrepancy among these candidates is 10.7cm. Fixing one set of cycle slips, the current epoch data should be used within the Kalman filter and the quadratic form of the residuals $QF_{77,-60}$ should be computed for each set of cycle slips. If the smallest $(QF_{77,-60})_{min}$ and $(QF_{77,-60})_i$ with respect to a cycle slip candidate set i are not consistent with the relation:

$$\frac{(QF_{77,-60})_i}{(QF_{77,-60})_{min}} < F \tag{5-32}$$

the cycle slip candidate set i should be rejected. F is also normally chosen as 2. If all other sets, except the one that has the smallest $(QF_{77,-60})_{min}$, are rejected, the cycle slip set derived $(QF_{77,-60})_{min}$ is selected as the correct cycle slip value. Otherwise all cycle slip sets that have passed the test (equation (5-32)) should be treated as candidates for the next epoch.

Table 5-3. Biases of different candidates on double-differenced ranges

$\Delta\nabla N_{1,-1}$ (cy)	$\Delta\nabla N_{-7,9}$ (cy)	$\Delta\nabla N_1$ (cy)	$\Delta\nabla N_2$ (cy)	$\Delta\nabla N_{77,-60}\cdot\lambda_{77,-60}$ (m)
-2	-2	-10	-8	-1.827
	0	-9	-7	-1.720
	+2	-8	-6	-1.613
-1	-1	-5	-4	-0.913
	+1	-4	-3	-0.806
0	-2	-1	-1	-0.107
	0	0	0	0
	2	+1	+1	0.107
+1	-1	+4	+3	0.806
	+1	+5	+4	0.913
+2	-2	+8	+6	1.613
	0	+9	+7	1.720
	+2	+10	+8	1.827

5.4 Cycle Slip Detection and Repair Without Precise Pseudo-Range Data

If there are more than four double-differences for L1 and L2 carrier phase and precise pseudo-range, the above procedure will be very powerful. However, precise pseudo-range data are not always available. Many GPS receivers do not output precise pseudo-range data when AS is on, including the Trimble 4000SSE, Leica System 200, and others. Although some receivers, such as the Ashtech Z12 and the new Leica System 300, output two precise pseudo-ranges on L1 and L2, the signal-to-noise ratio is relatively low, and the precise pseudo-ranges may not always be available even when L1 and L2 carrier tracking are maintained. If precise pseudo-range data are lost for a relatively long period, cycle slip detection and repair using the abovementioned procedure will become difficult. If the carrier phase observable is maintained, but no precise pseudo-range data is available, the cycle slip detection and repair step can be performed using a combination of the Ambiguity Function Method (AFM) and Kalman filtering. Details are presented below.

5.4.1 Cycle Slip Repair using the AFM and Kalman Filter

The Ambiguity Function Method is insensitive to integer biases such as cycle slips, and hence quite suitable for kinematic positioning applications. The equivalence of the AFM and least squares search methods has been proven (Lachapelle et al., 1992; Han, 1993). The AFM requires good initial positioning information in order to define the search region, and a relatively long wavelength carrier phase observable (formed from combinations of dual-frequency phase observations), in order to reduce the maxima points and the computation time (Han & Rizos, 1996b). The ionospheric effect is the main obstacle for its application in the long-range kinematic case, even when the precise ephemeris is available. If the AFM is not used for positioning, but rather for cycle slip detection and repair, the ionospheric delay can be computed at the previous epochs (equation (5-9)) using dual-frequency carrier phase observations and the known integer ambiguities. The ionospheric delay at the current epoch can be predicted with high precision if the prediction period is no more than a few minutes.

After the integer ambiguities are initialised, Kalman filter processing will be used to determine the position using the double-differenced carrier phase observations. The current version of the software considers the orbit as being known. The ionospheric

delay can be computed using equation (5-9). For the next epoch the ionospheric delay can be predicted, and the ionosphere-corrected carrier phase combination observations of $\Delta\nabla\hat{\varphi}_{1,-1}$ and $\Delta\nabla\hat{\varphi}_{-3,4}$ at the current epoch k can be used to compute the Ambiguity Function value:

$$A(X)=\left|\sum_{s=1}^{m_k}\exp\left[\vec{i}\cdot\left(2\pi\Delta\nabla\hat{\varphi}_{i,j}^{s}(k)-\frac{2\pi}{\lambda_{i,j}}\Delta\nabla\rho^{s}(X,k)\right)\right]\right| \tag{5-33}$$

where X is the trial position within the search region defined by the Kalman predicted position X(-) and its variance P(-); $\Delta\nabla\rho^{s}(X,k)$ is the computed double-differenced range for the double-differenced observation pair s at epoch k using the trial position X; m_k is the number of double-differenced observations at epoch k. When A(X) is larger than 95% of its expectation value, X will be considered to be a maxima point. If only one maxima point is obtained, this point is assumed to be the optimal position.

First, the AFM should be performed using the double-differenced observation $\Delta\nabla\hat{\varphi}_{-3,4}$ and the maxima positions obtained. The new search region should be centred at each maxima position and the AFM should be performed using $\Delta\nabla\hat{\varphi}_{1,-1}$, and then a set of cycle slip candidates can be obtained for each maxima position. The minimum distance among the maxima points is about twice the observation wavelength ($\lambda_{-3,4}=1.628\text{m}$) for six visible satellites, and about 1.2 times the observation wavelength in the case of five satellites (Han & Rizos, 1996b).

If only L1 carrier phase is available, the AFM can be performed using the L1 carrier phase observations. Because the wavelength is only 0.190m, the number of maxima points will be greater than for the dual-frequency case.

5.4.2. AFM with Constraints

Using the AFM, only fractions of the carrier phase observables are used, and hence the data processing is easily implemented. However, there is still other information valuable to positioning, such as the integer ambiguity values, which are not used. If two or three satellites are still tracking with no cycle slips, or cycle slips that can be repaired using the relevant precise pseudo-range data, their integer ambiguities can be used as constraints in the Ambiguity Function Method described above.

Assume the double-differenced observation s has known ambiguities ($\Delta\nabla N^s_{i,j}$) and has been corrected. The constraint can be written as:

$$\left|\Delta\nabla\hat{\varphi}^s_{i,j}(k+1) - \Delta\nabla N^s_{i,j} - \frac{1}{\lambda_{i,j}}\Delta\nabla\rho^s(X,k+1)\right| \le EPS \quad (31)$$

where EPS is a threshold value dependent on the observation accuracies, normally selected as three times the standard deviation of the observation. This constraint will make the search space reduce from three to two dimensions. If three satellites have no cycle slips, two constraints can be constructed and the search space will be reduced to one dimension. Figure 5-1 shows the search space reduced from two dimensions to one dimension. The maxima points will be reduced from 68 to 4.

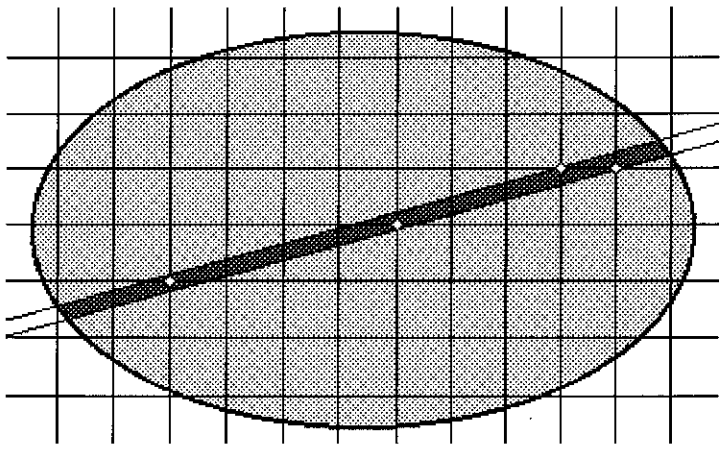

Figure 5-1. Maxima points reduced from two dimensions to one dimension

5.4.3 Validation Criteria for AFM in Long-Range Applications

Using all cycle slip candidate sets, the ionosphere-free observable at the current epoch can be formed and used in the Kalman filter. The quadratic form of the residuals $QF_{77,-60}$ should be computed for each set of cycle slips. The same test with equation (5-32) should be performed. If all sets except the one that has the smallest $(QF_{77,-60})_{min}$ are rejected, then the identified cycle slip set is selected as being the correct one. Otherwise all cycle slip sets that passed the test (equation (5-32)) should be treated as candidates for the next epoch.

5.5 Ambiguity Recovery Procedures

All data lost at certain epochs will cause gaps. This will occur if all satellite signals are obstructed or a failure within the receiver occurs. In general, the best observation environment should be selected for long-range kinematic positioning, and hence data gaps seldom occur and are usually only of short duration. The most frequent causes of data loss are due to obstructions of the signal, or a low signal-to-noise ratio caused by bad ionospheric conditions, multipath, high receiver dynamics, or low satellite elevation. Except in the case of a data gap, the data available at an epoch can be divided according to the three cases in Table 5-4.

Table 5-4. Cases of data loss

	Data Available
Case I	C/A, φ_1, φ_2, P1, or/and P2
Case II	C/A, φ_1, φ_2
Case III	C/A, φ_1

Case I: If four or more satellites have Case I data, it is considered that no data loss has occurred because one precise pseudo-range is enough to detect and repair cycle slips after a short data gap using the one-way cycle slip detection and repair procedure.

Case II: If less than four satellites have Case I data, but more than four satellites have Case II data, the Kalman filter and AFM procedure for the detection and repair of cycle slips can be used. If two or three satellites have precise pseudo-ranges which can be used to determine any cycle slips, the AFM with constraints procedure can be implemented. $\varphi_{1,-1}$ and $\varphi_{-3,4}$ will be used in this procedure. If the biases in the observations and the vehicle trajectory can be predicted with high precision, this procedure will be very powerful.

Case III: If four or less satellites have Case II data, but more than four satellites have Case III data, the Kalman filter and AFM with constraints procedure can be used for the single frequency case, but the maxima points will be more numerous than for the dual-frequency case due to its shorter wavelength (0.190m).

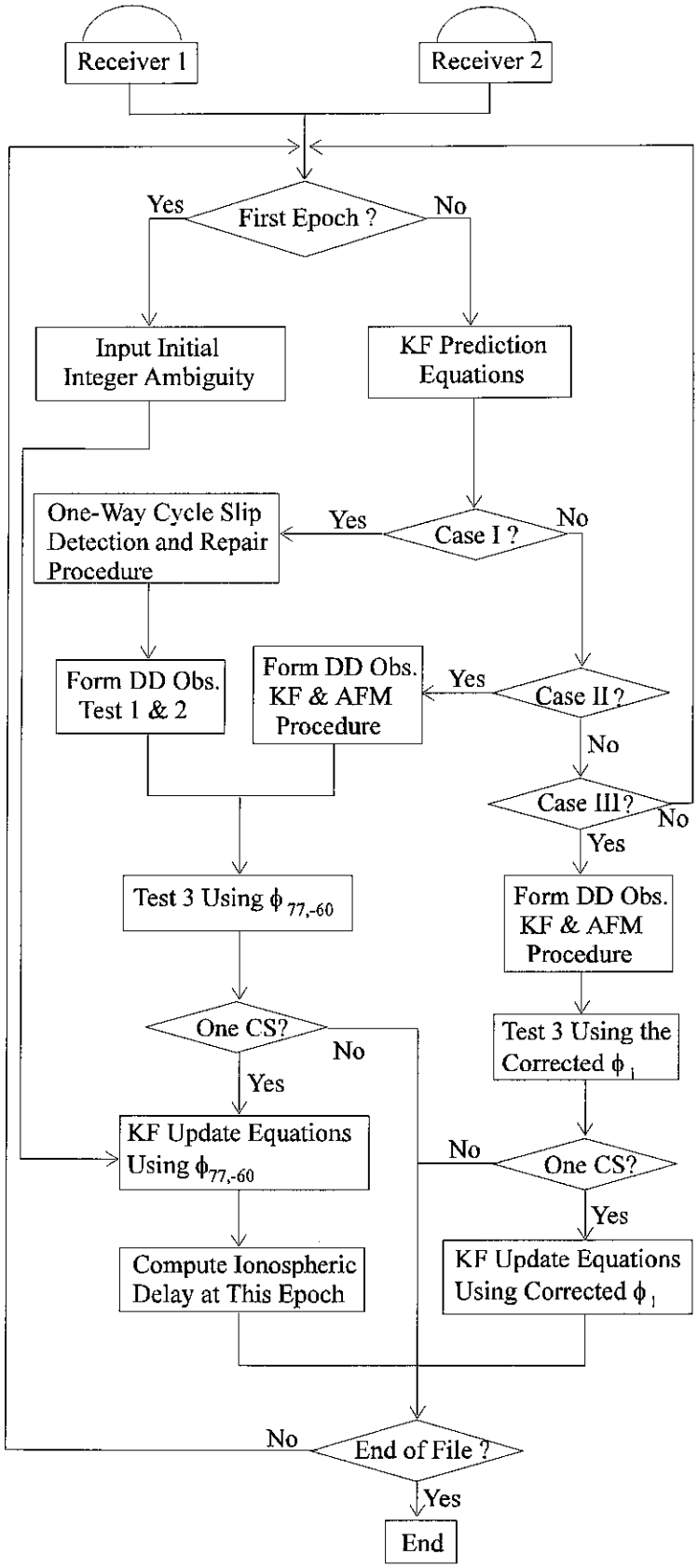

Figure 5-2. Cycle slip detection and repair procedure

Based on the above discussions, the ambiguity recovery procedure is summarised in Figure 5-2. After Test 3, if more than one candidate set is left, the current software deletes this epoch and then processes the next epoch. From data processing experience, this normally is due to multipath and having less than four precise pseudo-ranges available (Case II or III).

The one-way cycle slip detection and repair procedure can also be used in the ambiguity initialisation step. The cleaned data will then be used in the initialisation procedure.

5.6 Experiments

5.6.1 Aircraft Experiment

This experiment was carried out on 4 June, 1992, using Trimble 4000SST GPS receivers capable of measuring a single P-code pseudo-range on L2 (R2). The precise ephemeris was available. One receiver was mounted on a plane and the other was fixed at a site about 57.5 metres from the initial aircraft location. After 4-5 minutes static tracking the aircraft took off and its trajectory and height are plotted in Figures 5-3a and 5-3b. Equation (5-20) was used to compute $N_{1,-1}(k)$ and $N_{-7,9}(k)$, and then to predict $\bar{N}_{1,-1}(k)$ and $\bar{N}_{-7,9}(k)$ using the previous several epochs (ten epochs are chosen here). The differences between the predicted value and the computed value using real P-code pseudo-range data on L2 and dual-frequency carrier phase observations are plotted in Figures 5-4a and 5-4b for the aircraft receiver, and Figures 5-5a and 5-5b for the stationary receiver. For the roving receiver (Figures 5-4a and 5-4b), it can be seen that the noise of $DN_{-7,9}(k)$ is less than 0.25 cycles and $CS_{-7,9}(k)$ normally has one candidate set. If the noise of $DN_{1-1}(k)$ is greater than 0.5 cycles, $CS_{1,-1}(k)$ normally has more than one candidate set. The odd-even relationship will be very powerful for reducing the cycle slip candidate sets. For the stationary receiver (Figures 5-5a and 5-5b), the noise of $DN_{-7,9}(k)$ and $DN_{1-1}(k)$ is small enough to determine cycle slips. The elevation of this satellite (PRN 23) is plotted in Figure 5-5a. It can be seen that the lower the elevation, the higher the noise of $DN_{1-1}(k)$. Based on the cycle slip candidates in the one-way data, the double-differenced cycle slips can be formed and Test 1 and Test 2 then applied using the Kalman filter predicted position and the predicted ionospheric delay value. After Test 3 is applied, only one cycle slip candidate set is left at each epoch for this experiment.

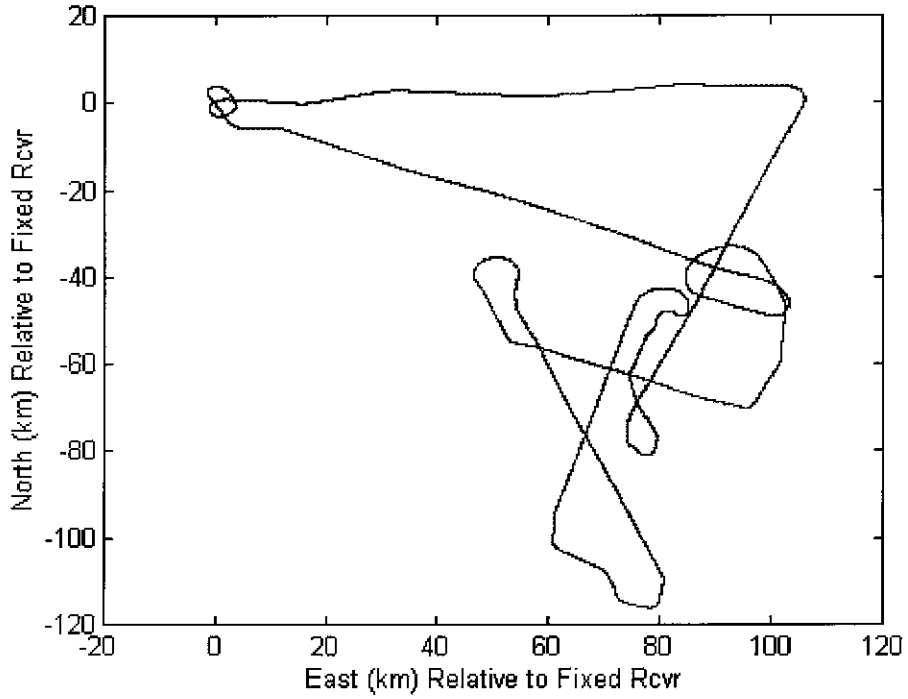

Figure 5-3a. Aircraft trajectory relative to fixed receiver for 4 June, 1992, experiment

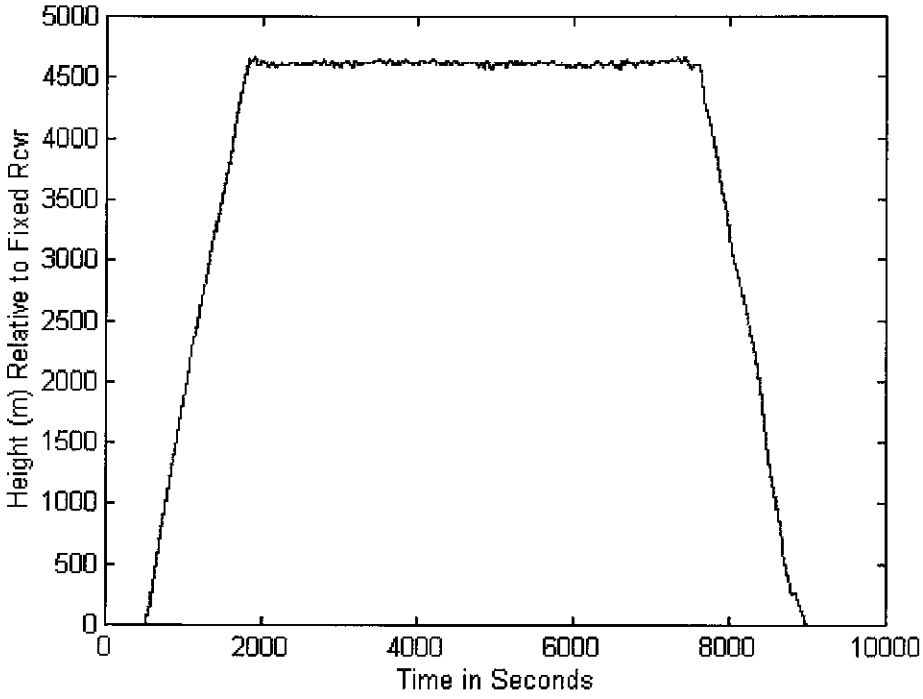

Figure 5-3b. Aircraft height relative to fixed receiver for 4 June, 1992, experiment

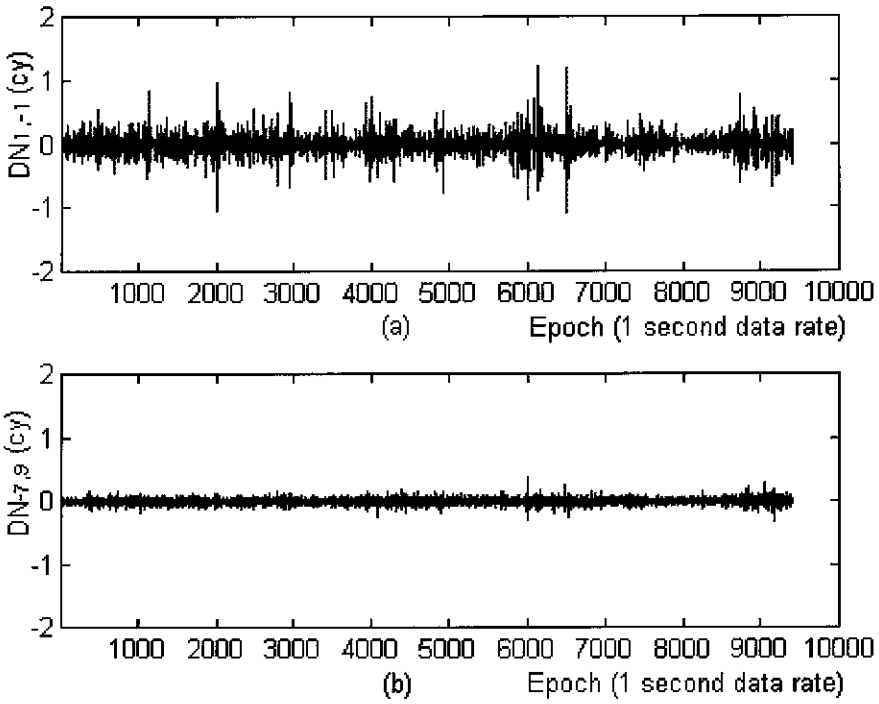

Figure 5-4. Real-valued cycle slip estimates ($DN_{1,-1}$ (a) and $DN_{-7,9}$ (b)) for aircraft receiver, 4 June, 1992, experiment

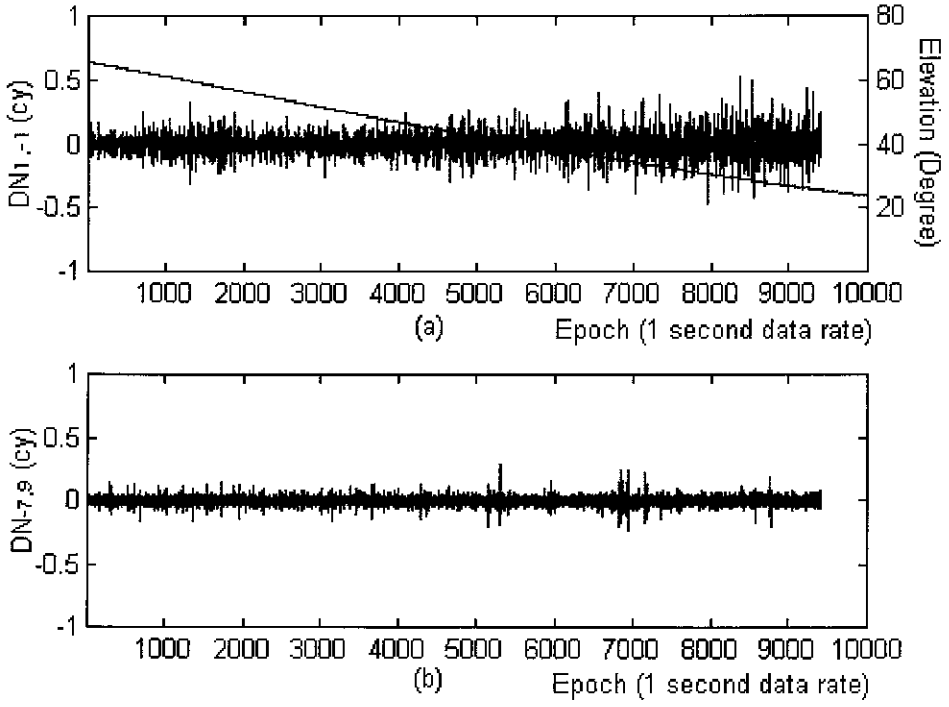

Figure 5-5. Real-valued cycle slip estimates ($DN_{1,-1}$ (a) and $DN_{-7,9}$ (b)) for fixed receiver, 4 June, 1992, experiment

In order to test the power of this procedure, a 60 second data gap after epoch k is simulated. The predicted $N^{-}_{1,-1}(k+60)$ and $N^{-}_{-7,9}(k+60)$ using 60 epochs of data before epoch k can be obtained. The computed real-valued cycle slips $DN_{1-1}(k+60)$ and $DN_{-7,9}(k+60)$ at each epoch are plotted in Figures 5-6a and 5-6b. It can be seen that the noise of $DN_{1-1}(k)$ does not change much, but the noise of $DN_{-7,9}(k)$ has increased significantly. The cycle slip detection and repair procedure can successfully determine one cycle slip candidate set. A 5 minute data gap simulation was then selected, but the data processing was not successful.

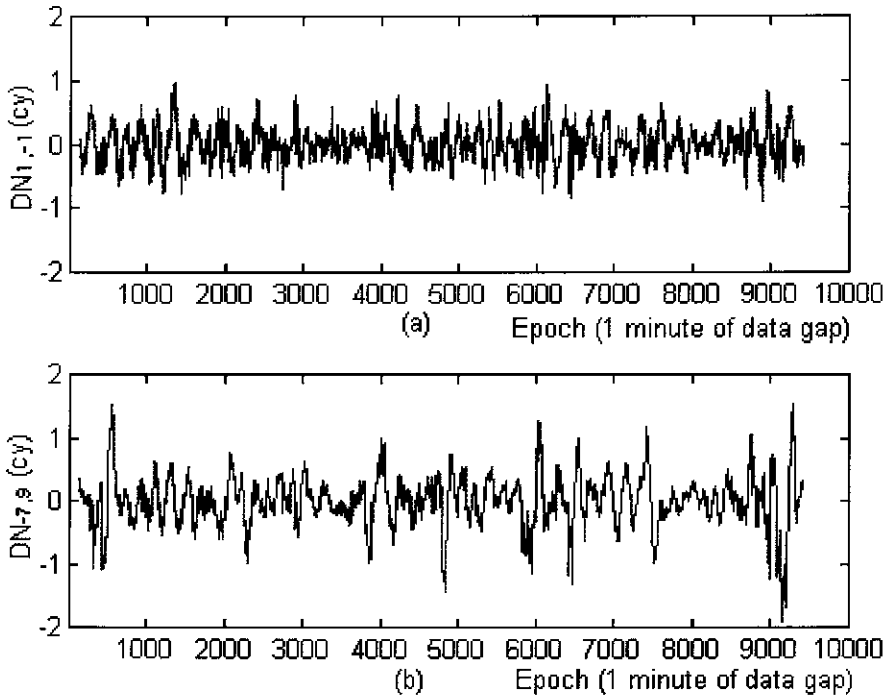

Figure 5-6. Real-valued cycle slip estimates ($DN_{1,-1}$ (a) and $DN_{-7,9}$ (b)) for aircraft receiver assuming 1 minute of data gap, 4 June, 1992, experiment

The Kalman filter and AFM procedure neglecting P2 pseudo-range is also used to detect and repair cycle slips. For 1-2 second data interval observations, the Kalman predicted position bias is less than 2.5 metres and the cycle slip detection and repair process was successful. For data sample interval greater than 2 seconds, more than one set of cycle slips are left and the process was not successful.

The initialisation is carried out using the first and last 5 minutes of static data (baseline length of the order of tens of metres), and the same double-differenced integer ambiguities were obtained, hence furnishing proof that indeed there are no cycle slips left in the data.

5.6.2 Train Experiment

This experiment was carried out on 6 October, 1994, using Ashtech Z12 GPS receivers, capable of measuring dual P-code pseudo-ranges when AS is on. The precise ephemeris was available. Two receivers were set up, separated by about 272 kilometres at the start. One was mounted on a train. After static tracking, the train receiver moved over a period of about 50 minutes. The trajectory and height are plotted in Figures 5-7a and 5-7b. Equations (5-17) and (5-20) were used to compute $N_{1,-1}(k)$ and $N_{-7,9}(k)$ and then to predict $\bar{N}_{1,-1}(k)$ and $\bar{N}_{-7,9}(k)$ using the previous several epochs of data (ten epochs are chosen here). The differences between the predicted value and the computed value ($DN_{1,-1}(k)$ and $DN_{-7,9}(k)$) are plotted in Figures 5-8a and 5-8b for the train receiver. The noise of $DN_{1,-1}(k)$ and $DN_{-7,9}(k)$ is less than about 0.1 cycles. This satellite (PRN 16) has the lowest elevation of the five satellites tracked, and is plotted in Figure 5-8a. It can be seen that cycle slip detection and repair is very easy for 1 second data rate observations if there is no data gap.

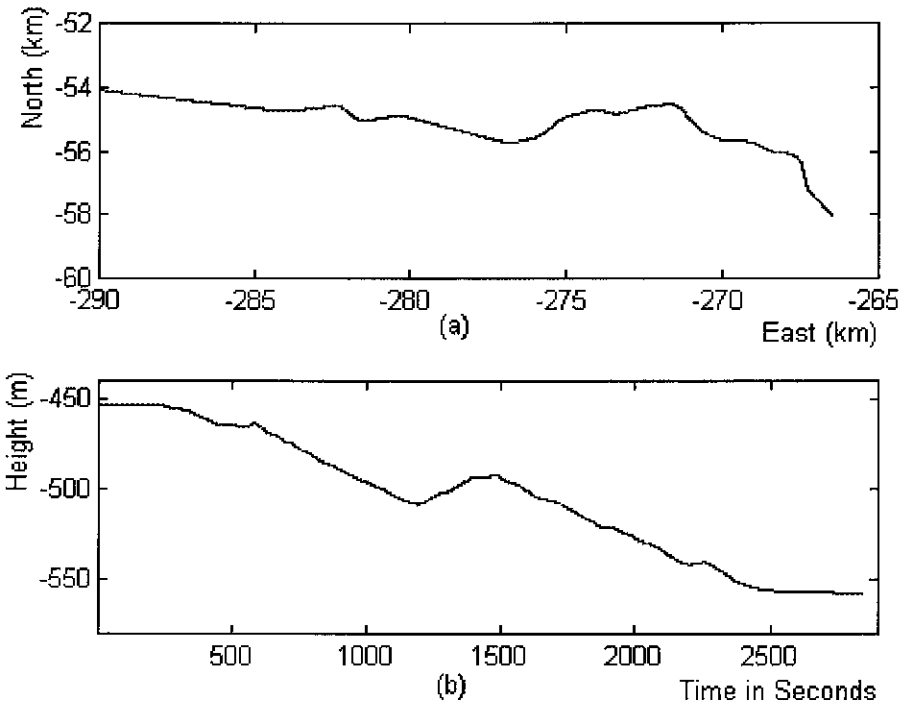

Figure 5-7. Train trajectory (a) and height (b) relative to fixed receiver for 6 October, 1994, experiment

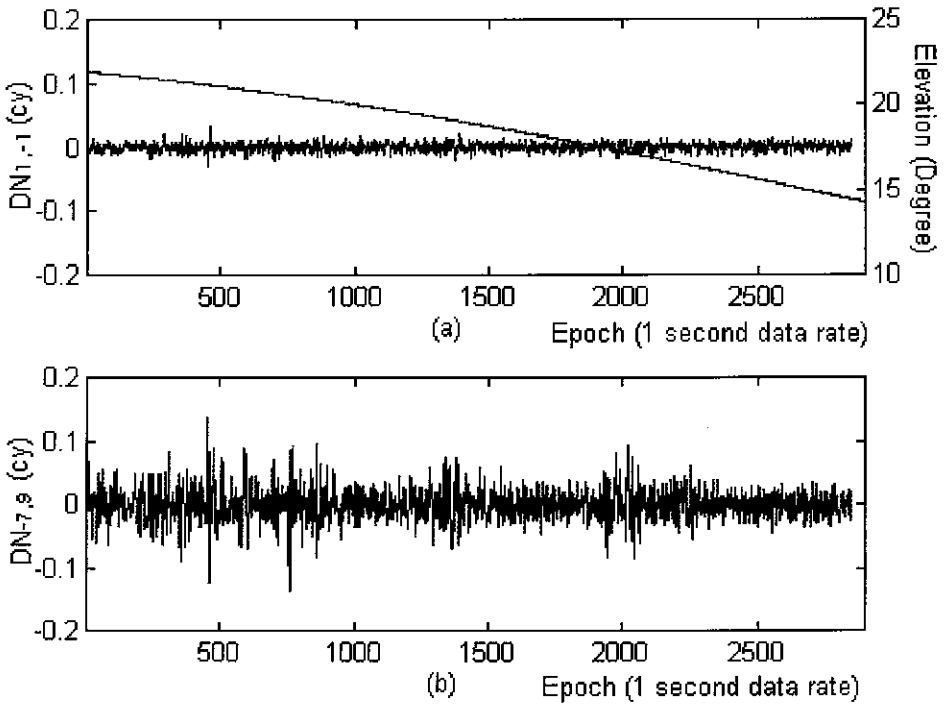

Figure 5-8. Real-valued cycle slip estimates ($DN_{1,-1}$ (a) and $DN_{-7,9}$ (b)) for train receiver for 6 October, 1994, experiment

A data gap of 5 minutes was simulated at each epoch, similar to what was done for the aircraft experiment, and the real-valued cycle slip estimates are plotted in Figures 5-9a and 5-9b. The suggested procedure can successfully determine one set of cycle slip values. The 5 minute cleaned data are used to predict $N^{-}_{1,-1}$ and $N^{-}_{-7,9}$ when DN_{1-1} and $DN_{-7,9}$ are computed.

Multipath and the bias caused by receiver internal filtering will cause the real-valued cycle slip estimates to be biased. Figure 5-10 gives an example of a cycle slip during a short data gap. The problem is that there are multipath effects or other biases before and after the data gap. In this case, the current software will delete all affected data which can be identified by the linear fitting procedure.

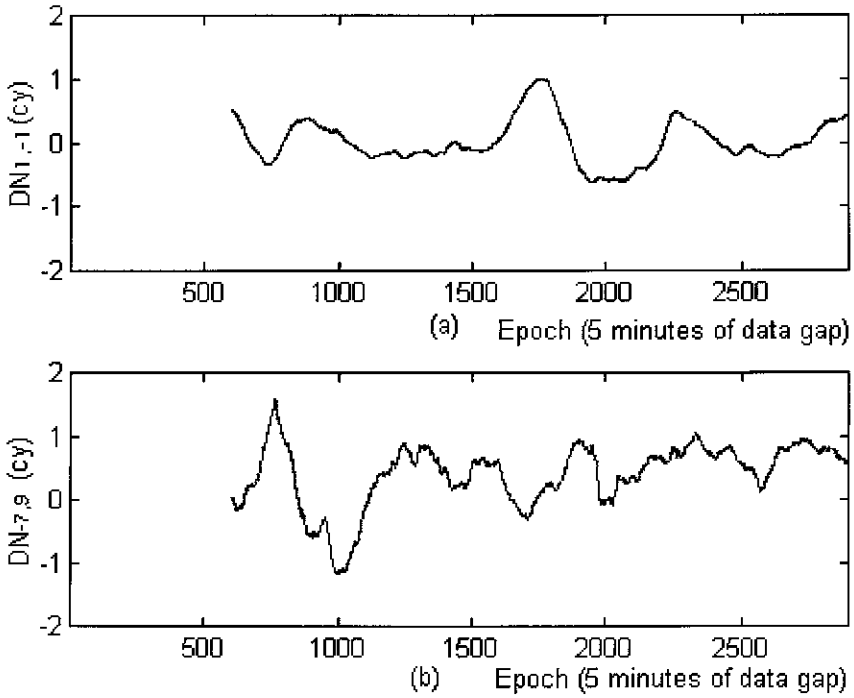

Figure 5-9. Real-valued cycle slip estimates ($DN_{1,-1}$ (a) and $DN_{-7,9}$ (b)) for train receiver assuming 5 minutes of data gap for 6 October, 1994, experiment

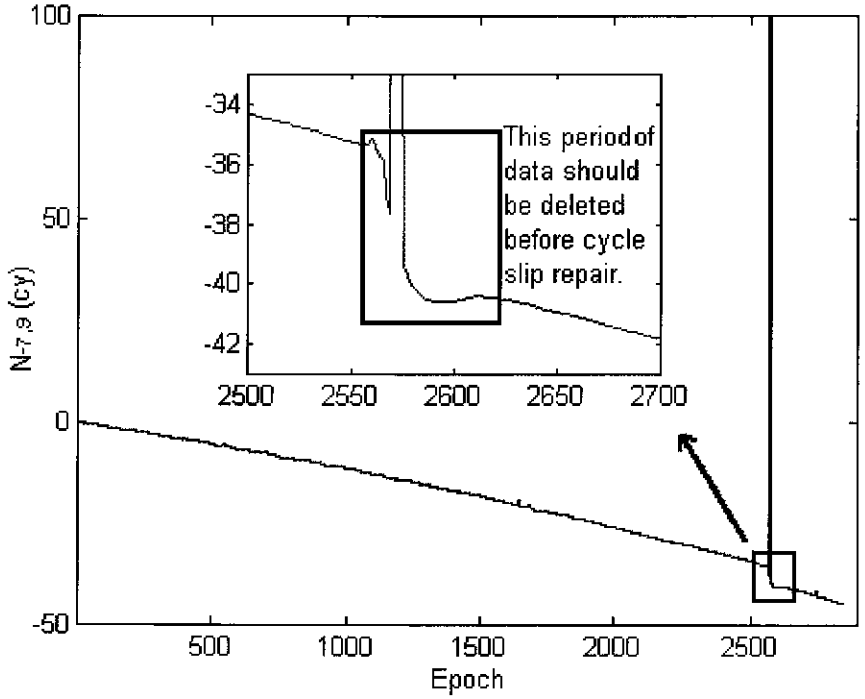

Figure 5-10. Cycle slip occurred in PRN 18 of train receiver for 6 October, 1994, experiment

The Kalman filter and AFM procedure is also used to detect and repair cycle slips. For data with 1-3 second sample rate selected from this data set, the predicted position biases are less than about 2.5 metre, and cycle slip detection and repair is successful. For the data with larger interval than 3 seconds, more than one set of cycle slip candidates will remain and the result is therefore not successful.

5.7 Concluding Remarks

If precise pseudo-range data are available, the combined carrier phase observations $\varphi_{1,-1}$ and $\varphi_{-7,9}$ are very useful for cycle slip detection and repair in kinematic data. The suggested procedure can repair data gaps up to 1-5 minutes, depending on the receiver type and the ionosphere conditions.

If dual-frequency, full wavelength carrier phase is available, but no precise pseudo-range data, the Kalman filter and AFM procedure will detect and repaire cycle slips. The length of data gap that can be repaired depends on the receiver dynamics and the antenna environment. Normally, if the predicted position bias is less than about 2.5 metres, the cycle slips can be repaired. For GPS receivers outputting precise pseudo-ranges, the Kalman filter and AFM procedure can be used together with the first procedure in order to detect and repair cycle slips during any period when pseudo-range data is not available.

The suggested procedure needs ambiguity initialisation at the beginning of a session. For short receiver separations at the beginning of a session, the traditional ambiguity resolution method for the static case, or ambiguity resolution "on-the-fly" for the kinematic case can be used. For large receiver separations at the beginning of a session, static methods are needed to initialise the ambiguities.

Multipath and the bias caused by receiver internal filtering are the main obstacle to the suggested procedure. In the current software all data seriously affected by multipath will be deleted.

This method can be used for real-time kinematic positioning. After initialising at the start of the session, and if there are no data gaps longer than a few minutes, the integer ambiguities can be resolved instantaneously and the roving receiver position can be determined in real-time.

Chapter 6

LONG-RANGE GPS KINEMATIC POSITIONING FOR SURVEYS WITHIN A SMALL AREA

6.1 Introduction

Centimetre accuracy GPS rapid static or kinematic positioning using current techniques requires fast ambiguity resolution (for the former) or ambiguity resolution "on-the-fly" (for the latter), in order to convert the ambiguous carrier phase data into unambiguous ranges with millimetre measurement precision. The use of two single frequency GPS receivers, which output C/A pseudo-range and L1 carrier phase measurements, separated by less than about 10km, with station occupancies of the order of 10-15 minutes, will generally permit rapid static positioning (Han, 1994c). However, ambiguity resolution on-the-fly for kinematic applications is difficult and unreliable. If the incorrect ambiguities are fixed, outliers will occur in the baseline, or trajectory, results and hence the accuracy will be significantly reduced. There are several remedies to this, including the use of dual-frequency instrumentation, longer station occupation times, and the requirement to keep baselines comparatively "short". Because of these constraints, GPS applications requiring high accuracy will therefore suffer from high cost and inefficiency.

Although there has been considerable progress recently in the development of "smart" ambiguity resolution algorithms, there are still several algorithmic and operational constraints (see Chapter 2). For example, although the Ambiguity Function Method does not require ambiguity resolution directly, it does require quite accurate *apriori* coordinates in order to define the initial search region that contains the sole maximum point (Remondi, 1989). The "stop & go" technique requires ambiguity resolution at the initial point (by whatever method), and these integer ambiguities are then valid for the subsequent survey points only if the satellite tracking is maintained (Remondi, 1985). All of these techniques require two receivers in order to determine the baseline vector between receivers. In addition they are very sensitive to systematic biases such as the

ionospheric delay and multipath (Sauer, 1994). These limitations tend to restrict the application of these techniques.

Continuously operating GPS reference receivers are being established at a rapid rate all over the world, and are expected to have quite a dense coverage within a few years. These receivers can therefore assist surveyors to perform GPS positioning with only one field receiver. Unfortunately, the surveyor's receiver is often more than 20km from the nearest GPS reference receiver, making conventional GPS rapid static positioning, or kinematic positioning, almost impossible because of the difficulties of ambiguity resolution for such baseline lengths using single frequency receivers. On the other hand, the known coordinated points for many applications such as detail surveys, profile surveys, large scale mapping, cadastral surveys, etc., are generally expressed in a local geodetic datum, with the baseline vector to the GPS reference station generally being required to a much lower accuracy than that necessary for determining the initial integer ambiguities. Even if a reference receiver were close to the surveyor's receiver (say within a few kilometres), the initial ambiguities must still be resolved using standard techniques.

Clearly, for such scenarios, GPS is unlikely to be favoured over traditional surveying techniques based on total stations. Developing a reliable and efficient GPS positioning technique for such applications is therefore a considerable challenge. In this chapter a new operational mode is suggested (Han & Rizos, 1996a; 1996h) which:

- makes use of permanent GPS reference stations, permitting the surveyor to employ just one single frequency receiver in the field (and only one technician!),
- requires only that the GPS receiver start and end the survey at known points in the local datum (not necessarily a geocentric datum),
- does not require ambiguity resolution in the normal sense,
- is not dependent on the distance from the surveyor's receiver to the reference receiver, and
- is insensitive to systematic biases such as ionospheric delay and multipath if the survey area is small (eg., 10km× 10km), no matter how distant the GPS reference receiver is.

The data processing will give centimetre accuracy relative coordinates between all points visited by the surveyor's roving receiver, rather than baselines from the surveyor's receiver to the reference receiver.

6.2 Principles of the Concept

6.2.1 Biased Vectors

GPS double-differenced carrier phase observations can be expressed as (equation (2-1)):

$$\nabla\Delta\phi_i \cdot \lambda = \nabla\Delta\rho_i + \nabla\Delta N \cdot \lambda - B + \varepsilon_i \tag{6-1}$$

where $\Delta\nabla N$ is the double-differenced integer ambiguity set estimated from using the initial coordinates or pseudo-range data; B is the bias term expressed in the form:

$$B = -\delta\nabla\Delta N \cdot \lambda \tag{6-2}$$

$\delta\nabla\Delta N$ is the bias vector of the estimated integer ambiguity set. The linearization of equation (6-1) gives:

$$V_i = A_i\delta X_i - (L_i + B) \tag{6-3}$$

where $L_i = \nabla\Delta\varphi_i \cdot \lambda - \nabla\Delta\rho_i^0 - \nabla\Delta N \cdot \lambda$; and $\nabla\Delta\rho_i^0$ is the double-differenced range implied by the initial coordinates X_i^0. The least squares estimate of the parameters is:

$$\delta X_i = (A_i^T P A_i)^{-1} A_i^T P (L_i + B) = \delta X_i' + \delta X_i'' \tag{6-4}$$

where

$$\delta X_i' = (A_i^T P A_i)^{-1} A_i^T P L_i \tag{6-5}$$

$$\delta X_i'' = (A_i^T P A_i)^{-1} A_i^T P B \tag{6-6}$$

and the coordinate results are:

$$\hat{X}_i = X_i^0 + \delta X_i = \hat{X}_i' + \delta X_i'' \tag{6-7}$$

It can be seen that $\hat{X}_i' = X_i^0 + \delta X_i''$ is easily estimated, and $\delta X_i''$ is the coordinate bias caused by the ambiguity bias component B .

6.2.2 Corrected Vectors

Approximate linearity of the elements in A_i with time

A GPS satellite is at an altitude of approximately 20,000km, and moves smoothly with an alongtrack velocity of about 4km/sec. The direction cosine therefore changes very slowly and this change is approximately linear (Sauer, 1994).

If it is assumed that the direction cosine at time t_0 is $\vec{n}_0$, the direction cosine n_i at time t_i can be approximated by:

$$\vec{n}_i = \vec{n}_0 + (t_i - t_0)\dot{\vec{n}}_0 \tag{6-8}$$

The elements of matrix A_i are formed by differencing the direction cosines between two satellites, and they are also approximately linear with time:

$$A_i = A_0 + (t_i - t_0)\dot{A} = A_0 + \Delta A_i \tag{6-9}$$

over short periods of time, such as about half an hour, where $\dot{A}$ is the mean rate of change of A for this period. Figure 6-1 illustrates the change of the elements of the design matrix A with time. It is obvious that they exhibit very good linearity.

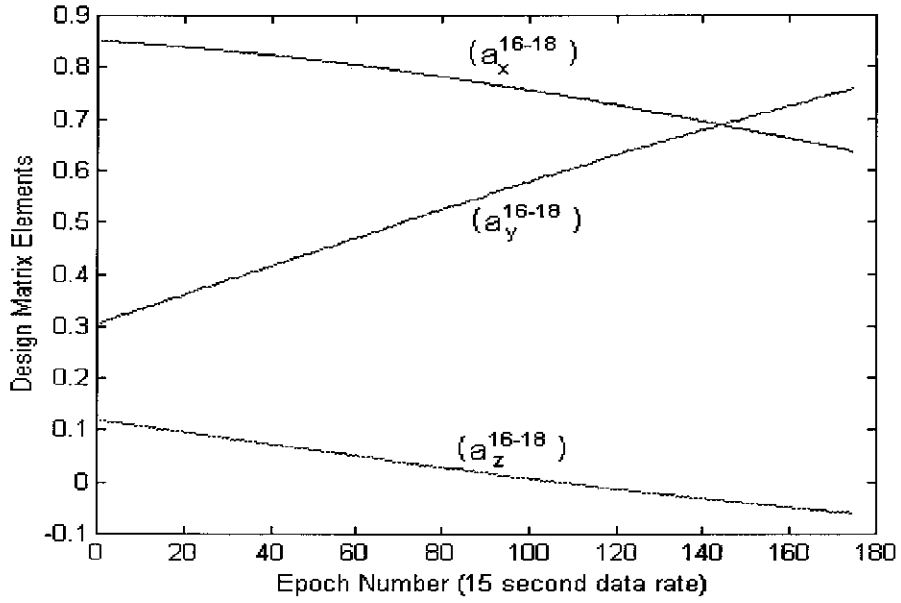

Figure 6-1. Linearity of the elements of the design matrix with time

Approximate linearity of δX_i with time

From equation (6-6) it is possible to derive $\delta X_0''$ at t_0:

$$\delta X_0'' = (A_0^T P A_0)^{-1} A_0^T P B \tag{6-10}$$

and at time t_i

$$(A_i^T P A_i)\delta X_i'' = A_i^T P B \tag{6-11}$$

Substituting equation (6-9):

$$\delta X_i'' = \delta X_0'' + (t_i - t_0)N^{-1}\left[\dot{A}^T P B - (\dot{A}^T P A_0 + A_0^T P \dot{A})\delta X_0''\right] + o^2(\Delta A_i) \tag{6-12}$$

where

$$o^2(\Delta A_i) = -N^{-1}\left[\Delta A_i^T P \Delta A_i \delta X_0'' + (A_0^T P \Delta A_i + \Delta A_i^T P A_0 + \Delta A_i^T P \Delta A_i)(\delta X_i'' - \delta X_0'')\right] \tag{6-13}$$

and $N = A_0^T P A_0$. $o^2(\Delta A_i)$ is a function of ΔA_i and $B = -\delta\nabla\Delta N \cdot \lambda$. It is necessary to make the bias $\delta\nabla\Delta N$ as small as possible, and the period as short as possible, in order to make $o^2(\Delta A_i)$ so small that it can be neglected.

A new GPS operational mode and the determination of the correction terms $\Delta\delta X_{1,i}''$

Consider the case of kinematic positioning from known station 1 in the local datum, while maintaining satellite tracking during movement of the antenna (Figure 6-2). The determination of the position of the GPS receiver at epoch i is of interest. In this example, two known stations are used (station 1 and station N, visited by the receiver at the beginning and then at the end of the field session). The known station coordinates in the local datum are not required with high accuracy relative to the reference station. However, these known stations should have centimetre accuracy relative to each other. (Alternatively, only one known station need be used, but it should be visited twice, once at the beginning and then at the end of the survey session.) It is the baseline vectors from station 1 to i which are required, not the baselines between the surveyor's receiver and the reference receiver. This can be expressed as (refer to equation (6-7) and Figure 6-2):

$$\Delta\hat{X}_{1,i} = \Delta\hat{X}'_{1,i} + \Delta\delta X''_{1,i} \tag{6-14}$$

where

$$\Delta\hat{X}_{1,i} = \hat{X}_i - \hat{X}_1 \tag{6-15}$$

$$\Delta\hat{X}'_{1,i} = \hat{X}'_i - \hat{X}'_1 \tag{6-16}$$

$$\Delta\delta X''_{1,i} = \delta X''_i - \delta X''_1 \tag{6-17}$$

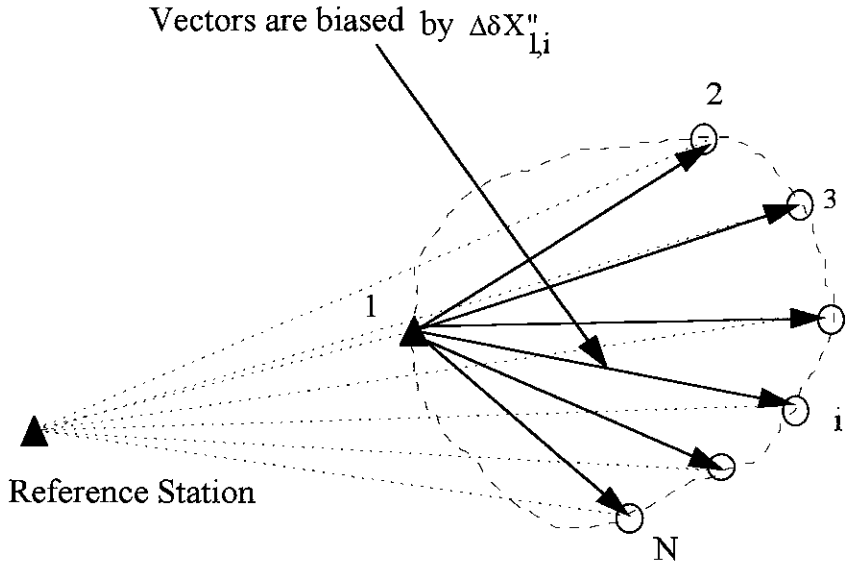

Figure 6-2. Configuration of the suggested GPS operational mode

If the known baseline vector from station 1 to station N is $\Delta X_{1,N}$, then $\Delta\delta X''_{1,N}$ can be estimated from:

$$\Delta\delta X''_{1,N} = \Delta X_{1,N} - \Delta\hat{X}'_{1,N} \tag{6-18}$$

$\delta X''_{1,i}$ can then be determined using the linearity property of $\delta X''_i$:

$$\Delta\delta X''_{1,i} = \frac{t_i - t_1}{t_N - t_1}\Delta\delta X''_{1,N} \tag{6-19}$$

Equation (6-14) can therefore be used to determine the position of station i relative to station 1.

Data processing will give centimetre accuracy relative positions between all visited points by the single surveyor's receiver, rather than baselines from the surveyor's receiver to the reference receiver. The operational mode is similar to that of the "stop & go" technique, however there is no requirement for initialisation, or to have the receivers close together. This procedure does not require the integer ambiguities to be resolved, and hence it is not sensitive to systematic GPS biases such as ionospheric delay and multipath, which are the most common reasons for incorrect ambiguity resolution.

6.3 Experiments

6.3.1 Kinematic Positioning

Short-range kinematic experiment

The first experiment was carried out on 19 January, 1996. After a few minutes of static observation at the known station, the roving GPS receiver (a Leica GPS System 300, but only C/A code pseudo-range and L1 carrier phase observations were used) started to move along Foreshore Road, Sydney, and then back to the same known station. The Mather Pillar station (a permanent station located on the roof of the Geography & Surveying Building, at The University of New South Wales, equipped with an Ashtech Z12 GPS receiver) was chosen as the reference GPS station, approximately 6km away from the roving receiver. The trajectory computed using the L1 carrier phase observations and fixing the integer ambiguities is considered to be the true trajectory, against which the suggested procedure's results will be compared, is plotted in Figure 6-3, in ISG (Integrated Survey Coordinates) coordinates.

Applying the suggested procedure, the biased vector from Mather Pillar to the rover receiver can be determined from equation (6-5). The initial ambiguity set can be determined using C/A pseudo-range observations from the first few epochs of data.

Figure 6-4 gives the offsets ($\delta X_i^{"}$) of the biased vector as East, North, and Height components.

The second step is the correction of the biased vector using equations (6-14, 6-18 and 6-19). The difference between the corrected vector and the true trajectory at each epoch is illustrated in Figure 6-5. If the errors of the known points at the start and the end are ignored, the differences shown in Figure 6-5 is the $o^2(\Delta A_i)$ term in equation (6-13). For some applications, such as profile surveys, these effects can be ignored.

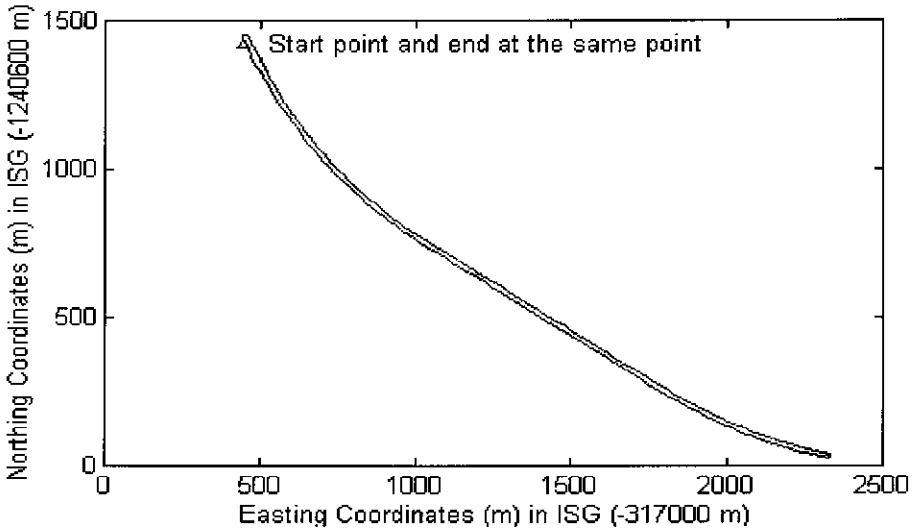

Figure 6-3. The user receiver trajectory on 19 January, 1996

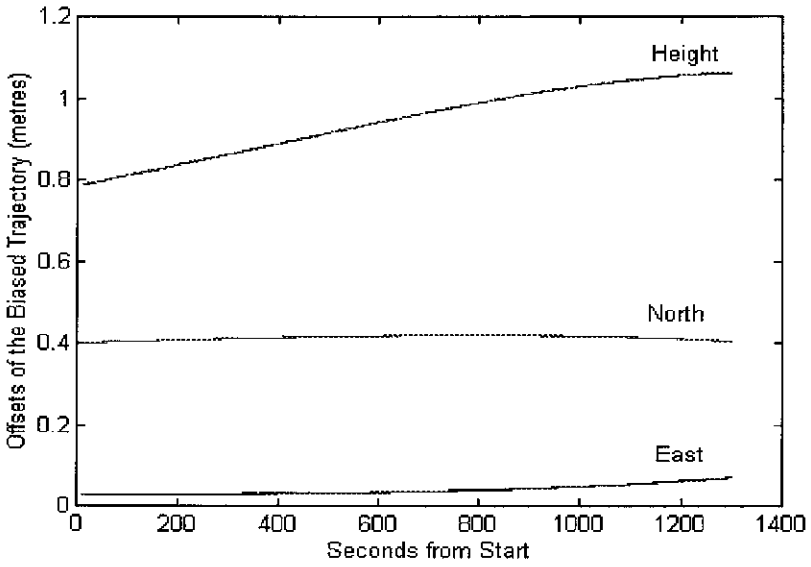

Figure 6-4. Offset of the biased vector determined by equation (6-5)

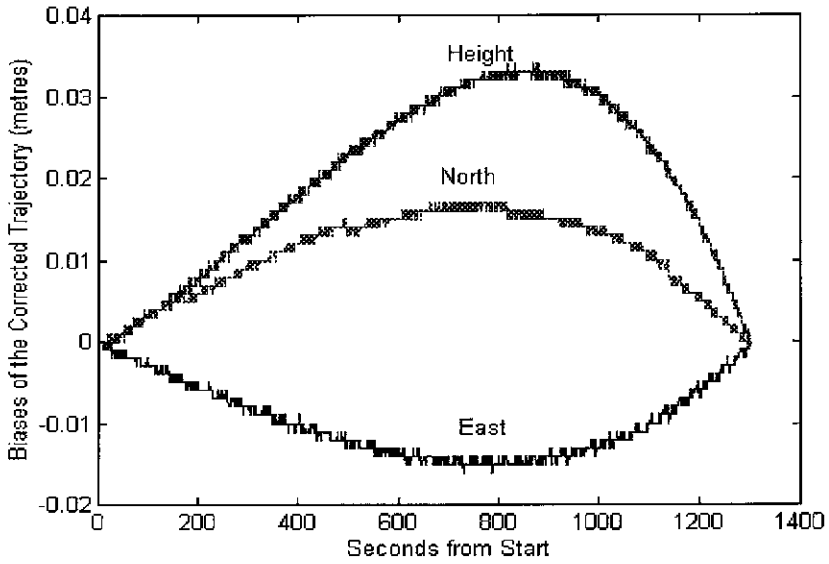

Figure 6-5. Biases of the corrected trajectory on 19 January, 1996

Medium-range kinematic experiment

This experiment was carried out on 7 April, 1996. After one minute of static observations at the known station (start point indicated in Figure 6-6), the roving GPS receiver (an Ashtech Z12 receiver, though only the C/A code pseudo-range and L1 carrier phase observations were used) mounted on a car started to move along a freeway, travelling west out of Sydney, and then back to the other known station (end point in Figure 6-6). The Mather Pillar was again chosen as the reference station, approximately 31.5 to 37.5 km away from the roving receiver. The data collection interval was 1 second for both receivers.

In order to compare the trajectory solution with results determined independently, a static GPS receiver (this time a Leica GPS 399 receiver) was set up close to the roving receiver. The trajectory of the roving receiver was then accurately determined relative to this static receiver using the L1 carrier phase observations, after fixing the integer ambiguities. This solution is the "standard" mode of data processing, and this trajectory (Figure 6-6) is considered to be the true trajectory against which the results of the suggested procedure are compared. Note, all coordinates are expressed in the TM projection system known as the Integrated Survey Grid (ISG) (Manual of the New South Wales Integrated Survey Grid, 1976).

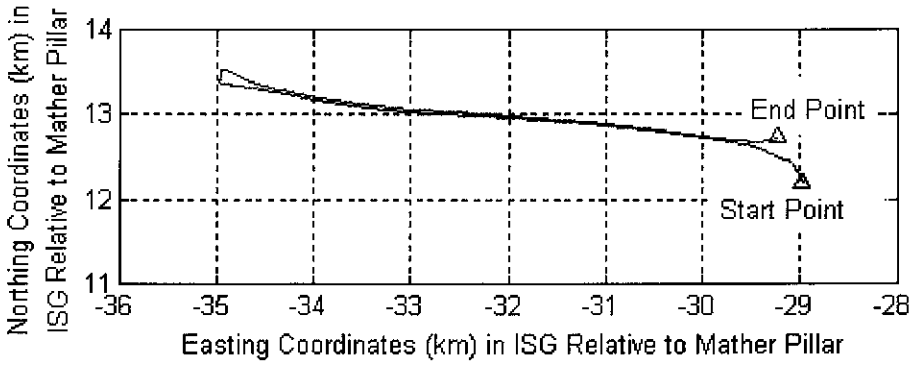

Figure 6-6. The user receiver trajectory

The first step is to compute the vectors $\hat{X}_i'$ using the fixed ambiguities determined by C/A pseudo-range and carrier phase observations over the whole obervation span. Because the estimated ambiguities are not correct (they maybe in error by several cycles, the "ambiguity bias"), the computed vectors will have biases ($\delta X_i''$), including an offset term, linear drift term and non-linear term as indicated in Figure 6-7 (refer to equations (6-7 and 6-12)). The second step is to compute the vectors relative to the start point (refer to equation (6-14)). This step will remove the offsets in the vectors relative to the start point, but they are still affected by the linear drift term and non-linear term. The third step is to correct the linear drift term using equation (6-19), based on the known coordinates of the start and end point. With these three steps the vectors relative to the start point will be only affected by the non-linear effect caused by the ambiguity biases, and this term can be neglected for centimetre-level accuracy surveys if the observation span is comparatively short (say, <30 minutes), and the ambiguity biases are smaller enough (say, <15 cycles). The difference between the corrected vector and the true trajectory at each epoch is plotted in Figure 6-8. This includes the errors of the known coordinates at the start and the end of the survey, errors of the assumed true trajectory determined from the L1 carrier phase observations, and errors due to the non-linear term. The maximum error in any component is about 3cm, certainly adequate for many large scale mapping applications. Note that the reference GPS receiver was from 31.5 to 37.5 km away from the roving receiver, yet centimetre accuracy positioning results were obtained relative to the trajectory itself.

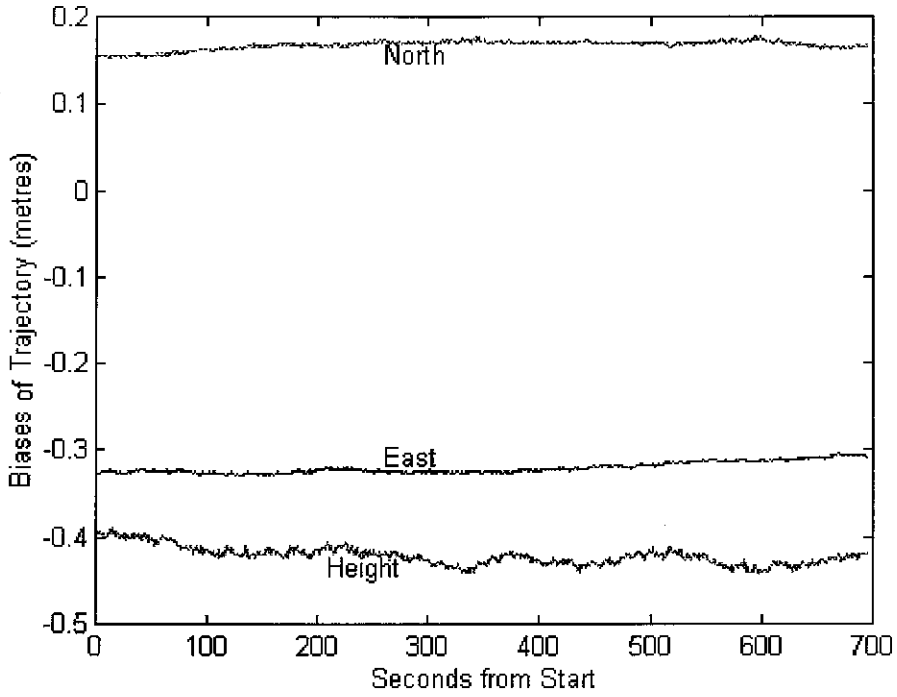

Figure 6-7. Biases of the vectors determined by equation (6-5)

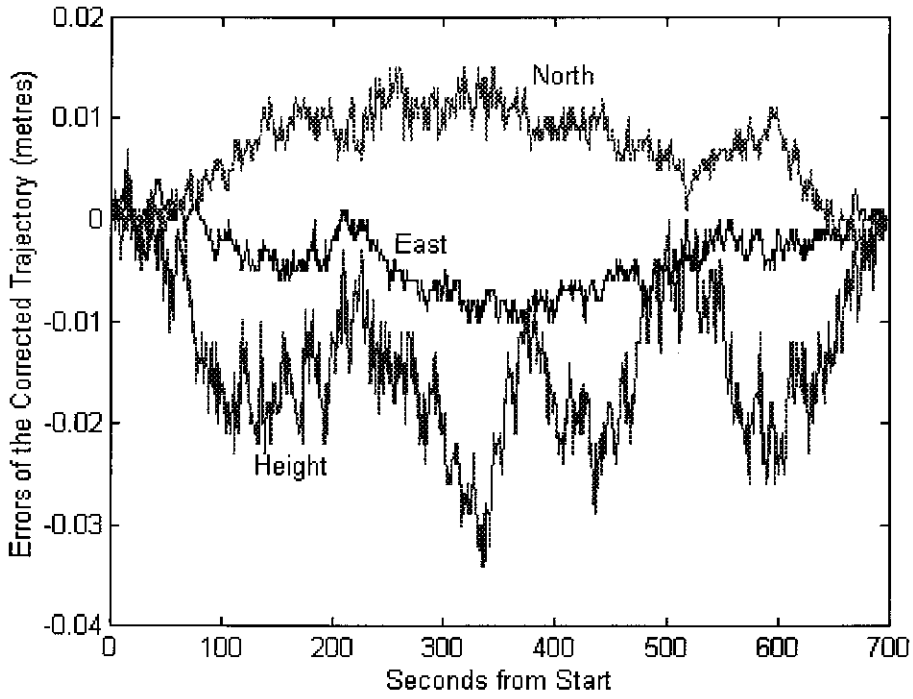

Figure 6-8. Errors of the trajectory vectors after corrections for the 7 April, 1996, experiment

6.3.2 Rapid Static Positioning

This experiment was carried out at Queens Park, in Sydney, on 19 January, 1996, using one Leica GPS 399 receiver (though only the C/A pseudo-range and L1 carrier phase observations were used). The Mather Pillar was again used as the reference station. The data collection interval was 1 second for both receivers. The experiment started from permanent mark PM58855, and involved visiting ten other sites before returning to PM58855. These sites are permanent survey marks with precise horizontal coordinates in the ISG system and heights in the Australian Height Datum (AHD). This survey mode is similar to the standard "stop & go" technique, although in this technique the distance from the surveyor's receiver to the reference receiver could be tens of kilometres. The initialisation procedure as employed in the standard "stop & go" technique is not required. For the first stage, the data processing procedure is the same as for the kinematic case. The second stage is to identify which epochs are collected at the survey marks, and compute the mean position of the positions using the data collected at each mark. The differences between the estimated coordinates and the known ISG/AHD coordinates are listed in Table 6-1. The maximum error is 2.6cm.

Table 6-1. Differences between the estimated ISG/AHD coordinates and the known coordinates at each site for the 19 January, 1996, experiment

Site Name	East (cm)	North (cm)	Height (cm)	Occupation time (sec)
PM58856	0.70	-1.50	1.90	160
PM58858	-0.30	-1.90	0.90	75
PM58859	-0.30	-2.20	0.80	71
PM58860	0.00	-2.50	1.70	74
PM58861	-0.50	-2.60	0.30	74
PM58863	-0.50	-2.10	-0.40	73
PM58864	-0.20	-1.30	-0.70	73
PM58865	0.10	-1.50	-0.90	76
PM58867	-1.00	-1.90	-1.70	66
PM58868	-0.40	-1.80	-0.90	131

The fixed integer ambiguity results were also computed using the L1 carrier phase data for each of the sites, and the differences with the results determined using the suggested procedure are listed in Table 6-2. These differences are primarily caused by the non-linear term in equaion (6-13). The maximum error is 1.1cm.

Table 6-2. The effect of the non-linear term in the corrections, a comparison with fixed ambiguity solution for the 19 January, 1996, experiment

Site Name	East (cm)	North (cm)	Height (cm)	Occupation time (sec)
PM58856	-0.80	-.60	-0.30	160
PM58858	-1.00	-.70	-0.30	75
PM58859	-1.10	-.80	-0.30	71
PM58860	-1.10	-.90	-0.30	74
PM58861	-1.10	-.90	-0.30	74
PM58863	-1.10	-.90	-0.30	73
PM58864	-1.10	-.80	-0.30	73
PM58865	-0.90	-.80	-0.30	76
PM58867	-0.90	-.70	-0.20	66
PM58868	-0.70	-.50	-0.10	131

6.4 Concluding Remarks

A new GPS operational mode and processing procedure for precise rapid static and kinematic positioning that does not require the fixing of the ambiguities to their integer values is described in this chapter. With the aid of data from a permanent GPS reference station (not necessarily located close to the surveyor's receiver), only one GPS single frequency receiver is needed to ensure centimetre to sub-decimetre-level accuracy relative to all visited points (in the case of the "stop & go" mode), or the trajectory itself (for the kinematic positioning mode), rather than for the vector from the surveyor's receiver to the reference receiver.

It must be emphasised that this procedure is an alternative to standard GPS surveying methods such as "rapid static", "stop & go", etc., which require a pair of dual-frequency instruments. It is, however, a low-cost alternative because of the need for only one

single frequency receiver (and a reference station that does not need to be within a few tens of kilometres of the survey site). Therefore, this technique is not only a lower cost and more efficient GPS method for some applications than the standard fixed integer ambiguity positioning methods ("rapid static", "stop & go", and kinematic positioning), but also traditional survey methods based on total stations. However, the technique is not suitable for real-time applications and requires that no cycle slips occur on at least four satellites while the antenna is moving. Potential applications of this technique include detail surveys, GIS database generation or update, profile surveys, large scale mapping, etc.

Chapter 7

CONCLUSIONS AND RECOMMENDATIONS

7.1 Summary and Conclusions

There are two main problems that must be overcome for carrier phase-based medium-range or long-range GPS kinematic positioning to be accurate and reliable: error or bias mitigation and appropriate ambiguity resolution technique. Successful ambiguity resolution requires that the magnitudes of all biases should be reduced to less than a quarter of the carrier wavelength. Three different ways to resolve integer ambiguity for medium-range or long-range kinematic positioning have been proposed. The first technique is to directly resolve ambiguity on-the-fly, or instantaneously, using multiple reference stations. The second technique is to resolve cycle slip, and hence to *recover* ambiguity on-the-fly, or instantaneously. The third technique is to leave the ambiguity parameters "free" and to then correct the baseline biases that result.

7.1.1 Ambiguity Resolution On-The-Fly for Medium-Range GPS Kinematic Positioning

Ambiguity resolution on-the-fly using multiple reference stations is based on a linear combination functional model, formed from the single-differenced functional equation for baselines from the user roving receiver to three or more reference stations. The linear coefficients are determined based on the location of the reference stations and the user's receiver. In this way, the orbit biases and ionospheric delay can be eliminated, and in addition, the tropospheric delay and multipath can be significantly reduced. If the double-differenced ambiguity sets for the reference stations have been determined, the double-differenced integer ambiguity set for the user roving receiver and one of the reference station can be determined using the suggested functional model. In addition, the improvements of the refined real-time stochastic model, a new criteria to verify the correct ambiguity set, and a fault detection and adaptive procedure, result in more reliable real-valued ambiguity estimates and their variance-covariances, and subsequently

a more reliable ambiguity resolution can be expected. This technique requires that reference stations be located such that they surround the survey area in order to efficiently account for the ionospheric delay by linear interpolation. The reference station positions should be known accurately. For real-time kinematic positioning, the integer ambiguity sets for the reference stations should be determined first and then used to correct the double-differenced observations between the user roving receiver and one of the reference stations.

The algorithm used for short-range and medium-range carrier phase-based kinematic positioning can resolve ambiguity resolution with one epoch of data. The average computation time for one epoch is less than 0.1 second. Four short-range experiments were carried out and the algorithm gave positioning results with success rates 100%, 100%, 99.7% and 98.4% over the total length of the data. These represent significant improvement on the rates 80.8%, 93.1%, 89.4% and 68.4% obtained using traditional ambiguity resolution techniques. The algorithm used for medium-range kinematic positioning gave similar results. The success rate for the experiment described in Section 4.7.2 is 100%, and the average computation time 0.071 seconds for each epoch. This algorithm can also be used for short-range or medium-range real-time GPS kinematic positioning.

For medium-range kinematic positioning, the reference stations are required to be dense enough in order to ensure that the linear interpolation for the ionospheric delay is accurate enough. Typically, the survey area of the interest should be located inside the triangle or quadrilateral formed by three or four reference stations, and these reference stations should be no more than about 200 km apart. Otherwise the ionosphere interpolation is of low accuracy, and the orbit bias and ionospheric delay will not be effectively eliminated. Furthermore, the tropospheric delay, multipath and observation noise will become larger, and subsequently ambiguity resolution becomes impossible.

7.1.2 Ambiguity Recovery Technique for Long-Range GPS Kinematic Positioning

The ambiguity recovery technique resolves the cycle slip(s) using a combination of cycle slip repair and ambiguity resolution procedures. This technique effectively involves "relative" ambiguity determination, rather than "absolute" ambiguity resolution. The concern is only with the biases affecting the carrier phase observations which change

with time. Two procedures have been implemented. One requires precise pseudo-range data and the other one does not.

The first procedure uses a combination of precise pseudo-range and carrier phase observations, which can eliminate the receiver and satellite clock biases, and the user receiver's movement. The remaining biases due to orbit error, ionosphere, troposphere and the static receiver's multipath change quite smoothly and can be fitted by a linear function for a short period of time. The selected widelane (wavelength 0.86 m) and $\varphi_{-7,9}$ (wavelength 14.65 m) combinations used for cycle slip detection minimise the effect of the noise from the pseudo-range data. Cycle slips in the carrier phase observations for satellites whose elevation is 40 degrees or higher can be detected in the one-way receiver-satellite data. If more than one set of one-way cycle slips are identified, the double-differenced cycle slip candidates will be formed. Because the double-differenced integer ambiguities at previous epochs are known, the ionospheric delay can be computed and this bias at the current epoch can be predicted with high precision if the data gap is shorter than about tens of seconds up to a few minutes. This means that the Ambiguity Function Method can then be used to detect and remove cycle slips. On the other hand, from the double-differenced cycle slip candidates derived from one-way data the integer ambiguity candidates can be derived, and the validation criteria used for the ambiguity search procedure in the estimated ambiguity domain can be used to verify the correct integer ambiguity set. This procedure can repair data gaps up to 1-5 minutes in length depending on the receiver type and the ionospheric conditions.

If dual-frequency, full wavelength carrier phase observations are available, but no precise pseudo-range data, the Ambiguity Function Method (AFM) with Kalman filtering will be a powerful combination for detecting and repairing cycle slips. The AFM can be used to determine the position and recover double-differenced integer ambiguities at the current epoch by using the ionosphere-corrected widelane and $\varphi_{-3,4}$ carrier phase observation combinations. The initial coordinates are provided by the Kalman filter. In general, if the predicted position bias is less than about 2.5 metres, the cycle slips can be repaired. For the experiments described in Chapter 5, the procedure can repair data gap up to a few seconds. For GPS receivers outputting precise pseudo-range data, the AFM and Kalman filter procedure can be used together with the first procedure in order to detect and repair cycle slips during any period of pseudo-range data loss. For GPS receivers without precise pseudo-range data, this procedure can be used to repair cycle slips, but the data gap must be short enough to ensure that the coordinate prediction accuracy from the Kalman filter is high enough.

The ambiguity recovery technique requires precise ephemeris data, such as is available from the International GPS Service for Geodynamics (IGS). The accuracy requirements are listed in Table B-1. This technique can be used for real-time kinematic positioning if the predicted precise ephemeris were available, as may be provided by the IGS in the near future. After initialising at the start of the session, and if there are no data gaps longer than a few minutes, the integer ambiguity can be resolved instantaneously and the roving receiver positioning can then be determined in real-time.

7.1.3 Long-Range GPS Kinematic Positioning for Surveys within a Small Area

The third technique assumes that only the trajectory of the roving receiver relative to itself is required to be of high accuracy. The biased position derived using biased or incorrect fixed ambiguities can be corrected to sub-decimetre accuracy using the known positions of the start point and end point of the survey. It is well known that the direction from a GPS antenna to a satellite changes slowly, hence the direction cosines also change slowly, in an approximately linear manner during a short period. Making use of this property, it can be shown that the incorrect initial ambiguity results bias the baseline vectors approximately linearly with time, provided the ambiguity error is small (a few cycles), and the time span is short (up to about half an hour). If the survey is from a known point to another known point, or back to the starting point, the biased vectors can be corrected relative to the first survey point using this linearity property. Therefore, this mode can give the centimetre to sub-decimtre accuracy vectors between all visited survey marks, or the trajectory relative to the first visited mark, rather than with respect to a distant reference GPS receiver. With the aid of data from a permanent GPS reference station (not necessarily located close to the surveyor's receiver), only one GPS single frequency receiver is required to carry out the survey.

The satellite change geometry is very important The smaller the satellite geometry changes, the better accuracy the positioning. The short-range constraint is required for distances between the points visited by a roving receiver, not the distance between the roving receiver and the reference (normally permanent) receiver. Any kind of GPS receiver that outputs carrier phase observations can be used in this operational mode. The applications include post-processed, small area, static or kinematic positioning, using one user receiver, with the aid of a continuously operating reference receiver (no matter how far it is from the user). However, the technique is not suitable for real-time applications and requires that no cycle slip occur on at least four satellites while the antenna is moving. This technique can be considered a low-cost alternative to standard

GPS surveying methods such as "rapid static", "stop & go", etc., because of the requirement for only one single frequency GPS receiver.

7.1.4 Other Contributions of the Research

Orbit bias elimination procedure

A well known "rule-of-thumb" states that the orbit bias $d\rho$ will cause the baseline to be degraded by $\left(\frac{d\rho}{\rho}\cdot 10^6\right)$ ppm. Local Area DGPS positioning will suffer from the effect of orbit bias and can be improved using the procedure suggested in Section 3.2. For high precision short-range positioning, e.g. such as for real-time deformation monitoring of engineering structures, volcanoes, etc., the orbit bias effect can be eliminated by the appropriate data processing of stable reference stations surrounding the survey area of interest.

Ionospheric delay interpolation using the epoch-by-epoch and satellite-by-satellite model

The ionospheric delay interpolation at the ionosphere layer using an epoch-by-epoch and satellite model was suggested by Webster & Kleusberg (1992); Wanninger (1995); Han & Rizos (1996e). The contribution in this thesis is a technique for interpolation in the ground Gauss plane, which is computationally much easier than the standard techniques interpolated at the single ionosphere layer. Based on this innovation, the ionospheric delay is eliminated in the suggested functional model using multiple reference station (see Section 4.2). Furthermore, the technique can be used to eliminate the ionospheric delay in high precision GPS positioning using single frequency receivers. For high precision short-range positioning, e.g. as in real-time deformation monitoring (Rizos et al., 1996), the ionospheric delay can be eliminated using data from the surrounding reference stations.

Three-step quality control improvements

A three-step quality control procedure which includes real-time stochastic model improvement, a new criteria for verifying the correct ambiguity set, and a fault detection and adaptive procedure, was developed to improve the performance of ambiguity resolution, and is suitable for both short-range or medium-range positioning. If precise

pseudo-range observations are available, the integrated model with the three-step quality control procedure can resolve integer ambiguity instantaneously. If precise pseudo-range observations are not available, the three-step quality control procedure can also be used to improve the performance of ambiguity resolution and significantly enhance the reliability of GPS carrier phase positioning.

A new method to construct multi-satellite ambiguity combination and comparison of the ambiguity resolution techniques

A new method to construct the multi-satellite ambiguity combinations for implementing the LAMBDA method is suggested, which can make the variance-covariance matrix significantly decorrelated. The transformation time is very short, typically between a few milliseconds and a few tens of milliseconds. Search methods such as FARA, Cholesky decomposition, FASF and the LDL^T decomposition methods are employed to search the transformed ambiguities and the results are shown to have been significantly improved. Hence, if the existing software packages employing such search methods were modified to implement the suggested transformation method, the data processing will become much more efficient. On the other hand, a comparison between the search procedures in the original ambiguity domain and the transformed ambiguity domain shows that the suggested transformation method can be easily combined with the Cholesky decomposition search procedure or the LDL^T decomposition search procedure, resulting in a procedure that is highly efficient in terms of computation time.

The effect of temporal correlation on ambiguity resolution

It is well known that the estimated variance-covariance matrix for an estimated GPS baseline vector is over-optimistic. Although the most realistic results can be obtained by considering between-epoch correlations, this will make the computation much more complicated. The differences in the GPS baseline vectors, between considering and neglecting between-epoch correlation, are very small, but the effect on the magnitudes of the variance-covariance terms is large. This will affect the search region for ambiguity resolution, and subsequently affect the reliability of the ambiguity resolution. The suggested procedure for accounting for the temporal correlation is to scale the variance-covariance matrix by a factor. This can be used for rapid static positioning or kinematic positioning.

Multipath extraction and mitigation method

Multipath is a periodic bias whose frequency characteristics are within a certain frequency band. The frequency band can be determined from a spectral analysis of the signal-to-noise ratio output by a GPS receiver. Therefore, the multipath can be extracted using band pass filtering, and can be mitigated using band stop filtering. The extracted multipath can be used for multipath correction if the antenna environment is unchanging. The multipath biases can therefore be corrected for at reference stations when preforming carrier phase-based medium-range or long-range kinematic positioning. The suggested method can be used for other applications such as deformation monitoring.

7.2 Limitations, Prospects and Recommendations

7.2.1 The Limitations

There are several constraints to current carrier phase-based medium-range or long-range kinematic GPS positioning systems. In terms of hardware, new generation GPS receivers such as the Ashtech Z12, Leica SR 399, or Trimble 4000SSi are required because the algorithms use precise pseudo-range data on L1 and/or L2 to assist in the recovery or resolution of the integer ambiguities. Multipath, or the biases caused by the receiver internal filtering, on carrier phase and pseudo-range observations will degrade the performance of the algorithms, even though pseudo-range accuracy has been improved significantly and multipath elimination technologies have been developed.

From the algorithm point of view, on-the-fly ambiguity resolution for medium-range kinematic positioning is possible if multiple reference receivers are used to significantly reduce the distance dependent errors. This technique requires a dense network of reference receivers in the survey area in order to ensure that the linear combination parameters are positive and less than 1, and that the linear interpolation of the ionospheric delay at a user receiver is of high accuracy. Ambiguity recovery techniques can repair the integer ambiguity for data gaps up to a few minutes in length for long-range GPS kinematic positioning. However, an integer ambiguity initialisation procedure will be required at the beginning of the survey, and any data gaps should be kept as short as possible during the observation session. The precise ephemeris is required if using the ambiguity recovery technique.

Although these two techniques can be used for real-time positioning, data latency will still be the main problem. The position output latency is mainly caused by: (a) receiver data download delay (about 0.2 seconds using serial communication with 38400 baud rate); (b) data link transmission delay (which may reach about 1 second using 9600 data link baud rate), and; (c) baseline computation delay (which is about 0.1 second for baseline computation and ambiguity recovery after signals are obstructed). There are two ways to resolve this problem: (a) synchronise reference data and mobile receiver data, which gives the maximum precision but a substantial delay; (b) use the latest reference data and extrapolate them to the time of the mobile receiver data, which will cause some additional error. The former is better for the carrier phase ambiguity resolution process, as all errors have to be minimised for maximum reliability and performance. However, the kinematic position will suffer due to a time delay of up to 1-2 seconds (which may be crucial for some real-time applications). The latter solution will introduce additional errors due to observation extrapolation. Experimental results show that the linear extrapolation model will introduce an additional double-differenced error of about 2cm for a 1 second delay and about 8cm for a 2 second delay. A quadratic extrapolation model will introduce an additional double-differenced error of about 4cm for a 2 second delay (Landau et al., 1995; Lapucha et al., 1995).

7.2.2 The Prospects

In the near future, the performance of medium-range or long-range kinematic GPS positioning will be improved because of the following factors: (1) It is possible that an additional civilian frequency will be transmitted by Block IIF satellites. The additional civilian signal will significantly improve the reliability of ambiguity resolution. (2) Selective Availability (S/A) may be turned off. Without S/A, double-differenced carrier phase extrapolation will be possible to a higher accuracy, and the extrapolation period may be much longer than the current 1-2 seconds. (3) IGS may soon provide predicted precise ephemerides with 30cm accuracy (Neilan, 1996). (4) New GPS receivers will have the ability to track the Glonass satellite signals, which means that almost twice the number of observations at each epoch will be available, hence improving reliability and availability. (5) Wide Area DGPS or Wide Area Augmentation Systems will require a dense network of permanent reference stations, which will also support centimetre-accuracy real-time kinematic positioning using one receiver. (6) It may be possible to improve the pseudo-range observation accuracy and reduce multipath effects by developing new GPS receiver and antenna technologies, thus improving the reliability of on-the-fly ambiguity resolution, or instantaneous ambiguity resolution, for medium-range

positioning applications. (7) Algorithm improvement is possible as well as improved characterisation of GPS errors.

7.2.3 Suggestions and Recommendations for Future Research

Carrier phase-based medium-range or long-range kinematic GPS positioning, in post-processed or real-time mode, has many applications, particularly for marine and airborne positioning where GPS reference receivers cannot be set up near the survey area. Once Wide Area DGPS systems or Wide Area Augmentation Systems are established, this technique will allow a user to precisely position a moving receiver in real-time. From the possible improvements of GPS and Glonass systems, user hardware and other facilities, such as the IGS service, the following investigations are recommended as a continuation of this research.

1. The impact of the third frequency on the carrier phase-based medium-range or long-range kinematic positioning systems should be investigated. It is possible to find other carrier phase combinations, which minimise the effect of pseudo-range noise, and which are optimised for ambiguity recovery or ambiguity search in the observation domain.

2. The differential correction message requirements from WADGPS or WAAS for carrier phase-based medium-range or long-range kinematic positioning should be investigated, so that the user may use these messages for sub-decimetre accuracy GPS kinematic positioning.

3. Ambiguity resolution for GPS/Glonass carrier phase data should be investigated. The amount of carrier phase and pseudo-range observation data will be almost double that of GPS alone.

4. The reliability of the ambiguity resolution, especially for the instantaneous case, should be further investigated. This includes stochastic model refinement for different functional models, and new detection and adaptive procedures.

5. System development using the suggested algorithms for real-time implementation should be carried out, and careful analysis of the data latency problems should be preformed.

6. The final output should be a user-friendly, carrier phase-based, medium-range or long-range GPS real-time kinematic positioning system. All technical problems should therefore have been addressed.

REFERENCES

Abidin, H. A. (1993). Computational and Geometrical Aspects of On-The-Fly Ambiguity Resolution. PhD Dissertation, Dept. of Surveying Eng. Tech. Rept. No.164, University of New Brunswick, Fredericton, New Brunswick, Canada, 314pp.

Abidin, H. A. and D. E. Wells (1990). Extrawidelaning for 'On The Fly' Ambiguity Resolution: Simulation of Ionospheric Effects. Proc. 2nd Int. Symp. on Precise Positioning with Global Positioning System, Ottawa, Canada, 3-7 September, 1217-1232.

Ashjaee, J. and R. Lorenz (1992). Precision GPS Surveying After Y-Code. Proc. ION GPS-92, 5th Int. Tech. Meeting of The Satellite Division of The U.S. Institute of Navigation, Albuquerque, New Mexico, 16-18 September, 657-659.

Axelrad, P., Comp, C. J. and MacDoran, P. F. (1994). Use of Signal-to-Noise Ratio for Multipath Error Correction in GPS Differential Phase Measurements: Methodology and Experimental Results. Proc. ION GPS-94, 7th Int. Tech. Meeting of The Satellite Division of The U.S. Institute of Navigation, Salt Lake City, Utah, 20-23 September, 655-666.

Black, H. D. (1978). An Easily Implemented Algorithm for the Tropospheric Range Correction. Journal of Geophysical Research, 83(B4), 1825-1828.

Blewitt, G. (1989). Carrier Phase Ambiguity Resolution for the Global Positioning System Applied to Geodetic Baselines up to 2000 km. Journal of Geophysical Research, 94(B8), 10187-10203.

Blewitt, G. (1990). An Automatic Editing Algorithm for GPS Data. Geophysical Research Letters, 17(3), 199-202.

Braun, J. and C. Rocken (1995). Vertical Height Errors when Mixing Trimble 4000SST and Trimble 4000SSE Observations. UNAVCO report at http://www.unavco.ucar.edu.

Brunner, F. K. and W. M. Welsch (1993). Effect of the Troposphere on GPS Measurements. GPS World, 4(1), 42-51.

Chen, D. (1993). Fast Ambiguity Search Filtering (FASF): A Novel Concept for GPS Ambiguity Resolution. Proc. ION GPS-93, 6th Int. Tech. Meeting of The Satellite

Division of The U.S. Institute of Navigation, Salt Lake City, Utah, 22-24 September, 781-787.

Chen, D. and G. Lachapelle (1994). A Comparison of the FASF and Least-Squares Search Algorithms for Ambiguity Resolution On The Fly. Proc. Int. Symp. on Kinematic Systems in Geodesy, Geomatics and Navigation, Banff, Canada, 30 August - 2 September, 241-253.

Chen, D. and G. Lachapelle (1995). A Comparison of the Fast and Least-Squares Search Algorithms for On-The-Fly Ambiguity Resolution. NAVIGATION, Journal of The U. S. Institute of Navigation, 42(2), 371-390.

Chen, X. (1994). Analysis of Continuous GPS Data from the Western Canada Deformation Array. Proc. ION GPS-94, 7th Int. Tech. Meeting of The Satellite Division of The U.S. Institute of Navigation, Salt Lake City, Utah, 20-23 September, 1339-1348.

Clark, T. (1992). GPS Antennas: De-Mystifying Multipath. NASA Goddard Internal Memorandum, March 5.

Cohen C. and B. Parkinson (1991). Mitigating Multipath Error in GPS Based Attitude Determination. Guidance and Control, 74, Advances in the Astronautical Sciences.

Cohen, C., B. Pervan and B. Parkinson (1992). Estimation of Absolute Ionospheric Delay Exclusively through Single-Frequency GPS Measurements. Proc. ION GPS-92, 5th Int. Tech. Meeting of The Satellite Division of The U.S. Institute of Navigation, Albuquerque, New Mexico, 16-18 September, 325-330.

Collins, J. P. and R. B. Langley (1996). Mitigating Tropospheric Propagation Delay Errors in Precise Airborne GPS Navigation. Proc. IEEE Position Location & Navigation Symp. PLANS'96, Atlanta, Georgia, 22-26 April, 582-589.

Colombo, O. L., C. Rizos and B. Hirsch (1995). Decimetre-Level DGPS Navigation Over Distances of More Than 1000km: Results of the Sydney Harbour Experiment. Proc. 4th Int. Conf. on Differential Satellite Navigation Systems, Bergen, Norway, 24-28 April, paper no. 61, 8pp.

Corbett, S. J. and P. A. Cross (1995). GPS Single Epoch Ambiguity Resolution. Survey Review, 33(257), 149-160.

Counselman, C. C. (1987). Method and System for Determining Position using Signals from Satellites. U.S. Patent 4667203. 19 May.

Counselman, C. C. and S. A. Gourevitch. (1981). Miniature Interferometer Terminals for Earth Surveying: Ambiguity and Multipath with the Global Positioning System. IEEE Transactions on Geoscience and Remote Sensing, GE-19(4), 244-252.

Cross, P. A. (1983). Advanced Least Squares Applied to Position Fixing. Working Paper No. 6, Department of Surveying, Polytechnic of East London, 205pp.

Cross, P. A. (1996). Trends in Estimation Techniques: Modern Least Squares for Surveyors. Seminar at School of Geomatic Engineering, The University of New South Wales, Sydney, Australia, 13 December.

Cross, P. A. and W. D. S. Roberts (1992). GPS Techniques for Precise Real-Time Offshore Positioning. Int. Workshop on Global Positioning Systems in the Geosciences, Technical University of Crete, Chania, Greece, 8-10 June, 259-271.

Davis, J. L., T. A. Herring, I. I. Shapiro, A. E. E. Rogers and G. Elgered (1985). Geodesy by Radio Interferometry: Effects of Atmospheric Modelling Errors on Estimates of Baseline Length. Radio Science, 20(6), 1593-1607.

Dodson, A. H. and P. J. Shardlow (1995). The Global Positioning System as a Passive Integrated Atmospheric Water Vapour Sensing Device. Proc. EUROPTA Satellite Remote Sensing II, Vol 2582, Paris, France, September, 166-177.

Dodson, A. H., P. J. Shardlow, L. C. M. Hubbard, G. Elgered and P. O. J. Jarlemark (1996). Wet Tropospheric Effects on Precise Relative GPS Height Determination. Journal of Geodesy, 70, 188-202.

Dong, D. N. and Y. Bock (1989). Global Positioning System Network Analysis With Phase Ambiguity Resolution Applied to Crustal Deformation Studies in California. Journal of Geophysical Research, 94(B4), 3949-3966.

El-Rabbany, A. E-S. (1994). The Effect of Physical Correlations on the Ambiguity Resolution and Accuracy Estimation in GPS Differential Positioning. Tech. Rept. No.170, Dept. of Geodesy & Geomatics Engineering, University of New Brunswick, Fredericton, New Brunswick, Canada, 161pp.

Enge, P. K. and A. J. Van Dierendonck (1996). Wide Area Augmentation System. In: Parkinson B. et al (ed), Global Positioning System: Theory and Applications, Vol II, American Institute of Aeronautics and Astronautics, Inc., Washington DC, 117-142.

Euler, H.-J. and H. Landau (1992). Fast GPS Ambiguity Resolution On-The-Fly for Real-Time Applications. Proc. 6th Int. Geodetic Symp. on Satellite Positioning, Columbus, Ohio, 17-20 March, 650-659.

Euler, H.-J. and B. Schaffrin (1990). On a Measure of the Discernibility between Different Ambiguity Solutions in the Static-Kinematic GPS-Mode. Banff, Canada, 10-13 September. In: K-P Schwarz and G. Lachapelle (ed.), Kinematic Systems in Geodesy, Surveying, and Remote Sensing, IAG Symposium No. 107, Springer-Verlag, 285-295.

Feng Y. and S. Han (1996). A Long-Range Dynamic GPS Positioning System and its Test Results. Proc. IEEE Position Location & Navigation Symp. PLANS'96, Atlanta, Georgia, 22-26 April, 711-718.

Feng Y., K. Kubik and S. Han (1996). A Long-Range Dynamic GPS System for Aircraft Navigation and Positioning. Int. Archives of Photogrammetry and Remote Sensing, Vol. XXXI, Part B1, 65-71.

Fenton, P. C., W. H. Falkenberg, T. J. Ford, K. K. Ng and A. J. Van Dierendonck (1991). NovAtel's GPS Receiver - the High Performance OEM Sensor of the Future. Proc. ION GPS-91, 4th Int. Tech. Meeting of The Satellite Division of The U.S. Institute of Navigation, Albuquerque, New Mexico, 11-13 September, 49-58.

Frei, E. and G. Beutler (1990). Rapid Static Positioning Based on the Fast Ambiguity Resolution Approach FARA: Theory and First Results. Manuscripta Geodaetica, 15, 325-356.

Frei E., J. Yau and D. Sauer (1993). Ambiguity Resolution on the Fly (AROF); Results, Facts, Limitations. Proc. ION GPS-93, 6th Int. Tech. Meeting of the Satellite Division of the Institute of Navigation, Salt Lake City, Utah, 22-24 September, 1059-1067.

Geiger, A., H, Hirter, M. Cocard, B. Bürki, A. Wiget, U. Wild, D. Schneider, M. Rothacher, S. Schaer and G. Beutler (1995). Mitigation of Tropospheric Effects in Local and Regional GPS Networks. IUGG XXI General Assembly, Colorado, 2-14 July, In: Beutler, G., G. W. Hein, W. G. Melbourne and G. Seeber (ed.): GPS Trends in Precise Terrestrial, Airborne, and Spaceborne Applications, IAG Symposium No. 115, Springer-Verlag, 1996, 263-267.

Georgiadou, Y. and A. Kleusberg (1988a). On the Effect of Ionospheric Delay on Geodetic Relative GPS Positioning. Manuscripta Geodaetica, 13, 1-9.

Georgiadou, Y. and A. Kleusberg (1998b). On Carrier Signal Multipath Effects in Relative GPS Positioning. Manuscripta Geodaetica, 13, 172-179.

Goad, C. C. (1985). Precise Relative Position Determination using Global Positioning System Carrier Phase Measurements in Nondifferenced Mode. Proc. 1st Int. Symp. on Precise Positioning with Global Positioning System, Rockville, Maryland, 15-19 April, 347-356.

Goad C. C. (1992). Robust Techniques for Determining GPS Phase Ambiguities. Proc. 6th Int. Geodetic Symp. on Satellite Positioning, Columbus, Ohio, 17-20 March, 245-254.

Goad, C. C. and Goodman, L. (1974). A Modified Hopfield Tropospheric Refraction Correction Model. Pres. at the Fall Annual Meeting of the American Geophysical Union, San Francisco, December.

Haji, G. A. (1990). The Multipath Simulator: A Tool Toward Controlling Multipath. Proc. 2nd Symp. on GPS Applications in Space, Hanscom AFB, February.

Han, S. (1991). Equivalence of the Methods for GPS Data Processing with Carrier Phase Observations. Journal of Wuhan Technical University of Surveying and Mapping, 16(1), 68-76.

Han, S. (1993). Improved Ambiguity Function Method and Its Application in Kinematic Positioning. Pres. at IAG General Meeting, Beijing, P. R. China, 9-13 August, 17pp.

Han, S. (1994a). Equivalence between the Ambiguity Function Method and the Least Squares Method with GPS Carrier Phase Observables and the Improved Ambiguity Function Method. ACTA GEODAETICA et CARTOGRAPHICA SINICA, Journal of Chinese Society of Geodesy, Photogrammetry and Cartography, 23(4), 282-288.

Han, S. (1994b). Ambiguity Function Method with Constrained Conditions and its Application in GPS Kinematic Positioning. Journal of Wuhan Technical University of Surveying & Mapping, 19(1), 7-14.

Han, S. (1994c). Theory of GPS Rapid Static Positioning and Numerical Results. Journal of Wuhan Technical University of Surveying & Mapping, 19(2), 136-142.

Han, S. (1995a). Theory and Applications of the Combinations of GPS Dual Frequency Carrier Phase Observations. ACTA GEODAETICA et CARTOGRAPHICA SINICA, Journal of Chinese Society of Geodesy, Photogrammetry and Cartography, 24(2), 8-13.

Han, S. (1995b). Ambiguity Recovery for GPS Long Range Kinematic Positioning. Proc. ION GPS-95, 8th Int. Tech. Meeting of The Satellite Division of The U.S. Institute of Navigation, Palm Springs, California, 12-15 September, 349-360. Accepted by NAVIGATION, Jouranl of The U. S. Institute of Navigation.

Han, S. (1995c). Ambiguity Resolution Techniques Using Integer Least Squares Estimation for Rapid Static or Kinematic Positioning. Proc. Satellite Navigation Technology 1995 and Beyond, Brisbane, Australia, 26-28 June, paper no. 34, 9pp.

Han, S. (1996). Quality Control Issues Relating to Ambiguity Resolution for Real-Time GPS Kinematic Positioning. Proc. ION GPS-96, 9th Int. Tech. Meeting of The Satellite Division of The U.S. Institute of Navigation, Kansas City, Missouri, 17-20 September, 1419-1430. Accepted by Journal of Geodesy.

Han, S. and C. Rizos (1995a). A Suggested Procedure for On-The-Fly Ambiguity Resolution for Long Range Kinematic Positioning. Proc. 4th Int. Conf. on Differential Navigation Systems, Bergen, Norway, 24-28 April, paper no. 67, 8pp.

Han, S. and C. Rizos (1995b). A New Method of Constructing Multi-Satellite Ambiguity Combinations for Improved Ambiguity Resolution. Proc. ION GPS-95, 8th Int. Tech. Meeting of The Satellite Division of The U.S. Institute of Navigation, Palm Springs, California, 12-15 September, 1145-1153.

Han, S. and C. Rizos (1995c). Standardization of the Variance-Covariance Matrix for GPS Rapid Static Positioning. Geomatics Research Australasia, 62, 37-54.

Han, S. and C. Rizos (1995d). On-The-Fly Ambiguity Resolution for Long Range GPS Kinematic Positioning. IUGG XXI General Assembly, Colorado, 2-14 July, In: Beutler, G., G. W. Hein, W. G. Melbourne and G. Seeber (ed.): GPS Trends in Precise Terrestrial, Airborne, and Spaceborne Applications, IAG Symposium No. 115, Springer-Verlag, 1996, 290-294.

Han, S. and C. Rizos (1995e). Selection and Scaling of Simultaneous Baseline for GPS Network Adjustment, or Correct Procedures for Processing Trivial Baselines. Geomatics Research Australasia, 63, 51-66.

Han, S. and C. Rizos (1995f). GPS Network Design and Adjustment for Rapid Static Operational Mode. Proc. 5th South East and 36th Australian Surveyor Congress, Singapore, 16-20 July, 11pp.

Han, S. & C. Rizos (1996a). A New Operation Mode and Processing Procedure for Centimetre Accuracy Rapid Static Positioning and Kinematic Positioning Using Single Frequency GPS Receivers. Proc. 37th Australian Surveyor Congress, Perth, Australia, 13-19 April, 203-212.

Han, S. and C. Rizos (1996b). Improving the Computational Efficiency of the Ambiguity Function Algorithm. Journal of Geodesy, 70, 330-341.

Han, S. & C. Rizos (1996c). Integrated Method for Instantaneous Ambiguity Resolution Using New Generation GPS Receivers. Proc. IEEE Position Location & Navigation Symp. PLANS'96, Atlanta, Georgia, 22-26 April, 254-261.

Han, S. and C. Rizos (1996d). Validation and Rejection Criteria for Integer Least Squares Estimation. Survey Review, 33(260), 375-382.

Han, S. and C. Rizos (1996e). GPS Network Design and Error Mitigation for Real-Time Continuous Array Monitoring Systems. Proc. ION GPS-96, 9th Int. Tech. Meeting of The Satellite Division of The U.S. Institute of Navigation, Kansas City, Missouri, 17-20 September, 1827-1836.

Han, S. and C. Rizos (1996f). Progress and Constraints of Real-Time Carrier Phase-Based Marine GPS Positioning. Proc. Int. Symp. Gravity, Geoid and Marine Geodesy 1996 (GraGeoMar96), Tokyo, Japan, 30 September - 5 October.

Han, S. and C. Rizos (1996g). Comparison of GPS Ambiguity Resolution Techniques. Int. Symp. on Global Positioning Systems, Digital Photogrammetry Systems, Remote Sensing and Geographical Systems (Geo-Informatics'96), Wuhan, P. R. China, 16-19 October, 136-146.

Han, S. and C. Rizos (1996h). Centimetre GPS Kinematic or Rapid Static Survey Without Ambiguity Resolution. Surveying and Land Information System, Journal of the American Congress on Surveying and Mapping, September, in press.

Harvey, B. (1995). Practical Least Squares and Statistics for Surveyors. Monograph 13, School of Geomatic Engineering , The University of New South Wales, Sydney, Australia, 319pp.

Hatch, R. R. (1986). Dynamic Differential GPS at the Centimeter Level. Proc. 4th Int. Geodetic Symp. on Satellite Positioning, Las Cruces, New Mexico, 28 April - 2 May, 1287-1298.

Hatch, R.R. (1990). Instantaneous Ambiguity Resolution. In: Schwarz, K. P. and G. Lachapelle (ed.): Kinematic Systems in Geodesy, Surveying and Remote Sensing, IAG Symposium 107, Springer-Verlag, 299-308.

Hatch, R. R., R. Keegan and T. A. Stansell (1992). Kinematic Receiver Technology from Magnavox. Proc. 6th Int. Geodetic Symp. on Satellite Positioning, Columbus, Ohio, 17-20 March, 174-183.

Hofmann-Wellenhof, B., H. Lichtenegger and J. Collins (1994). GPS Theory and Practice. Third Revised Edition, Springer-Verlag, Wien New York, 355pp.

Hopfield, H. S. (1969). Two-Quartic Tropospheric Refractivity Profile for Correcting Satellite Data. Journal of Geophysical Research, 74(18), 4487-4499.

Jin, X. X. (1995). The Change of GPS Code Accuracy with Satellite Elevation. Proc. 4th Int. Conf. on Differential Satellite Navigation Systems, Bergen, Norway, 24-28 April, poster no. 6, 8pp.

Johnson, J., J. Braun, C. Rocken, and T. VanHove (1995). The Role of Multipath in Antenna Height Tests at Table Mountain. UNAVCO Home Page, July 1995.

Kee, C. (1996). Wide Area Differential GPS. In: Parkinson B. et al (ed), Global Positioning System: Theory and Applications, Vol II, American Institute of Aeronautics and Astronautics, Inc., Washington DC, 81-115.

Klobuchar, J. A. (1987). Ionospheric Time-Delay Algorithm for Single-Frequency GPS Users. IEEE Transactions on Aerospace and Electronic Systems, AES-23, 325-331.

Kraus, T. P., J. N. Little and L. Schure (1994). Signal Processing Toolbox. The MathWorks Inc.

Lachapelle, G., M.E. Cannon, C. Erickson and W. Falkenberg (1992). High Precision C/A Code Technology for Rapid Static DGPS Surveys. Proc. 6th Int. Geodetic Symp. on Satellite Positioning, Ohio, Columbus, 17-20 March, 165-173.

Landau, H. and H. J. Euler (1992). On-The-Fly Ambiguity Resolution for Precision Differential Positioning. Proc. of the ION GPS-92, 5th Int. Tech. Meeting of the Satellite Division of the Institute of Navigation, Albuquerque, New Mexico, 22-24 September, 607-613.

Landau H., C. Pagels and U. Vollath (1995). Development and Implementation of a Centimeter-Accurate Real-Time-Kinematic Positioning System. Proc. ION GPS-95, Proc. ION GPS-95, 8th Int. Tech. Meeting of The Satellite Division of The U.S. Institute of Navigation, Palm Springs, California, 12-15 September, 1485-1491.

Langley, R. B. (1993). The GPS Observables. GPS World, 4(4), 52-59.

Langley, R. B. (1996). Propagation of the GPS Signals. In: Kleusberg A. and P. J. G. Teunissen (ed.): GPS for Geodesy, Lecture Notes in Earth Sciences, Springer-Verlag, Berlin, 103-140.

Lapucha D., R. Barker & Z. Liu (1995). High-Rate Precise Real-Time Positioning Using Differential Carrier Phase. Proc. ION GPS-95, 8th Int. Tech. Meeting of The Satellite Division of The U.S. Institute of Navigation, Palm Springs, California, 12-15 September, 1443-1449.

Leick, A. (1995). GPS Satellite Surveying. Second Edition, John Wiley & Sons, Inc., 560pp.

Lu, G. (1995). Development of a GPS Multi-Antenna System for Attitude Determination. PhD Dissertation, UCGE Reports Number 20073, Department of Geomatics Engineering, The University of Calgary, Calgary, Canada, 185pp.

Mader, G. L. (1992). Rapid Static and Kinematic Global Positioning System Solutions Using the Ambiguity Function Technique. Journal of Geophysical Research, 97(B3), 3271-3283.

Manual of the New South Wales Integrated Survey Grid, New South Wales Department of Lands, Sydney, Australia, January, 1976.

Mendes, V. B. and R. B. Langley (1995). Zenith Wet Tropospheric Delay Determination using Prediction Models: Accuracy Analysis. Cartografia e Cadastro, 2, 41-47.

Merminod, B. (1990). Resolution of the Cycle Ambiguities. In: Rizos, C. (ed.): Contributions to GPS Studies. UNISURV S-38, School of Surveying, The University of New South Wales, Sydney, Australia, 104-154.

Mervert, L., G. Beutler, M. Rothacher and U. Wild (1994). Ambiguity Resolution Strategies using the Results of the International GPS Geodynamics Service (IGS), Bulletin Géodésique, 68, 29-38.

Mok, E. (1996). A New Ambiguity Function Algorithm for Short Baseline Engineering Surveying Applications. PhD Dissertation, Department of Geomatics, University of Newcastle upon Tyne, U.K., 192 pp.

Mok, E. and P. Cross (1996). Optimum Rejection Threshold Determination for Ambiguity Function Testing. International Symposium on Global Positioning Systems, Digital Photogrammetry Systems, Remote Sensing and Geographical Systems (Geo-Informatics'96), Wuhan, P. R. China, 16-19 October, 317-335.

Neilan, R. E. (1996). The International GPS Service for Geodynamics. Pres. AGU's Western Pacific Geophysics Meeting, Brisbane, Australia, 23-27 July.

Qiu W., G. Lachapelle and M. E. Cannon (1995). Ionospheric Effect Modelling for Single Frequency GPS Users. Manuscripta Geodaetica, 20, 96-109.

Remondi, B.W. (1984), Using the Global Positioning System (GPS) Phase Observable for Relative Geodesy: Modeling, Processing, and Results. PhD Dissertation, Center for Space Research, The University of Texas at Austin, 360pp.

Remondi, B. W. (1985), Performing Centimeter Accuracy Relative Surveys in Seconds using GPS Carrier Phase, Proc. 1st Int. Symp. on Precise Positioning with GPS, Rockville, Marryland, 15-19 April, 789-797.

Remondi, B.W. (1988). Kinematic and Pseudo-Kinematic GPS. Proc. ION GPS-88, 1st Int. Tech. Meeting of The Satellite Division of The U.S. Institute of Navigation, Colorado Springs, Colorado, 19-23 September, 115-121.

Remondi, B. W. (1989). Pseudo-Kinematic GPS Results Using the Ambiguity Function Method. NAVIGATION, Journal of The U.S. Institute of Navigation, 38(1), 17-36.

Remondi B. W. and S. A. Hilla (1993). Pseudo-Kinematic Surveying Based on Upon Full-Wavelength Dual-Frequency GPS Observations. NOAA Technical Memorandum NOS NGS-56, 20pp.

Rizos, C. (1996). Principles and Practice of GPS Surveying, Monograph 17, School of Geomatic Engineering, The University of New South Wales, Sydney, Australia, 560pp.

Rizos, C., R. Galas and C. Reigber (1996). Design Challenges in the Development of a GPS-Based Volcano Monitoring System. Proc. 8th FIG Int. Symp. on Deformation Measurements, Hong Kong, 25-28 June, 7-15.

Roberts, W. D. S. and P. A. Cross (1993). The Effects of DGPS Temporal Correlation within the Kalman Filter Applied to Offshore Positioning. The Hydrographic Journal, 67, 5-11.

Saastamoinen, J. (1973). Contribution to the Theory of Atmospheric Refraction. Bulletin Geodesique, 107, 13-34

Sauer, D. B. (1994). Determination of High-Precision Trajectories without Fixing Integer Ambiguities. Proc. IEEE Position Location & Navigation Symp. PLANS'94, Las Vegas, Nevada, 11-15 April, 402-409.

Schwarz, K. P., N. El-Sheimy and Z. Liu (1994). Fixing GPS Cycle Slip by INS/GPS - Methods and Experiences. In: Cannon M. E. and G. Lachapelle (ed.): Proc. Int. Symp. on Kinematic Systems in Geodesy, Geomatics and Navigation, Banff, Canada, 30 August - 2 September, 265-275.

Shi, P. (1988). Atmospheric Refraction on the Results of GPS Phase Differential Measurements. In: Brunner, F. K. (Ed.): Atmospheric Effects on Geodetic Space Measurements, Monograph 12, School of Surveying, The University of New South Wales, Sydney, Australia, 45-62.

Shi, P. and S. Han (1992). Centralized Undifferential Method for GPS Network Adjustment. Australian Journal of Geodesy, Photogrammetry and Surveying, 57, 89-100.

Teunissen, P. J. G. (1994). A New Method for Fast Carrier Phase Ambiguity Estimation. Proc. IEEE Position Location & Navigation Symp. PLANS'94, Las Vegas, Nevada, 11-15 April, 562-573.

Teunissen, P. J. G. (1996a). On the Geometry of the Ambiguity Search Space with and without Ionosphere. Zeitschrift für Vermessungswesen, 121, 332-341.

Teunissen, P. J. G. (1996b). An Analytical Study of Ambiguity Decorrelation Using Dual Frequency Code and Carrier Phase. Journal of Geodesy, 70(8), 515-528.

Tiberius, C. C. J. M. and P. J. de Jonge (1995). Fast Positioning Using the LAMBDA-Method. Proc. 4th Int. Conf. on Differential Satellite Navigation Systems, Bergen, Norway, 24-28 April, paper no.30, 8pp.

Wanninger, L. (1995). Improved Ambiguity Resolution by Regional Differential Modelling of the Ionosphere. Proc. ION GPS-95, 8th Int. Tech. Meeting of The Satellite Division of The U.S. Institute of Navigation, Palm Springs, Calfornia, 12-15 September, 55-62.

Webster, I. and A. Kleusberg (1992). Regional Modelling of the Ionosphere for Single Frequency Users of the Global Positioning System. Proc. 6th Int. Geodetic Symp. on Satellite Positioning, Columbus, Ohio, 17-20 March, 230-239.

Wei, M. and K. P. Schwarz (1995). Fast Ambiguity Resolution Using an Integer Nonlinear Programming Method. Proc. ION GPS-95, 8th Int. Tech. Meeting of The Satellite Division of The U.S. Institute of Navigation, Palm Springs, California, 12-15 September, 1101-1110.

Wells, D. E., N. Beck, D. Delikaraoglou, A. Kleusberg, E. J. Krakiwsky, G. Lachapelle, R. B. Langley, M. Nakiboglu, K. P. Schwarz, J. M. Tranquilla and P. Vaníček. (1987). Guide to GPS Positioning. Canadian GPS Associates, Fredericton, N. B., Canada.

Wild, U., G. Beutler, W. Gurtner and M. Rothacher (1989). Estimating the Ionosphere using One or More Dual Frequency GPS Receivers. Proc. 5th International Geodetic Symposium on Satellite Positioning, Las Cruces, New Mexico, March 1989, Vol. II, 724-736.

Wu, J. T. (1994). Weighted Differential GPS Method for Reducing Ephemeris Error. Manuscripta Geodaetica, 20, 1-7.

Wübbena,G. (1989). The GPS Adjustment Software Package - GEONAP - Concepts and Models. Proc. 5th Int. Geodetic Symp. on Satellite Positioning, Las Cruces, New Mexico, 13-17 March, 452-461.

Wübbena, G., A. Bagge, G. Seeber, V. Böder and P. Hankemeier (1996). Reducing Distance Dependent Errors for Real-Time Precise DGPS Applications by Establishing Reference Station Networks. Proc. ION GPS-96, 9th Int. Tech. Meeting of The Satellite Division of The U.S. Institute of Navigation, Kansas City, Missouri, 17-20 September, 1845-1852.

Zhang, Q. J. and Schwarz, K. P. (1996). Estimating Double Difference GPS Multipath under Kinematic Conditions. Proc. IEEE Position Location & Navigation Symp. PLANS'96, Atlanta, Georgia, 22-26 April, 285-291.

Appendix A

IONOSPHERE INTERPOLATION USING AN EPOCH-BY-EPOCH AND SATELLITE-BY-SATELLITE MODEL

The epoch-by-epoch and satellite-by-satellite ionospheric model has been proposed for use as a high accuracy ionospheric delay prediction model (Webster & Kleusberg, 1992; Wanninger, 1995; Han & Rizos, 1996e). The ionospheric delay of a user receiver is estimated from an interpolation of ionospheric delay observations at three or more surrounding reference, dual-frequency GPS receivers, using the intersection points of the GPS signal paths with an ionospheric single-layer model at a height of 350 km (Figure 3-5). Actual implementation will involve the computation of the positions of the intersection points, and the transformation from TEC to VEC and from VEC to TEC. Due to the fact that precise TEC can only be computed in the double-differenced form, an approximation will also be necessary. For an area of approximately 200×200 km^2 in extent, the computation procedure can be reduced simply to that of the interpolation of the single-differenced TEC between receivers, or double-differenced TEC based on the receiver positions in the Gauss plane coordinate system. This appendix will give the proof.

For a satellite with elevation angle E at a reference station, the plane containing the satellite, the station and the earth's centre will intersect with the earth's surface as the line AB. $\overline{AB} = 200$ km is selected in the thesis. Also C and D points can be found to form a square. The intersection points A', B', C' and D' can be found by the lines from A, B, C, D to a satellite and the ionospheric layer with height H. Because the area is very small compared with the earth's radius, the point on the earth within ABCD can be considered to lie within the square ABCD. Any point within the square ABCD can be mapped onto the plane A'B'C'D'.

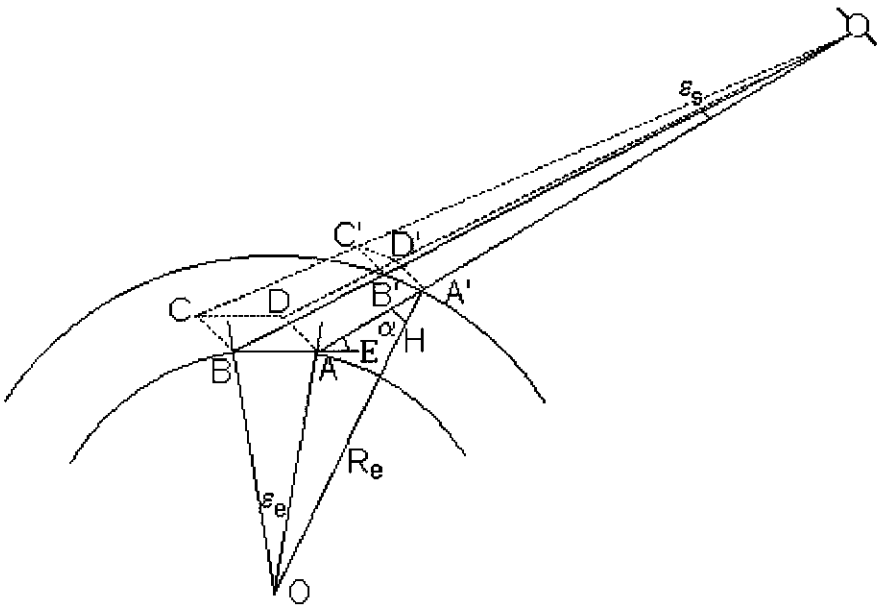

Figure A-1. Geometry relation between the coordinate systems on the ground and on the ionosphere layer

From the similar triangles, the following relations can be derived:

$$\overline{B'C'} = \frac{20,000 - \overline{BB'}}{20,000} \cdot \overline{BC} \tag{A-1}$$

and

$$\overline{A'D'} = \frac{20,000 - \overline{AA'}}{20,000} \cdot \overline{AD} \tag{A-2}$$

The distance $\overline{AA'}$ can be expressed as:

$$\sin\alpha = \frac{R_e}{R_e + H} \cdot \sin(90 + E) \tag{A-3}$$

$$\overline{AA'} = \frac{R_e + H}{\sin(90 + E)} \cdot \sin(90 - E - \alpha) \tag{A-4}$$

and $\overline{BB'}$ can also be expressed as a function of the elevation angle $(E-\varepsilon_e-\varepsilon_s)$ at B. The maximum distance $\overline{BB'}<1303\text{km}$ if the lowest elevation angle is selected as 10 degrees. The maximum value of the difference $\overline{BB'}-\overline{AA'}<100\text{km}$ if H=350 km. Therefore the relations (A-1) and (A-2) can be simplified to:

$$\overline{A'D'}=S_y\cdot\overline{AD} \tag{A-5}$$

and

$$\overline{B'C'}=S_y\cdot\overline{BC} \tag{A-6}$$

where

$$S_y=\frac{20,000-\overline{AA'}}{20,000}\approx\frac{20,000-\overline{BB'}}{20,000} \tag{A-7}$$

Based on the geometry in Figure A-1, the following relation can be derived:

$$\overline{A'B'}=S_y\cdot\frac{\sin(E-\varepsilon_e-\varepsilon_s)}{\sin(90+\alpha+\varepsilon_s)}\cdot\overline{AB}=S_x\cdot\overline{AB} \tag{A-8}$$

A similar relation for $\overline{CD}$ and $\overline{C'D'}$ can be derived:

$$\overline{C'D'}=S_x\cdot\overline{CD} \tag{A-9}$$

The mapping from plane ABCD to the plane A'B'C'D' can be performed through a scaling by S_x and S_y, and then ABCD can be translated to Gauss plane coordinate system, as shown in Figure A-2. x is the North axis and y is the East axis. The coordinate origin is at the point B. θ is the satellite azimuth.

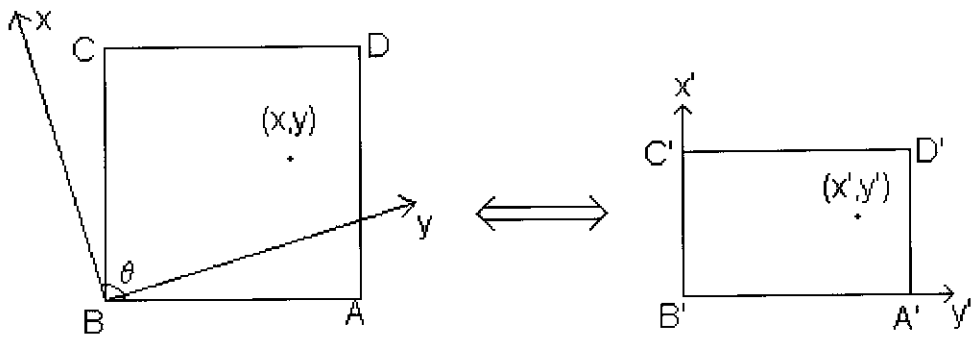

Figure A-2. Coordinate Transformation from the Gauss plane to ionosphere layer

From equations (A-5, A-6, A-8, A-9), the coordinates in a Gauss plane coordinate system can be transformed to the ionospheric layer coordinate system, and vice versa:

$$\begin{bmatrix} x' \\ y' \end{bmatrix} = \begin{bmatrix} S_x & 0 \\ 0 & S_y \end{bmatrix} \cdot \begin{bmatrix} \cos(\theta - 90) & \sin(\theta - 90) \\ -\sin(\theta - 90) & \cos(\theta - 90) \end{bmatrix} \cdot \begin{bmatrix} x \\ y \end{bmatrix} = T \cdot \begin{bmatrix} x \\ y \end{bmatrix} \tag{A-10}$$

Assume that B is the reference GPS receiver and the other two reference receivers are located at (x_1, y_1) and (x_2, y_2) in the Gauss coordinate system. The transformed coordinates at the ionospheric layer coordinate system are (x'_1, y'_1) and (x'_2, y'_2), respectively. The single-differenced ΔVEC_1 and ΔVEC_2 at points 1 and 2 relative to point B can be represented by a linear model:

$$\begin{bmatrix} \Delta VEC_1 \\ \Delta VEC_2 \end{bmatrix} = \begin{bmatrix} x'_1 & y'_1 \\ x'_2 & y'_2 \end{bmatrix} \cdot \begin{bmatrix} \alpha_x \\ \alpha_y \end{bmatrix} \tag{A-11}$$

where α_x and α_y are the VEC change rate at the axis x' and y' and can be determined if ΔVEC_1 and ΔVEC_2 are known:

$$\begin{bmatrix} \alpha_x \\ \alpha_y \end{bmatrix} = \begin{bmatrix} x'_1 & y'_1 \\ x'_2 & y'_2 \end{bmatrix}^{-1} \cdot \begin{bmatrix} \Delta VEC_1 \\ \Delta VEC_2 \end{bmatrix} = \left(T^T\right)^{-1} \cdot \begin{bmatrix} x_1 & y_1 \\ x_2 & y_2 \end{bmatrix}^{-1} \cdot \begin{bmatrix} \Delta VEC_1 \\ \Delta VEC_2 \end{bmatrix} \tag{A-12}$$

For any point (x,y) in the Gauss coordinate system, the intersection point at the ionospheric layer is (x',y'), and the single-differenced VEC can be interpolated as:

$$\Delta VEC = \begin{bmatrix} x' & y' \end{bmatrix} \begin{bmatrix} \alpha_x \\ \alpha_y \end{bmatrix} = \begin{bmatrix} x & y \end{bmatrix} \cdot T^T \cdot \begin{bmatrix} \alpha_x \\ \alpha_y \end{bmatrix} = \begin{bmatrix} x & y \end{bmatrix} \cdot \begin{bmatrix} x_1 & y_1 \\ x_2 & y_2 \end{bmatrix}^{-1} \cdot \begin{bmatrix} \Delta VEC_1 \\ \Delta VEC_2 \end{bmatrix} \quad \text{(A-13)}$$

This means that the single-differenced VEC can be obtained by interpolating in the Gauss coordinate system, which is equivalent to an interpolation at the ionospheric layer.

Furthermore, the maximum difference angle between $\sin^{-1}(0.94792\cos E)$ for any point within the area ABCD is smaller than 2.2 degrees for a 200 km square area. Therefore, the TEC interpolation formula can be derived by multiplying by $\frac{1}{\cos[\sin^{-1}(0.94792\cos E)]}$:

$$\Delta TEC = \begin{bmatrix} x & y \end{bmatrix} \cdot \begin{bmatrix} x_1 & y_1 \\ x_2 & y_2 \end{bmatrix}^{-1} \cdot \begin{bmatrix} \Delta TEC_1 \\ \Delta TEC_2 \end{bmatrix} \quad \text{(A-14)}$$

where ΔTEC, ΔTEC_1 and ΔTEC_2 are the single-differenced total electron content referenced to station B.

Note that the single-differenced TEC interpolation function is not dependent on the satellite, and only dependent on the GPS receiver positions. Therefore, for any two satellites, the double-differenced TEC can be derived from the interpolated single-differenced TEC as:

$$\nabla\Delta TEC = \begin{bmatrix} x & y \end{bmatrix} \cdot \begin{bmatrix} x_1 & y_1 \\ x_2 & y_2 \end{bmatrix}^{-1} \cdot \begin{bmatrix} \nabla\Delta TEC_1 \\ \nabla\Delta TEC_2 \end{bmatrix} \quad \text{(A-15)}$$

Although the single-differenced TEC cannot be accurately determined, the double-differenced TEC can be determined using dual-frequency carrier phase observations with known double-differenced integer ambiguities:

$$\nabla\Delta TEC(k) = \frac{1}{\alpha} \cdot \frac{f_2^2}{f_1^2 - f_2^2} \cdot \left(\left(\nabla\Delta\phi_1(k) - \lambda_1 \cdot \nabla\Delta N_1 \right) - \left(\nabla\Delta\phi_2(k) - \lambda_2 \cdot \nabla\Delta N_2 \right) \right) \quad \text{(A-16)}$$

If there are three reference GPS receivers set up around the survey area of interest, and the integer ambiguity can be determined relative to one of the reference station, the double-differenced TEC ($\nabla\Delta TEC_1$, $\nabla\Delta TEC_2$ for the other two stations) can be used to interpolate double-differenced TEC at the roving receiver.

Appendix B

AMBIGUITY RESOLUTION FOR LONG-RANGE GPS STATIC BASELINES

Appendix B will mainly discuss the ambiguity resolution technique for long-range static positioning. Cycle slip detection and repair techniques are described in Blewitt (1990) and Han (1995b).

B-1. Fundamental Observation Equations

The observation equations and the ambiguity resolution procedure for high precision long-range static positioning were described by Blewitt (1989), Dong & Bock (1989) and Goad (1992), and are based on the following equations:

$$R_1 = \rho + \frac{I}{f_1^2} + \varepsilon_{R_1} \tag{B-1}$$

$$\varphi_1\lambda_1 = \rho - \frac{I}{f_1^2} + N_1\lambda_1 + \varepsilon_{\varphi_1} \tag{B-2}$$

$$R_2 = \rho + \frac{I}{f_2^2} + \varepsilon_{R_2} \tag{B-3}$$

$$\varphi_2\lambda_2 = \rho - \frac{I}{f_2^2} + N_2\lambda_2 + \varepsilon_{\varphi_2} \tag{B-4}$$

where R_1 and R_2 are the one-way precise pseudo-ranges; φ_1 and φ_2 are the one-way carrier phase observations in units of cycles; ρ is the geometric range from station to satellite; I is a function of the Total Electron Content; f_1, f_2 and λ_1, λ_2 are the frequencies and wavelengths of the L1 and L2 carrier waves respectively; N_1 and N_2 are the integer cycle ambiguities of the L1 and L2 carrier phase observations; and ε is the

observation noise with respect to the observation type indicated by its subscript. The carrier phase combination (i, j) can be represented by (Han & Rizos, 1996b):

$$\varphi_{i,j} = i \cdot \varphi_1 + j \cdot \varphi_2 \tag{B-5}$$

and the integer ambiguity and wavelength are expressed by:

$$N_{i,j} = i \cdot N_1 + j \cdot N_2 \tag{B-6}$$

$$\lambda_{i,j} = c \Big/ (i \cdot f_1 + j \cdot f_2) \tag{B-7}$$

where c in equation (B-7) is the speed of light in a vacuum.

The ionosphere-free combination of the L1 and L2 carrier phase observations can be derived as:

$$\varphi_{77,-60}\lambda_{77,-60} = \rho + N_{77,-60}\lambda_{77,-60} + \varepsilon_{\varphi_{77,-60}\lambda_{77,-60}} \tag{B-8}$$

and subsequently the double-differenced ionosphere-free observations are:

$$\Delta\nabla\varphi_{77,-60}\lambda_{77,-60} = \Delta\nabla\rho + \Delta\nabla N_{77,-60}\lambda_{77,-60} + \varepsilon_{\Delta\nabla\varphi_{77,-60}\lambda_{77,-60}} \tag{B-9}$$

Although $\Delta\nabla N_{77,-60}$ is an integer, it is almost impossible to resolve it using the above observation directly due to the small value of the wavelength $\lambda_{77,-60}$ ($\approx$0.63cm). Therefore the following ambiguity resolution techniques for $\Delta\nabla N_{77,-60}$ are considered.

B-2. Widelane Integer Ambiguity Determination Methods

There are different way to determine widelane integer ambiguities using available observations. If the precise pseudo-range observations on L1 and L2 are available, e.g. as output by GPS receivers such as the Ashtech Z12, Leica SR 399 or Trimble 4000SSi, Method 1 can be used, as discussed in Section B-2-1. If the precise pseudo-range observations on L1 and L2 are not available, but the difference between the precise pseudo-range observations on L1 and L2 is available, e.g. as output by GPS receivers such as the Rogue SNR 8000 or Trimble 4000SSE, Method 2 can be used, as discussed

in Section B-2-2. If the precise pseudo-range observations are not available or cannot be used, Method 3 can be used, as discussed in Section B-2-3.

B-2-1. Method 1 - Using Precise Pseudo-Range Observations on L1 and L2

Based on equations (B-1 to B-4), the real-valued ambiguity ($N_{i,j}$) estimation formula for a carrier phase combination $\varphi_{i,j}$ can be written as:

$$N_{i,j} = \varphi_{i,j} - \frac{9240\cdot(i+j)+289\cdot i}{2329\cdot\lambda_1}\cdot R_1 + \frac{9240\cdot(i+j)+289\cdot i}{2329\cdot\lambda_2}\cdot R_2 \qquad \text{(B-10)}$$

Hence the double-differenced widelane ambiguity can be written as:

$$\Delta\nabla N_{1,-1} = \Delta\nabla\varphi_{1,-1} - \frac{17}{137\cdot\lambda_1}\Delta\nabla R_1 - \frac{17}{137\cdot\lambda_2}\Delta\nabla R_2 \qquad \text{(B-11)}$$

For static data, $\Delta\nabla N_{1,-1}$ can generally be determined by time-averaging a few tens of minutes of data. Using this technique, widelane integer ambiguity determination is independent of the knowledge of orbits, station location, etc., and so can be applied to baselines of any length provided there is sufficient common visibility of satellites.

B-2-2. Method 2 - Using Differences of the Precise Pseudo-Ranges on L1 and L2

In order to overcome Anti-Spoofing, GPS receivers such as the Trimble 4000SSE and Rogue SNR 8000 use the cross-correlation tracking technique to output full wavelength L1 and L2 carrier phase and the *difference* between the two precise pseudo-ranges ($R_1 - R_2$). Therefore, the following equation can be derived from equations (B-1 to B-4):

$$-(R_1 - R_2) = \varphi_1\lambda_1 - \varphi_2\lambda_2 + N_1\lambda_1 - N_2\lambda_2$$

$$= \varphi_1\lambda_1 - \varphi_2\lambda_2 - \frac{f_1^2 - f_2^2}{f_1 f_2}\left[N_{1,-1}\lambda_{1,-1} - N_{77,-60}\lambda_{77,-60}\right] \qquad \text{(B-12)}$$

and can be represented by the following double-differenced form:

$$\Delta\nabla N_{1,-1} = \frac{4620}{2329\cdot\lambda_{1,-1}}\cdot\left[(\Delta\nabla R_1 - \Delta\nabla R_2) + (\Delta\nabla\varphi_1\lambda_1 - \Delta\nabla\varphi_2\lambda_2)\right] + \frac{1}{\lambda_{1,-1}}\cdot\Delta\nabla N_{77,-60}\lambda_{77,-60} \qquad \text{(B-13)}$$

The term $\Delta\nabla N_{77,-60}\lambda_{77,-60}$ can be easily estimated from the ambiguity-float solution of the ionosphere-free carrier phase observation with an accuracy better than 10 cm, and hence the effect of this term can be neglected. The effect of the term $(\Delta\nabla\varphi_1\lambda_1 - \Delta\nabla\varphi_2\lambda_2)$ can also be neglected due to its noise being less than a few centimetres. The significant effect is therefore the noise of $(\Delta\nabla R_1 - \Delta\nabla R_2)$, which needs quite a long observation period in order to average out this noise and the pseudo-range multipath. Using this technique, widelane integer ambiguity determination is also independent of the knowledge of orbits, station location, etc., and hence can be applied to baselines of any length provided there is sufficient common visibility of satellites.

B-2-3. Method 3 - No Precise Pseudo-Range Observations

The widelane carrier phase observation equation can be derived from equations (B-2) and (B-4) as:

$$\Delta\nabla\varphi_{1,-1}\lambda_{1,-1} = \Delta\nabla\rho + \Delta\nabla N_{1,-1}\lambda_{1,-1} + \frac{77}{60}\cdot\frac{\Delta\nabla I}{f_1^2} + \varepsilon_{\Delta\nabla\varphi_{1,-1}\lambda_{1,-1}} \qquad \text{(B-14)}$$

If the ionospheric delay is $\frac{\Delta\nabla I}{f_1^2} = \lambda_1$, then the $\Delta\nabla N_1$ will be biased by one cycle, but the $\Delta\nabla N_{1,-1}$ will be biased by 0.3636 cycles. Therefore, from the point of view of ambiguity resolution, $\Delta\nabla N_{1,-1}$ has a smaller ionosphere effect. Hence, the maximum baseline length for which the ionospheric delay can be neglected when resolving $\Delta\nabla N_{1,-1}$ is longer than that for which the ionospheric delay can be neglected when resolving $\Delta\nabla N_1$. If the ionospheric delay is neglected, the widelane integer ambiguity can be resolved for baselines up to about 30 km in length using equation (B-14), while the L1 integer ambiguity can be resolved for baselines up to 15 km in length using equation (B-2).

Dong & Bock (1989) have proposed that $\frac{\Delta\nabla I}{f_1^2}$ be considered an unknown parameter with zero mean value and a small uncertainty. The method is expected to derive the more reliable results than simply neglecting ionospheric delay term.

The functional model of equation (B-14) is also affected by orbit bias. The effect of the orbit bias on $\Delta\nabla N_{1,-1}$ can be approximated by:

$$d\Delta\nabla N_{1,-1} = \frac{1}{\lambda_{1,-1}\bar{\rho}}\left[\Delta X\cdot\left(dX^i - dX^j\right) + \Delta Y\cdot\left(dY^i - dY^j\right) + \Delta Z\cdot\left(dZ^i - dZ^j\right)\right] \quad \text{(B-15)}$$

where $(\Delta X,\ \Delta Y,\ \Delta Z)$ is the baseline vector; $\left(dX^i,\ dY^i,\ dZ^i\right)$ and $\left(dX^j,\ dY^j,\ dZ^j\right)$ are the orbit errors for the three components of the satellites i and j; $\bar{\rho}$ (≈20,000km) is the mean distance from receivers to satellites. If it is assumed that the orbit errors at the three components are the same, and are random for different satellites, the effect of an orbit bias on $\Delta\nabla N_{1,-1}$ can be approximated by:

$$m_{\Delta\nabla N_{1,-1}} = \frac{\sqrt{6}}{3\lambda_{1,-1}\bar{\rho}}\cdot D\cdot m_S \quad \text{(B-16)}$$

where D is the baseline length; m_S is the standard deviation of the satellite orbit information and $m_{\Delta\nabla N_{1,-1}}$ is the standard deviation of the effect of the orbit bias on the value $\Delta\nabla N_{1,-1}$. If it is assumed that $m_{\Delta\nabla N_{1,-1}} < 0.25$ cycles, the maximum length of the baseline for different magnitudes of orbit bias are listed in Table B-1.

Table B-1.Maximum length of baseline for different magnitudes of orbit bias

Orbit Bias (m)	0.2	0.5	1.0	2.0	5.0	10.0
Maximal Length (km) for $\Delta\nabla N_{1,-1}$	26391	10556	5278	2639	1056	528
Maximal Length (km) for $\Delta\nabla N_1$	3275	1310	655	328	131	66

B-3. Ambiguity Resolution for Long-Range Static Positioning

Using the double-differenced ionosphere-free combination observation equation (B-9), $\Delta\nabla N_{77,-60}$ is very difficult to determine because the wavelength of the ionosphere-free combination is very small (0.63cm). However, after the widelane ambiguities $\Delta\nabla N_{1,-1}$ are fixed, $\Delta\nabla N_{77,-60}$ can be represented by:

$$\Delta\nabla N_{77,-60} = \frac{60\cdot i + 77\cdot j}{i+j}\cdot\Delta\nabla N_{1,-1} + \frac{17}{i+j}\cdot\Delta\nabla N_{i,j} \quad \text{(B-17)}$$

and then substituting in equation (B-9), the following form of the observation equation can be obtained:

$$\Delta\nabla\varphi_{77,-60}\lambda_{77,-60} = \Delta\nabla\rho + \Delta\nabla N_{i,j}\cdot\left(\frac{17}{i+j}\cdot\lambda_{77,-60}\right) + \Delta\nabla N_{1,-1}\cdot\left(\frac{60\cdot i+77\cdot j}{i+j}\cdot\lambda_{77,-60}\right) + \varepsilon_{\Delta\nabla\varphi_{77,-60}\lambda_{77,-60}} \tag{B-18}$$

The third term on the right hand side is therefore a known quantity. The search techniques in the estimated ambiguity domain can be used to resolve $\Delta\nabla N_{i,j}$. The larger the coefficient of $\Delta\nabla N_{i,j}$, the smaller the search region for $\Delta\nabla N_{i,j}$. The maximum value is obtained when i+j=1, hence $\Delta\nabla N_{i,j}$ can be represented by $\Delta\nabla N_1$, $\Delta\nabla N_2$ or other combinations which satisfy the condition i+j=1, and the same search region will result. If $\Delta\nabla N_1$ is used, equation (B-18) can be simply expressed as:

$$\Delta\nabla\varphi_{77,-60}\lambda_{77,-60} = \Delta\nabla\rho + \Delta\nabla N_1\cdot\left(17\lambda_{77,-60}\right) + \Delta\nabla N_{1,-1}\cdot\left(60\lambda_{77,-60}\right) + \varepsilon_{\Delta\nabla\varphi_{77,-60}\lambda_{77,-60}} \tag{B-19}$$

Comparing this equation with the L1 double-differenced phase observation equation, the wavelength of $\Delta\nabla N_1$ in equation (B-19) is equivalent to 10.7cm ($17\lambda_{77,-60} = 10.7\text{cm}$). On the other hand, the orbit bias will affect the ambiguity determination and though this can be neglected in the short-range positioning mode (due to the assumptions for differential processing), the precise ephemeris should be used for long baselines. The effect of orbit bias on $\Delta\nabla N_1$ can be approximated by equations similar to equations (B-15) and (B-16):

$$d\Delta\nabla N_1 = \frac{1}{51\lambda_{77,-60}\bar{\rho}}\left[\Delta X\cdot\left(dX^i - dX^j\right) + \Delta Y\cdot\left(dY^i - dY^j\right) + \Delta Z\cdot\left(dZ^i - dZ^j\right)\right] \tag{B-20}$$

and

$$m_{\Delta\nabla N_1} = \frac{\sqrt{6}}{51\lambda_{77,-60}\bar{\rho}}\cdot D\cdot m_S \tag{B-21}$$

Assuming that $m_{\Delta\nabla N_1} < 0.25$ cycles, the maximum length of the baseline for different magnitudes of orbit bias are listed in Table B-1.

After determination of the initial ambiguities $\Delta\nabla N_{77,-60}$ from $\Delta\nabla N_{1,-1}$ and $\Delta\nabla N_1$, the double-differenced ionosphere-free combination observation equation (B-9) can be used for GPS long-range static positioning.

Publications from

THE SCHOOL OF GEOMATIC ENGINEERING

(Formerly School of Surveying)

THE UNIVERSITY OF NEW SOUTH WALES

All prices include postage by surface mail. Air mail rates on application. (Effective August 1997)

To order, write to Publications Officer, School of Geomatic Engineering
The University of New South Wales, Sydney 2052, AUSTRALIA

NOTE: ALL ORDERS MUST BE PREPAID

UNISURV REPORTS - S SERIES

S8 - S20	Price (including postage) :		$10.00
S29 onwards	Price (including postage) :	Individuals	$25.00
		Institutions	$30.00

S8 A. Stolz, "Three-D Cartesian co-ordinates of part of the Australian geodetic network by the use of local astronomic vector systems", Unisurv Rep. S8, 182 pp, 1972.

S10 A.J. Robinson, "Study of zero error & ground swing of the model MRA101 tellurometer", Unisurv Rep. S10, 200 pp, 1973.

S12. G.J.F. Holden, "An evaluation of orthophotography in an integrated mapping system", Unisurv Rep. S12, 232 pp, 1974.

S14. Edward G. Anderson, "The Effect of Topography on Solutions of Stokes` Problem", Unisurv Rep. S14, 252 pp, 1976.

S16. K. Bretreger, "Earth Tide Effects on Geodetic Observations", Unisurv S16, 173 pp, 1978.

S17. C. Rizos, "The role of the gravity field in sea surface topography studies", Unisurv S17, 299 pp, 1980.

S18. B.C. Forster, "Some measures of urban residential quality from LANDSAT multi-spectral data", Unisurv S18, 223 pp, 1981.

S19. Richard Coleman, "A Geodetic Basis for recovering Ocean Dynamic Information from Satellite Altimetry", Unisurv S19,332 pp, 1981.

S20. Douglas R. Larden, "Monitoring the Earth's Rotation by Lunar Laser Ranging", Unisurv Report S20, 280 pp, 1982.

S29 Gary S Chisholm, "Integration of GPS into hydrographic survey operations", Unisurv S29, 190 pp, 1987.

S30. Gary Alan Jeffress, "An investigation of Doppler satellite positioning multi-station software", Unisurv S30, 118 pp, 1987.

S31. Jahja Soetandi, "A model for a cadastral land information system for Indonesia", Unisurv S31, 168 pp, 1988.

S33. R. D. Holloway, "The integration of GPS heights into the Australian Height Datum", Unisurv S33, 151 pp.,1988.

S34. Robin C. Mullin, "Data update in a Land Information Network", Unisurv S34, 168 pp. 1988.

S35. Bertrand Merminod, "The use of Kalman filters in GPS Navigation", Unisurv S35, 203 pp., 1989.

S36. Andrew R. Marshall, "Network design and optimisation in close range Photogrammetry", Unisurv S36, 249 pp., 1989.

S37. Wattana Jaroondhampinij, "A model of Computerised parcel-based Land Information System for the Department of Lands, Thailand," Unisurv S37, 281 pp., 1989.

S38. C. Rizos (Ed.), D.B. Grant, A. Stolz, B. Merminod, C.C. Mazur "Contributions to GPS Studies", Unisurv S38, 204 pp., 1990.

S39. C. Bosloper, "Multipath and GPS short periodic components of the time variation of the differential dispersive delay", Unisurv S39, 214 pp., 1990.

S40. John Michael Nolan, "Development of a Navigational System utilizing the Global Positioning System in a real time, differential mode", Unisurv S40, 163 pp., 1990.

S41. Roderick T. Macleod, "The resolution of Mean Sea Level anomalies along the NSW coastline using the Global Positioning System", 278 pp., 1990.

S42. Douglas A. Kinlyside, "Densification Surveys in New South Wales - coping with distortions", 209 pp., 1992.

S43. A. H. W. Kearsley (ed.), Z. Ahmad, B. R. Harvey and A. Kasenda, "Contributions to Geoid Evaluations and GPS Heighting", 209 pp., 1993.

S44. Paul Tregoning, "GPS Measurements in the Australian and Indonesian Regions (1989-1993)", 134 + xiii pp, 1996.

S45. Wan-Xuan Fu, "A study of GPS and other navigation systems for high precision navigation and attitude determinations", 332pp, 1996.

S46. Peter Morgan et al, "A zero order GPS network for the Australia region", 187 + xii pp, 1996.

S47. Yongru Huang, "A digital photogrammetry system for industrial monitoring", 145 + xiv pp, 1997.

S48. Kim Mobbs, "Tectonic interpretation of the Papua New Guine Region from repeat satellite measurements", 256 + xc pp, 1997.

S49. Shaowei Han, "Carrier phase-based long-range GPS kinematic positioning", 185 + xi pp, 1997.

S50. Mustafa D Subari, "Low-cost GPS systems for intermediate surveying and mapping accuracy applications", 179 + xiii pp, 1997.

MONOGRAPHS

Prices include postage by surface mail

		Price
M1.	R.S. Mather, "The theory and geodetic use of some common projections", (2nd edition), 125 pp., 1978.	$15.00
M2.	R.S. Mather, "The analysis of the earth's gravity field", 172 pp., 1971.	$8.00
M3.	G.G. Bennett, "Tables for prediction of daylight stars", 24 pp.,1974.	$5.00
M4.	G.G. Bennett, J.G. Freislich & M. Maughan, "Star prediction tables for the fixing of position", 200 pp., 1974.	$8.00
M8.	A.H.W. Kearsley, "Geodetic Surveying", 96 pp, (revised) 1988.	$12.00
M11.	W.F. Caspary, "Concepts of Network and Deformation Analysis",183 pp., 1988.	$25.00
M12.	F.K. Brunner, "Atmospheric Effects on Geodetic Space Measurements", 110 pp., 1988.	$16.00
M13.	Bruce R. Harvey, "Practical Least Squares and Statistics for Surveyors", (2nd edition), 319 pp., 1994.	$30.00
M14.	Ewan G. Masters & John R. Pollard (Ed.), "Land Information Management", 269 pp., 1991. (Proceedings LIM Conference, July 1991).	$20.00
M15/1	Ewan G. Masters & John R. Pollard (Ed.), "Land Information Management - Geographic Information Systems - Advance Remote Sensing Vol 1" 295 pp., 1993 (Proceedings of LIM & GIS Conference, July 1993).	$30.00
M15/2	Ewan G. Masters & John R. Pollard (Ed.), "Land Information Management - Geographic Information Systems - Advance Remote Sensing Vol 2" 376 pp., 1993 (Proceedings of Advanced Remote Sensing Conference, July 1993).	$30.00
M16.	A. Stolz, "An Introduction to Geodesy", 112 pp., 1994.	$20.00
M17	Chris Rizos, "Principles and Practice of GPS Surveying", 565 pp., 1997.	$50.00